

Dark matter effects on the properties of neutron stars: compactness and tidal deformability

Hong-Ming Liu (刘宏铭)^{1,2}, Jin-Biao Wei (魏金标)³, and Zeng-Hua Li (李增花)^{1,2*}

¹ Institute of Modern Physics, Key Laboratory of Nuclear Physics and Ion-Beam Application, MOE, Fudan University, Shanghai 200433, People's Republic of China

² Shanghai Research Center for Theoretical Nuclear Physics, NSFC and Fudan University, Shanghai 200438, China

³ School of Mathematics and Physics, China University of Geosciences, Lumi Road 388, 430074 Wuhan, China

G. F. Burgio⁴, H. C. Das⁴, and H.-J. Schulze⁴

⁴ Istituto Nazionale di Fisica Nucleare, Sezione di Catania, Dipartimento di Fisica, Università di Catania,

Via Santa Sofia 64, 95123 Catania, Italy

(Dated: March 27, 2024)

We systematically study the observable properties of dark-matter admixed neutron stars, employing a realistic nuclear EOS in combination with self-interacting fermionic dark matter respecting constraints on the self-interaction cross section. Deviations from universal relations valid for nucleonic neutron stars are analyzed over the whole parameter space of the model and unequivocal signals for the presence of dark matter in neutron stars are identified.

I. INTRODUCTION

Dark matter (DM), realized by yet unknown elementary particles within or beyond the standard model [1–3], is one of the most enigmatic aspects of current astrophysics [4, 5]. It must make up nearly 90% of the matter in the Universe in order to explain observations at galactic and super-galactic scales [6–10]. Most of its properties like its mass and interactions with other particles are presently unknown [11–14].

Theoretically several kinds of bosonic and fermionic DM candidates have been hypothesized, such as a weakly-interacting massive particle (WIMP) [15–19], especially neutralino [20–28], asymmetric dark matter (ADM) [29–32] like mirror matter [33–35], axion [36, 37], and strangelets [38–41].

A particular environment to reveal features of DM are neutron stars (NSs), the densest objects known in the Universe, for which more and more precise observational data become available. Their hypothetical capability to accumulate DM might provide possibilities to deduce related DM properties. It is thus of great interest to theoretically analyze DM-admixed NS (DNS) models, combining a more or less well-known nuclear-matter (NM) EOS with a hypothetical DM EOS within a general-relativistic two-fluid approach [34, 42, 43].

The fundamental theoretical challenge of the eventual presence of DM in NSs is the fact that their mass-radius relation is not anymore a unique function, but depends on an additional degree of freedom, the DM content. The absence of any knowledge regarding the nature of DM, combined with the persisting uncertainty of the high-density NM EOS, then renders any theoretical conclusion regarding either DM or high-density NM doubtful. The simplest example would be the observation of a very massive ‘NS’, which could simply be caused by the presence of a massive DM halo, but also by a very stiff NM EOS. Therefore theoretical methods have to be devised to unequivocally identify the presence and quantity of DM in NSs.

It is generally believed that most or all observed ‘NSs’ are such, namely standard hadronic stars with very little admixture of DM. We note at this point that current estimates of the acquired DM content by accretion during the NS lifetime yield extremely small results of $\lesssim 10^{-10} M_{\odot}$ [13, 15, 17, 29, 30, 32, 44–47], which would be unobservable. The existence of DNSs with large DM fractions (of the order of percent or larger) assumed in this article, therefore requires exotic capture or formation mechanisms [12, 47–54], which remain so far very speculative. Keeping this in mind, we study in this work in a qualitative manner DNSs with arbitrary DM fraction up to 100%, corresponding to pure dark stars (DSs) [50, 55–57].

The effects of DM on the properties of NM and NSs have been intensely investigated in recent years. Apart from its fundamental impact on NS mass and radius [11, 58–64], a large number of works studied the possibility of DM acquisition by NSs [65–70] and related phenomena like heating [14, 17, 44, 46, 71–75] or internal black hole formation and collapse [15, 18, 30, 32, 34, 45, 76–79]. Recently, more quantitative studies have been performed, like the DM effects on the derived properties of NM [23], or the validity of universal relations between the NS compactness M/R and the moment of inertia I , tidal deformability Λ , and quadrupole moment Q [80–83], in the presence of DM [51, 84, 85]. Refs. [86, 87] examined the possibility of the LIGO/Virgo events GW170817 [88] and GW190425 [89] being realized by a DNS scenario. Many recent works [22, 24–26, 28, 35, 51–53, 90–98] focused on DM effects on the NS tidal deformability and related observables [99–102], which are directly accessible by recent and future GW detectors. The impact of DM on the pulsar x-ray profile [103, 104] and on NS cooling processes [19, 27] were also examined recently.

The purpose of the present article is to continue and extend our previous study of DNS optical radii and tidal deformability [105] over the full parameter space of a given DM model. We will now assume self-interacting fermionic DM particles with an interaction strength constrained by observational limits on the self-interaction cross section.

The optical radius R_N is perhaps the most relevant and at

* zhli09@fudan.edu.cn

the same time the most easily accessible observable of a NS (apart from the gravitational mass M), and therefore merits particular attention before studying more intricate features of a NS. We will also analyze the validity and breakdown of universal relations between stellar compactness M/R_N and tidal deformability Λ . The purpose is to devise unequivocal methods to deduce and quantify the presence of DM in NSs.

This article is organized as follows. In the next section II, the EOSs of ordinary NM and DM used in this work are briefly described. The detailed calculations and discussion are presented in Sec. III. A summary is given in Sec. IV.

II. FORMALISM

A. Equation of state for nuclear matter

As in [105], we employ here the latest version of a Brueckner-Hartree-Fock (BHF) EOS obtained with the Argonne V18 NN potential and compatible three-body forces [106–108], see [109, 110] for a more detailed account. This EOS is compatible with all current low-density constraints [111–113] and in particular also with those imposed on NS maximum mass $M_{\max} > 2M_{\odot}$ [114–116], radius $R_{1.4} \approx 11 - 13$ km [117–120], and tidal deformability $\Lambda_{1.4} \approx 70 - 580$ [88, 121–123].

Therefore observation of compact objects violating these constraints will be interpreted as indicating DM admixture according to the following detailed analysis.

B. Equation of state for dark matter

We employ in this work the frequently used [49, 51–53, 59, 61, 91, 92, 95, 124–126] DM model of fermions with mass μ self-interacting via a repulsive Yukawa potential

$$V(r) = \alpha \frac{e^{-mr}}{r} \quad (1)$$

with coupling constant α and mediator mass m . Following Ref. [124] we write pressure and energy density of the resulting DM EOS as

$$p_D = \frac{\mu^4}{8\pi^2} \left[x \sqrt{1+x^2} (2x^2/3 - 1) + \text{arsinh}(x) \right] + \delta, \quad (2)$$

$$\epsilon_D = \frac{\mu^4}{8\pi^2} \left[x \sqrt{1+x^2} (2x^2 + 1) - \text{arsinh}(x) \right] + \delta, \quad (3)$$

where

$$x = \frac{k_F}{\mu} = \frac{(3\pi^2 n)^{1/3}}{\mu} \quad (4)$$

is the dimensionless kinetic parameter with the DM particle density n , and the self-interaction term is written as

$$\delta = \frac{2}{9\pi^3} \frac{\alpha \mu^6}{m^2} x^6 \equiv \mu^4 \left(\frac{y}{3\pi^2} \right)^2 x^6 = \left(\frac{yn}{\mu} \right)^2, \quad (5)$$

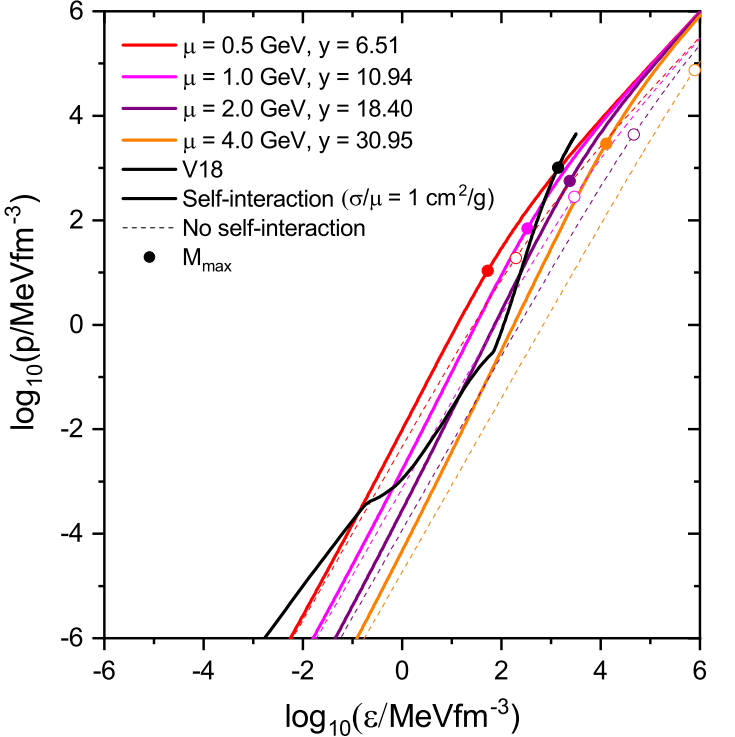


FIG. 1. EOSs of different pure DM models and the nuclear V18 EOS. The markers indicate the values of the maximum-mass M_{\max} configurations. The interaction parameter y , Eq. (10), is also listed.

introducing the interaction parameter $y^2 = 2\pi\alpha\mu^2/m^2$. Ref. [124] contains interesting scaling relations regarding the EOS and mass-radius relations of pure fermionic DM stars.

Within this model, y is not a free parameter, but constrained by observational limits imposed on the DM self-interaction cross section σ [127–130],

$$\sigma/\mu \sim 0.1 - 10 \text{ cm}^2/\text{g}. \quad (6)$$

In [49, 51, 125] it has been shown that the Born approximation

$$\sigma_{\text{Born}} = \frac{4\pi\alpha^2}{m^4} \mu^2 = \frac{y^4}{\pi\mu^2} \quad (7)$$

is very accurate for $\mu \lesssim 1$ GeV and in any case remains valid in the limit $\alpha \rightarrow 0$ for larger masses. We therefore employ here this approximation, choosing for simplicity the fixed constraint

$$\sigma/\mu = 1 \text{ cm}^2/\text{g} = 4560 / \text{GeV}^3, \quad (8)$$

which appears compatible with all current observations. This implies

$$y^4 = \pi\mu^3\sigma/\mu \sim \pi(16.58\mu_1)^3, \quad (9)$$

$$y \sim 10.94\mu_1^{3/4} \quad (10)$$

with $\mu_1 \equiv \mu/1$ GeV. After this, the DM EOS depends only on the parameter μ .

This is demonstrated in Fig. 1, which compares the DM EOS with and without self interaction for four typical masses

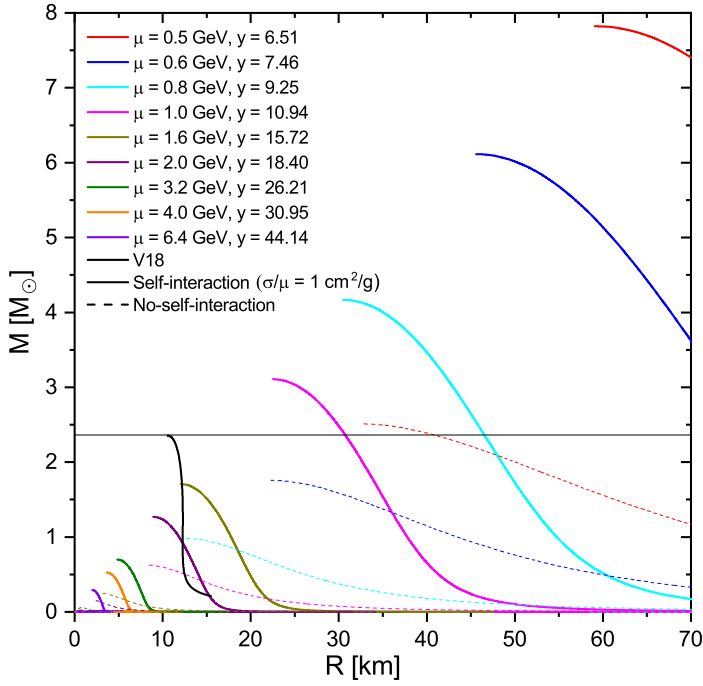


FIG. 2. Mass-radius relations of pure dark stars for different values of the DM particle mass μ , with (solid) and without (dashed) self-interaction, in comparison with the NM EOS V18 (solid black). The horizontal black line indicates the maximum mass of a pure NS, $M_{\max} = 2.36 M_\odot$.

$\mu = 0.5, 1, 2, 4 \text{ GeV}$, in comparison with the nucleonic EOS. Markers indicate the configurations of maximum stellar mass. It can be seen that the self-interaction is always important in the relevant density domains and stiffens substantially the EOS. The nucleonic EOS exhibits different trends for core, inner crust, and outer crust of a NS.

C. Hydrostatic configuration

The stable configurations of the DNSs are obtained from a two-fluid version of the TOV equations [34, 42, 43]:

$$\frac{dp_D}{dr} = -[p_D + \varepsilon_D] \frac{dv}{dr}, \quad (11)$$

$$\frac{dp_N}{dr} = -[p_N + \varepsilon_N] \frac{dv}{dr}, \quad (12)$$

$$\frac{dm}{dr} = 4\pi r^2 \varepsilon, \quad (13)$$

$$\frac{dv}{dr} = \frac{m + 4\pi r^3 p}{r(r - 2m)}, \quad (14)$$

where r is the radial coordinate from the center of the star, and $p = p_N + p_D$, $\varepsilon = \varepsilon_N + \varepsilon_D$, $m = m_N + m_D$ are the total pressure, energy density, and enclosed mass, respectively.

The total gravitational mass of the DNS is

$$M = m_N(R_N) + m_D(R_D), \quad (15)$$

where the stellar radii R_N and R_D are defined by the vanishing of the respective pressures. There are thus in general two scenarios: DM-core ($R_D < R_N$) or DM-halo ($R_D > R_N$) stars.

We first analyze the mass-radius relations of pure DSs in Fig. 2, comparing the results with and without self interaction for various values of μ . Consistent with the DM EOS, one notes that the self interaction is always very important and leads to stars with much larger masses and radii for the same μ . In this work we only employ values of $\mu \sim \mathcal{O}(1 \text{ GeV})$, such that the corresponding values of M_{\max} are of the same order as those of ordinary NSs, $\sim \mathcal{O}(1 M_\odot)$, for which the mass-radius relation of the nucleonic V18 EOS is shown for comparison. Otherwise the observable effects on NS structure will be very small [105]. We note that in [124] the following scaling relations for M_{\max} and the corresponding radius $R(M_{\max})$ were derived for $y \gg 1$,

$$M_{\max}/M_\odot = (0.627 + 0.269y)/\mu_1^2 \quad (16)$$

$$= (0.627 + 2.943\mu_1^{3/4})/\mu_1^2, \quad (17)$$

$$R(M_{\max})/\text{km} = (8.114 + 1.921y)/\mu_1^2, \quad (18)$$

$$= (8.114 + 21.01\mu_1^{3/4})/\mu_1^2, \quad (19)$$

which are reasonably well fulfilled for our range of μ and associated y , Eq. (10), given also in the figure.

After analyzing our models of pure NSs and pure DM stars, we now examine in detail the properties of DNSs within the two-fluid scenario, assuming that the two fluids interact only via gravity. The resulting scenario is very rich because the stellar configurations depend on the DM fraction $f = M_D/M$. The following Fig. 3 gives a detailed account of the possible mass-radius relations of DNSs (including DM self-interaction) with $\mu = 1 \text{ GeV}$ over the full range of DM fraction f . Both $M(R_N)$ and $M(R_D)$ relations, Eq. (15), are shown as solid or dotted curves, respectively.

The maximum gravitational mass is $2.36 M_\odot$ for the $f = 0$ pure NS (black solid curve) and $3.11 M_\odot$ for the $f = 1$ pure DS in this case (orange dotted curve), whereas intermediate mixed stars have lower M_{\max} . Those are plotted in intervals of f varying by 0.02. One can classify the stars as either DM-core or DM-halo, and for each fixed- f curve a marker denotes the transition $R_D = R_N$ between these configurations, if present. For example, for $f = 0.1$ all stars are DM-core, whereas for $f = 0.2$ there are two transitions at $(M, R) = (1.69 M_\odot, 10.64 \text{ km})$ and $(M, R) = (0.18 M_\odot, 15.69 \text{ km})$ from DM core to DM halo and back. Many (M, R_N) points are double- or triple-occupied, as for example the $f = 0.1, 0.9, 0.99994$ stars with a common $(M, R_N) = (1.11 M_\odot, 11.07 \text{ km})$. These multiple-occupied configurations, characterized by different f , belong to the class of the so-called “twin” stars, which differ substantially in their internal structure and DM radius, but would be indistinguishable by just mass and optical radius observations. A more detailed discussion can be found in [105].

Another interesting aspect are configurations of nearly pure NSs or DSs, with a very small fraction of the minority component. Those correspond to small amounts of minority matter trapped in a container majority star, and are characterized by

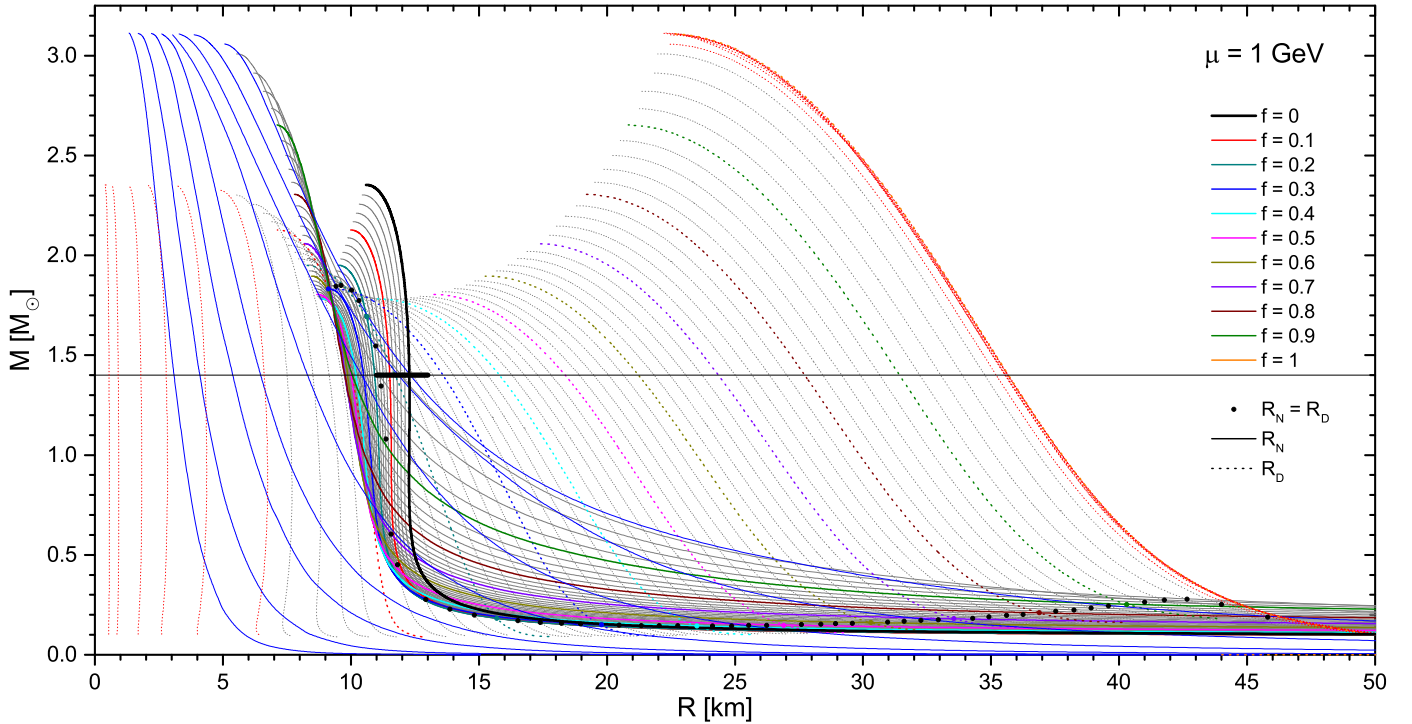


FIG. 3. Total gravitational mass M as function of nuclear (solid curves) or dark (dotted curves) radius for the $\mu = 1$ GeV model with different DM fractions $f = M_D/M$. Markers indicate $R_D = R_N$ configurations. The range of NS radii $R_{1.4} = 11\text{--}13$ km is represented by a horizontal bar on the $M = 1.4M_\odot$ line. The values of f are in intervals of 0.02, apart from those close to the boundaries: $f = 10^{-2,-3,\dots,-7}$ (thin dotted red curves) and $f = 1 - 10^{-2,-3,\dots,-9}$ (thin solid blue curves).

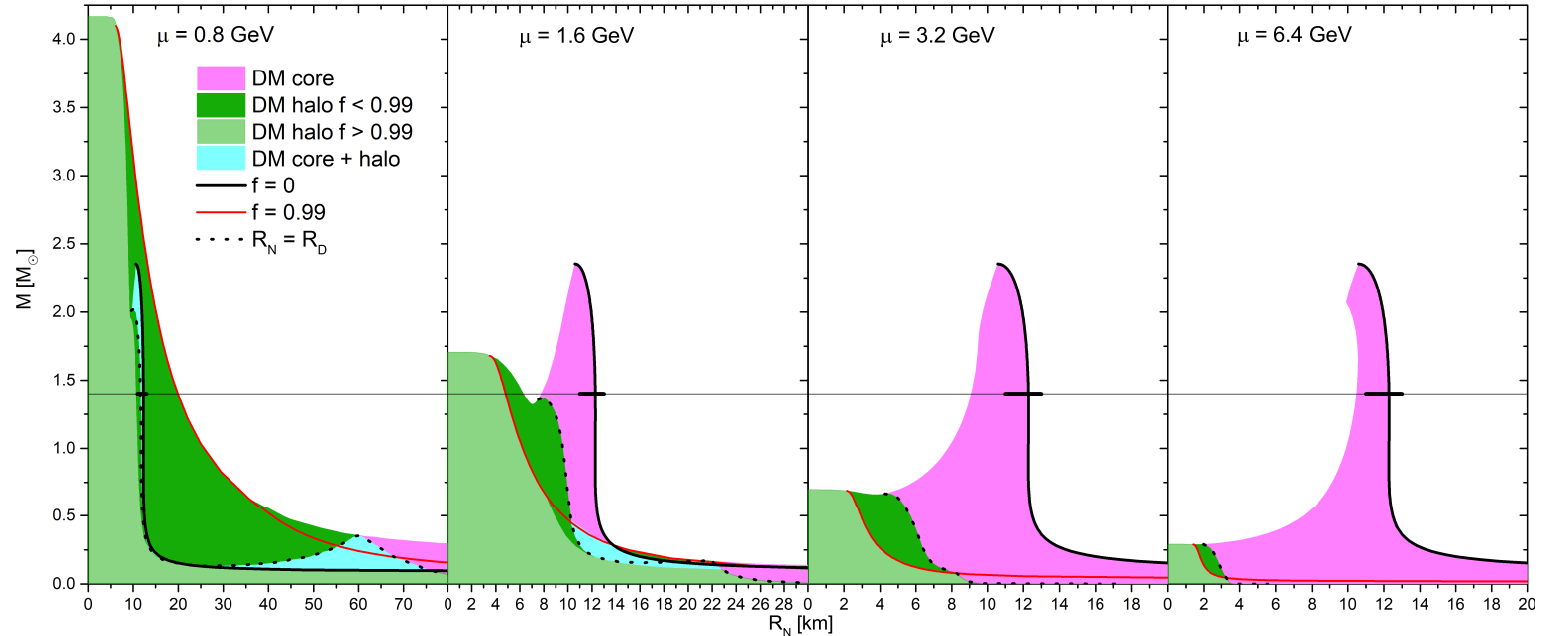


FIG. 4. The domains of stable DM-core (magenta shading), DM-halo (green), and both (cyan) DNSs in the (M, R_N) plane for different DM models. Note the different R_N axes. See extended discussion in the text.

small minority radii. Those are shown in the figure by thin solid blue curves ($f \rightarrow 1$) for DSs containing a small amount of pure NM, plotted in intervals of $f = 1 - 10^{-2,-3,\dots,-9}$, or thin dotted red ($f \rightarrow 0$) curves which correspond to pure NM configurations with a tiny amount of DM equal to $f =$

$10^{-2,-3,\dots,-7}$.

According to this discussion, one can prepare for a given μ a configuration plot in the (M, R_N) plane [64, 105], that shows all possible DM-core or DM-halo stars, corresponding to the domain covered by solid curves in Fig. 3, for example. This is

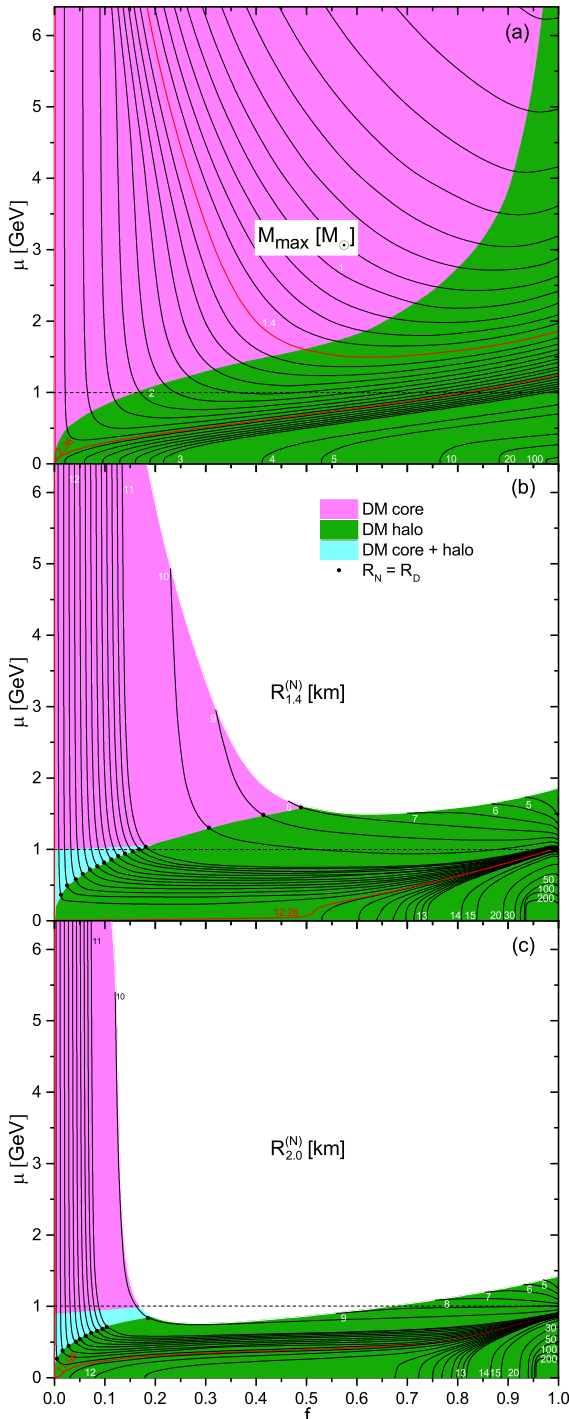


FIG. 5. Contour plots of (a) M_{\max} (thin contours are in intervals of $0.1 M_\odot$; 2.36 is the value for the pure NS) and (b,c) optical $R_{1.4}^{(N)}$ and $R_{2.0}^{(N)}$ (indicated by numbers in km; thin contours are in intervals of 0.1 km; 12.28 and 11.95 are the values for the pure NS), as functions of (f, μ) . The color scheme is as in Fig. 4. The horizontal dashed line at $\mu = 1$ GeV is to guide the eye.

done in Fig. 4 for $\mu = 0.8, 1.6, 3.2, 6.4$ GeV. According to the previous discussion, magenta domains contain only DM-core stars, delimited by the black solid curve ($f = 0$), whereas the green domains (dark green $f < 0.99$ and light green $f > 0.99$ for clarity) host only DM-halo stars. In the cyan domain both kind of configurations are present. One notes that for ‘large’

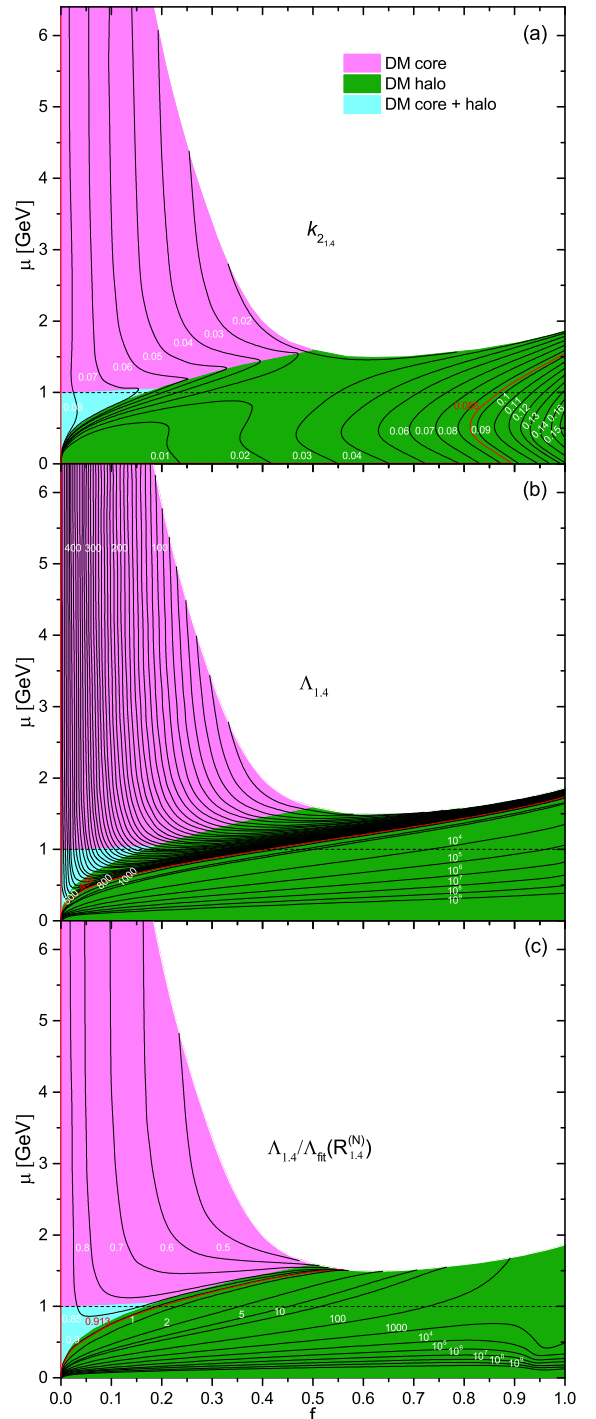


FIG. 6. Contour plots of (a) Love number $(k_2)_{1.4}$ (contours are in intervals of 0.01; 0.086 is the value for the pure NS), (b) tidal deformability $\Lambda_{1.4}$ (thin contours are in intervals of 10; 430 is the value for the pure NS), and (c) the ratio $\Lambda_{1.4}/\Lambda_{\text{fit}}(R_{1.4}^{(N)})$, Eq. (22), as functions of (f, μ) . The color scheme is as in Fig. 4. The horizontal dotted line at $\mu = 1$ GeV is to guide the eye. The observation of GW170817 was reported as $\Lambda_{1.4} = 70\text{--}580$ [121].

μ nearly all stellar configurations are DM core (magenta), and added DM causes always a reduction of radius and maximum DNS mass. However, these possible changes become smaller and smaller with increasing μ . With decreasing μ instead, DM halo configurations (green) become increasingly dominant. They feature a wide range of possible optical radii R_N

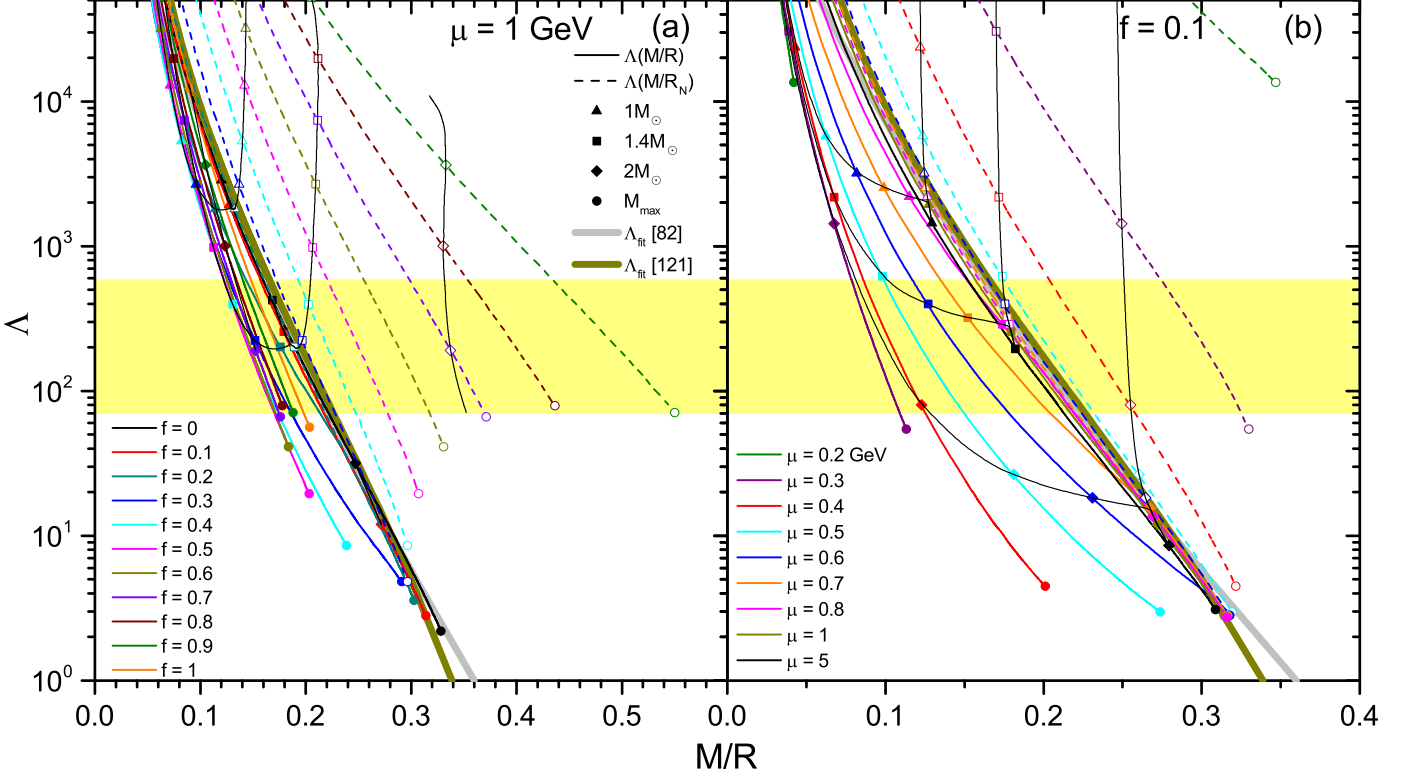


FIG. 7. Λ vs. M/R (dashed curves) and M/R_N (solid curves) for (a) $\mu = 1 \text{ GeV}$, varying f and (b) $f = 0.1$, varying μ . Configurations of fixed $M = 1, 1.4, 2M_\odot, M_{\max}$ are indicated by markers and joined by black lines. The universal relations for pure NSs of [82, 83] are shown as wide curves. The shaded band indicates the range 70–580 for $M = 1.4M_\odot$ (square markers) deduced from GW170817 [121].

from zero (for very diluted NM, $f \rightarrow 1$) to very large values $\gg R(f=0)$. Also the possible maximum mass becomes larger than the pure NS one for $\mu < 1.11 \text{ GeV}$, increasing with decreasing μ .

Therefore, the possible DNS configurations depend strongly on the DM particle mass μ , and this fact can be exploited to conversely deduce the values of μ and f from eventual DNS observations. This possibility will be examined in detail in the following.

III. RESULTS

A. Mass and radius

We begin in Fig. 5 with the most significant observables mass and radius, namely the maximum mass M_{\max} (a) and the optical radii $R_{1.4}^{(N)}$ (b) and $R_{2.0}^{(N)}$ (c) as contour plots of the two model parameters μ and f . According to the preceding discussion, and roughly dividing into the cases $\mu \gtrsim 1 \text{ GeV}$ and $\mu \lesssim 1 \text{ GeV}$, in the first case $M_{\max} < M_{\max}(f=0) = 2.36M_\odot$ (indicated by a red contour) for any f (mostly DM-core stars), whereas in the second case M_{\max} might reach very large values with increasing f (all DM-halo stars). The (red) $M = 1.4M_\odot$ contour identifies the maximum value of μ as a function of f , for which a $1.4M_\odot$ DNS is possible.

We examine the optical radius $R_{1.4}^{(N)}$ of such stars in panel

(b). Again dividing roughly into the two cases, for high masses $\mu \gtrsim 1 \text{ GeV}$ there are only DM-core stars, where the DM core pulls together also the nuclear matter, always reducing the radius with increasing f from the $f=0$ pure NS value 12.28 km. The maximum possible DM fraction f is limited in this regime by the condition that a stable $1.4M_\odot$ DNS can be formed.

On the other hand, most $\mu \lesssim 1 \text{ GeV}$ configurations are DM-halo, without upper limits on f , and for sufficiently large f also the optical radius is stretched out to large values by the surrounding DM halo. This concurs with very large M_{\max} in panel (a). These stars feature ‘low-density’ NM (described by the NS crust EOS in this work) embedded in a larger DM ‘container’ star. Similar as pointed out for Fig. 3, in this domain for a fixed μ two or three configurations with the same $R_{1.4}^{(N)}$ but different f (and different $R_{1.4}$) exist; therefore, only knowing μ and $R_{1.4}^{(N)}$, a unique classification of a DNS is not possible here.

Qualitatively similar results for $R_{2.0}^{(N)}$ are shown in panel (c). Naturally the parameter space is more restricted here due to the $M = 2M_\odot$ condition.

B. Tidal deformability

An observable closely related to the radius R is the tidal deformability (quadrupole polarizability) Λ , obtained from the

tidal Love number k_2 [131–135],

$$\Lambda = \frac{2}{3} \left(\frac{R}{M} \right)^5 k_2, \quad (20)$$

where R is the gravitational-mass radius, i.e., the outer DNS radius in our formalism. The relevant equations to compute k_2 in the two-fluid formalism can be found in [92–94, 102], for example.

In Fig. 6(a) we display $(k_2)_{1.4}(f, \mu)$ as a contour plot, just as $R_{1.4}^{(N)}$ in Fig. 5(b). One can see that for not very large values of f the effect of DM admixture is always a reduction of k_2 . Only for very dark stars with $f \gtrsim 0.8$ values of $k_2 > 0.086$ (the one of a pure NS) are reached again. However, k_2 is not directly observable, but the relevant quantity is the tidal deformability $\Lambda_{1.4}(f, \mu)$ shown in panel (b). Obviously, the dependence of $\Lambda_{1.4}$ on the fifth power of the radius $R_{1.4}$ then implies also a very strong dependence on (f, μ) that can clearly be seen in the figure. For DM-core configurations $\Lambda_{1.4}$ is reduced compared to the pure NS value 430 (red contour), as is the radius $R_{1.4} = R_{1.4}^{(N)}$ reported in Fig. 5(b), whereas for DM-halo configurations with large f and $R_{1.4} = R_{1.4}^{(D)}$, $\Lambda_{1.4}$ becomes enormous. Thus any non-tiny admixture of DM causes a substantial effect that we analyze as follows.

A universal relation between the tidal deformability and the compactness M/R of pure NSs was introduced in Ref. [80], and in Ref. [82, 123] the following fit was proposed

$$\frac{M}{R} = 0.36 - 0.0355 \ln \Lambda + 0.000705 (\ln \Lambda)^2, \quad (21)$$

or equivalently

$$\log \Lambda_{\text{fit}}(R) = 10.9 - 16.4 \sqrt{\frac{M}{R} + 0.087}, \quad (22)$$

which holds to within 7% for a large set of NS nucleonic EOSs [82]. Recently an equivalent but more sophisticated fit was derived in [83]. Substantial deviations from this fit formula therefore indicate ‘non-nucleonic’ compact stars, and we illustrate this by displaying in Fig. 6(c) the ratio $\Lambda_{1.4}/\Lambda_{\text{fit}}(R_{1.4}^{(N)})$ between the DNS value and the expected value of a pure NS with the same optical radius $R_{1.4}^{(N)}$ as the DNS.

In the $\mu \gtrsim 1$ GeV DM-core regime we have $R_{1.4}^{(N)} = R_{1.4}$ and therefore the reduction of $\Lambda_{1.4}$ simply reflects the moderate reduction of the radius in this domain, leading also to a moderate reduction of $\Lambda_{1.4}/\Lambda_{\text{fit}}(R_{1.4}^{(N)})$. However, in the $\mu \lesssim 1$ GeV DM-halo regime with $R_{1.4}^{(N)} \ll R_{1.4}$, apart from the very large values of $\Lambda_{1.4}$ due to the extended halo, the value of $\Lambda_{\text{fit}}(R_{1.4}^{(N)})$ is also too small and this amplifies the ratio $\Lambda_{1.4}/\Lambda_{\text{fit}}(R_{1.4}^{(N)})$.

even more, to increases of several orders of magnitude with $f \rightarrow 1$ but in particular $\mu \rightarrow 0$. Thus DNSs in this regime should exhibit very clear observational signatures by just analyzing their optical radius and tidal deformability, in the way just presented.

For a different illustration of this feature, we compare in Fig. 7 explicitly the universal relation $\Lambda_{\text{fit}}(M/R_N)$ with the actual DNS relations for either fixed $\mu = 1$ GeV (a) or fixed $f = 0.1$ (b), varying the other variable. The enormous enhancement of Λ relative to Λ_{fit} for DM-halo stars is evident in both cases, increasing with $f \rightarrow 1$ and $\mu \rightarrow 0$, respectively, as explained before. The results for the $M = 1.4M_\odot$ configurations (square markers) in the figure correspond to those analyzed before in Figs. 5 and 6, but the qualitative behavior is the same for any mass M (or compactness M/R). Equivalent results but limited to very small DM fractions were also obtained recently in [84, 85]. It is obvious that the GW170817 constraint $\Lambda_{1.4} = 70\text{--}580$ is compatible with a very wide range of parameters (μ, f) as can be seen more clearly in Fig. 6(a).

The figure in addition shows the relation between Λ and the true compactness M/R (dashed curves), should one be able to deduce the gravitational radius R observationally. In this case the actual values lie always below the fit formula due to the large difference between R and R_N in DM-halo stars. Thus also in this kind of analysis there would be a unique signature of DM in DNSs.

IV. SUMMARY

We have analyzed the properties of DNSs with substantial DM fraction, combining a well-constrained nucleonic EOS with a fermionic DM EOS respecting an important constraint on the self-interaction cross section. The analysis was focused on the most important and accessible observables: mass, radius, and tidal deformability. Already at this level, there are very pronounced observational features (violation of universal relations) that would clearly discern a DNS from a ‘standard’ NS, provided the DM fraction is not tiny. Registration of future GW events will allow to perform such analysis with good precision, allowing a search for DM in this way.

ACKNOWLEDGMENTS

This work is sponsored by the National Key R&D Program of China No. 2022YFA1602303 and the National Natural Science Foundation of China under Grant Nos. 11975077, 12147101, and 12205260.

-
- [1] F. Zwicky, *Gen. Relativ. Gravit.* **41**, 207 (2009).
 - [2] G. Bertone, D. Hooper, and J. Silk, *Phys. Rep.* **405**, 279 (2005).
 - [3] J. L. Feng, *Annu. Rev. Astron. Astrophys.* **48**, 495 (2010).
 - [4] V. Trimble, *Annu. Rev. Astron. Astrophys.* **25**, 425 (1987).
 - [5] L. Bergström, *Rep. Prog. Phys.* **63**, 793 (2000).

- [6] K. G. Begeman, A. H. Broeils, and R. H. Sanders, *Mon. Not. R. Astron. Soc.* **249**, 523 (1991).
- [7] E. Abdalla, L. R. Abramo, L. Sodré, and B. Wang, *Phys. Lett. B* **673**, 107 (2009).
- [8] E. Abdalla, L. R. Abramo, and J. C. C. de Souza, *Phys. Rev. D* **82**, 023508 (2010).
- [9] D. M. Wittman, J. A. Tyson, D. Kirkman, I. Dell’Antonio, and G. Bernstein, *Nature (London)* **405**, 143 (2000).
- [10] R. Massey, T. Kitching, and J. Richard, *Rep. Prog. Phys.* **73**, 086901 (2010).
- [11] A. B. Henriques, A. R. Liddle, and R. G. Moorhouse, *Nucl. Phys. B* **337**, 737 (1990).
- [12] P. Ciarcelluti and F. Sandin, *Phys. Lett. B* **695**, 19 (2011).
- [13] T. Güver, A. E. Erkoca, M. H. Reno, and I. Sarcevic, *J. Cosmol. Astropart. Phys.* **2014**, 013 (2014).
- [14] N. Raj, P. Tanedo, and H.-B. Yu, *Phys. Rev. D* **97**, 043006 (2018).
- [15] I. Goldman and S. Nussinov, *Phys. Rev. D* **40**, 3221 (1989).
- [16] S. Andreas, T. Hambye, and M. H. G. Tytgat, *J. Cosmol. Astropart. Phys.* **2008**, 034 (2008).
- [17] C. Kouvaris, *Phys. Rev. D* **77**, 023006 (2008).
- [18] C. Kouvaris, *Phys. Rev. Lett.* **108**, 191301 (2012).
- [19] S. A. Bhat and A. Paul, *Eur. Phys. J. C* **80**, 544 (2020).
- [20] D. Hooper and L.-T. Wang, *Phys. Rev. D* **69**, 035001 (2004).
- [21] G. Panopoulos and I. Lopes, *Phys. Rev. D* **96**, 083004 (2017).
- [22] A. Das, T. Malik, and A. C. Nayak, *Phys. Rev. D* **99**, 043016 (2019).
- [23] H. C. Das, A. Kumar, B. Kumar, S. K. Biswal, T. Nakatsukasa, A. Li, and S. K. Patra, *Mon. Not. R. Astron. Soc.* **495**, 4893 (2020).
- [24] H. C. Das, A. Kumar, and S. K. Patra, *Phys. Rev. D* **104**, 063028 (2021).
- [25] H. C. Das, A. Kumar, and S. K. Patra, *Mon. Not. R. Astron. Soc.* **507**, 4053 (2021).
- [26] H. C. Das, A. Kumar, B. Kumar, and S. K. Patra, *Galaxies* **10**, 14 (2022).
- [27] A. Kumar, H. C. Das, and S. K. Patra, *Mon. Not. R. Astron. Soc.* **513**, 1820 (2022).
- [28] O. Lourenço, C. H. Lenzi, T. Frederico, and M. Dutra, *Phys. Rev. D* **106**, 043010 (2022).
- [29] C. Kouvaris and P. Tinyakov, *Phys. Rev. D* **83**, 083512 (2011).
- [30] S. D. McDermott, H.-B. Yu, and K. M. Zurek, *Phys. Rev. D* **85**, 023519 (2012).
- [31] M. I. Gresham and K. M. Zurek, *Phys. Rev. D* **99**, 083008 (2019).
- [32] O. Ivanytskyi, V. Sagun, and I. Lopes, *Phys. Rev. D* **102**, 063028 (2020).
- [33] L. B. Okun’, *Physics Uspekhi* **50**, 380 (2007).
- [34] F. Sandin and P. Ciarcelluti, *Astropart. Phys.* **32**, 278 (2009).
- [35] M. Hippert, J. Setford, H. Tan, D. Curtin, J. Noronha-Hostler, and N. Yunes, *Phys. Rev. D* **106**, 035025 (2022).
- [36] L. D. Duffy and K. van Bibber, *New. J. Phys.* **11**, 105008 (2009).
- [37] A. V. Balatsky, B. Fraser, and H. S. Røising, *Phys. Rev. D* **105**, 023504 (2022).
- [38] D. M. Jacobs, G. D. Starkman, and B. W. Lynn, *Mon. Not. R. Astron. Soc.* **450**, 3418 (2015).
- [39] S. Ge, K. Lawson, and A. Zhitnitsky, *Phys. Rev. D* **99**, 116017 (2019).
- [40] J. P. VanDevender *et al.*, *Universe* **7**, 116 (2021).
- [41] A. Zhitnitsky, *Mod. Phys. Lett. A* **36**, 2130017 (2021).
- [42] T. Kodama and M. Yamada, *Prog. Theor. Phys.* **47**, 444 (1972).
- [43] G. L. Comer, D. Langlois, and L. M. Lin, *Phys. Rev. D* **60**, 104025 (1999).
- [44] C. Kouvaris and P. Tinyakov, *Phys. Rev. D* **82**, 063531 (2010).
- [45] J. Bramante and F. Elahi, *Phys. Rev. D* **91**, 115001 (2015).
- [46] M. Baryakhtar, J. Bramante, S. W. Li, T. Linden, and N. Raj, *Phys. Rev. Lett.* **119**, 131801 (2017).
- [47] M. Deliyergiyev, A. Del Popolo, L. Tolos, M. Le Delliou, X. Lee, and F. Burgio, *Phys. Rev. D* **99**, 063015 (2019).
- [48] I. Goldman, R. N. Mohapatra, S. Nussinov, D. Rosenbaum, and V. Teplitz, *Phys. Lett. B* **725**, 200 (2013).
- [49] C. Kouvaris and N. G. Nielsen, *Phys. Rev. D* **92**, 063526 (2015).
- [50] J. Eby, C. Kouvaris, N. G. Nielsen, and L. C. R. Wijewardhana, *J. High Energy Phys.* **2016**, 28 (2016).
- [51] A. Maselli, P. Pnigouras, N. G. Nielsen, C. Kouvaris, and K. D. Kokkotas, *Phys. Rev. D* **96**, 023005 (2017).
- [52] J. Ellis *et al.*, *Phys. Rev. D* **97**, 123007 (2018).
- [53] A. E. Nelson, S. Reddy, and D. Zhou, *J. Cosmol. Astropart. Phys.* **2019**, 012 (2019).
- [54] F. Di Giovanni, S. Fakhry, N. Sanchis-Gual, J. C. Degollado, and J. A. Font, *Phys. Rev. D* **102**, 084063 (2020).
- [55] M. Colpi, S. L. Shapiro, and I. Wasserman, *Phys. Rev. Lett.* **57**, 2485 (1986).
- [56] F. E. Schunck and E. W. Mielke, *Class. Quantum Grav.* **20**, R301 (2003).
- [57] S. L. Liebling and C. Palenzuela, *Living Rev. Rel.* **15**, 6 (2012).
- [58] S.-C. Leung, M.-C. Chu, and L.-M. Lin, *Phys. Rev. D* **84**, 107301 (2011).
- [59] A. Li, F. Huang, and R.-X. Xu, *Astropart. Phys.* **37**, 70 (2012).
- [60] L. Tolos and J. Schaffner-Bielich, *Phys. Rev. D* **92**, 123002 (2015).
- [61] A. Del Popolo, M. Deliyergiyev, and M. Le Delliou, *Phys. Dark Universe* **30**, 100622 (2020).
- [62] H. Das, A. Kumar, B. Kumar, S. Biswal, and S. Patra, *J. Cosmol. Astropart. Phys.* **2021**, 007 (2021).
- [63] S.-H. Yang, C.-M. Pi, and X.-P. Zheng, *Phys. Rev. D* **104**, 083016 (2021).
- [64] B. Kain, *Phys. Rev. D* **103**, 043009 (2021).
- [65] I. Lopes, J. Casanellas, and D. Eugénio, *Phys. Rev. D* **83**, 063521 (2011).
- [66] A. Del Popolo, M. Le Delliou, and M. Deliyergiyev, *Universe* **6** (2020).
- [67] N. F. Bell, G. Busoni, T. F. Motta, S. Robles, A. W. Thomas, and M. Virgato, *Phys. Rev. Lett.* **127**, 111803 (2021).
- [68] T. N. Maity and F. S. Queiroz, *Phys. Rev. D* **104**, 083019 (2021).
- [69] F. Anzuini, N. F. Bell, G. Busoni, T. F. Motta, S. Robles, A. W. Thomas, and M. Virgato, *J. Cosmol. Astropart. Phys.* **2021**, 056 (2021).
- [70] D. Bose, T. N. Maity, and T. S. Ray, *J. Cosmol. Astropart. Phys.* **2022**, 001 (2022).
- [71] D. Gonzalez and A. Reisenegger, *A&A* **522**, A16 (2010).
- [72] B. Bertoni, A. E. Nelson, and S. Reddy, *Phys. Rev. D* **88**, 123505 (2013).
- [73] R. Garani, A. Gupta, and N. Raj, *Phys. Rev. D* **103**, 043019 (2021).
- [74] J. Coffey, D. McKeen, D. E. Morrissey, and N. Raj, *Phys. Rev. D* **106**, 115019 (2022).
- [75] M. Fujiwara, K. Hamaguchi, N. Nagata, and J. Zheng, *Phys. Rev. D* **106**, 055031 (2022).
- [76] A. de Lavallaz and M. Fairbairn, *Phys. Rev. D* **81**, 123521 (2010).

- [77] J. Bramante, K. Fukushima, and J. Kumar, *Phys. Rev. D* **87**, 055012 (2013).
- [78] J. Bramante and T. Linden, *Phys. Rev. Lett.* **113**, 191301 (2014).
- [79] D. Liang and L. Shao, *JCAP* **2023**, 016 (2023).
- [80] K. Yagi and N. Yunes, *Phys. Rev. D* **88**, 023009 (2013).
- [81] K. Yagi and N. Yunes, *Science* **341**, 365 (2013).
- [82] K. Yagi and N. Yunes, *Phys. Rep.* **681**, 1 (2017).
- [83] D. A. Godzieba, R. Gamba, D. Radice, and S. Bernuzzi, *Phys. Rev. D* **103**, 063036 (2021).
- [84] P. Routaray, A. Quddus, K. Chakravarti, and B. Kumar, *MNRAS* **525**, 5492 (2023).
- [85] P. Thakur, T. Malik, A. Das, T. K. Jha, and C. Providência, *Phys. Rev. D* **109**, 043030 (2024).
- [86] K. Zhang, G.-Z. Huang, J.-S. Tsao, and F.-L. Lin, *Eur. Phys. J. C* **82**, 366 (2020).
- [87] K. Zhang, G.-Z. Huang, J.-S. Tsao, and F.-L. Lin, *EPJC* **82**, 366 (2022).
- [88] B. P. Abbott *et al.* (LIGO Scientific Collaboration and Virgo Collaboration), *Phys. Rev. Lett.* **119**, 161101 (2017).
- [89] B. P. Abbott *et al.*, *Astrophys. J. Lett.* **892**, L3 (2020).
- [90] A. Quddus *et al.*, *J. Phys. G: Nucl. Part. Phys.* **47**, 095202 (2020).
- [91] W. Husain and A. W. Thomas, *J. Cosmol. Astropart. Phys.* **2021**, 086 (2021).
- [92] K.-L. Leung, M.-C. Chu, and L.-M. Lin, *Phys. Rev. D* **105**, 123010 (2022).
- [93] D. Rafiei Karkevandi, S. Shakeri, V. Sagun, and O. Ivanytskyi, *Phys. Rev. D* **105**, 023001 (2022).
- [94] Y. Dengler *et al.*, *Phys. Rev. D* **105**, 043013 (2022).
- [95] M. Collier, D. Croon, and R. K. Leane, *Phys. Rev. D* **106**, 123027 (2022).
- [96] M. Dutra, C. H. Lenzi, and O. Lourenço, *Mon. Not. R. Astron. Soc.* **517**, 4265 (2022).
- [97] R. F. Diedrichs, N. Becker, C. Jockel, J.-E. Christian, L. Sagunski, and J. Schaffner-Bielich, *Phys. Rev. D* **108**, 064009 (2023).
- [98] D. Rafiei Karkevandi, S. Shakeri, V. Sagun, and O. Ivanytskyi, in *The Sixteenth Marcel Grossmann Meeting* (WORLD SCIENTIFIC, 2023).
- [99] H. C. Das, A. Kumar, S. K. Biswal, and S. K. Patra, *Phys. Rev. D* **104**, 123006 (2021).
- [100] M. Emma, F. Schianchi, F. Pannarale, V. Sagun, and T. Dietrich, *Particles* **5**, 273 (2022).
- [101] A. Bauswein, G. Guo, J. Lien-Hua, Y.-H. Lin, and M.-R. Wu, *Phys. Rev. D* **107**, 083002 (2023).
- [102] K. Zhang, L.-W. Luo, J.-S. Tsao, C.-S. Chen, and F.-L. Lin, *Results in Physics* **53**, 106967 (2023).
- [103] Z. Miao, Y. Zhu, A. Li, and F. Huang, *Astrophys. J.* **936**, 69 (2022).
- [104] S. Shakeri and D. R. Karkevandi, *Phys. Rev. D* **109**, 043029 (2024).
- [105] H.-M. Liu, J.-B. Wei, Z.-H. Li, G. F. Burgio, and H. J. Schulze, *Physics of the Dark Universe* **42**, 101338 (2023).
- [106] Z. H. Li, U. Lombardo, H.-J. Schulze, and W. Zuo, *Phys. Rev. C* **77**, 034316 (2008).
- [107] Z. H. Li and H.-J. Schulze, *Phys. Rev. C* **78**, 028801 (2008).
- [108] H.-M. Liu, J. Zhang, Z.-H. Li, J.-B. Wei, G. F. Burgio, and H. J. Schulze, *Phys. Rev. C* **106**, 025801 (2022).
- [109] M. Baldo, ed., *Nuclear Methods and The Nuclear Equation of State* (World Scientific, Singapore, 1999).
- [110] M. Baldo and G. F. Burgio, *Rep. Prog. Phys.* **75**, 026301 (2012).
- [111] J.-B. Wei, J.-J. Lu, G. F. Burgio, Z.-H. Li, and H.-J. Schulze, *Eur. Phys. J. A* **56**, 63 (2020).
- [112] G. F. Burgio, H.-J. Schulze, I. Vidaña, and J.-B. Wei, *Prog. Part. Nucl. Phys.* **120**, 103879 (2021).
- [113] G. F. Burgio, H.-J. Schulze, I. Vidaña, and J.-B. Wei, *Symmetry* **13**, 400 (2021).
- [114] J. Antoniadis *et al.*, *Science* **340**, 1233232 (2013).
- [115] Z. Arzoumanian *et al.*, *Astrophys. J., Suppl. Ser.* **235**, 37 (2018).
- [116] H. T. C. *et al.*, *Nature Astronomy* **4**, 72 (2020).
- [117] T. E. Riley *et al.*, *Astrophys. J. Lett.* **918**, L27 (2021).
- [118] M. C. Miller *et al.*, *Astrophys. J. Lett.* **918**, L28 (2021).
- [119] P. T. H. Pang, I. Tews, M. W. Coughlin, M. Bulla, C. Van Den Broeck, and T. Dietrich, *Astrophys. J.* **922**, 14 (2021).
- [120] G. Raaijmakers *et al.*, *Astrophys. J. Lett.* **918**, L29 (2021).
- [121] B. P. Abbott *et al.*, *Phys. Rev. Lett.* **121**, 161101 (2018).
- [122] G. F. Burgio, A. Drago, G. Pagliara, H.-J. Schulze, and J.-B. Wei, *Astrophys. J.* **860**, 139 (2018).
- [123] J.-B. Wei, A. Figura, G. F. Burgio, H. Chen, and H.-J. Schulze, *J. Phys. G: Nucl. Part. Phys.* **46**, 034001 (2019).
- [124] G. Narain, J. Schaffner-Bielich, and I. N. Mishustin, *Phys. Rev. D* **74**, 063003 (2006).
- [125] S. Tulin, H.-B. Yu, and K. M. Zurek, *Phys. Rev. D* **87**, 115007 (2013).
- [126] M. Cassing, A. Brisebois, M. Azeem, and J. Schaffner-Bielich, *Astrophys. J.* **944**, 130 (2023).
- [127] M. Markevitch, A. H. Gonzalez, D. Clowe, A. Vikhlinin, W. Forman, C. Jones, S. Murray, and W. Tucker, *Astrophys. J.* **606**, 819 (2004).
- [128] M. Kaplinghat, S. Tulin, and H.-B. Yu, *Phys. Rev. Lett.* **116**, 041302 (2016).
- [129] L. Sagunski, S. Gad-Nasr, B. Colquhoun, A. Robertson, and S. Tulin, *J. Cosmol. Astropart. Phys.* **2021**, 024 (2021).
- [130] A. Loeb, *Astrophys. J. Lett.* **929**, L24 (2022).
- [131] J. B. Hartle, *Astrophys. J.* **150**, 1005 (1967).
- [132] T. Binnington and E. Poisson, *Phys. Rev. D* **80**, 084018 (2009).
- [133] T. Hinderer, B. D. Lackey, R. N. Lang, and J. S. Read, *Phys. Rev. D* **81**, 123016 (2010).
- [134] T. Damour and A. Nagar, *Phys. Rev. D* **81**, 084016 (2010).
- [135] S. Postnikov, M. Prakash, and J. M. Lattimer, *Phys. Rev. D* **82**, 024016 (2010).

Tidal deformability as a probe of dark matter in neutron stars

D. Rafiei Karkevandi

*ICRANet-Isfahan, Isfahan University of Technology,
Isfahan, 84156-83111, Iran
E-mail: davood.rafiei64@gmail.com*

S. Shakeri

*Department of Physics, Isfahan University of Technology,
ICRANet-Isfahan, Isfahan University of Technology,
Isfahan, 84156-83111, Iran
E-mail: s.shakeri@iut.ac.ir*

V. Sagun

*CFisUC, Department of Physics, University of Coimbra,
Coimbra, 3004-516, Portugal
E-mail: violetta.sagun@uc.pt*

O. Ivanytskyi

*Institute of Theoretical Physics, University of Wroclaw,
Wroclaw, 50-204, Poland
E-mail: oleksii.ivanytskyi@uwr.edu.pl*

The concept of boson stars (BSs) was first introduced by Kaup and Ruffini and Bonazzola in the 1960s. Following this idea, we investigate an effect of self-interacting asymmetric bosonic dark matter (DM) according to Colpi et al. model for BSs (1986) on different observable properties of neutron stars (NSs). In this paper, the bosonic DM and baryonic matter (BM) are mixed together and interact only through gravitational force. The presence of DM as a core of a compact star or as an extended halo around it is examined by applying different boson masses and DM fractions for a fixed coupling constant. The impact of DM core/halo formations on a DM admixed NS properties is probed through the maximum mass and tidal deformability of NSs. Thanks to the recent detection of Gravitational-Waves (GWs) and the latest X-ray observations, the DM admixed NS's features are compared to LIGO/Virgo and NICER results.

Keywords: Bosonic Dark matter, Complex scalar field, Neutron Star, Gravitational-Wave

1. Introduction

The evidence for the existence of dark matter (DM) which constitutes up to 85% of the matter in the universe, is implied from various astrophysical and cosmological observations. However, despite the enormous experimental efforts in the past decades, the nature of these particles remains elusive. In addition to various terrestrial experiments, compact astrophysical objects such as neutron stars (NSs) can be served as valuable natural detectors to constrain the properties of DM. The presence

of DM in NS interior depending on the various hypothesis of introducing them and their features, could have significant effects on the properties of NSs.^{1–8}

There are different scenarios assuming existence of DM in the NS interiors, which are mostly based on the DM accumulation during different stages of stellar evolution. The main of these stages are : a) progenitor, b) main sequence star, c) supernova explosion with formation of a proto-NS, and d) equilibrated NS.^{4,9–13} As an alternative way, DM can be produced during the supernova explosion or NS merger leading to presence of DM in the NSs.^{2,3} High level of DM fraction inside NS is reachable through other mechanisms such as (i) dark compact objects or DM clumps as the accretion center of baryonic matter (BM),^{3,14,15} (ii) DM captured by NS in a binary system including Dark star and Dark star–NS merger,^{7,15,16} (iii) NS can pass through a region in the Galaxy with extremely high DM density leading to accumulation of vast amount of DM.^{16–19}

Two main and qualitatively different pictures leading to potentially observable impact of DM on the NS properties are a) Self-annihilating DM affecting luminosity, effective temperature and cooling process of NSs^{20–25} and b) Asymmetric DM (ADM) with negligible annihilation rate caused by particle-antiparticle asymmetry in the dark sector.^{26–29} We consider the second possibility allowing stable and massive DM particles to reside in a core of the NS. It was pointed out that the presence of DM particles in stellar cores can significantly decrease the mass of a compact object.^{18,19,30,31} However, it was shown that light DM particles form an extended halo around the NS and can increase its gravitational mass.^{2,4} It is worth mentioning that both of the aforementioned cases for combination of DM and BM within NS are known as DM admixed NS.

Regarding the ADM model, generally two methods have been utilized so far to extract the properties of the DM admixed NS from the Tolman-Oppenheimer-Volkof (TOV) equations.^{32,33} 1) Single fluid formalism, for which an Equation of State (EoS) is considered for the whole star by inserting DM-BM interactions.^{1,7,34–37} 2) Two-fluid formalism, for which DM and BM interact only through gravitational force, and two individual EoSs have to be considered for the DM and BM fluids.^{15,16,38–41}

In this research, we apply a two-fluid formalism for the DM admixed NS. Bosonic DM is described by a complex scalar field with repulsive self-interaction. Historically, this model has been applied to describe hypothetical self-gravitating objects composed of bosons, so called boson stars. The idea of BS was first proposed by Kaup⁴² and Ruffini-Bonazzola⁴³ for non-interacting bosons. The Heisenberg uncertainty principle was the only source of pressure of the BS matter resisting gravitational contraction. This leads to much lower maximum mass of BS compared to the Chandrasekhar mass. The pressure of the BS matter was significantly increased by introducing repulsive self-interaction proposed by Colpi et al.⁴⁴ Within this approach, stellar mass objects are supported by the DM particle mass about hundreds MeV and dimensionless coupling constant is of order of unity (see a comprehensive

review on BSs in^{45–47}). Another component, i.e. BM, is modeled by the induced surface tension (IST) EoS. It was successfully applied to describe the nuclear matter, heavy-ion collision data and dense matter existing inside NS.^{48–50}

With this set up we study effects of self-repulsive bosonic ADM on the mass-radius (M-R) profile and tidal deformability parameter^{2,3,13,36,37,51–54} inferred from the GW signals related to post-merger stages of NSs.^{55–59} Such a combined analysis based on the recent LIGO/Virgo results^{60,60,61,61} opens a new possibility to study the internal structure of compact objects which may contain DM.

To be specific, in this work we consider a model of Colpi et al.⁴⁴ with sub-GeV DM particles of mass $m_\chi \sim \mathcal{O}(100 \text{ MeV})$ and self-coupling constant $\lambda = \pi$. We analyze two key observational constraints of NSs, i.e. maximum mass and tidal deformability. The first of them is based on the NICER observation of the heaviest known pulsar PSR J0740+6620 with mass $2.072^{+0.067}_{-0.066} M_\odot$ ⁶² and corresponds to requiring the maximal stellar mass to be at least $M_{max} = 2M_\odot$. The merger event GW170817⁶³ leads to the second constraint on the dimensionless tidal deformability $\Lambda \leq 580$ for $M = 1.4M_\odot$.⁶⁴ Using these constraints we probe DM admixed NSs at various masses and fractions of DM.

The rest of the paper is organized as follows. In Sec. 2 the DM and BM EoSs are described. In Sec. 3 we explain the two-fluid TOV formalism, DM halo and DM core formations and their impacts on mass-radius profile of DM admixed NSs. Sec. 4 is devoted to probing the effect of DM halo/core configurations on the tidal deformability. Our conclusions will be presented in Sec. 5. We use units in which $\hbar = c = G = 1$.

2. Bosonic DM and BM models

2.1. Dark Boson Star

In the following we apply a model of complex scalar field as the bosonic DM with repulsive self-interaction potential, $V(\phi) = \frac{\lambda}{4}|\phi|^4$, minimally coupled to gravity and described by the action

$$S = \int d^4x \sqrt{-g} \left[\frac{M_{Pl}^2}{2} R - \frac{1}{2} \partial_\mu \phi \partial^\mu \phi^* - \frac{1}{2} m_\chi^2 |\phi|^2 - \frac{1}{4} \lambda |\phi|^4 \right], \quad (1)$$

where m_χ is the boson mass, λ stands for the dimensionless coupling constant and M_{Pl} corresponds to the Planck mass.^{44,65} In this setup a coherent scalar field is governed by both Klein-Gordon and Einstein equations which can potentially form Bose-Einstein Condensate (BEC) if the temperature is sufficiently low.^{66,67} It has been assumed a spherically symmetric configuration for the scalar field $\phi(r, t) = \Phi(r)e^{i\omega t}$ and a static metric to rewrite Klein-Gordon-Einstein (K.G.E) equations to a set of ordinary differential equations.⁴⁴ This leads to the following EoS describing

a self-interacting and self-gravitating bosonic system so-called BS

$$P = \frac{m_\chi^4}{9\lambda} \left(\sqrt{1 + \frac{3\lambda}{m_\chi^4}} \rho - 1 \right)^2. \quad (2)$$

We recently presented an alternative derivation of this EoS in locally flat space-time by using the mean-field approximation (see appendix of⁶⁸). This equation is valid in the parameter region for λ as

$$\lambda \gg 4\pi(m_\chi/M_{Pl})^2 = 8.43 \times 10^{-36} \left(\frac{m_\chi}{100 \text{ MeV}} \right)^2 \quad (3)$$

In this limit which is called strong coupling regime, the system can be approximated as a perfect fluid and the anisotropy of pressure will be ignored.^{45, 69, 70} Stellar mass BSs can be formed for $\lambda \sim \mathcal{O}(1)$ and $m_\chi \sim \mathcal{O}(100 \text{ MeV})$,^{45, 71} in this section, we focus on this range of model parameters.

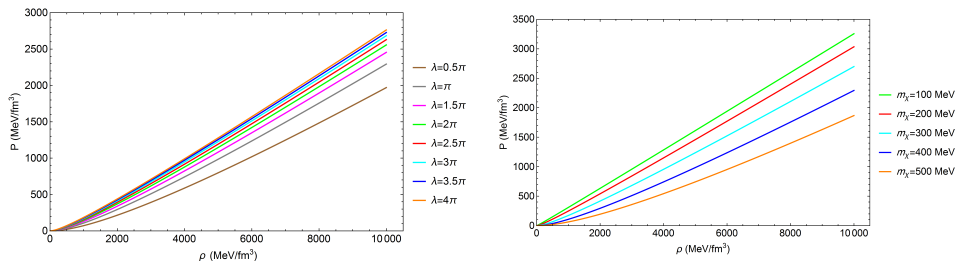


Fig. 1. Pressure as a function of density for bosonic matter obtained for $\lambda = \pi$ and various DM masses as labeled (right); for $m_\chi = 400$ MeV and different values of coupling constant (left).

Fig. 1 shows pressure of bosonic matter as a function of density for different masses and coupling constants as labeled. As it is shown in Fig. 1, (right panel) the pressure decreases with increasing of boson masses and (left panel) the pressure rises with the enhancement of the coupling constant or equivalently increasing the repulsive force between bosons.

In different density limits one can approximate Eq. (2) in a typical polytrope form $P = K\rho^\gamma$, where polytropic index at low density $\gamma \approx 2$ and it smoothly reaches to $\gamma \approx 1$ at high density. At low density regime, the bosonic DM EoS, Eq. (2), is reduced to

$$P \approx \frac{\lambda}{4m_\chi^4} \rho^2. \quad (4)$$

However, for high density regime or correspondingly for very light bosons or high coupling constant, Eq. (2) reaches to radiation EoS with $P \approx \rho/3$. Similar equation to Eq. (4) has been obtained so far for a dilute self-interacting boson gas in a self-gravitating system (BS) known as Gross-Pitaevskii-Poisson (G.P.P) equation.^{70, 72, 73} In fact, the G.P.P equation describes the BEC phase in a dilute

gas where only two-body mean field interaction is considered near zero temperature.^{74–76}

In Fig. 2, we present the M-R diagrams of BSs obtained by solving TOV equation for Eq. (2). As it is indicated in the right panel, by decreasing the boson mass, the maximum gravitational mass of BSs increases and even goes above $2M_{\odot}$ ^{62,77,78} and the corresponding radius goes well above typical NS radius. In the left panel, it is shown that higher self-coupling constant at fixed mass $m_{\chi} = 400$ MeV leads to higher maximum masses of BSs. Both the decreasing of boson mass and increasing of the coupling constant cause an enhancement in pressure of the system and consequently the rise of the maximum mass.

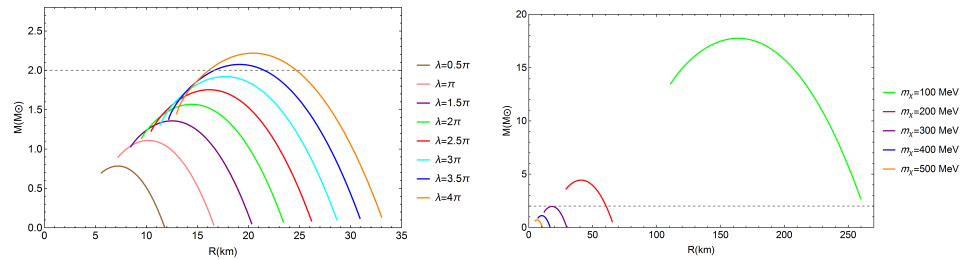


Fig. 2. M-R profile for BSs based on Eq. (2), (right panel) for the fixed value of coupling constant $\lambda = \pi$ and different boson masses. (Left panel) Calculations are made for fixed boson mass $m_{\chi} = 400$ MeV and different values of coupling constant as labeled at the figure. The gray dashed line shows the $2M_{\odot}$ limit.

Moreover, the variation of compactness $\mathcal{C} = M/R$ with respect to mass of BSs for different values of m_{χ} and λ is presented in Fig. 3. It shows the same dimensionless maximum compactness $\mathcal{C}_{(max)} \simeq 0.16$ for all cases. We see that the maximum compactness of a BS based on Eq. (2) is independent of free parameters of the model, namely m_{χ} and λ and for all the parameter space is well below the black hole formation limit $\mathcal{C} = 0.5$.^{46,79}

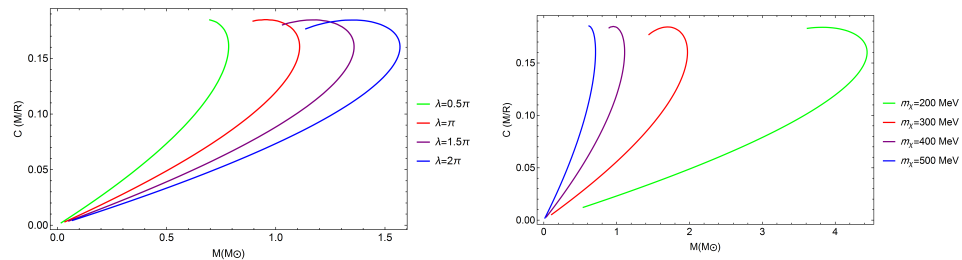


Fig. 3. Compactness of BSs as a function of their mass obtained for a fixed coupling constant $\lambda = \pi$ and different values of boson mass (right); fixed particle's mass $m_{\chi} = 400$ MeV and various λ values (left).

2.2. Neutron Star

For the baryon component (NS matter), we use the unified EoS with induced surface tension (IST) where both the short-range repulsion and long-range attraction between baryons have been taken into account.^{49,50} The IST EoS reproduces the nuclear matter properties,⁸⁰ fulfills the proton flow constraint,⁸¹ provides a high-quality description of hadron multiplicities created during the nuclear-nuclear collision experiments⁸² as well as the matter inside compact stars.^{48–50} The EoS is in a very good agreement with latest NS observations providing the maximum mass $M_{max} = 2.08M_\odot$ and radius of the $1.4M_\odot$ star equals to $R_{1.4} = 11.37$ km.⁸³ In our work the crust part of the NS's EoS is described via the polytropic EoS with $\gamma = 4/3$.⁴ In Fig. 4, the change of pressure for a same density regime is plotted for BM and DM EoSs (left panel) and we show the M-R profiles of the NS and BS based on our considered EoSs (right panel).

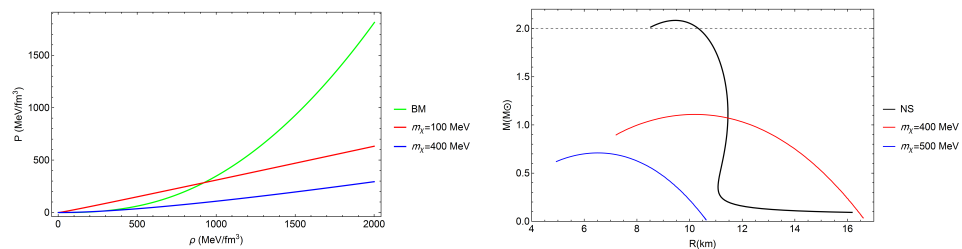


Fig. 4. Comparing BM and DM EoSs, left panel shows pressure vs. energy density for two different values of boson mass and $\lambda = \pi$. Right panel indicates M-R profiles for the NSs and BSs, considering $m_\chi = 400, 500$ MeV and the same coupling constant.

3. Two-fluid TOV equations and maximum mass

In order to study compact objects formed by the admixture of BM and DM that interact only through gravity, we use two-fluid TOV formalism^{15,16} shown by Eqs. (5-6). Here $p = p_B + p_D$ and $M = M_T = \int_0^r 4\pi r^2 \epsilon_B(r) dr + \int_0^r 4\pi r^2 \epsilon_D(r) dr$. It can be seen that the total pressure and mass of the object have two contributions from BM and DM fluids shown by B and D indices. In order to solve two-fluid TOV equations

$$\frac{dp_B}{dr} = -(p_B + \epsilon_B) \frac{M + 4\pi r^3 p}{r(r - 2M)}, \quad (5)$$

$$\frac{dp_D}{dr} = -(p_D + \epsilon_D) \frac{M + 4\pi r^3 p}{r(r - 2M)}, \quad (6)$$

two central conditions related to both of the fluids have to be considered. By fixing two central pressures (p_B and p_D) together with the initial conditions at the center

of the star ($M_B(r \simeq 0) = M_D(r \simeq 0) \simeq 0$) the Eqs. (5-6) are numerically integrated up to the radius at which the pressure of one of the components vanishes. In principle this radius can be realized as DM radius R_D or BM radius R_B . In the former case the DM distributed only inside the core while BM extends to larger radius ($R_B > R_D$), then we set $p_D(r > R_D) = 0$ and continue the numerical integration to reach the visible radius of the star where $p_B(R_B) = 0$. When we have a BM core, DM can exist as an extended halo around the core with $R_D > R_B$, where $p_B(r > R_B) = 0$. It should be mentioned that for both DM core and DM halo cases, the core of the object is a mixture of DM and BM. Based on our extensive analysis there is another possibility of DM admixed NSs' configurations for which $R_B \approx R_D$ and DM distributed within the entire NS (see Fig. 5).

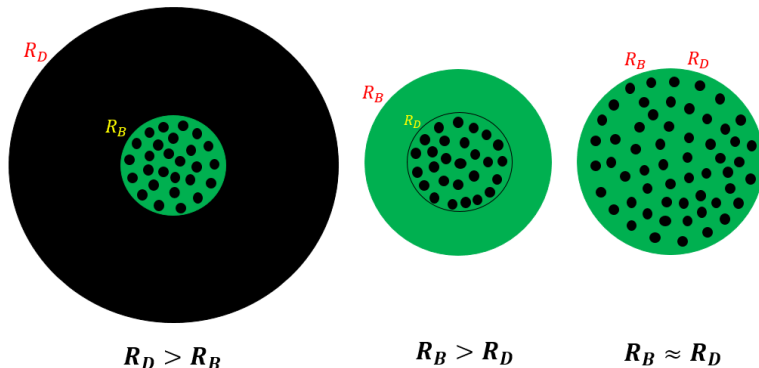


Fig. 5. Three possible configurations of a DM admixed NS, (left) DM halo, (middle) DM core and (right) DM is distributed in a whole NS. Note that for the DM core and halo cases the core of the object is a mixture of BM and DM. Green and black colors denote BM and DM, respectively.

For all of the possible DM admixed NSs' structures, the total gravitational mass of the mixed object is

$$M_T = M_B(R_B) + M_D(R_D). \quad (7)$$

However, the observable radius of the star is still defined by R_B , this is due to the visibility of R_B compare to R_D and technical difficulties of indirect detection of dark radius R_D . Furthermore, the DM fraction that determines the amount of DM in a DM admixed NS is defined as

$$F_\chi = \frac{M_D(R_D)}{M_T}. \quad (8)$$

Hereafter an effect of DM on NS properties is studied for m_χ of about hundreds MeV and fixed coupling constant $\lambda = \pi$. Fig. 6 shows energy density profiles for a DM admixed NS where the BM (dashed red curves) and DM (solid red curves)

components are plotted separately. The energy density profiles for pure BM and DM stars are presented by solid black and green curves, respectively. Here we consider $\lambda = \pi$ and $F_\chi = 20\%$, while the central values of pressure for BM and DM components are chosen in such a way that a desired DM fraction F_χ has been obtained.

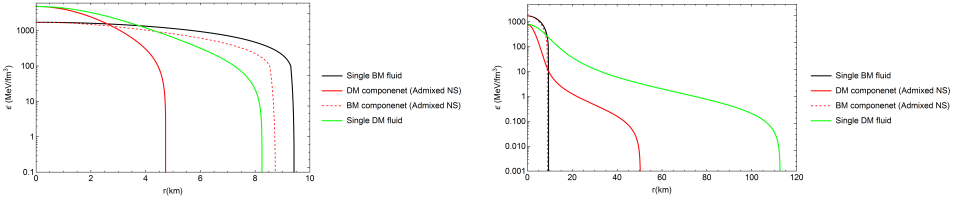


Fig. 6. Energy density profiles for pure BM and DM stars (black and green curves) shown together with the slotted DM and BM components of a DM admixed NS (solid and dashed red curves). Left panel corresponds to a DM core formation, while the right one to a DM halo, for $m_\chi = 400$ MeV and $m_\chi = 100$ MeV, respectively. For both of the cases, coupling constant is fixed at $\lambda = \pi$ and $F_\chi = 20\%$.

On the left panel which is obtained for $m_\chi = 400$ MeV, a DM core with $R_D \approx 5$ km is embedded in a BM structure with a larger radius. On the right panel, we fixed DM mass to $m_\chi = 100$ MeV which leads to the formation of a DM halo around the BM fluid with much larger radius. Interestingly, we see that for both DM core and DM halo formations, a reduction occurs in the energy density and the radius of DM and BM fluids in the mixed object compare to pure BM/DM star. This effect is much larger for the DM component and shows that the properties of the single DM fluid have significant effects in the admixed NS and in fact underly their features.

By comparing the left and right panels of Fig. 6, we see a transition from DM core to DM halo by changing m_χ from 400 MeV to 100 MeV. Therefore, by a thorough analysis of an effect of model parameters, as a general behaviour, we can conclude that light DM particles with $m_\chi < 200$ MeV, for low DM fractions, tend to form a halo around a NS, while heavier ones would mainly create a DM core inside a compact star (for more detailed analysis see⁶⁸).

The M-R profiles for DM admixed NSs are shown in Fig. 7 in which $M = M_B + M_D$. Here R is the outermost radius of the star which is determined by R_B for the DM core and R_D for the DM halo. The solid black curve shows the M-R relation for the BM fluid (without DM), the gray dashed line indicates the $2M_\odot$ constraint on maximum mass of NSs and the shaded regions colored in magenta and cyan denote the causality and GR limits, respectively.

As it is shown in Fig. 7, two different boson masses, 100 MeV and 400 MeV lead to a DM halo and a DM core formations, respectively. In the left panel ($m_\chi = 400$ MeV), it is indicated that DM core formation causes a decrease of the maximum

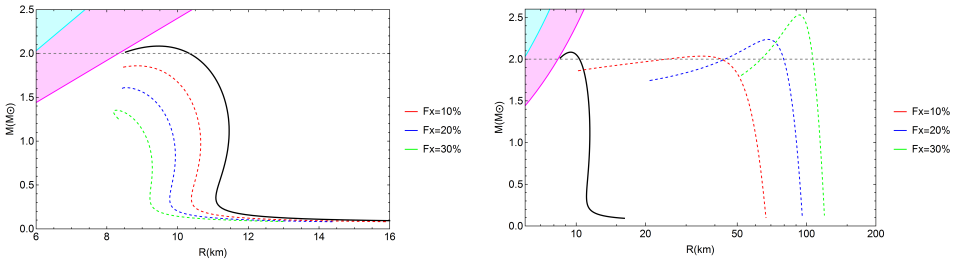


Fig. 7. Mass-Radius profiles for DM admixed NSs for $m_\chi = 400$ MeV (left) which corresponds to a DM core formation and $m_\chi = 100$ MeV (right) that represents an extended DM halo formation around a NS. Coupling constant is fixed to $\lambda = \pi$ and different F_χ are considered as labeled.

mass well below the $2M_\odot$ constraint,^{62,77,78} and also a reduction of the corresponding radius. However, for $m_\chi = 100$ MeV (see the right panel in Fig. 7) for which a DM halo is formed around a NS, both maximum mass and radius are increased. Regarding the radius of the object for DM halo formation, it is increased significantly since is determined by R_D . It is seen that higher DM fractions enhance both of the above behaviours for DM core/halo structures. Note that for the cases in which a DM halo is formed ($R_D > R_B$), the visible radius of the star remains to be R_B .

To summarize, we see here that an effect of bosonic DM with repulsive self-interaction onto NSs is in agreement with previous studies which considered different DM models. Thus, an existence of a DM core decreases the maximum star's mass and the corresponding radius, while the formation of a DM halo increases these quantities.^{2–4,30} In this regard, the most massive NS observed by NICER,⁶² PSR J0740+6620 ($M_{max} \simeq 2M_\odot$) is compatible with the DM admixed NS scenario.

4. Tidal deformability of a DM admixed NS

GW signal from NS-NS mergers introduce tidal deformability as a new observable quantity to probe the internal structure of NSs and constrain their macroscopic features.^{84–87} In this section, we analyse an impact of self-interacting bosonic DM on the tidal deformability of a DM admixed NS.

The idea of tidal deformability was first proposed by Tanja Hinderer in 2008^{88,89} which comes from the fact that in a binary system of NSs both of the objects are deformed owing to the imposed tidal forces.^{90–92} The tidal deformability expresses the ability of the gravitational field to change the quadrupole structure of a NS which alter the rotational phase of the binary system. Therefore, the GW signal is influenced during the inspiral phase due to the deformation effects of NSs when the binary orbital radius becomes comparable to the radius of NS. In fact, taking tidal deformability into account produces a phase shift in GW signal and accelerates the inspiral which leads to an earlier merging.^{37,85,93}

The induced quadrupole moment Q_{ij} of a NS due to the external tidal field of its companion \mathcal{E}_{ij} can be parameterized as follows^{88,90}

$$Q_{ij} = \lambda_t \mathcal{E}_{ij}, \quad (9)$$

where λ_t is the tidal deformability parameter and can be defined based on k_2 , the tidal love number, which is calculated from the system of equations including the TOV one. As is evident, k_2 and the tidal deformability strongly depend on the star's EoS.^{88–90}

$$\lambda_t = \frac{2}{3} k_2 R^5 \quad (10)$$

Unlike λ_t which has dimension, dimensionless tidal deformability Λ can be defined as,

$$\Lambda = \frac{\lambda_t}{M^5} = \frac{2}{3} k_2 \left(\frac{R}{M} \right)^5. \quad (11)$$

where R and M are the radius and mass of the compact star. It should be mentioned that R in a DM admixed NS is the outermost radius of the object which for a DM halo $R = R_D$ and for a DM core $R = R_B$. As an observational constraint on the tidal deformability, we take $\Lambda_{1.4} = 190^{+390}_{-120}$ reported by⁶⁴ for $M = 1.4M_\odot$ in the case of GW170817.

In the following, we investigate the effect of self-interacting bosonic DM, as a DM core or a DM halo, on the tidal deformability Λ of a mixed object at various m_χ and F_χ . In Figs. 8 and 9 the variation of Λ is shown in terms of total mass and radius of DM admixed NSs. In these figures the gray horizontal dashed lines indicate the LIGO/Virgo upper bound $\Lambda_{1.4} = 580$,⁶⁴ the gray solid vertical lines show $M_T = 1.4M_\odot$ and the colored dashed and solid vertical lines stand for $R_{1.4}$ radius for the corresponding model parameters. The tidal deformability calculated for the pure baryonic EoS is denoted by the solid black curve and its $\Lambda_{1.4}$ value is about 285 which is well below the LIGO/Virgo constraint.

As a general behaviour in these plots, it can be seen that tidal deformability is a decreasing function of total mass and rises by increasing the radius which is related to the definition of this parameter as a function of R/M through Eq. (11). It follows from the M-R profile of a combined system NS+DM, that approaching the maximum mass of the equilibrium sequence decreases the stellar radius and, consequently, R/M . In other words the lowest value of Λ corresponds to the maximum mass and minimum radius of the DM admixed NS.

The effect of variation of Λ caused by changing the DM mass at fixed coupling constant $\lambda = \pi$ and DM fraction $F_\chi = 10\%$ is shown on Fig. 8. It is seen that for low DM masses $m_\chi = 100, 120, 150$ MeV, leading to formation of the DM halo, $\Lambda_{1.4}$ is higher than in the cases of higher m_χ and purely baryonic NS. Indeed, the corresponding $R_{1.4}$ significantly exceeds the values obtained for purely baryonic NS. For $m_\chi = 300, 400, 500$ MeV, however, the situation is different. Formation of the

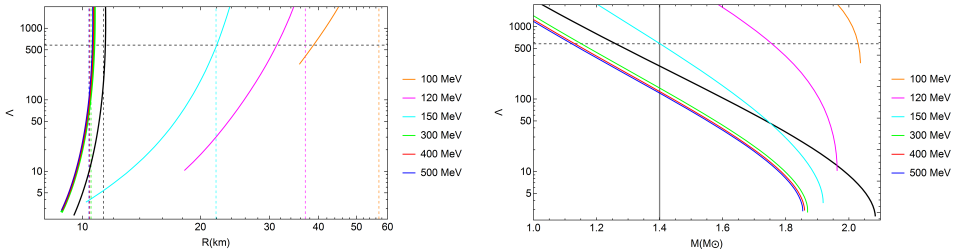


Fig. 8. Tidal deformability (Λ) in terms of total mass (right) and outermost radius (left) for stable sequences of DM admixed NSs. Various boson masses are considered, $m_\chi = 100, 120, 150$ MeV correspond to a DM halo formation while for $m_\chi = 300, 400, 500$ MeV a DM core is formed inside NS. Coupling constant and DM fraction are fixed at π and 10%, respectively.

DM core reduces the corresponding tidal polarizability, for which the $\Lambda - R$ curves are very similar to purely baryonic case. Regarding Fig. 8, we can conclude that DM halo yields large $\Lambda_{1.4}$, which even can exceed the observational constraint, while the DM core lowers Λ making it consistent with $\Lambda_{1.4} \leq 580$. This is related to the effect, which was mentioned in the previous section. Namely, DM halo increases the mass and radius of DM admixed NSs while DM core decreases these quantities. It is worth mentioning that GW observations during the inspiral phase of NS-NS coalescence correspond to lower frequencies detectable by Ad. LIGO. At this regime typical interstellar separation is $r < 150$ km. In order to prevent the technical difficulties caused by the overlap of DM halos we restrict their radii as $R_D \leq 75$ km.^{2,3}

To give more insight, Fig. 9 shows modification of tidal polarizability due to variation of the DM fraction from 5% to 15% calculated at fixed $\lambda = \pi$ and $m_\chi = 100, 400$ MeV, corresponding to DM halo and DM core, respectively. As it is seen, higher F_χ increases $\Lambda_{1.4}$ and $R_{1.4}$ at $m_\chi = 100$ MeV and decreases these parameters at $m_\chi = 400$ MeV. Remarkably, for $m_\chi = 100$ MeV (solid lines) tidal polarizability of the $M = 1.4M_\odot$ star exceeds 580 even at $F_\chi = 5\%$ since in this case Λ is more sensitive to DM fraction than at $m_\chi = 400$ MeV. Despite at this later case depicted by the dashed lines $\Lambda_{1.4}$ is in agreement with the upper observational constraint, the reduction of tidal deformability and $R_{1.4}$ should be consistent with the lower observational limits $\Lambda_{1.4} \gtrsim 70$ and $R_{1.4} \gtrsim 11$ km.^{64,94–97}

As the final remark of this section, in Fig. 10, we show the effect of increasing and decreasing tidal deformability in a NS with DM halo/core and purely baryonic one. It was explained in the beginning of this section that tidal deformability parameter shows how much the compact object is deformed due to the gravitational potential of its companion. Thus in this illustration, we see that DM admixed NS with a DM halo can be more deformed since it has higher values of Λ compared to purely baryonic NS and the DM admixed one with the DM core. In addition, considering tidal love number k_2 we note that mixed compact objects with stiffer EoS are more deformable due to the DM halo compared to the ones with softer EoS producing the DM core.

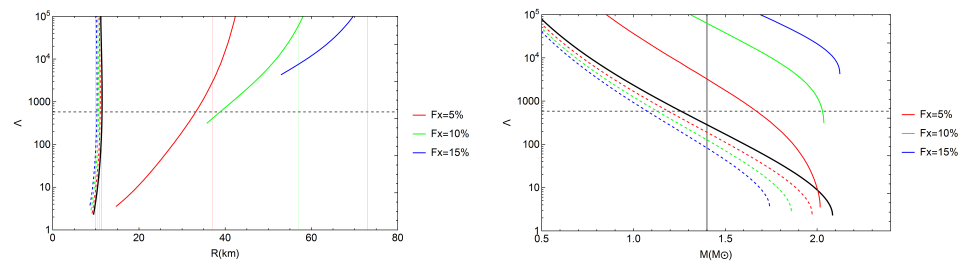


Fig. 9. Tidal deformability (Λ) in terms of total mass (right) and outermost radius (left) for stable sequences of DM admixed NSs. Two boson masses are considered, $m_\chi = 100 \text{ MeV}$ (solid lines) and $m_\chi = 400 \text{ MeV}$ (dashed lines) which correspond to DM halo and DM core formations, respectively. Various DM fractions are considered as labeled.

In summary, we note that in full agreement with the previous studies^{2,3} DM halo increases tidal deformability, while DM core decreases it. Meanwhile, upper constraint on tidal deformability, $\Lambda_{1.4} = 580$, related to GW170817 event,⁶⁴ has been considered.

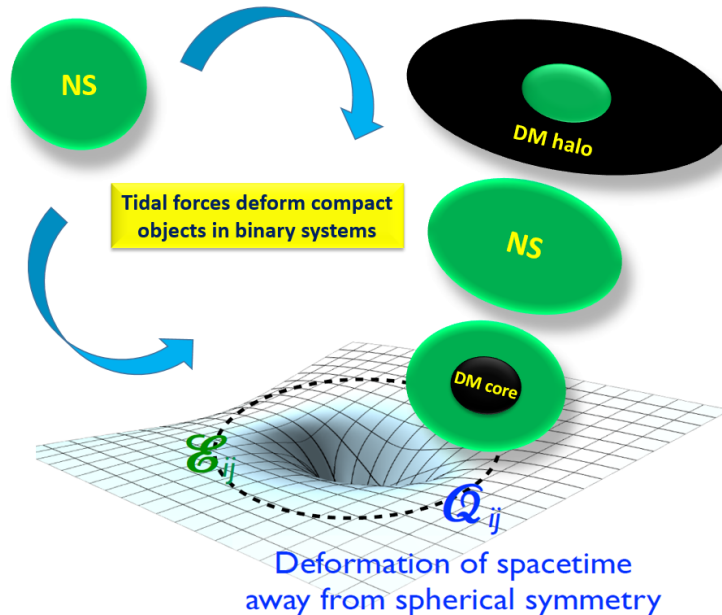


Fig. 10. The effect of increasing and decreasing of tidal deformability on DM admixed NS's deformation is compared with the pure BM object (NS). It is shown that higher value of Λ indicates more deformation in the compact object, therefore a DM halo deforms more in comparison with a pure NS and DM admixed NS with a DM core.

5. Conclusion and Outlook

Treating DM as a self-repulsing complex scalar field, various properties of single fluid BSs and two-fluid NSs has been studied within the TOV formalism. It is shown that for $\lambda = \pi$, light DM particles ($m_\chi \lesssim 200$ MeV) form BSs with much larger maximum mass and radius compared with typical NSs, while heavy DM particles lead to formation of BSs with much smaller radius and mass. Furthermore, we showed that for low DM fractions ($F_\chi < 20\%$), light bosons create a halo around the DM admixed NSs, while heavier DM particles form a DM core inside the BM component.

The effect of bosonic DM as a halo/core has been examined by considering the maximum mass, radius and tidal deformability of a DM admixed NS. We have indicated that DM halo formation causes an increase in the aforementioned observable quantities while a DM core reduces all of them. Considering various m_χ and F_χ , the maximum mass and tidal deformability of the mixed object has been compared to the latest upper observational bounds, $M_{max} = 2M_\odot$ and $\Lambda_{1.4} \leq 580$ inferred from NICER (PSR J0740+6620) and LIGO/Virgo (GW170817) detections.

Regarding the impact of DM halo and DM core formations on NS's observable parameters and applying the observational limits for NSs' features, one could constrain the parameter space of DM model such as mass and coupling constant and also the amount of DM inside the compact object. In this regard, an extensive investigation has been done recently in⁶⁸ by the same authors of the present paper in which a constraint has been imposed on F_χ for sub-GeV DM particles by taking M_{max} and $\Lambda_{1.4}$ bounds. Moreover, as DM core decreases the visible radius of the DM admixed NS (R_B) and DM halo increases the invisible dark radius of the object (R_D), radius constraint for typical NSs ($M \approx 1.4M_\odot$) and most massive ones ($M \approx 2M_\odot$)^{62,96,97} could be utilized to impose more stringent limits on DM parameter space and its fraction. In addition, any unusual observational results of NSs' properties could be explained by the DM admixed NS model. For instance, there are many effort among the community to explain the nature of the secondary compact object in the GW190814⁹⁸ event with the mass about $2.6M_\odot$ being higher than the maximum NS one. There are some works explaining the mass of this strange object by the DM core or halo formation within the DM admixed NS scenario.^{52,99,100} Regarding our model, as an example, $m_\chi = 50$ MeV, $\lambda = \pi$ and $F_\chi \approx 20\%$ lead to formation of a DM admixed NS with $M_T = 2.6M_\odot$ and detectable radius about 10 km. As a final remark, upcoming modern facilities such as X-ray (NICER,¹⁰¹ ATHENA,¹⁰² eXTP¹⁰³ and STROBE-X¹⁰⁴) and radio (MeerKAT,¹⁰⁵ ngVLA¹⁰⁶ and SKA¹⁰⁷) telescopes, as well as GW (LIGO/Virgo/KAGRA¹⁰⁸ and Einstein^{109,110}) detectors, shown in Fig. 11, would provide vast numbers of promising results for NSs' features bringing us to a golden age of NS investigations and consequently could help us to shed light on the nature of DM and its possible existence in compact objects.



Fig. 11. Applying various innovative telescopes covering all kinds of observations from GW and X-ray to radio waves provide a unique opportunity for compact objects' research which may solve the puzzle of DM.

Acknowledgments

V.S. acknowledges the support from the Fundação para a Ciéncia e Tecnologia (FCT) within the projects UID/04564/2021. The work of O.I. was supported by the Polish National Science Center under the grant No. 2019/33/B/ST9/03059.

References

1. G. Panopoulos and I. Lopes, Dark matter effect on realistic equation of state in neutron stars, *Physical Review D* **96** (Oct 2017).
2. A. E. Nelson, S. Reddy and D. Zhou, Dark halos around neutron stars and gravitational waves, *Journal of Cosmology and Astroparticle Physics* **2019**, p. 012–012 (Jul 2019).
3. J. Ellis, G. Hütsi, K. Kannike, L. Marzola, M. Raidal and V. Vaskonen, Dark Matter Effects On Neutron Star Properties, *Phys. Rev. D* **97**, p. 123007 (2018).
4. O. Ivanytskyi, V. Sagun and I. Lopes, Neutron stars: New constraints on asymmetric dark matter, *Phys. Rev. D* **102**, p. 063028 (Sep 2020).
5. Z. Rezaei, Study of Dark-Matter Admixed Neutron Stars using the Equation of State from the Rotational Curves of Galaxies, *Astrophys. J.* **835**, p. 33 (2017).
6. A. de Lavallaz and M. Fairbairn, Neutron Stars as Dark Matter Probes, *Phys. Rev. D* **81**, p. 123521 (2010).
7. M. I. Gresham and K. M. Zurek, Asymmetric Dark Stars and Neutron Star Stability, *Phys. Rev. D* **99**, p. 083008 (2019).

8. Y. Dengler, J. Schaffner-Bielich and L. Tolos, The Second Love Number of Dark Compact Planets and Neutron Stars with Dark Matter, *arXiv e-prints*, p. arXiv:2111.06197 (November 2021).
9. J. F. Navarro, C. S. Frenk and S. D. M. White, The Structure of cold dark matter halos, *Astrophys. J.* **462**, 563 (1996).
10. R. Ruffini, C. R. Argüelles and J. A. Rueda, On the core-halo distribution of dark matter in galaxies, *Monthly Notices of the Royal Astronomical Society* **451**, p. 622–628 (May 2015).
11. C. Argüelles, A. Krut, J. Rueda and R. Ruffini, Novel constraints on fermionic dark matter from galactic observables i: The milky way, *Physics of the Dark Universe* **21**, p. 82–89 (Sep 2018).
12. A. Del Popolo, M. Le Delliou and M. Deliyergiyev, Neutron Stars and Dark Matter, *Universe* **6**, p. 222 (November 2020).
13. R. Ciancarella, F. Pannarale, A. Addazi and A. Marciano, Constraining mirror dark matter inside neutron stars, *Phys. Dark Univ.* **32**, p. 100796 (2021).
14. I. Goldman, R. Mohapatra, S. Nussinov, D. Rosenbaum and V. Teplitz, Possible implications of asymmetric fermionic dark matter for neutron stars, *Physics Letters B* **725**, p. 200–207 (Oct 2013).
15. P. Ciarcelluti and F. Sandin, Have neutron stars a dark matter core?, *Physics Letters B* **695**, p. 19–21 (Jan 2011).
16. F. Sandin and P. Ciarcelluti, Effects of mirror dark matter on neutron stars, *Astroparticle Physics* **32**, p. 278–284 (Dec 2009).
17. A. Del Popolo, M. Deliyergiyev and M. Le Delliou, Solution to the hyperon puzzle using dark matter, *Phys. Dark Univ.* **30**, p. 100622 (2020).
18. M. Deliyergiyev, A. Del Popolo, L. Tolos, M. Le Delliou, X. Lee and F. Burgio, Dark compact objects: An extensive overview, *Physical Review D* **99** (Mar 2019).
19. A. Li, F. Huang and R.-X. Xu, Too massive neutron stars: The role of dark matter?, *Astropart. Phys.* **37**, 70 (2012).
20. C. Kouvaris, WIMP Annihilation and Cooling of Neutron Stars, *Phys. Rev. D* **77**, p. 023006 (2008).
21. S. A. Bhat and A. Paul, Cooling of Dark-Matter Admixed Neutron Stars with density-dependent Equation of State, *Eur. Phys. J. C* **80**, p. 544 (2020).
22. J. Fuller and C. Ott, Dark Matter-induced Collapse of Neutron Stars: A Possible Link Between Fast Radio Bursts and the Missing Pulsar Problem, *Mon. Not. Roy. Astron. Soc.* **450**, L71 (2015).
23. J. F. Acevedo, J. Bramante and A. Goodman, Nuclear fusion inside dark matter, *Phys. Rev. D* **103**, p. 123022 (2021).
24. A. Sedrakian, Axion cooling of neutron stars, *Phys. Rev. D* **93**, p. 065044 (2016).
25. A. Sedrakian, Axion cooling of neutron stars. II. Beyond hadronic axions, *Phys. Rev. D* **99**, p. 043011 (2019).
26. D. E. Kaplan, M. A. Luty and K. M. Zurek, Asymmetric Dark Matter, *Phys. Rev. D* **79**, p. 115016 (2009).
27. J. Shelton and K. M. Zurek, Darkogenesis: A baryon asymmetry from the dark matter sector, *Phys. Rev. D* **82**, p. 123512 (2010).
28. K. Petraki and R. R. Volkas, Review of asymmetric dark matter, *Int. J. Mod. Phys. A* **28**, p. 1330028 (2013).
29. C. Kouvaris and N. G. Nielsen, Asymmetric Dark Matter Stars, *Phys. Rev. D* **92**, p. 063526 (2015).
30. S. Leung, M. Chu and L. Lin, Dark-matter admixed neutron stars, *Phys. Rev. D* **84**, p. 107301 (2011).

31. Q.-F. Xiang, W.-Z. Jiang, D.-R. Zhang and R.-Y. Yang, Effects of fermionic dark matter on properties of neutron stars, *Phys. Rev. C* **89**, p. 025803 (Feb 2014).
32. R. C. Tolman, Static solutions of Einstein's field equations for spheres of fluid, *Phys. Rev.* **55**, 364 (1939).
33. J. R. Oppenheimer and G. M. Volkoff, On Massive neutron cores, *Phys. Rev.* **55**, 374 (1939).
34. A. Das, T. Malik and A. C. Nayak, Confronting nuclear equation of state in the presence of dark matter using GW170817 observation in relativistic mean field theory approach, *Phys. Rev. D* **99**, p. 043016 (2019).
35. H. C. Das, A. Kumar, B. Kumar, S. Kumar Biswal, T. Nakatsukasa, A. Li and S. K. Patra, Effects of dark matter on the nuclear and neutron star matter, *Mon. Not. Roy. Astron. Soc.* **495**, 4893 (2020).
36. D. Sen and A. Guha, Implications of Feebly Interacting Dark Sector on Neutron Star Properties and Constraints from GW170817, *Mon. Not. Roy. Astron. Soc.* **504**, p. 3 (2021).
37. H. C. Das, A. Kumar and S. K. Patra, Effects of dark matter on the inspiral properties of the binary neutron star (4 2021).
38. S. Mukhopadhyay, D. Atta, K. Imam, D. Basu and C. Samanta, Compact bifluid hybrid stars: Hadronic Matter mixed with self-interacting fermionic Asymmetric Dark Matter, *Eur. Phys. J. C* **77**, p. 440 (2017), [Erratum: Eur. Phys. J. C 77, 553 (2017)].
39. X. Li, F. Wang and K. Cheng, Gravitational effects of condensate dark matter on compact stellar objects, *Journal of Cosmology and Astroparticle Physics* **2012**, p. 031–031 (Oct 2012).
40. X. Li, T. Harko and K. Cheng, Condensate dark matter stars, *JCAP* **06**, p. 001 (2012).
41. L. Tolos and J. Schaffner-Bielich, Dark compact planets, *Physical Review D* **92** (Dec 2015).
42. D. J. Kaup, Klein-Gordon Geon, *Phys. Rev.* **172**, 1331 (1968).
43. R. Ruffini and S. Bonazzola, Systems of selfgravitating particles in general relativity and the concept of an equation of state, *Phys. Rev.* **187**, 1767 (1969).
44. M. Colpi, S. Shapiro and I. Wasserman, Boson Stars: Gravitational Equilibria of Selfinteracting Scalar Fields, *Phys. Rev. Lett.* **57**, 2485 (1986).
45. F. E. Schunck and E. W. Mielke, General relativistic boson stars, *Class. Quant. Grav.* **20**, R301 (2003).
46. S. L. Liebling and C. Palenzuela, Dynamical Boson Stars, *Living Rev. Rel.* **20**, p. 5 (2017).
47. L. Visinelli, Boson Stars and Oscillations: A Review (9 2021).
48. K. A. Bugaev, V. V. Sagun, A. I. Ivanytskyi, I. P. Yakimenko, E. G. Nikonov, A. V. Taranenko and G. M. Zinovjev, Going beyond the second virial coefficient in the hadron resonance gas model, *Nucl. Phys. A* **970**, 133 (February 2018).
49. V. V. Sagun, I. Lopes and A. I. Ivanytskyi, The induced surface tension contribution for the equation of state of neutron stars, *Astrophys. J.* **871**, p. 157 (2019).
50. V. Sagun, I. Lopes and A. Ivanytskyi, Neutron stars meet constraints from high and low energy nuclear physics, *Nucl. Phys. A* **982**, 883 (2019).
51. A. Quddus, G. Panopoulos, B. Kumar, S. Ahmad and S. K. Patra, GW170817 constraints on the properties of a neutron star in the presence of WIMP dark matter, *J. Phys. G* **47**, p. 095202 (2020).
52. K. Zhang and F.-L. Lin, Constraint on hybrid stars with gravitational wave events, *Universe* **6**, p. 231 (2020).

53. A. Le Tiec and M. Casals, Spinning Black Holes Fall in Love, *Phys. Rev. Lett.* **126**, p. 131102 (2021).
54. A. Das, T. Malik and A. C. Nayak, Confronting nuclear equation of state in the presence of dark matter using gw170817 observation in relativistic mean field theory approach, *Physical Review D* **99** (Feb 2019).
55. J. Ellis, A. Hektor, G. Hütsi, K. Kannike, L. Marzola, M. Raidal and V. Vaskonen, Search for Dark Matter Effects on Gravitational Signals from Neutron Star Mergers, *Phys. Lett. B* **781**, 607 (2018).
56. M. Bezares, D. Viganò and C. Palenzuela, Gravitational wave signatures of dark matter cores in binary neutron star mergers by using numerical simulations, *Phys. Rev. D* **100**, p. 044049 (2019).
57. M. Bezares and C. Palenzuela, Gravitational Waves from Dark Boson Star binary mergers, *Class. Quant. Grav.* **35**, p. 234002 (2018).
58. C. Horowitz and S. Reddy, Gravitational Waves from Compact Dark Objects in Neutron Stars, *Phys. Rev. Lett.* **122**, p. 071102 (2019).
59. A. Bauswein, G. Guo, J.-H. Lien, Y.-H. Lin and M.-R. Wu, Compact Dark Objects in Neutron Star Mergers (12 2020).
60. B. P. Abbott *et al.*, GW170817: Observation of Gravitational Waves from a Binary Neutron Star Inspiral, *Phys. Rev. Lett.* **119**, p. 161101 (2017).
61. B. P. Abbott *et al.*, GW190425: Observation of a Compact Binary Coalescence with Total Mass $\sim 3.4M_{\odot}$, *Astrophys. J. Lett.* **892**, p. L3 (2020).
62. T. E. Riley *et al.*, A NICER View of the Massive Pulsar PSR J0740+6620 Informed by Radio Timing and XMM-Newton Spectroscopy, *Astrophys. J. Lett.* **918**, p. L27 (2021).
63. B. Abbott, R. Abbott, T. Abbott, F. Acernese, K. Ackley, C. Adams, T. Adams, P. Addesso, R. Adhikari, V. Adya and et al., Gw170817: Observation of gravitational waves from a binary neutron star inspiral, *Physical Review Letters* **119** (Oct 2017).
64. B. P. Abbott *et al.*, GW170817: Measurements of neutron star radii and equation of state, *Phys. Rev. Lett.* **121**, p. 161101 (2018).
65. A. Maselli, P. Pnigouras, N. G. Nielsen, C. Kouvaris and K. D. Kokkotas, Dark stars: Gravitational and electromagnetic observables, *Phys. Rev. D* **96**, p. 023005 (2017).
66. A. Arbey, J. Lesgourgues and P. Salati, Galactic halos of fluid dark matter, *Phys. Rev. D* **68**, p. 023511 (Jul 2003).
67. A. Suárez, V. H. Robles and T. Matos, A Review on the Scalar Field/Bose-Einstein Condensate Dark Matter Model, *Astrophys. Space Sci. Proc.* **38**, 107 (2014).
68. D. Rafiei Karkevandi, S. Shakeri, V. Sagun and O. Ivanovtskyi, Bosonic Dark Matter in Neutron Stars and its Effect on Gravitational Wave Signal, *arXiv e-prints*, p. arXiv:2109.03801 (September 2021).
69. E. W. Mielke and F. E. Schunck, Boson stars: Alternatives to primordial black holes?, *Nucl. Phys. B* **564**, 185 (2000).
70. P.-H. Chavanis and T. Harko, Bose-Einstein Condensate general relativistic stars, *Phys. Rev. D* **86**, p. 064011 (2012).
71. C. Pacilio, M. Vaglio, A. Maselli and P. Pani, Gravitational-wave detectors as particle-physics laboratories: Constraining scalar interactions with a coherent inspiral model of boson-star binaries, *Phys. Rev. D* **102**, p. 083002 (2020).
72. X. Li, T. Harko and K. Cheng, Condensate dark matter stars, *JCAP* **06**, p. 001 (2012).
73. P.-H. Chavanis, Mass-radius relation of self-gravitating Bose-Einstein condensates with a central black hole, *Eur. Phys. J. Plus* **134**, p. 352 (2019).

74. F. Dalfovo, S. Giorgini, L. P. Pitaevskii and S. Stringari, Theory of bose-einstein condensation in trapped gases, *Reviews of Modern Physics* **71**, p. 463–512 (Apr 1999).
75. J. Rogel-Salazar, The gross-pitaevskii equation and bose-einstein condensates, *European Journal of Physics* **34**, p. 247–257 (Jan 2013).
76. C. J. Pethick and H. Smith, *Bose-Einstein Condensation in Dilute Gases*, 2 edn. (Cambridge University Press, 2008).
77. J. Antoniadis *et al.*, A Massive Pulsar in a Compact Relativistic Binary, *Science* **340**, p. 6131 (2013).
78. H. T. Cromartie *et al.*, Relativistic Shapiro delay measurements of an extremely massive millisecond pulsar, *Nature Astron.* **4**, 72 (2019).
79. P. Amaro-Seoane, J. Barranco, A. Bernal and L. Rezzolla, Constraining scalar fields with stellar kinematics and collisional dark matter, *JCAP* **11**, p. 002 (2010).
80. V. V. Sagun, A. I. Ivanovtskyi, K. A. Bugaev and I. N. Mishustin, The statistical multifragmentation model for liquid-gas phase transition with a compressible nuclear liquid, *Nucl. Phys. A* **924**, 24 (2014).
81. A. I. Ivanovtskyi, K. A. Bugaev, V. V. Sagun, L. V. Bravina and E. E. Zabrodin, Influence of flow constraints on the properties of the critical endpoint of symmetric nuclear matter, *Phys. Rev. C* **97**, p. 064905 (2018).
82. V. V. Sagun, K. A. Bugaev, A. I. Ivanovtskyi, I. P. Yakimenko, E. G. Nikonov, A. V. Taranenko, C. Greiner, D. B. Blaschke and G. M. Zinovjev, Hadron resonance gas model with induced surface tension, *European Physical Journal A* **54**, p. 100 (June 2018).
83. V. Sagun, G. Panotopoulos and I. Lopes, Asteroseismology: radial oscillations of neutron stars with realistic equation of state, *Phys. Rev. D* **101**, p. 063025 (2020).
84. C. Raithel, F. Özel and D. Psaltis, Tidal deformability from GW170817 as a direct probe of the neutron star radius, *Astrophys. J. Lett.* **857**, p. L23 (2018).
85. K. Chatzioannou, Neutron star tidal deformability and equation of state constraints, *Gen. Rel. Grav.* **52**, p. 109 (2020).
86. E. R. Most, L. R. Weih, L. Rezzolla and J. Schaffner-Bielich, New constraints on radii and tidal deformabilities of neutron stars from GW170817, *Phys. Rev. Lett.* **120**, p. 261103 (2018).
87. S. De, D. Finstad, J. M. Lattimer, D. A. Brown, E. Berger and C. M. Biwer, Tidal Deformabilities and Radii of Neutron Stars from the Observation of GW170817, *Phys. Rev. Lett.* **121**, p. 091102 (2018), [Erratum: *Phys. Rev. Lett.* 121, 259902 (2018)].
88. T. Hinderer, Tidal Love numbers of neutron stars, *Astrophys. J.* **677**, 1216 (2008).
89. T. Hinderer, B. D. Lackey, R. N. Lang and J. S. Read, Tidal deformability of neutron stars with realistic equations of state and their gravitational wave signatures in binary inspiral, *Phys. Rev. D* **81**, p. 123016 (2010).
90. S. Postnikov, M. Prakash and J. M. Lattimer, Tidal Love Numbers of Neutron and Self-Bound Quark Stars, *Phys. Rev. D* **82**, p. 024016 (2010).
91. T. Zhao and J. M. Lattimer, Tidal Deformabilities and Neutron Star Mergers, *Phys. Rev. D* **98**, p. 063020 (2018).
92. S. Han and A. W. Steiner, Tidal deformability with sharp phase transitions in (binary) neutron stars, *Phys. Rev. D* **99**, p. 083014 (2019).
93. B. D. Lackey and L. Wade, Reconstructing the neutron-star equation of state with gravitational-wave detectors from a realistic population of inspiralling binary neutron stars, *Phys. Rev. D* **91**, p. 043002 (2015).
94. M. C. Miller *et al.*, PSR J0030+0451 Mass and Radius from NICER Data and Implications for the Properties of Neutron Star Matter, *Astrophys. J. Lett.* **887**, p. L24 (2019).

95. T. E. Riley *et al.*, A NICER View of PSR J0030+0451: Millisecond Pulsar Parameter Estimation, *Astrophys. J. Lett.* **887**, p. L21 (2019).
96. G. Raaijmakers, S. K. Greif, K. Hebeler, T. Hinderer, S. Nissanke, A. Schwenk, T. E. Riley, A. L. Watts, J. M. Lattimer and W. C. G. Ho, Constraints on the dense matter equation of state and neutron star properties from NICER’s mass-radius estimate of PSR J0740+6620 and multimessenger observations (5 2021).
97. M. C. Miller *et al.*, The Radius of PSR J0740+6620 from NICER and XMM-Newton Data, *Astrophys. J. Lett.* **918**, p. L28 (2021).
98. R. Abbott *et al.*, GW190814: Gravitational Waves from the Coalescence of a 23 Solar Mass Black Hole with a 2.6 Solar Mass Compact Object, *Astrophys. J. Lett.* **896**, p. L44 (2020).
99. H. C. Das, A. Kumar and S. K. Patra, Dark matter admixed neutron star as a possible compact component in the GW190814 merger event, *Phys. Rev. D* **104**, p. 063028 (2021).
100. B. K. K. Lee, M.-c. Chu and L.-M. Lin, Can the GW190814 secondary component be a bosonic dark matter admixed compact star? (10 2021).
101. A. L. Watts, Constraining the neutron star equation of state using Pulse Profile Modeling, *AIP Conf. Proc.* **2127**, p. 020008 (2019).
102. R. Cassano *et al.*, SKA-Athena Synergy White Paper (7 2018).
103. J. J. M. in ’t Zand *et al.*, Observatory science with eXTP, *Sci. China Phys. Mech. Astron.* **62**, p. 029506 (2019).
104. P. S. Ray *et al.*, STROBE-X: X-ray Timing and Spectroscopy on Dynamical Timescales from Microseconds to Years (3 2019).
105. M. Bailes *et al.*, MeerTime - the MeerKAT Key Science Program on Pulsar Timing, *PoS MeerKAT2016*, p. 011 (2018).
106. R. J. Selina, The next generation very large array: A technical overview <https://arxiv.org/ftp/arxiv/papers/1806/1806.08405.pdf> (2018).
107. A. Weltman *et al.*, Fundamental physics with the Square Kilometre Array, *Publ. Astron. Soc. Austral.* **37**, p. e002 (2020).
108. R. Abbott *et al.*, Observation of Gravitational Waves from Two Neutron Star–Black Hole Coalescences, *Astrophys. J. Lett.* **915**, p. L5 (2021).
109. M. Punturo *et al.*, The Einstein Telescope: A third-generation gravitational wave observatory, *Class. Quant. Grav.* **27**, p. 194002 (2010).
110. M. Maggiore *et al.*, Science Case for the Einstein Telescope, *JCAP* **03**, p. 050 (2020).

Confronting nuclear equation of state in the presence of dark matter using GW170817 observation in relativistic mean field theory approach

Arpan Das,^{1,*} Tuhin Malik,^{2,†} and Alekha C. Nayak^{1,‡}

¹Physical Research Laboratory, Ahmedabad 380009, India

²Department of Physics, BITS-Pilani, K.K. Birla Goa Campus, Goa 403726, India

(Received 2 August 2018; published 28 February 2019)

We confront the admixture of dark matter inside a neutron star using gravitational wave constraints coming from binary neutron star merger. We consider a relativistic mean field model including $\sigma - \omega - \rho$ meson interaction with NL3 parametrization. We study fermionic dark matter interacting with nucleonic matter via Higgs portal mechanism. We show that admixture of dark matter inside the neutron star softens the equation state and lowers the value of tidal deformability. Gravitational wave GW170817 observation puts an upper bound on tidal deformability of a binary neutron star with low spin prior at 90% confidence level, which disfavors stiff equation of state such as the Walecka model with NL3 parametrization. However, we show that the Walecka model with NL3 parametrization with a fermionic dark matter component satisfies the tidal deformability bound coming from the GW170817 observation.

DOI: 10.1103/PhysRevD.99.043016

I. INTRODUCTION

Compact objects like neutron stars (NS) are nature's laboratory which can shed light directly or indirectly on the different branches of physics such as low energy nuclear physics, QCD under extreme conditions, the general theory of relativity etc. A neutron star is one of the remnants of a dying star undergoing gravitational collapse. Gravitational collapse of stars with a mass range between $1.4\text{--}3.0 M_{\odot}$ evolve into a neutron star. Neutron degeneracy pressure inside the neutron star makes it hydrostatically stable against the gravitational collapse. If the mass of a dying star is very large (beyond $10 M_{\odot}$) then the stellar remnant will overcome the neutron degeneracy pressure and gravitational collapse will produce a black hole. Matter density inside the neutron star can be as large as a few times the nuclear saturation density ($n_B = 0.16 \text{ fm}^{-3}$). Interior of a neutron star provides a situation to study the behavior of matter at extreme conditions. In this context, the possible equation of state (EoS) of infinite nuclear matter has been explored extensively (for a brief review see [1]). The main challenge in the description of matter at high densities inside neutron stars is to develop a model which not only

describes matter at high densities, but also the properties of matter observed at saturation densities [2–4]. Valid nuclear EoS has to satisfy presently well accepted empirical and experimental constraints [5–7], e.g., ground state properties of spherical and deformed nuclei, saturation density, binding energy, symmetry energy, compression modulus etc. as well as constraints coming from infinite nuclear matter e.g., neutron star mass radius relation, tidal deformability etc. Rotating neutron stars or pulsars give important information about superfluid nature of nucleon inside the neutron star [8,9]. Superfluidity of nucleons is important to explain timing irregularities (glitch) of pulsars. From the high energy nuclear physics point of view, neutron star provides an ideal condition where high density QCD matter (quark matter phase, color superconducting phase etc.) can exist [10–13]. Historically the neutron star mass radius relationship coming from solving the Tolman-Oppenheimer-Volkoff (TOV) equation has been studied extensively to put constraints on the nuclear EoS [1]. However recent observation of gravitational waves from neutron star mergers opens up another dimension in the study of the nuclear EoS [14,15].

On August 17, 2017, the Advanced LIGO and Virgo observatories detected the gravitational waves (GW) from a merging binary NS [14]. GW170817 data open up a new way to understand the neutron star structure and the underlying EoS of dense matter. Details of the internal structure of the neutron stars in the binary mergers become important as the orbital separation become comparable with the size of the bodies. For neutron star binary merger the tidal field of the companion induces a quadrupole moment to the other neutron star. The relation of the induced quadrupole moment to the external tidal field is

*arpan@prl.res.in

†tuhin.malik@gmail.com

‡alekha@prl.res.in

Published by the American Physical Society under the terms of the [Creative Commons Attribution 4.0 International license](#). Further distribution of this work must maintain attribution to the author(s) and the published article's title, journal citation, and DOI. Funded by SCOAP³.

proportional to the tidal deformability. Tidal deformability is sensitive to the mass, radius, and tidal love number, which in turn depends on the nuclear EoS. Using observed tidal deformability parameters of the neutron star merger one can put strong constraints on the neutron star EoS, for details and related studies see [16–22] and references therein. The GW170817 observation puts an upper bound on tidal deformability of the combined binary NSs at 90% confidence [15]. Consequently, this can be used to rule out certain equation of states of neutron stars.

Observations of the kinematics of self-gravitating objects such as galaxies and clusters of galaxies give strong hint of the existence of dark matter (DM). Cosmological observations tell us that this invisible matter cannot consist of baryons, it must be a new kind of matter which interacts with the rest of the standard model particles very weakly. The exact nature of the dark matter, its coupling between standard model particles and the mass is still not known. However extensive studies on the particle physics dark matter models have put strong constraints on the coupling constant and mass of the dark matter particles (for a recent review on dark matter physics see [23]). Among different proposals of dark matter, weakly interacting massive particle (WIMP) scenario has gained favor because it gives the correct prediction of the measured relic abundance of the dark matter today very naturally.

The presence of dark matter inside neutron star and its consequences have been discussed in the literature [24–35]. These discussions include dark matter capture by neutron star and heating of old neutron star in the galactic halo to a temperature detectable by upcoming infrared telescopes [24], trapped WIMPs inside the neutron star [25], charged massive dark matter particle and its effect on neutron star [26], heating of a neutron star due to dark matter annihilation [27–29], or the collapse of a neutron star due to accretion of nonannihilating dark matter [30] etc. In Ref. [32] authors have considered possible effects of a self-interacting dark matter core on the maximum mass of a neutron star, mass-radius relation and on the NS tidal deformability parameter. They have computed radial density and pressure profiles of the baryonic and dark matter components for different nuclear EoS and different dark matter fractions. In Ref. [35], the authors have considered the Walecka relativistic mean field model including $\sigma - \omega$ interaction for the nucleonic part [2,3,5,6] and fermionic dark matter inside the neutron star. Using mean field approximation they have calculated effective nucleon mass, variation of σ field, EoS and the corresponding mass radius relation in this model. However, it is important to mention that the simple relativistic mean field model (RMF) model taken in this work is unsuccessful in producing nuclear saturation properties. This simple model is ruled out due to the fact that it gives high nuclear incompressibility (≈ 500 MeV) and very low nucleon mass [36]. Keeping this limitation of the simple $\sigma - \omega$ in this work we have

considered the a generalized Lagrangian for the nucleonic sector including $\sigma - \omega - \rho$ meson interaction with NL3 parametrization [37,38]. The EoS of this model is disfavored by GW170817 tidal deformability upper bound limit. However, we show that if we consider fermionic dark matter interaction via Higgs portal mechanism, then it can evade the GWs tidal deformability upper bound constraint. We have also considered nongravitational interaction of the dark matter and the nucleon field in a relativistic mean field approach.

This paper is organized as follows: in Sec. II we discuss generalized Walecka model with NL3 parameterization. In Sec. III, we discuss fermionic dark matter model and its interaction with nuclear matter. The EoS of total Lagrangian density of dark matter and nuclear matter is presented in Sec. IV. Constraint from GWs tidal deformability on EoS is discussed in Sec. V. Finally, we conclude in Sec. VI.

II. WALECKA MODEL WITH NL3 PARAMETRIZATION

In this section, we briefly summarize the taken RMF model [2,3,5,6], which is also known as quantum hadron dynamics (QHD) [39]. In this framework, nucleons are quasiparticles with an effective medium dependent mass and baryon chemical potential. They move in the mean field of mesons. The simplest QHD model is known as the $\sigma - \omega$ model. In this model nucleon-nucleon interaction is mediated by the exchange of σ and ω mesons. Properties of symmetric nuclear matter has been studied in this model. In general σ mesons give rise to a strong attractive central force and a spin-orbit nuclear force, on the other hand, ω -mesons are responsible for the repulsive central force. However, this simple model does not reproduce nuclear saturation properties, e.g., compressibility [36]. More advanced versions of QHD includes ρ meson exchange interaction between nucleons [37]. Since protons and neutrons only differ in terms of their isospin projections, ρ mesons are included to distinguish between these baryons and to give a better account of the symmetry energy. These vector mesons are charged, hence the reaction between ρ meson and proton will differ from the reaction between ρ meson and neutron. In general one can also include photon field, however, neutron star is assumed to be charge neutral, hence the contribution from the photon field can be neglected.

Lagrangian including nucleon field, σ , ω and ρ mesons and their interactions can be written as [37],

$$\begin{aligned} \mathcal{L} = & \bar{\psi} [\gamma^\mu (i\partial_\mu - g_v V_\mu - g_\rho \boldsymbol{\tau} \cdot \mathbf{b}_\mu) - (M_n + g_s \phi)] \psi \\ & + \frac{1}{2} \partial_\mu \phi \partial^\mu \phi - \frac{1}{2} m_s^2 \phi^2 - \frac{1}{3} g_2 \phi^3 - \frac{1}{4} g_3 \phi^4 \\ & - \frac{1}{4} V^{\mu\nu} V_{\mu\nu} + \frac{1}{2} m_V^2 V^\mu V_\mu - \frac{1}{4} \mathbf{b}^{\mu\nu} \cdot \mathbf{b}_{\mu\nu} + \frac{1}{2} m_\rho^2 \mathbf{b}^\mu \mathbf{b}_\mu \quad (1) \end{aligned}$$

In general one can also include terms quartic in ω meson and $\omega - \rho$ interactions. However in the present work we have used NL3 parametrization of the above Lagrangian. In this parametrization coupling of terms quartic in ω meson and $\omega - \rho$ interactions are taken to be zero. In the above equation ψ is nucleon doublet, ϕ , V_μ , and \mathbf{b}_μ denotes σ , ω , ρ meson field, respectively. m_s , m_V , and m_ρ are the masses of the mesons and M_n denotes the nucleon mass. g_s , g_v , and g_ρ are the scalar, vector, and isovector coupling constants, respectively. Field strength tensor of the vector and isovector mesons are given by,

$$V_{\mu\nu} = \partial_\mu V_\nu - \partial_\nu V_\mu, \quad (2)$$

and,

$$\mathbf{b}_{\mu\nu} = \partial_\mu \mathbf{b}_\nu - \partial_\nu \mathbf{b}_\mu \quad (3)$$

ρ meson field can be written explicitly as, $\mathbf{b}^\mu = (b_1^\mu, b_2^\mu, b_3^\mu)$. b_3^μ represents neutral ρ^0 meson and ρ^\pm are the orthogonal linear superposition of b_1^μ and b_2^μ .

$$b_\pm^\mu = \frac{1}{\sqrt{2}}(b_1^\mu \pm b_2^\mu). \quad (4)$$

$\tau = (\tau_1, \tau_2, \tau_3)$ are the Pauli matrices, these are also the isospin operators. Proton and neutron are the different projections of nucleon in isospin space. Operation of τ_3 on neutron and proton is as follows,

$$\tau_3|p\rangle = +1|p\rangle \quad \text{and} \quad \tau_3|n\rangle = -1|n\rangle \quad (5)$$

Numerical values of the all the parameter of the Lagrangian are given in the Table I [37].

III. INTERACTION LAGRANGIAN BETWEEN NUCLEAR MATTER AND DARK MATTER

Due to the galaxy rotation, the compact object like neutron star pass through the dark matter halo and capture dark matter particle from it. Because of the high baryon density inside neutron star, the DM particle loses energy due to its interaction with neutrons. The strong gravitational force of the NS trap the DM after it loses some energy [27,34,40]. There are also other mechanism such as conversion neutrons to scalar dark matter, scalar DM production via bremsstrahlung increases the dark matter density inside the neutron star [32,33]. Since dark matter composed of 95% total matter density, one could possible imagine that many compact objects composed of DM. The amount of dark matter inside NS also depend on the evolution history of NS, the environment where it lives. In Ref. [41], the authors have shown that the binary neutron star systems might enhance DM accumulation probability inside NS.

We consider fermionic dark matter (χ) inside the neutron star. Here we consider the lightest neutralino which acts as a fermionic dark matter candidate [35,42]. Dark matter is not directly coupled with the nucleons rather they are coupled to the Higgs field h . Coupling between the dark matter and the Higgs field is y . For neutralino mass ($M_\chi = 200$ GeV), the value of y varies from 0.001–0.1. We fix $y = 0.07$ for the rest of our analysis [35,42]. The Higgs field is also coupled to the nucleons through effective Yukawa coupling $\frac{f M_n}{v}$, where f the proton-Higgs form factor and its value has been estimated to be approximately 0.35 [43]. We have not considered h^3 and h^4 term in the Higgs potential, because in the mean field approximation the value of the h is small and the only dominant term is the h^2 . So, the dark sector Lagrangian and its interaction with the nucleons and Higgs field is given by [35]

$$\begin{aligned} \mathcal{L}_{\text{DM}} = & \bar{\chi}[i\gamma^\mu \partial_\mu - M_\chi + yh]\chi + \frac{1}{2}\partial_\mu h \partial^\mu h - \frac{1}{2}M_h^2 h^2 \\ & + f \frac{M_n}{v} \bar{\psi} h \psi. \end{aligned} \quad (6)$$

Direct detection experiment such as LUX [44] and XENON [45] excluded dark matter-nucleon cross section above $\sim 8 \times 10^{-47}$ cm² for dark matter mass range 30–50 GeV at 90% C.L.. The invisible Higgs decay width tightly constraint the dark matter below $M_h/2$, hence the dark matter mass $M_\chi = 200$ GeV evades these constraints. It is important to mention that dark matter may not be a single component, it may well be a multicomponent system. Dark matter can consist of low mass as well as high mass particles. As an example in Ref. [35] authors have considered heavy dark matter particles inside the neutron star.

Here we have considered the average number density of nuclear matter is 10^3 times larger than the average dark matter density (n_{DM}), which gives the ratio between mass of the dark matter inside neutron star and mass of the neutron star to be $\sim \frac{1}{6}$ [35]. We know that nuclear saturation density $n_B \sim 0.16$ fm⁻³, so dark matter number density is $n_{\text{DM}} \sim 10^{-3} n_B \sim 0.16 \times 10^{-3}$ fm⁻³. Number density of dark matter $n_{\text{DM}} = \frac{(k_F^{\text{DM}})^3}{3\pi^2}$, which gives $k_F^{\text{DM}} \sim 0.033$ GeV. In our calculations we have varied k_F^{DM} from 0.02 GeV to 0.06 GeV. For these values of k_F^{DM} corresponding dark matter density will be different.

IV. NEUTRON STAR EQUATION OF STATE AND BETA EQUILIBRIUM

The Euler Lagrange equation of motion for nucleon doublet (ψ), scalar(ϕ), vector(V^μ), isovector (\mathbf{b}^μ), DM particle (χ) and Higgs boson (h) can be derived from Lagrangian densities Eqs. (1) and (6) as,

TABLE I. Nucleon masses (M_n), σ meson mass (m_s), ω meson mass (m_v), ρ mass m_ρ and couplings g_s , g_v , g_ρ , g_2 , g_3 of NL3 parametrization [37].

M_n (MeV)	m_s (MeV)	m_v (MeV)	m_ρ (MeV)	g_s	g_v	g_ρ	g_2 (fm $^{-1}$)	g_3
939	508.194	782.501	763.000	10.217	12.868	4.474	-10.431	-28.885

$$\begin{aligned} & \left[\gamma^\mu (i\partial_\mu - g_v V_\mu - g_\rho \boldsymbol{\tau} \cdot \mathbf{b}_\mu) - \left(M_n + g_s \phi - \frac{f M_n}{v} h \right) \right] \psi = 0, \\ & \partial_\mu \partial^\mu \phi + m_s^2 \phi + g_2 \phi^2 + g_3 \phi^3 + g_s \bar{\psi} \psi = 0, \\ & \partial_\mu V^\mu + m_V^2 V^\nu = g_v \bar{\psi} \gamma^\nu \psi, \\ & \partial_\mu \mathbf{b}^\mu + m_\rho^2 \mathbf{b}^\nu = g_\rho \bar{\psi} \gamma^\nu \boldsymbol{\tau} \psi, \\ & (i\gamma_\mu \partial^\mu - M_\chi + y h) \chi = 0, \\ & \partial_\mu \partial^\mu h + M_h^2 h = y \bar{\chi} \chi + \frac{f M_n}{v} \bar{\psi} \psi, \end{aligned} \quad (7)$$

respectively. The DM particle mass and Higgs particle mass are denoted as M_χ and M_h , respectively. Applying standard relativistic mean field approximation we get,

$$\begin{aligned} \phi_0 &= \frac{1}{m_s^2} (-g_s \langle \bar{\psi} \psi \rangle - g_2 \phi_0^2 - g_3 \phi_0^3), \\ V_0 &= \frac{g_v}{m_V^2} \langle \psi^\dagger \psi \rangle = \frac{g_v}{m_V^2} (\rho_p + \rho_n), \\ h_0 &= \frac{y \langle \bar{\chi} \chi \rangle + f \frac{M_n}{v} \langle \bar{\psi} \psi \rangle}{M_h^2}, \\ b_0 &= \frac{g_\rho}{M_\rho^2} \langle \psi^\dagger \tau_3 \psi \rangle = \frac{g_\rho}{M_\rho^2} (\rho_p - \rho_n), \\ (i\gamma^\mu \partial_\mu - g_v \gamma^0 V_0 - g_\rho \tau_3 \gamma^0 b_0 - M_n^*) \psi &= 0, \\ (i\gamma^\mu \partial_\mu - M_\chi^*) \chi &= 0, \end{aligned} \quad (8)$$

where M_n^* and M_χ^* are nucleon and dark matter effective mass, respectively. ρ_p and ρ_n are the densities of proton and neutron, respectively. The effective mass of nucleon and dark matter can be given as,

$$\begin{aligned} M_n^* &= M_n + g_s \phi_0 - \frac{f M_n}{v} h_0, \\ M_\chi^* &= M_\chi - y h_0. \end{aligned} \quad (9)$$

$$\begin{aligned} \epsilon &= g_v V_0 (\rho_p + \rho_n) + g_\rho b_0 (\rho_p - \rho_n) + \frac{1}{\pi^2} \int_0^{k_p} dk k^2 \sqrt{k^2 + (M_n^*)^2} + \frac{1}{\pi^2} \int_0^{k_n} dk k^2 \sqrt{k^2 + (M_n^*)^2} + \frac{1}{\pi^2} \int_0^{k_F^{\text{DM}}} dk k^2 \sqrt{k^2 + (M_\chi^*)^2} \\ &+ \frac{1}{2} m_s^2 \phi_0^2 + \frac{1}{3} g_2 \phi_0^3 + \frac{1}{4} g_3 \phi_0^4 - \frac{1}{2} m_V^2 V_0^2 - \frac{1}{2} m_\rho^2 b_0^2 + \frac{1}{2} M_h h_0^2. \end{aligned} \quad (12)$$

$$\begin{aligned} P &= \frac{1}{3\pi^2} \int_0^{k_p} \frac{k^4 dk}{\sqrt{k^2 + (M_n^*)^2}} + \frac{1}{3\pi^2} \int_0^{k_n} \frac{k^4 dk}{\sqrt{k^2 + (M_n^*)^2}} + \frac{1}{3\pi^2} \int_0^{k_F^{\text{DM}}} \frac{k^4 dk}{\sqrt{k^2 + (M_\chi^*)^2}} \\ &- \frac{1}{2} m_s^2 \phi_0^2 - \frac{1}{3} g_2 \phi_0^3 - \frac{1}{4} g_3 \phi_0^4 + \frac{1}{2} m_V^2 V_0^2 + \frac{1}{2} m_\rho^2 b_0^2 - \frac{1}{2} M_h h_0^2, \end{aligned} \quad (13)$$

The baryon density (ρ), scalar density (ρ_s), and dark matter scalar density (ρ_s^{DM}) are

$$\begin{aligned} \rho &= \langle \psi^\dagger \psi \rangle = \frac{\gamma}{(2\pi)^3} \int_0^{k_F} d^3 k, \\ \rho_s &= \langle \bar{\psi} \psi \rangle = \frac{\gamma}{(2\pi)^3} \int_0^{k_F} \frac{M_n^*}{\sqrt{M_n^{*2} + k^2}} d^3 k, \\ \rho_s^{\text{DM}} &= \langle \bar{\chi} \chi \rangle = \frac{\gamma}{(2\pi)^3} \int_0^{k_F^{\text{DM}}} \frac{M_\chi^*}{\sqrt{M_\chi^{*2} + k^2}} d^3 k, \end{aligned} \quad (10)$$

where k_F and k_F^{DM} are the Fermi momentum for the nucleonic matter and dark matter respectively. γ is the spin degeneracy factor of nucleon and $\gamma = 2$ for neutron and proton individually.

The masses for both nucleon and dark matter depends on baryon density for fixed values of dark matter Fermi momentum k_F^{DM} and coupling constants. These masses and coupling values are discussed in Table I and Sec. III. To get the density dependent profile for M_n^* and M_χ^* , one needs to solve numerically Eq. (10) together with the field equations Eq. (8) in self-consistent manner. In this work, we have taken the average dark matter number density approximately 1000 times smaller than the average neutron number density. This implies the dark matter mass fraction with respect to the neutron star mass is $\approx 1/6$. The expectation values of the energy-momentum tensor or the stress tensor provide the energy density and pressure of the system in the static case, i.e., the EoS, which is given by,

$$\epsilon = \langle T^{00} \rangle \quad \text{and} \quad P = \frac{1}{3} \langle T^{ii} \rangle. \quad (11)$$

The expression for the total energy density (ϵ) and the pressure (P) can be obtained by combining the Lagrangian density Eqs. (1) and (6):

ρ_n and ρ_p are the neutron and proton number density with k_F^n and k_F^p are the corresponding Fermi momentum of neutron and proton, respectively. The number densities and corresponding Fermi momenta are equal for the symmetric nuclear matter. The matter inside the neutron star is mainly composed of neutrons. However, the neutron will eventually $\beta-$ decays as,

$$n \rightarrow p + e^- + \bar{\nu}, \quad (14)$$

$$n + \nu \rightarrow p + e^-. \quad (15)$$

To maintain the neutron star matter charge neutral, muons (μ) will appear when the chemical potential of the electrons reaches the muon rest mass ($m_\mu = 106$ MeV). For a given baryon density ($\rho = \rho_n + \rho_p$), the charge neutrality is given as,

$$\rho_p = \rho_e + \rho_\mu \quad (16)$$

and the $\beta-$ equilibrium condition is given as,

$$\mu_n = \mu_p + \mu_e \quad \text{and} \quad \mu_e = \mu_\mu \quad (17)$$

Where, the chemical potentials μ_p , μ_n , μ_e , and μ_μ are given as,

$$\mu_p = \frac{\partial e}{\partial \rho_p} = g_v V_0 + g_\rho b_0 + \sqrt{k_p^2 + (M_n^*)^2} \quad (18)$$

$$\mu_n = \frac{\partial e}{\partial \rho_n} = g_v V_0 - g_\rho b_0 + \sqrt{k_n^2 + (M_n^*)^2} \quad (19)$$

$$\mu_e = \sqrt{k_e^2 + m_e^2} \quad (20)$$

$$\mu_\mu = \sqrt{k_\mu^2 + m_\mu^2} \quad (21)$$

The particle fractions of neutrons and protons will depend on both charge neutrality and the $\beta-$ equilibrium condition as given above. The self-consistent numerical solution of Eqs. (16) and (17) will set the fraction of neutron, proton, electron, and muon number density for a given baryon density. The total energy density and pressure of leptons are given as,

$$\epsilon_l = \sum_{l=e,\mu} \frac{1}{\pi^2} \int_0^{k_l} k^2 \sqrt{k^2 + m_l^2} dk \quad (22)$$

$$P_l = \sum_{l=e,\mu} \frac{1}{3\pi^2} \int_0^{k_l} \frac{k^4 dk}{\sqrt{k^2 + m_l^2}} \quad (23)$$

The total energy density and pressure for $\beta-$ equilibrated neutron star matter are

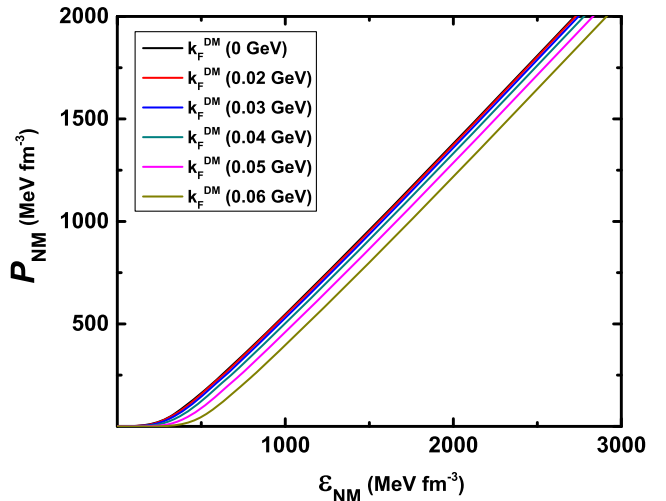


FIG. 1. The equation of states of NS with different dark matter Fermi momenta k_F^{DM} , 0.0–0.06 GeV with a step of 0.02 GeV. The black line corresponds to EoS of NS without dark matter. The EoS becomes softer with increasing number density of dark matter inside the NS.

$$\epsilon_{\text{NM}} = \epsilon_l + \epsilon, \quad (24)$$

$$P_{\text{NM}} = P_l + P. \quad (25)$$

In Fig. 1, we plot pressure (P_{NM}) as function of the total energy density (ϵ_{NM}) for different dark matter Fermi momentum $k_F^{\text{DM}} = 0.0\text{--}0.06$ GeV. Fermi momentum $k_F^{\text{DM}} = 0.0$ GeV corresponds equation of state without dark matter. Increasing the value of k_F^{DM} from 0.02 GeV to 0.06 GeV, the EoS becomes softer, i.e., with increasing density of dark matter pressure reduces, which is consistent with earlier work [35]. This behavior is evident from the expression of energy density and pressure from Eqs. (12) and (13), i.e., with increasing k_F^{DM} the dark matter contribution in energy density increases much faster than the pressure.

Neutron star mass radius relationship can be obtained by solving the TOV equation for a given nuclear matter EoS [46]. The EoS for the core is obtained from the Walecka Model with NL3 parameterization in the presence and absence of dark matter components. Crust EoS is modeled using the BPS EoS [47] for the range of density $\rho \sim 4.8 \times 10^{-9}$ to 2.6×10^{-4} fm $^{-3}$. We use the polytropic form $P_{\text{NM}}(\epsilon_{\text{NM}}) = a_1 + a_2 \epsilon_{\text{NM}}^{\gamma'}$ [48] to join the core and crust of the NS, where a_1 and a_2 are obtained by matching the edge of the core at one end with the inner edge of the outer crust at other end, and γ' is taken 4/3 [49]. In Fig. 2 we plot the mass radius of NS using the EoS as shown in Fig. 1. It is clear from Fig. 1 that the equation state is softer in the presence of larger dark matter density. A softer equation of state gives a lower value of the maximum mass of neutron star. From Fig. 2, the maximum mass without dark matter

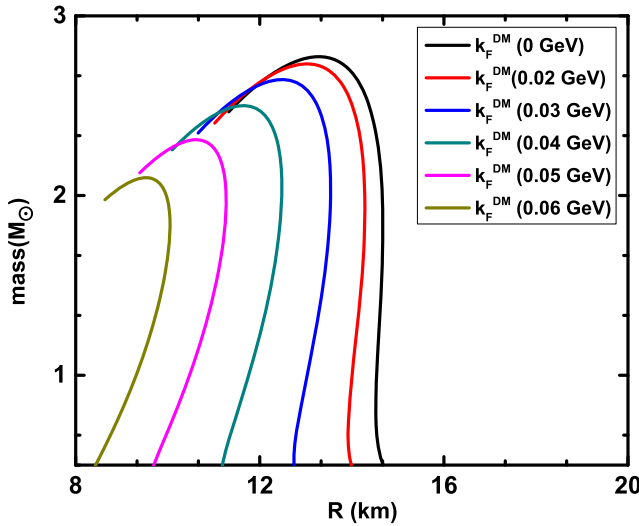


FIG. 2. Mass radius relation of NS for different EoS with dark matter Fermi momentum $k_F^{\text{DM}} = 0.0\text{--}0.06 \text{ GeV}$. The maximum mass of NS without dark matter is $2.8 M_\odot$ and $2.1 M_\odot$ with dark matter Fermi momentum $k_F^{\text{DM}} = 0.06 \text{ GeV}$.

($k_F^{\text{DM}} = 0$) $\sim 2.8 M_\odot$ and the value of the maximum mass of NS decreases with increasing dark matter density.

In the context of dark matter inside the neutron star it is very natural to consider the formation of dark matter core-like structure inside the neutron star with nonuniform distribution of the dark matter. This picture has been explored in various literatures [32,34]. We would like to point out that we are focusing on the mainly qualitative aspect of the presence of dark matter inside the neutron star. The effect of nonuniformly distributed dark matter inside the neutron star on its properties has been discussed in Ref. [34]. In Ref. [34] authors have invoked two-fluid picture of the neutron star containing nuclear matter fluid as well as dark matter fluid inside the neutron star. In that work, authors also have considered the RMF picture for both nuclear fluid as well as dark matter fluid, the mass radius relation in the presence of dark matter for some specific EOS is qualitatively similar to our result, e.g., in the presence of dark matter, mass of neutron star can decrease. They have also shown that for mass of the dark matter (M_{DM}) can be large e.g., $0.33 M_\odot$. However, if one assumes a RMF kind of situation for the dark matter sector then the coupling of the dark matter particle with a scalar, vector particles etc. will be free parameters of the theory. In the nuclear matter sector, the coupling constants have been fixed keeping in mind the finite nuclei properties, but for the dark matter, these constraints are not available. Hence these free coupling constants in the dark matter sector will make the model less predictive.

Tidal deformability also depends upon the compactness and equation of state. In the next section, we study the effect of dark matter on nuclear matter EoS using the tidal deformability constraint from GW170817 observation.

V. TIDAL DEFORMABILITY CONSTRAINT

One of the important measurable structural properties of a binary merger is the tidal deformability. In a coalescing binary NS system, during the last stage of inspiral, each NS develops a mass quadrupole due to the tidal gravitational field induced by the other NS forming the binary. The tidal deformability describes the degree of deformation of a NS due to the tidal field of the companion NS and is sensitive to the nature of the EoS. The tidal deformability is defined as,

$$\lambda = \frac{2}{3} k_2 R^5, \quad (26)$$

where R is the radius of the NS. The value of k_2 is typically in the range $\approx 0.05\text{--}0.15$ [16–18] for NSs and depends on the stellar structure. This quantity can be calculated using the following expression [16]

$$\begin{aligned} k_2 = & \frac{8C^5}{5} (1 - 2C)^2 [2 + 2C(y_R - 1) - y_R] \\ & \times \{2C(6 - 3y_R + 3C(5y_R - 8)) \\ & + 4C^3[13 - 11y_R + C(3y_R - 2) + 2C^2(1 + y_R)] \\ & + 3(1 - 2C)^2[2 - y_R + 2C(y_R - 1)] \log(1 - 2C)\}^{-1}, \end{aligned} \quad (27)$$

where C ($\equiv M/R$) is the compactness parameter of the star of mass M . The quantity y_R ($\equiv y(R)$) can be obtained by solving the following differential equation

$$r \frac{dy(r)}{dr} + y(r)^2 + y(r)F(r) + r^2Q(r) = 0 \quad (28)$$

with

$$\begin{aligned} F(r) &= \frac{r - 4\pi r^3(\epsilon(r) - p(r))}{r - 2M(r)}, \\ Q(r) &= \frac{4\pi r(5\epsilon(r) + 9p(r) + \frac{\epsilon(r) + p(r)}{\partial p(r)/\partial \epsilon(r)} - \frac{6}{4\pi r^2})}{r - 2M(r)} \\ &\quad - 4 \left[\frac{M(r) + 4\pi r^3 p(r)}{r^2(1 - 2M(r)/r)} \right]^2, \end{aligned}$$

along with the TOV equation with proper boundary conditions [46,50]. One can then define the dimensionless tidal deformability: $\Lambda = \frac{2}{3} k_2 C^{-5}$.

Individual dimensionless tidal deformability of two stars, Λ_1 and Λ_2 cannot be extracted independently from the observed gravitational waveform. Instead, an effective dimensionless tidal deformability of the binary $\tilde{\Lambda}$ can be extracted, which is a mass-weighted average of the individual dimensionless tidal deformability Λ_1 and Λ_2 . The effective tidal deformability ($\tilde{\Lambda}$) of binary system in terms of Λ_1 and Λ_2 is defined as [51]

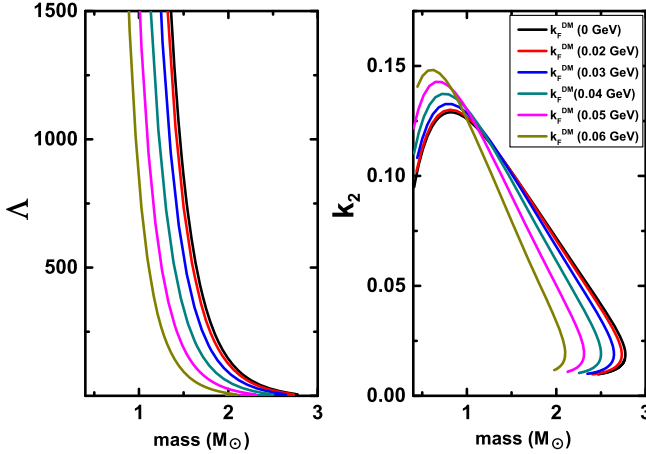


FIG. 3. Dimensionless tidal deformability (Λ) of NS and Love number (k_2) as a function of neutron star mass for different dark matter Fermi momentum is shown.

$$\tilde{\Lambda} = \frac{16}{13} \frac{(m_1 + 12m_2)m_1^4\Lambda_1 + (m_2 + 12m_1)m_2^4\Lambda_2}{(m_1 + m_2)^5} \quad (29)$$

where m_1 and m_2 are the masses of the neutron stars in the binary. Similarly, masses of the two companion neutron stars cannot be measured directly, rather the chirp mass, $\mathcal{M}_c = (m_1 m_2)^{3/5}(m_1 + m_2)^{-1/5}$, which is measured directly. By assuming low-spin prior which is consistent with the binary neutron star systems that have been observed in, GW170817 put an upper bound on the NSs combined dimensionless tidal deformability and chirp mass with 90% confidence [15]. This analysis predicts that the combined dimensionless tidal deformability of the NS merger is $\tilde{\Lambda} \leq 800$. It is important to note that a reanalysis of GW170817 observation has been done assuming the same EoS for both stars and this puts an upper limit on the dimensionless tidal deformability, $\tilde{\Lambda} \leq 1000$ [52]. However lower bound on dimensionless tidal deformability can be put using the investigation of the UV/optical/infrared counterpart of GW170817 with kilonova models [53]. The lower bound of dimensionless tidal deformability is $\tilde{\Lambda} \geq 400$.

One of the important goals of this work is to study the structural properties of neutron stars in the presence of the dark matter component. For the sake of arguments it is important to understand the behavior of dimensionless tidal deformability and the tidal Love number of the companion neutron stars. Solving Eq. (28) and the TOV equation with appropriate boundary conditions, we get y_R . Using the value of y_R and compactness one can get k_2 using the expression Eq. (27). Left plot in Fig. 3 shows the dimensionless tidal deformability Λ and the right plot shows tidal Love number k_2 as a function of the NS mass for our EoS with different dark matter density. The value of k_2 is of the range 0.09–0.13 for a typical neutron star of mass $1.5 M_\odot$, which is expected [16,17]. For a given

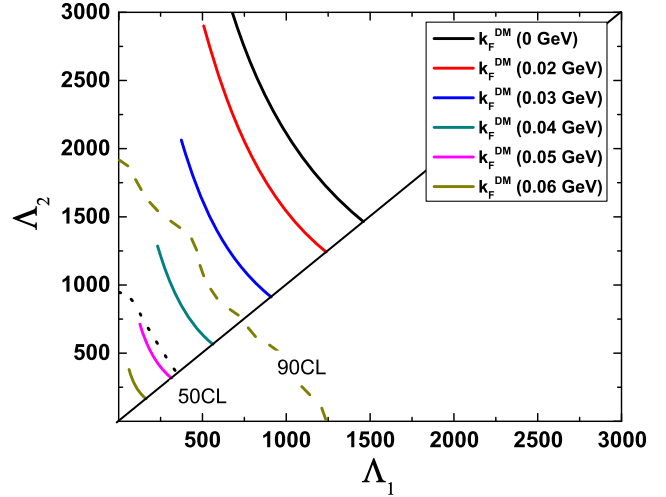


FIG. 4. Tidal deformability parameters of the low and high mass components of binary neutron star merger (GW170817 observation). Dashed line and dotted line indicates 90% and 50% confidence limit for low spin priors [15]. The diagonal solid line corresponds to $\Lambda_1 = \Lambda_2$ boundary. The Walecka model with NL3 parametrization is disfavored by GW observation at 90% C.L. in the absence of dark matter, i.e., $k_F^{\text{DM}} = 0.0$ GeV. Note that low dark matter density, e.g., $k_F^{\text{DM}} = 0.03$ GeV is also disfavored. However, the Walecka model in NL3 parametrization with relatively higher DM density, e.g., $k_F^{\text{DM}} = 0.04$ –0.06 GeV is allowed by 90% C.L. of the GW170817 observation.

neutron star mass (say around $1.5 M_\odot$) EoS without the dark matter predicts larger radius and with increasing dark matter density radius decreases. Since the dimensionless tidal deformability is inversely proportional to the compactness ($C = M/R$), its value is larger in the absence of dark matter.

To study the tidal deformability constraint from the GW170817 observation on EoS of NS, we plot the combined tidal deformability of the binary system in Λ_1 , Λ_2 plane in Fig. 4. Λ_1 and Λ_2 are the individual dimensionless tidal deformability of the high mass m_1 and low mass m_2 neutron stars in a binary, respectively. The curves are corresponding to the EoS with different dark matter density and obtained by varying m_1 and m_2 independently. m_1 has been taken in the range $1.365 < m_1/M_\odot < 1.60$ and the range of the m_2 is determined by keeping the chirp mass \mathcal{M}_c fixed at $1.188 M_\odot$. The dashed and the dot lines represent, respectively, the 90% and 50% confidence limits of the combined dimensionless tidal deformability obtained from the GW170817 for the low spin prior. One can see from this plot that EoS given by the NL3 parametrization without dark matter component can be excluded at 90% confidence level using the upper bound on tidal deformability of a binary system. However if we consider dark matter component in neutron stars, then NL3 parametrized EoS comes within the 90% confidence level. Hence a small component of dark matter inside a neutron

star can revive well-known EoS, which otherwise might be excluded by the GW170817 observation.

VI. CONCLUSIONS

We have confronted the neutron star equation of state in the presence of dark matter component using the gravitational wave constraint from the binary star merger. We have shown that for a uniformly distributed dark matter inside neutron star, the EoS becomes softer which eventually produces lower NS mass with increasing dark matter density. We have taken the Walecka model with NL3 parametrization in the nuclear matter sector. The Walecka model with NL3 parametrization without dark matter admixture gives rise to a maximum mass of NS $\sim 2.8 M_{\odot}$. By increasing dark matter density (Fermi momentum) inside neutron star reduces the value of maximum mass. The value of the maximum mass of neutron star changes from $2.8 M_{\odot}$ to $2.1 M_{\odot}$ by increasing

dark matter Fermi momentum from 0.0 GeV to 0.06 GeV. One of the striking results of our analysis is that the stiffer equation of states such as relativistic mean field model (Walecka model) with NL3 parametrization is ruled out at 90% C.L. using the GW170817 observation. However, in the presence of dark matter this constraint can be evaded and NL3 parametrization can be brought within 90% C.L.

ACKNOWLEDGMENTS

T. M. acknowledges the hospitality provided by Physical Research Laboratory (PRL), Ahmedabad, India, during his visit, where the work has been initiated. T. M. is also grateful to the Science and Engineering Research Board (SERB), Govt. of India for the international travel support (ITS/2018/002448). We would like to thank Prof. Hiramaya Mishra for constant encouragement and support.

-
- [1] J. M. Lattimer, *Annu. Rev. Nucl. Part. Sci.* **62**, 485 (2012).
 - [2] J. D. Walecka, *Ann. Phys. (N.Y.)* **83**, 491 (1974).
 - [3] B. D. Serot and J. D. Walecka, *Int. J. Mod. Phys. E* **06**, 515 (1997).
 - [4] J. Boguta and A. R. Bodmer, *Nucl. Phys.* **A292**, 413 (1977); J. Boguta and H. Stoecker, *Phys. Lett.* **120B**, 289 (1983); J. Boguta, *Phys. Lett.* **106B**, 255 (1981).
 - [5] Y. K. Gambhir, P. Ring, and A. Thimet, *Ann. Phys. (N.Y.)* **198**, 132 (1990).
 - [6] P. Ring, *Prog. Part. Nucl. Phys.* **37**, 193 (1996).
 - [7] M. Dutra, O. Lourenço, S. S. Avancini, B. V. Carlson, A. Delfino, D. P. Menezes, C. Providência, S. Typel, and J. R. Stone, *Phys. Rev. C* **90**, 055203 (2014).
 - [8] G. Baym, C. Pethick, D. Pines, and M. Ruderman, *Nature (London)* **224**, 872 (1969).
 - [9] W. C. G. Ho, C. M. Espinoza, D. Antonopoulos, and N. Andersson, *J. Phys. Soc. Jpn. Conf. Proc.* **14**, 010805 (2017).
 - [10] F. Weber, *J. Phys. G* **25**, R195 (1999).
 - [11] M. Prakash, *J. Phys. G* **34**, S253 (2007).
 - [12] F. Weber, M. Meixner, P. Negreiros, and M. Malheiro, *Int. J. Mod. Phys. E* **16**, 1165 (2007).
 - [13] F. Weber, O. Hamil, K. Mimura, and R. Negreiros, *Int. J. Mod. Phys. D* **19**, 1427 (2010).
 - [14] B. P. Abbott *et al.*, *Phys. Rev. Lett.* **119**, 161101 (2017).
 - [15] B. P. Abbott *et al.*, *Phys. Rev. Lett.* **121**, 161101 (2018).
 - [16] T. Hinderer, *Astrophys. J.* **677**, 1216 (2008).
 - [17] T. Hinderer, B. D. Lackey, R. N. Lang, and J. S. Read, *Phys. Rev. D* **81**, 123016 (2010).
 - [18] S. Postnikov, M. Prakash, and J. M. Lattimer, *Phys. Rev. D* **82**, 024016 (2010).
 - [19] K. Yagi and N. Yunes, *Science* **341**, 365 (2013); *Phys. Rev. D* **88**, 023009 (2013).
 - [20] K. Yagi, L. C. Stein, G. Pappas, N. Yunes, and T. A. Apostolatos, *Phys. Rev. D* **90**, 063010 (2014).
 - [21] L. Rezzolla, E. R. Most, and L. R. Weih, *Astrophys. J.* **852**, L25 (2018).
 - [22] L. Rezzolla, E. R. Most, L. R. Weih, and J. Schaffner-Bielich, *Phys. Rev. Lett.* **120**, 261103 (2018).
 - [23] M. Bauer and T. Plehn, *arXiv:1705.01987*.
 - [24] N. Raj, P. Tanedo, and H. B. Yu, *Phys. Rev. D* **97**, 043006 (2018).
 - [25] I. Goldman and S. Nussinov, *Phys. Rev. D* **40**, 3221 (1989).
 - [26] A. Gould, B. T. Draine, R. W. Romani, and S. Nussinov, *Phys. Lett. B* **238**, 337 (1990).
 - [27] C. Kouvaris, *Phys. Rev. D* **77**, 023006 (2008).
 - [28] C. Kouvaris and P. Tinyakov, *Phys. Rev. D* **82**, 063531 (2010).
 - [29] A. de Lavallaz and M. Fairbairn, *Phys. Rev. D* **81**, 123521 (2010).
 - [30] T. Guver, A. E. Erkoca, M. H. Reno, and I. Sarcevic, *J. Cosmol. Astropart. Phys.* **05** (2014) 013.
 - [31] Yi-zhong Fan, Rui-zhi Yang, and J. Chang, *arXiv:1204.2564*.
 - [32] J. Ellis, G. Hutsi, K. Kannike, L. Marzola, M. Raidal, and V. Vaskonen, *Phys. Rev. D* **97**, 123007 (2018).
 - [33] J. Ellis, A. Hektor, G. Hutsi, K. Kannike, L. Marzola, M. Raidal, and V. Vaskonen, *Phys. Lett. B* **781**, 607 (2018).
 - [34] Q.-F. Xiang, W.-Z. Jiang, D.-R. Zhang, and R.-Y. Yang, *Phys. Rev. C* **89**, 025803 (2014).
 - [35] G. Panotopoulos and I. Lopes, *Phys. Rev. D* **96**, 083004 (2017).
 - [36] K. C. Chung, C. S. Wang, A. J. Santiago, and J. W. Zhang, *Eur. Phys. J. A* **11**, 137 (2001).

- [37] G. A. Lalazissis, J. Konig, and P. Ring, *Phys. Rev. C* **55**, 540 (1997).
- [38] J. Boguta, *Phys. Lett.* **106B**, 245 (1981).
- [39] *Advances in Nuclear Physics*, edited by J. W. Negele and E. Vogt (Plenum, New York, 1986), Vol. 16.
- [40] I. Goldman and S. Nussinov, *Phys. Rev. D* **40**, 3221 (1989).
- [41] L. Brayer and P. Tinyakov, *Phys. Rev. Lett.* **109**, 061301 (2012).
- [42] S. P. Martin, *Adv. Ser. Dir. High Energy Phys.* **21**, 1 (2010); B. Murakami and J. D. Wells, *Phys. Rev. D* **64**, 015001 (2001).
- [43] J. M. Cline, K. Kainulainen, P. Scott, and C. Weniger, *Phys. Rev. D* **88**, 055025 (2013); **92**, 039906(E) (2015).
- [44] C. Frederico Pascoal da Silva (LUX Collaboration), arXiv:1710.03572.
- [45] E. Aprile *et al.* (Xenon Collaboration), *Phys. Rev. Lett.* **119**, 181301 (2017).
- [46] J. R. Oppenheimer and G. M. Volkoff, *Phys. Rev.* **55**, 374 (1939).
- [47] G. Baym, C. Pethick, and P. Sutherland, *Astrophys. J.* **170**, 299 (1971).
- [48] J. Carriere, C. J. Horowitz, and J. Piekarewicz, *Astrophys. J.* **593**, 463 (2003).
- [49] T. Malik, K. Banerjee, T. K. Jha, and B. K. Agrawal, *Phys. Rev. C* **96**, 035803 (2017).
- [50] T. Malik, N. Alam, M. Fortin, C. Providencia, B. K. Agrawal, T. K. Jha, B. Kumar, and S. K. Patra, *Phys. Rev. C* **98**, 035804 (2018).
- [51] C. Raithel, F. Ozel, and D. Psaltis, *Astrophys. J.* **857**, L23 (2018).
- [52] S. De, D. Finstad, J. M. Lattimer, D. A. Brown, E. Berger, and C. M. Biwer, *Phys. Rev. Lett.* **121**, 091102 (2018); **121**, 259902(E) (2018).
- [53] D. Radice, A. Perego, F. Zappa, and S. Bernuzzi, *Astrophys. J. Lett.* **852**, L29 (2018).



Cooling of dark-matter admixed neutron stars with density-dependent equation of state

Sajad A. Bhat^a, Avik Paul^b

Astroparticle Physics and Cosmology Division, Saha Institute of Nuclear Physics, HBNI, 1/AF Bidhannagar, Kolkata 700064, India

Received: 12 August 2019 / Accepted: 23 May 2020 / Published online: 16 June 2020
© The Author(s) 2020

Abstract We propose a dark-matter (DM) admixed density-dependent equation of state where the fermionic DM interacts with the nucleons via Higgs portal. Presence of DM can hardly influence the particle distribution inside neutron star (NS) but can significantly affect the structure as well as equation of state (EOS) of NS. Introduction of DM inside NS softens the equation of state. We explored the effect of variation of DM mass and DM Fermi momentum on the NS EOS. Moreover, DM-Higgs coupling is constrained using dark matter direct detection experiments. Then, we studied cooling of normal NSs using APR and DD2 EOSs and DM admixed NSs using dark-matter modified DD2 with varying DM mass and Fermi momentum. We have done our analysis by considering different NS masses. Also DM mass and DM Fermi momentum are varied for fixed NS mass and DM-Higgs coupling. We calculated the variations of luminosity and temperature of NS with time for all EOSs considered in our work and then compared our calculations with the observed astronomical cooling data of pulsars namely Cas A, RX J0822-43, 1E 1207-52, RX J0002+62, XMMU J17328, PSR B1706-44, Vela, PSR B2334+61, PSR B0656+14, Geminga, PSR B1055-52 and RX J0720.4-3125. It is found that APR EOS agrees well with the pulsar data for lighter and medium mass NSs but cooling is very fast for heavier NS. For DM admixed DD2 EOS, it is found that for all considered NS masses, all chosen DM masses and Fermi momenta agree well with the observational data of PSR B0656+14, Geminga, Vela, PSR B1706-44 and PSR B2334+61. Cooling becomes faster as compared to normal NSs in case of increasing DM mass and Fermi momenta. It is inferred from the calculations that if low mass super cold NSs are observed in future that may support the fact that heavier WIMP can be present inside neutron stars.

1 Introduction

Neutron stars are excellent celestial laboratories for investigating the supradense nuclear matter which is otherwise inaccessible to terrestrial laboratories. The density inside neutron stars is several times the saturated nuclear density, hence exotic particles like hyperons [1,2], pion or kaon condensate [3,4] and quarks [5] are believed to be present inside the core. Dark matter (DM) particles may also be captured and accumulated inside neutron stars [6–8]. Exotic particles soften the equation of state (EOS) and reduce the tidal deformability of the neutron star [9]. Exact nature of the matter is a challenging task and yet to be known. Any model suggested should not only describe the superdense matter but also reproduce the properties of matter observed at saturation densities [10,11]. Recently, the unprecedented joint detection of neutron star merger GW170817 by Advanced LIGO and Virgo observatories has put stronger constraints on the equation of state by constraining tidal deformability of NSs [12,13]. Using Shapiro delay measurements, a very massive neutron star has been found in the form of PSRJ0740+6620 with mass $2.17^{+0.11}_{-0.10}$ [14]. This can put stringent constraint on the equation of state.

Nowadays there are various cosmological and astrophysical indications for the existence of dark matter in the Universe like rotation curves of spiral galaxies, large-scale structures of the Universe, anisotropies of cosmic microwave background radiation (CMBR), gravitational lensing etc. The detection of dark matter is attempted following three different ways i.e. direct detection, indirect detection and collider searches (LHC). However, till now no experimental signature of dark matter has been discovered. Direct detection experiments put upper bounds on the dark matter-nucleon elastic scattering cross-sections for different DM masses. In the literature, many theoretical particle dark matter models are proposed to indirectly detect the dark matter and to explain the existence of few unsolved phenomenological evi-

^a e-mail: sajad.bhat@saha.ac.in (corresponding author)

^b e-mail: avik.paul@saha.ac.in

dences such as gamma ray excesses observed by Fermi-LAT gamma ray telescope [15, 16], positron excesses measured by PAMELA [17], AMS-02 [18], DAMPE [19] experiments etc. Till now many particle candidates of dark matter are proposed like Weakly Interacting Massive Particles (WIMPs) [20–24], Axions [25, 26], Fuzzy dark matter [29, 30], neutralino [20], Kaluza Klein dark matter [31] etc. In this work our proposed particle candidate of dark matter is WIMP. In the early Universe, WIMPs are produced thermally and initially they are at thermal equilibrium but when the temperature drops below the WIMPs mass they are decoupled at a particular temperature ($\sim \frac{M_\chi}{20}$) called freeze-out temperature. After decoupling, WIMP would possibly be a relic particle and may constitute a particle candidate of cold dark matter (CDM). WIMPs can cluster with stars gravitationally and also form a background density in the universe.

Several studies have indicated that neutron stars being highly compact objects can capture more dark matter particles during the formation stage in the supernova explosion as compared to the non-compact objects [32]. Recently, it is shown that the admixture of DM inside NSs softens the equation of state and hence tidal deformability is reduced [7]. It has been proven in [33] that the DM capture could be highly improved if it happens in binary pulsars. Since the DM present inside DM admixed NSs can possibly change the global properties of neutron stars, this open another indirect window to study DM apart from the other numerous ways. The structures of DM admixed NSs have been studied recently. It is shown that mass and radius of NSs can be remarkably affected by mirror DM [34]. It has been shown that fermionic DM could soften the equation of state and hence reduce the maximum mass supported by the NS [7]. This effect is sensitive to the mass of DM particle and the self-interaction within the dark matter. Since the normal matter and DM are believed to interact gravitationally, presence of DM can hardly influence the the particle distribution inside NS but can significantly affect the structure as well as EOS of NS.

Cooling of neutron stars have been well studied by several authors [35–39]. Some study has been done on the effect of DM on cooling of NSs [40–42]. It has been found that the heating due to dark matter annihilation can affect the temperature of the stars older than 10^7 years and consequently flattening out the temperature at 10^4 K for the neutron stars [41]. Moreover, recently it has been found that slowdown in the pulsar rotation can drive the NS matter out of beta equilibrium and the resultant imbalance in chemical potentials can induce late-time heating, named as rotochemical heating which can heat a NS up to 10^6 K for $t = 10^6 - 10^7$ years [42]. In Ref. [40], the authors have studied the cooling of DM admixed NS with dark matter mass ranging from 0.1 GeV to

1.3 GeV. In the present work, we have considered low as well as high dark matter masses (upto 500 GeV) and also varied the dark matter Fermi momenta for the cooling calculations. For these calculations, we have considered dark-matter modified density-dependent (DD2) EOS [43,44] and the results are compared with the observational data. Also, our work is different from the above mentioned works [41,42] because we don't consider heating due to WIMP annihilation owing to the very small annihilation cross-section. We consider indirect effect on cooling of NS stars due to change in the neutron star structure in presence of dark matter. With the introduction of dark matter, cooling properties can change significantly as compared to the normal NSs mainly because of changes in neutrino emissivity, neutrino luminosity and heat capacity. For given mass, neutron emissivity will be different due to significant change in stellar structures and consequently, neutrino luminosity will also be different. Heat capacity related to EOS will be different for normal NSs and DM admixed NSs because of softening of the EOS in case of the latter. Thus, normal NSs can be distinguished from DM admixed NSs using astronomical observation data related to surface temperature and age of pulsars. We have considered the complete set of cooling data of both young and cool and old and warm neutron stars namely Cas A, RX J0822-43, 1E 1207-52, RX J0002+62, XMMU J17328, PSR B1706-44, Vela, PSR B2334+61, PSR B0656+14, Geminga, PSR B1055-52 and RX J0720.4-3125. We adopted the temperature data sets of the above mentioned pulsars from the Refs. [7,45,48] and the luminosity data from the Ref. [49] (Table 1 and 3). As representatives for late time-cooling, a group of above mentioned three NSs (PSR B0656+14, Geminga and PSR B1055-52) is chosen forming a class of nearby objects that allows spectral fits to their X-ray emission ([50–53] and references therein). We studied NS cooling of both normal NSs using DD2 EOS [43,44] and Akmal-Pandharipande-Ravenhall (APR) EOS [54] and DM admixed NSs using DD2 EOS modified with DM sector. It is important to mention here that although DD2 is marginally allowed by the tidal deformability constraint obtained from the analysis of GW170817 with Phenom PNRT model [55], DM admixed DD2 will be softened and might be considerably allowed by the GW170817 constraints. Earlier DM admixed NSs are studied by some groups [6–8] where they adopted σ - ω - ρ model but our approach differs from theirs in the sense that meson-nucleon couplings are density-dependent in our model which gives rise to an extra term called rearrangement term [44,56] in the nucleon chemical potential.

This paper is organised as follows. In Sect. 2, we describe baryonic EOS model and DM admixed baryonic EOS model. We constrain dark matter-Higgs coupling parameter from the direct detection experiments as discussed in Sect. 3. In Sect. 4, we discuss the cooling mechanism of neutron star.

Furthermore, the results and calculations are presented in Sect. 5. Finally, we conclude our work in Sect. 6.

2 Equation of state model

In this section, we utilize density-dependent relativistic hadron field theory for describing strongly interacting super-dense nuclear matter inside neutron stars. Nucleon-nucleon strong interaction is mediated by the exchanges of scalar σ meson, responsible for strong attractive force, vector ω , responsible for strong repulsive force and ρ meson, responsible for symmetry energy. The Lagrangian density [43,44] is given by

$$\begin{aligned} \mathcal{L}_B = & \sum_B \bar{\psi}_B (i\gamma_\mu \partial^\mu - m_B + g_{\sigma B} \sigma - g_{\omega B} \gamma_\mu \omega^\mu \\ & - g_{\rho B} \gamma_\mu \boldsymbol{\tau}_B \cdot \boldsymbol{\rho}^\mu) \psi_B \\ & + \frac{1}{2} (\partial_\mu \sigma \partial^\mu \sigma - m_\sigma^2 \sigma^2) - \frac{1}{4} \omega_{\mu\nu} \omega^{\mu\nu} \\ & + \frac{1}{2} m_\omega^2 \omega_\mu \omega^\mu \\ & - \frac{1}{4} \boldsymbol{\rho}_{\mu\nu} \cdot \boldsymbol{\rho}^{\mu\nu} + \frac{1}{2} m_\rho^2 \boldsymbol{\rho}_\mu \cdot \boldsymbol{\rho}^\mu, \end{aligned} \quad (1)$$

where ψ_B denotes the nucleon fields, $\boldsymbol{\tau}_B$ is the isospin operator and g_s represent the density-dependent meson-baryon couplings. These couplings are determined by following the prescription adopted by Typel et al. [44,57]. The functional dependence of the couplings on density was introduced for the first time in [58] as described here

$$g_{\alpha B}(\rho_b) = g_{\alpha B}(\rho_0) f_\alpha(x), \quad (2)$$

where ρ_b is the total baryon density, $x = \rho_b/\rho_0$ and $f(x) = a_\alpha \frac{1+b_\alpha(x+d_\alpha)}{1+c_\alpha(x+d_\alpha)}$ for $\alpha = \omega, \sigma$. In order to reduce parameters, the functions are constrained as $f_\sigma(1) = f_\omega(1) = 1$, $f'_\sigma(0) = f'_\omega(0) = 0$, $f''_\sigma(1) = f''_\omega(1)$. Exponential density dependence i.e. $f(x) = \exp[-a_\alpha(x-1)]$ [58] is considered for the isovector meson $\boldsymbol{\rho}_\mu$ because $g_{\rho B}$ decreases at higher densities. Finite nuclear properties are fitted to determine the saturation density, the mass of σ meson, the couplings $g_{\alpha B}(\rho_0)$ and the coefficients $a_\alpha, b_\alpha, c_\alpha$ and d_α [44,57]. The fit provides the saturation density $\rho_0 = 0.149065 \text{ fm}^{-3}$, binding energy per nucleon as -16.02 MeV and compressibility factor $K = 242.7 \text{ MeV}$. The nucleon mass M_n is considered to be 939 MeV through out our work.

Leptons are treated as non-interacting particles and described by the free Lagrangian density

$$\mathcal{L}_l = \sum_l \bar{\psi}_l (i\gamma_\mu \partial^\mu - m_l) \psi_l, \quad (3)$$

where $l = e^-, \mu^-$ and $m_l = m_e, m_\mu$. The energy and pressure due to leptons will be explicitly mentioned in Sect. 2.1.

2.1 Effect of dark matter on equation of state

A uniformly distributed fermionic dark matter (WIMP) is considered inside neutron star. Dark matter interacts with Higgs field h with coupling strength y . DM-Higgs coupling y is explicitly discussed in Sect. 3. Three different WIMP masses ($M_\chi = 50 \text{ GeV}, 200 \text{ GeV}, 500 \text{ GeV}$) are considered in our calculations. Higgs field h interacts with the nucleons via effective Yukawa coupling $f M_n/v$, where f denotes the nucleon-Higgs form factor and is estimated to be approximately 0.3 [59] and $v = 246.22 \text{ GeV}$ denotes Higgs vacuum expectation value (VEV). In the Higgs potential, terms higher than quadratic are dropped because they are negligible in the mean field approximation (MFA). Hence the dark sector and its interaction with nucleons and Higgs field is described by the Lagrangian density

$$\begin{aligned} \mathcal{L}_{DM} = & \bar{\chi} (i\gamma_\mu \partial^\mu - M_\chi + yh) \chi + \frac{1}{2} \partial_\mu h \partial^\mu h \\ & - \frac{1}{2} M_h^2 h^2 + f \frac{M_n}{v} \bar{\psi} h \psi. \end{aligned} \quad (4)$$

Here we consider the assumption that the average dark matter number density inside neutron star is 10^3 times smaller than saturated nuclear matter number density [6,60] and the Fermi momentum of dark matter is constant [6] through out the neutron star. With these assumptions, the fractional mass of dark matter inside neutron star for $M_\chi = 200 \text{ GeV}$ can be expressed as

$$\frac{M_\chi}{M_{NS}} \approx \frac{1}{6}.$$

Given $\rho_0 = 0.149065 \text{ fm}^{-3}$, dark matter number density is $\rho_{DM} \sim 10^{-3} \rho_0 \sim 0.15 \times 10^{-3} \text{ fm}^{-3}$. Number density of dark matter is related to Fermi momentum via $\rho_{DM} = \frac{(k_F^{DM})^3}{3\pi^2}$ which gives $k_F^{DM} \sim 0.033 \text{ GeV}$. We vary k_F^{DM} in our calculations from 0.01 GeV to 0.06 GeV and dark matter densities ρ_{DM} will also vary accordingly. Equations of motion for nucleon doublet

$$\psi = \begin{bmatrix} \psi_p \\ \psi_n \end{bmatrix},$$

scalar meson (σ), vector meson (ω^μ) and isovector meson ($\boldsymbol{\rho}^\mu$), DM particle (χ) and Higgs boson h can be derived from Eqs. (1) and (4) as

$$\begin{aligned} & \left[\gamma^\mu (i\partial_\mu - \Sigma_B) - \left(M_n - g_{\sigma B} \sigma - \frac{f M_n}{v} h \right) \right] \psi_B = 0, \\ & \partial_\mu \partial^\mu \sigma + m_\sigma^2 \sigma = g_{\sigma B} \bar{\psi}_B \psi_B, \\ & \partial_\mu \omega^{\mu\nu} + m_\omega^2 \omega^\nu = g_{\omega B} \bar{\psi}_B \gamma^\nu \psi_B, \\ & \partial_\mu \boldsymbol{\rho}^{\mu\nu} + m_\rho^2 \boldsymbol{\rho}^\nu = g_{\rho B} \bar{\psi}_B \gamma^\nu \boldsymbol{\tau}_B \psi_B, \\ & (i\gamma_\mu \partial^\mu - M_\chi + yh) \chi = 0, \end{aligned}$$

Table 1 Meson masses and parameters of meson-nucleon couplings in DD2 EOS

Meson α	m_α in MeV	$g_{\alpha B}(\rho_0)$	a_α	b_α	c_α	d_α
ω	783.0	13.342362	1.369718	0.496475	0.817753	0.638452
σ	546.212459	10.686681	1.357630	0.634442	1.005358	0.575810
ρ	763.0	3.626940	0.518903			

$$\partial_\mu h \partial^\mu h + M_h^2 h^2 = y \bar{\chi} \chi + f \frac{M_n}{v} \bar{\psi}_B \psi_B, \quad (5)$$

where masses of DM particle and Higgs particle are denoted by M_χ and $M_h = 125.09$ GeV respectively. $\Sigma_B = \Sigma_B^0 + \Sigma_B^r$ is the vector self energy in which the first term consists of the usual non-vanishing components of vector mesons i.e. $\Sigma_B^0 = g_{\omega B} \omega_0 - g_{\rho B} \tau_{3B} \rho_{03}$ and the second term is the rearrangement term i.e. $\Sigma_B^r = \sum_B \left[-g'_{\sigma B} \sigma \rho_B^s + g'_{\omega B} \omega_0 \rho_B + g'_{\rho B} \tau_{3B} \rho_{03} \rho_B \right]$ which appears because of density-dependence of meson-nucleon couplings [56]. Here $g'_{\alpha B} = \frac{\partial g_{\alpha B}}{\partial \rho_B}$ where $\alpha = \sigma, \omega, \rho$ and τ_{3B} is the isospin projection of $B = n, p$. Due to density dependence of nucleon-meson couplings, chemical potential of the nucleons takes the form

$$\mu_B = \sqrt{k_B^2 + M_n^{*2}} + \Sigma_B^0 + \Sigma_B^r.$$

In the mean-field approximation (MFA), fields are replaced by their expectation values and above equations are simplified as

$$\begin{aligned} \sigma &= \frac{1}{m_\sigma^2} (g_{\sigma B} \langle \bar{\psi}_B \psi_B \rangle), \\ \omega_0 &= \frac{g_{\omega B}}{m_\omega^2} \langle \psi_B^\dagger \psi_B \rangle = \frac{g_{\omega B}}{m_\omega^2} (\rho_p + \rho_n), \\ h_0 &= \frac{y \langle \bar{\chi} \chi \rangle + f \frac{M_n}{v} \langle \bar{\psi}_B \psi_B \rangle}{M_h^2}, \\ \rho_{03} &= \frac{g_{\rho B}}{m_\rho^2} \langle \psi_B^\dagger \tau_{3B} \psi_B \rangle = \frac{g_{\rho B}}{m_\rho^2} (\rho_p - \rho_n), \\ (i\gamma^\mu \partial_\mu - \Sigma_B - M_n^*) \psi_B &= 0, \\ (i\gamma^\mu \partial_\mu - M_\chi^*) \chi &= 0. \end{aligned} \quad (6)$$

The effective masses of nucleons and dark matter are respectively given as

$$\begin{aligned} M_n^* &= M_n - g_{\sigma B} \sigma - \frac{f M_n}{v} h_0, \\ M_\chi^* &= M_\chi - y h_0. \end{aligned} \quad (7)$$

The baryon density (ρ), scalar density (ρ_s) and dark matter density (ρ_s^{DM}) are

$$\begin{aligned} \rho &= \langle \psi^\dagger \psi \rangle = \frac{\gamma}{(2\pi)^3} \int_0^{k_F} d^3 k, \\ \rho_s &= \langle \bar{\psi} \psi \rangle = \frac{\gamma}{(2\pi)^3} \int_0^{k_F} \frac{M_n^*}{\sqrt{k^2 + M_n^{*2}}} d^3 k, \end{aligned}$$

$$\rho_s^{DM} = \langle \bar{\chi} \chi \rangle = \frac{\gamma}{(2\pi)^3} \int_0^{k_F^{DM}} \frac{M_\chi^*}{\sqrt{k^2 + M_\chi^{*2}}} d^3 k, \quad (8)$$

where k_F and k_F^{DM} are the Fermi momenta for nucleonic matter and dark matter respectively and $\gamma = 2$ is the spin degeneracy factor of nucleons. The masses of mesons and meson-nucleon couplings at saturation density ρ_0 are given in Table 1 [44,57]. In order to get the density dependent profile for M_n^* and M_χ^* , Eqs. (6) and (8) should be solved self consistently. The energy and pressure i.e. EOS are provided by expectation values of energy-momentum tensor in the static case as $\epsilon = \langle T^{00} \rangle$ and $P = \frac{1}{3} \langle T^{ii} \rangle$.

The total energy density and pressure for the combined Lagrangian $\mathcal{L}_B + \mathcal{L}_{DM}$ are obtained as

$$\begin{aligned} \epsilon &= g_{\omega B} \omega_0 (\rho_p + \rho_n) + g_{\rho B} \rho_{03} (\rho_p - \rho_n) \\ &\quad + \frac{1}{\pi^2} \int_0^{k_F^p} dk k^2 \sqrt{k^2 + M_n^{*2}} \\ &\quad + \frac{1}{\pi^2} \int_0^{k_F^n} dk k^2 \sqrt{k^2 + M_n^{*2}} \\ &\quad + \frac{1}{\pi^2} \int_0^{k_F^{DM}} dk k^2 \sqrt{k^2 + M_\chi^{*2}} \\ &\quad + \frac{1}{2} m_\sigma^2 \sigma^2 - \frac{1}{2} m_\omega^2 \omega_0^2 - \frac{1}{2} m_\rho^2 \rho_{03}^2 + \frac{1}{2} M_h^2 h_0^2, \end{aligned} \quad (9)$$

$$\begin{aligned} P &= \frac{1}{3\pi^2} \int_0^{k_F^p} dk \frac{k^4}{\sqrt{k^2 + M_n^{*2}}} + \frac{1}{3\pi^2} \int_0^{k_F^n} dk \frac{k^4}{\sqrt{k^2 + M_n^{*2}}} \\ &\quad + \frac{1}{3\pi^2} \int_0^{k_F^{DM}} dk \frac{k^4}{\sqrt{k^2 + M_\chi^{*2}}} \\ &\quad - \frac{1}{2} m_\sigma^2 \sigma^2 + \frac{1}{2} m_\omega^2 \omega_0^2 + \frac{1}{2} m_\rho^2 \rho_{03}^2 - \frac{1}{2} M_h^2 h_0^2, \end{aligned} \quad (10)$$

where ρ_n and ρ_p are the neutron and proton number densities and k_F^n and k_F^p are the corresponding Fermi momenta of neutron and proton, respectively. The nuclear matter inside the neutron star will be charge neutral and β -equilibrated. The conditions of charge neutrality and β -equilibrium are given as

$$\rho_p = \rho_e + \rho_\mu, \quad (11)$$

and

$$\begin{aligned} \mu_n &= \mu_p + \mu_e, \\ \mu_e &= \mu_\mu, \end{aligned} \quad (12)$$

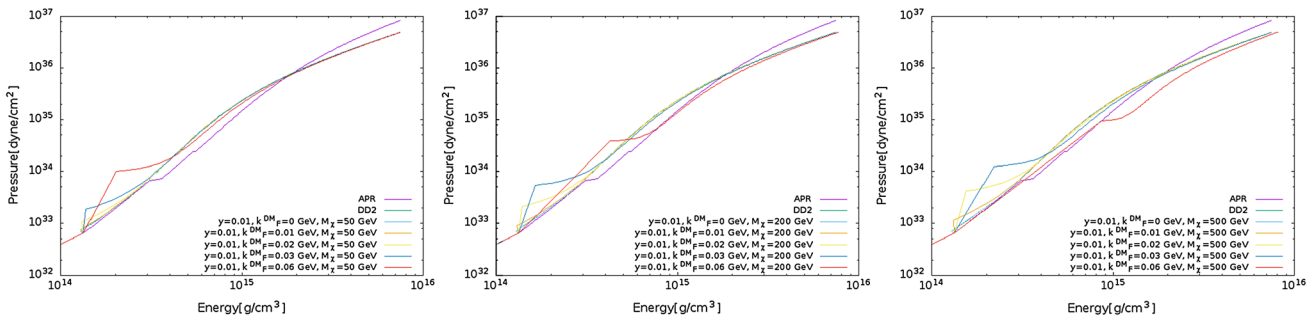


Fig. 1 Pressure vs energy plots for $M_\chi = 50$ GeV (left panel), $M_\chi = 200$ GeV (middle panel), $M_\chi = 500$ GeV (right panel) with varying DM Fermi momenta in each panel

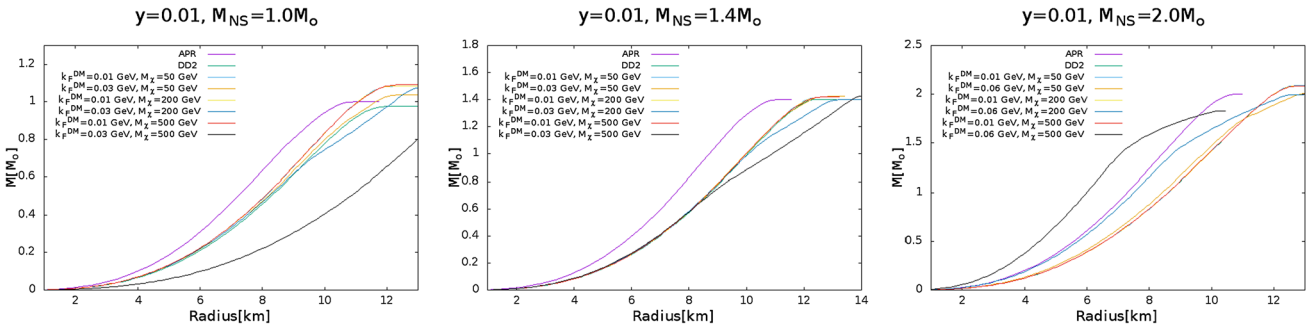


Fig. 2 Enclosed mass vs radius plots for $M_{NS} = 1.0M_\odot$ (left panel), $M_{NS} = 1.4M_\odot$ (middle panel), $M_{NS} = 2.0M_\odot$ (right panel) with varying DM mass and Fermi momentum in each panel

respectively. Here, the chemical potentials μ_e and μ_μ are given as

$$\begin{aligned}\mu_e &= \sqrt{k_e^2 + m_e^2}, \\ \mu_\mu &= \sqrt{k_\mu^2 + m_\mu^2},\end{aligned}\quad (13)$$

whereas the nucleon chemical potentials contain the rearrangement term also because of density-dependence of couplings as mentioned earlier. The particle fractions of neutron, proton, electron and muon will be determined by the self consistent solution of Eqs. (11) and (12) for a given baryon density. The energy density and pressure due to the non-interacting leptons are given as

$$\epsilon_l = \frac{1}{\pi^2} \sum_l \int_0^{k_F^l} dk k^2 \sqrt{k^2 + m_l^2}, \quad (14)$$

$$P_l = \frac{1}{3\pi^2} \sum_l \int_0^{k_F^l} dk \frac{k^4}{\sqrt{k^2 + m_l^2}}. \quad (15)$$

So the total energy density and pressure of the charge neutral β -equilibrated neutron star matter are

$$\epsilon_{NM} = \epsilon_l + \epsilon, \quad (16)$$

$$P_{NM} = P_l + P. \quad (17)$$

For all the EOSs considered in our work, we solve numerically Tolman-Oppenheimer-Volkoff (TOV) [61] equations

of hydrostatic equilibrium to generate the mass-radius and pressure-radius profiles as shown in Figs. 2, 3. In Fig. 1, we present EOSs for different DM masses and Fermi momenta along with APR and DD2 EOSs. It is important to mention that all of these EOSs satisfy the causality condition i.e. $c_s^2 < 1$. It is evident that for a fixed DM-Higgs coupling y and fixed DM mass, EOS becomes softer for higher values of DM Fermi momentum and is softest for $k_F^{DM} = 0.06$ GeV for lower to moderate values of density and APR is stiffest for higher values of density. Moreover, it is inferred from the comparison of three panels of Fig. 1 that for fixed values of y and k_F^{DM} , higher values of DM masses leads to softer EOS. It is important to mention here that for the higher DM mass $M_\chi = 500$ GeV, the EOS corresponding to $k_F^{DM} = 0.06$ GeV becomes softest among all the cases of DM masses. This sudden softening of EOS for $k_F^{DM} = 0.06$ GeV at $M_\chi = 500$ GeV might be due to dominance of dark matter over baryonic matter at such extreme parameters of DM. Nevertheless all the neutron star configurations for the dark matter densities considered in this work are stable and will not undergo black hole formation [60]. In Fig. 2, mass-radius profile is plotted for NS masses $1M_\odot$, $1.4M_\odot$ and $2M_\odot$. These plots can be explained the same way as in case of Fig. 1. Here also mass-radius profile for $k_F^{DM} = 0.06$ GeV at $M_\chi = 500$ GeV follows a trend contrary to other combinations of k_F^{DM} and M_χ . In this case the majority of mass

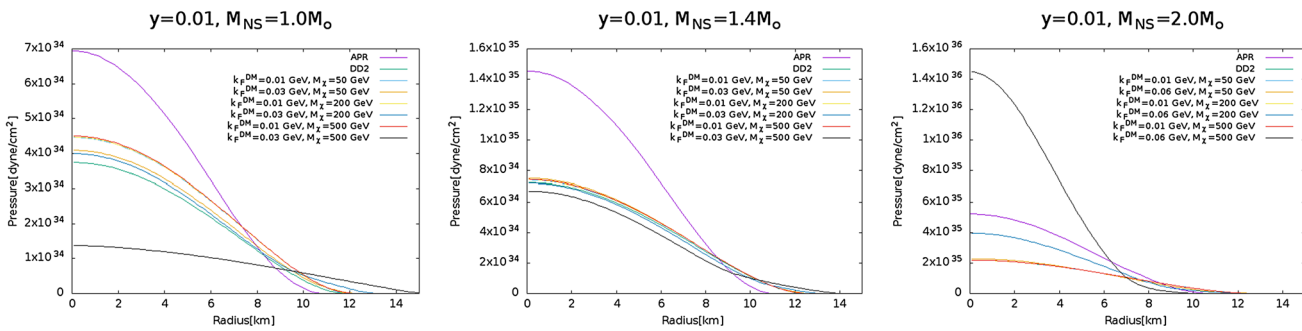


Fig. 3 Pressure vs radius plots for $M_{NS} = 1.0M_{\odot}$ (left panel), $M_{NS} = 1.4M_{\odot}$ (middle panel), $M_{NS} = 2.0M_{\odot}$ (right panel) with varying DM mass and Fermi momentum in each panel

contribution is from DM and hence leading to smaller radius than other cases due to enhanced gravitational contraction. Fig. 3 shows the pressure-radius profile for different NS masses where it is evident that for fixed DM mass and NS mass, higher values of k_F^{DM} leads to lower pressure except for the case of $M_{\chi} = 500$ GeV and $M_{NS} = 2M_{\odot}$ where $k_F^{DM} = 0.06$ GeV leads to higher pressure in the inner region of the star. This is because the star becomes more centrally condensed at very high DM mass.

3 Direct detection

Dark matter direct detection experiments do not show any signatures of collision events as of now. These experiments give an upper bound on the elastic scattering cross-section as a function of dark matter mass. In the present scenario, fermionic dark matter (WIMP) can undergo an elastic collision with the detector nucleus (quark level) by the Higgs exchange. Therefore, the effective Lagrangian contains the scalar operator $\bar{\chi}\chi\bar{q}q$ and can be written as

$$\mathcal{L}_{\text{eff}} = \alpha_q \bar{\chi}\chi\bar{q}q, \quad (18)$$

where q represent the valence quarks and $\alpha_q = yf(\frac{m_q}{v}) \left(\frac{1}{m_h^2} \right)$. This scalar operator contributes to the spin independent (SI) scattering cross-section for the fermionic dark matter candidate and can be expression as

$$(\sigma_{\text{SI}}) = \frac{y^2 f^2 M_n^2}{4\pi} \frac{m_r^2}{v^2 M_h^4}. \quad (19)$$

In Eq. (19), $m_r = \frac{M_n M_{\chi}}{M_n + M_{\chi}}$ is the reduced mass. We calculate the SI scattering cross-section using Eq. (19) and then constrain the parameter “y” using the direct detection experiments in such a way that calculated scattering cross-section for different dark matter masses are below the experimental bounds. In the present scenario, we use XENON-1T [62],

Table 2 Calculated values of spin independent DM-nucleon scattering cross-section for three chosen DM masses at fixed DM-Higgs coupling y

m_{χ} in GeV	y	$\sigma_{\text{SI}} \text{ cm}^2$
50	0.01	1.4115×10^{-47}
200	0.01	1.4514×10^{-47}
500	0.01	1.4596×10^{-47}

PandaX-II [63], LUX [64] and DarkSide-50 [65] experimental bounds for constraining the parameter “y”. We checked that by varying the value of the parameter “y” in the cooling calculations, no significant differences are found and hence, we accordingly fixed “y” to be 0.01 and calculate the corresponding scattering cross-section for three chosen DM masses as tabulated in Table 2.

4 Cooling mechanism of neutron stars

It is well known that the surface temperature of the neutron star decreases with time which is the direct indication of cooling. In order to calculate the thermal evolution of the neutron star, one needs to solve the the energy balance equation for the neutron star which can be expressed as [66]

$$\frac{dE_{\text{th}}}{dt} = C_v \frac{dT}{dt} = -L_v(T) - L_{\gamma}(T_e) + H(T) \quad (20)$$

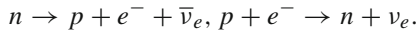
where E_{th} represents the thermal energy content of the star, T and T_e are the internal and effective temperatures of the star, respectively, C_v is the heat capacity of the core and H is the source term which includes different “heating mechanisms” important in the later stage of neutron star evolution. In Eq. (20), L_v and L_{γ} denote the neutrino and photon luminosities, respectively. $H(T)$ is considered here to be zero. The photon luminosity is calculated using the Stefan-Boltzmann law [67]

as

$$L_\gamma = S T^{2+4\alpha} = 4\pi \sigma R^2 T_e^4. \quad (21)$$

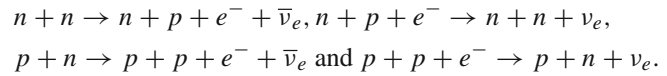
This relation is obtained using $T_e \propto T^{0.5+\alpha}$ ($\alpha \ll 1$), where R is the radius of the star and σ denotes the Stefan-Boltzmann constant. NSCool code [68] is utilised in the present work for calculating the neutrino and photon luminosities.

Several neutrino emitting processes contribute in the cooling of neutron stars [53, 66, 69]. Direct Urca processes and modified Urca processes are the two main neutrino emitting processes for the cooling. The direct Urca processes are



These are possible in neutron stars only if the proton fraction crosses a critical threshold. The two processes are fast and the luminosity varies with the temperature as $L_v^{fast} \propto T_9^6$. The baryon direct Urca processes are the strongest and open for some EOSs satisfying the threshold condition at sufficiently high densities. Cooling of neutron stars becomes rapid (enhanced) if these processes are allowed. If these processes are forbidden, then baryon modified Urca and baryon bremsstrahlung processes are the main neutrino emitting processes which lead to slow (standard) cooling. These reactions are abundant and the number of this type of open reactions grows quickly as density increases. However, one should not be bothered about this wealth of reactions because as the density increases direct Urca process will be determining the neutrino luminosity since the modified Urca and bremsstrahlung processes are negligible compared to it. Inside the neutron star core, direct Urca is the basic process bringing nucleons into the state of beta-equilibrium with chemical potentials satisfying the equality $\mu_n = \mu_p + \mu_e$. In equilibrium both reactions take place at the same rate, and the direct Urca process leaves the nucleon composition of matter unchanged. Threshold is the most important feature of direct Urca process. Since the process is several orders of magnitude more efficient than other neutrino processes, it is very important to know the threshold exactly. The reaction is allowed only if the Fermi momenta k_F^n , k_F^p and k_F^e satisfy the triangle condition (can be sides of one triangle). In other words, the value of each Fermi momentum should be smaller than the sum of two others. In neutron star matter k_F^n is larger than k_F^p and k_F^e , and the triangle condition reads: $k_F^n < k_F^p + k_F^e$. For $\rho \sim \rho_0$ one typically has $k_F^n \sim 340 \text{ MeV}/c$, $k_F^e \sim k_F^p \sim (60-100) \text{ MeV}/c$ and the condition is invalid, i.e., the direct Urca is forbidden [69]. However, k_F^p and k_F^e may grow with density faster than k_F^n , and the process can be open at higher densities, a few times ρ_0 . The direct Urca process in the npe matter is allowed for the EOSs having large symmetry energy at densities several times the nuclear saturation density. For APR EOS, the direct Urca process is allowed only for $M \gtrsim 1.97 M_\odot$ [36].

Modified Urca process will become more dominant provided the proton fraction is below the threshold for direct Urca. The modified Urca processes are



These are slow processes and luminosity varies with the temperature as $L_v^{slow} \propto T_9^8$. The neutron and proton branches of modified Urca process have similar emissivity with main difference in the threshold for the proton branch which is allowed at $k_F^n < 3k_F^p + k_F^e$. The neutron branch doesn't have the threshold. In the npe matter, this inequality is equivalent to $k_F^n < 4k_F^e$, i.e., to the proton fraction Y_p exceeding the critical value $Y_{cp} = 1/65 = 0.0154$ [69]. The latter condition is satisfied almost anywhere in the neutron star core. It can be violated only for the equations of state with very low symmetry energy at $\rho \lesssim \rho_0$, forbidding the proton branch in the outermost part of the core [69]. Contrary to the case of the direct Urca process, the emissivity increases smoothly from zero while the density exceeds the threshold value. The proton process is especially efficient at higher densities, near the threshold of the direct Urca process. Both branches of the modified Urca process are the leading standard (slow) neutrino generating mechanisms in non-superfluid neutron star cores, provided the direct Urca processes are forbidden.

For understanding the cooling mechanism of neutron stars, neutron star in Cassiopeia A (Cas A) supernova remnant is very important. It is the youngest known thermally emitting isolated neutron star in our galaxy and is also the first neutron star for which cooling has been observed directly. Moreover, it is among very few isolated neutron stars whose age and surface temperatures are very well determined and hence is important in understanding the thermal evolution and interior properties of neutron stars. Nearly 20 years of monitoring of this neutron star, since it was discovered by Chandra X-ray Observatory in 1999, has shown that there is a decrease in its temperature by 2–3% per decade. This cooling rate is significantly faster than that can be explained by standard neutron star cooling theories. This provides a strong evidence for the existence of superfluidity in neutron star cores [70–72]. Once the temperature is below the critical temperature of superfluid transition, neutron superfluidity and proton superconductivity opens a new channel for neutrino emission by continuous breaking and formation of cooper pairs. Hence the cooling of the neutron star is enhanced. This rapid cooling is expected to continue for several more decades. In future, Chandra observations will be more reliable and temperature measurements of this neutron star will be more accurate.

Free neutrons in the crust and both neutrons and protons in the core of a neutron star are likely to be in the superfluid (SF) state. We assume the singlet-state pairing of the protons, and either singlet-state or triplet-state pairing of the neutrons. In

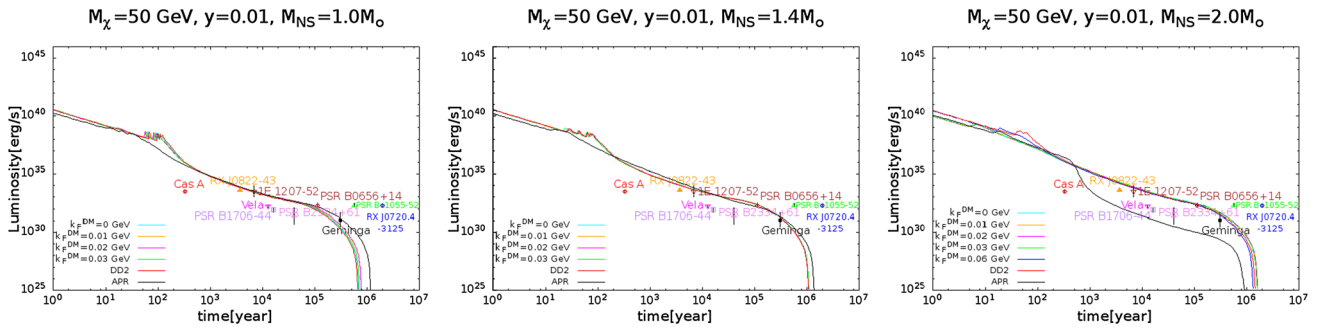


Fig. 4 Variation of luminosity with time three differently chosen NS masses $M_{NS} = 1.0M_{\odot}$ (Left panel), $M_{NS} = 1.4M_{\odot}$ (middle panel), $M_{NS} = 2.0M_{\odot}$ (right panel) with varying k_F^{DM} and fixed $M_{\chi} = 50$ GeV in each panel. The theoretical calculations are compared

with the observational data of pulsars namely Cas A, RX J0822-43, 1E 1207-52, PSR B1706-44, Vela, PSR B2334+61, PSR B0656+14, Geminga, PSR B1055-52 and RX J0720.4-3125 shown by dots with error bars from left to right

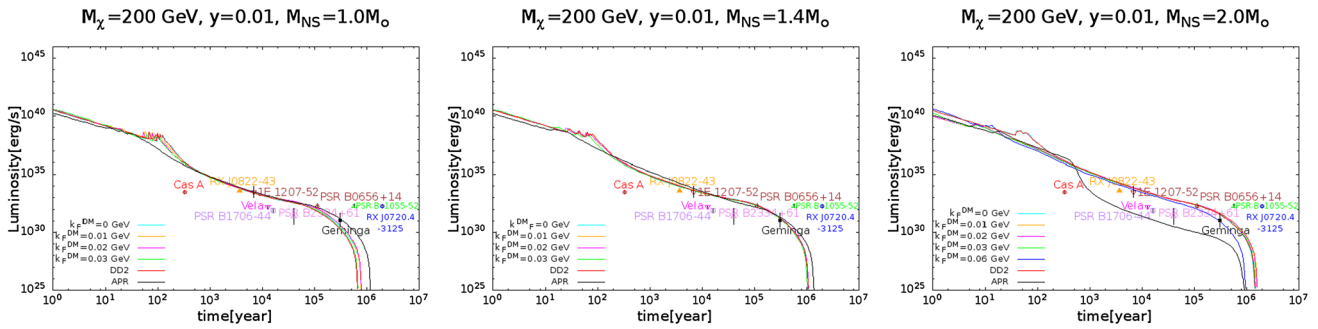


Fig. 5 Same as in Fig. 4 but for $M_{\chi} = 200$ GeV

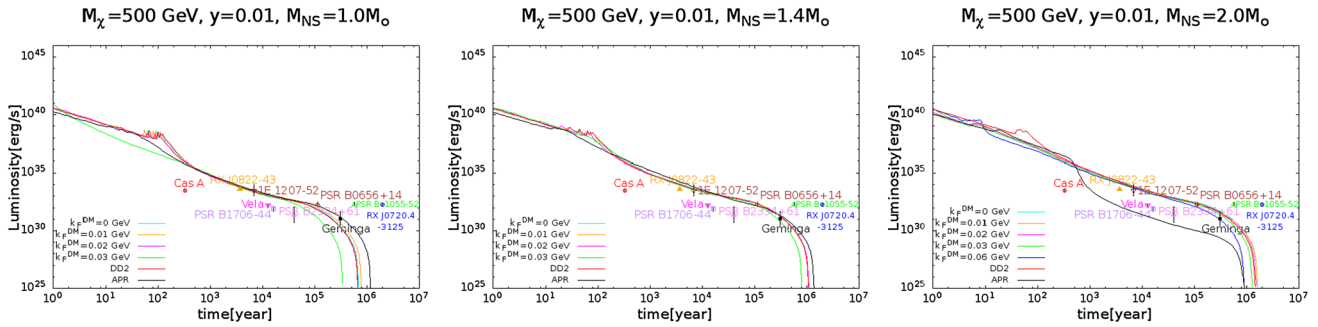


Fig. 6 Same as in Fig. 4 but for $M_{\chi} = 500$ GeV

a uniform, low-density matter (near the core-crust interface) the neutron pairing is known to be of the singlet type, but it switches to the triplet-state type at higher densities. Once the superfluidity is taken into account, the neutrino emissivity is highly suppressed at low temperature. The reason of this suppression is the gap in the energy spectrum which suppresses the excitation around the Fermi surface [73]. But at the same time another important neutrino emitting channel so called the Cooper pair breaking and formation (PBF) comes in play. It is associated with the Cooper pair breaking due to the thermal disturbance and its subsequent reformation. The triplet pairing in the core dominates the neutron PBF. The

PBF neutrino emitting processes are given as

$$n + n \rightarrow [nn] + \nu + \bar{\nu}, p + p \rightarrow [pp] + \nu + \bar{\nu}.$$

These are medium processes where luminosity varies with temperature as $L_{\nu}^{medium} \propto T_9^7$. It has been shown earlier that superfluidity in the crust affects the cooling curves at the initial thermal relaxation stage, while superfluidity in the core accelerates cooling at later stages. The duration of the thermal relaxation stage is greatly reduced by the effect of superfluidity on heat capacity of free neutrons in the stellar crust [69]. When thermal relaxation is over and the isothermal state is established throughout the star, the cooling is mainly

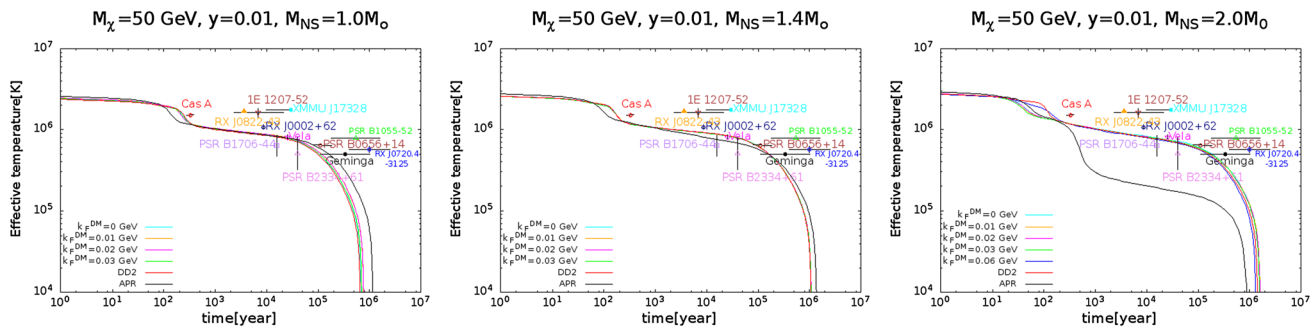


Fig. 7 Variation of effective temperature with time for three differently chosen NS masses $M_{NS} = 1.0M_{\odot}$ (Left panel), $M_{NS} = 1.4M_{\odot}$ (middle panel), $M_{NS} = 2.0M_{\odot}$ (right panel) with varying k_F^{DM} and fixed $M_{\chi} = 50 \text{ GeV}$ in each panel. The theoretical calculations are

compared with the observational data of pulsars namely Cas A, RX J0822-43, 1E 1207-52, XMMU J17328, PSR B1706-44, Vela, PSR B2334+61, PSR B0656+14, Geminga, PSR B1055-52 and RX J0720.4-3125 shown by dots with error bars from left to right

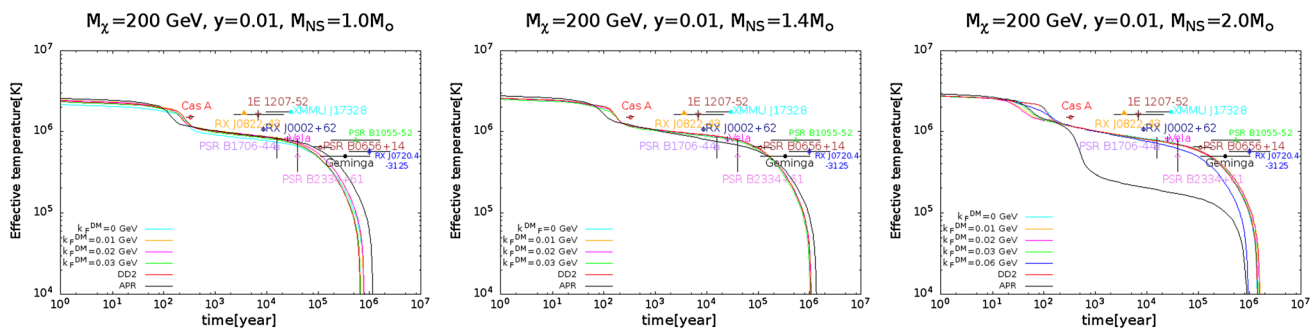


Fig. 8 Same as in Fig. 7 but for $M_{\chi} = 200 \text{ GeV}$

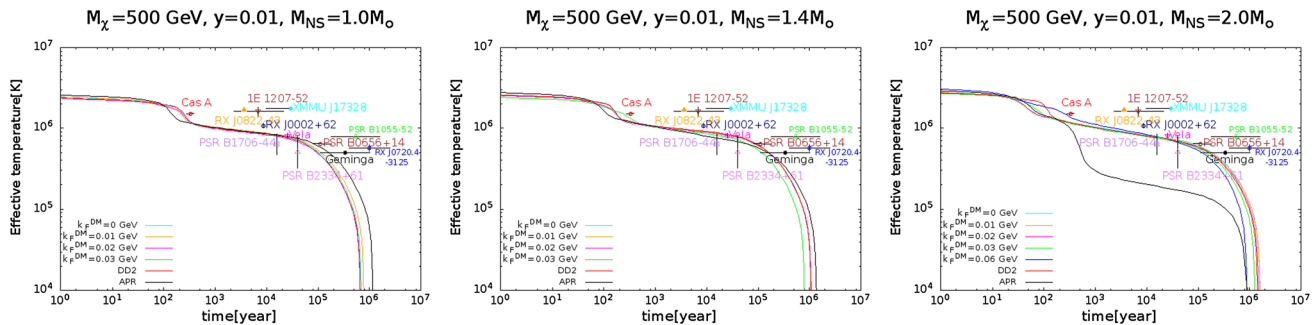


Fig. 9 Same as in Fig. 7 but for $M_{\chi} = 500 \text{ GeV}$

regulated by the neutrino luminosity and heat capacity of the stellar core. The neutrino processes and heat capacity of the crust cease to play a significant role except for the very low-mass stars with large crusts. However, it has been found that for some superfluid models the neutrino luminosity of the crust may affect the cooling for a short period of time during the transition from the neutrino cooling era to the photon era [69].

There are several other neutrino emitting processes involved in the cooling as follows

$$e^- + e^+ \rightarrow \nu + \bar{\nu} \text{ (electron-positron pair annihilation)}, \\ e^- \rightarrow e^- + \nu + \bar{\nu} \text{ (electron synchrotron)},$$

$\gamma + e^- \rightarrow e^- + \nu + \bar{\nu}$ (photoneutrino emission),
 $e^- + Z \rightarrow e^- + Z + \nu + \bar{\nu}$ (electron-nucleus bremsstrahlung),
 $n + n \rightarrow n + n + \nu + \bar{\nu}$ (neutron-neutron bremsstrahlung) and

$n + Z \rightarrow n + Z + \nu + \bar{\nu}$ (neutron-nucleus bremsstrahlung). For these processes, emissivity is numerically sub-dominant compared to the modified Urca process.

5 Calculations and results

We utilised NSCool Numerical code [68] for studying cooling of NSs adopting different EOSs like APR, DD2 and DM

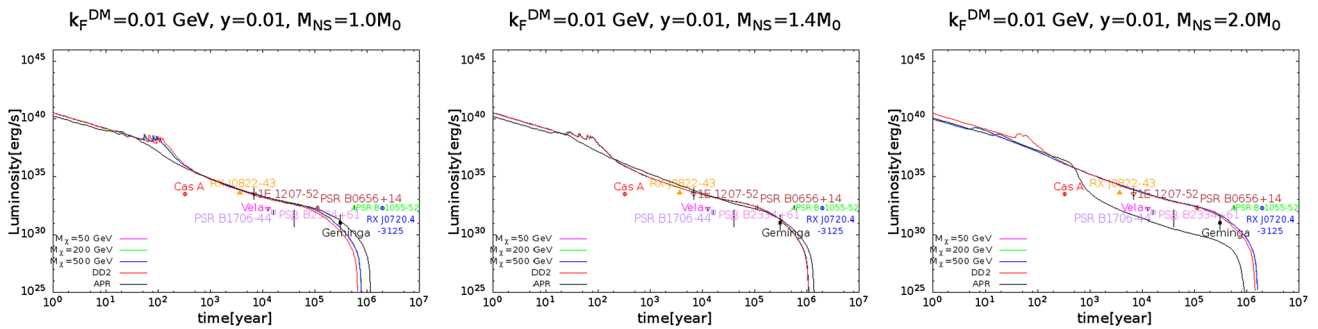


Fig. 10 Variation of luminosity with time for three differently chosen NS masses $M_{NS} = 1.0M_{\odot}$ (left panel), $M_{NS} = 1.4M_{\odot}$ (middle panel), $M_{NS} = 2.0M_{\odot}$ (right panel) with varying M_{χ} and fixed $k_F^{DM} = 0.01$ GeV in each panel. The theoretical calculations are com-

pared with the observational data of pulsars namely Cas A, RX J0822-43, 1E 1207-52, PSR B1706-44, Vela, PSR B2334+61, PSR B0656+14, Geminga, PSR B1055-52 and RX J0720.4-3125 shown by dots with error bars from left to right

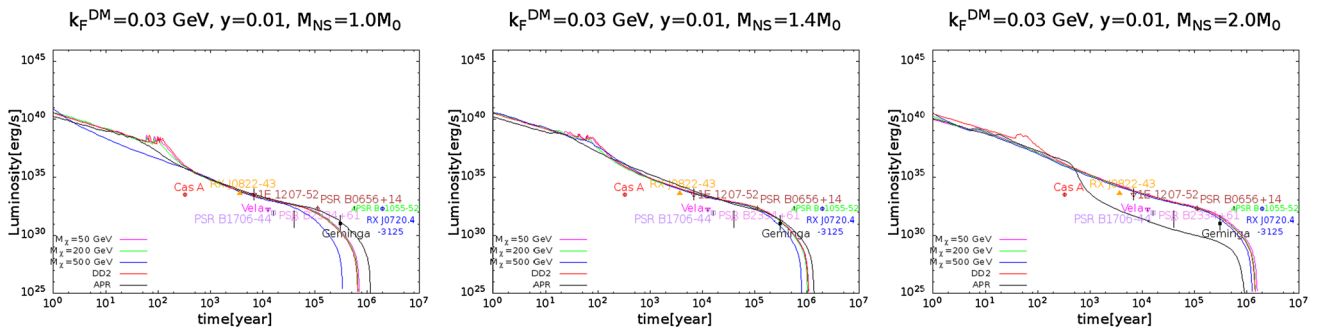


Fig. 11 Same as in Fig. 10 but for $k_F^{DM} = 0.03$ GeV

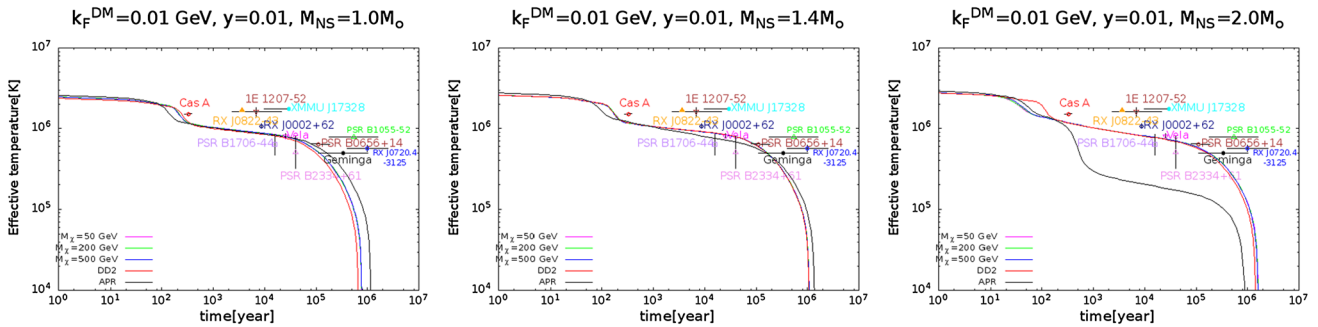


Fig. 12 Variation of tuminosity with time for chosen three different NS masses $M_{NS} = 1.0M_{\odot}$ (left panel), $M_{NS} = 1.4M_{\odot}$ (middle panel), $M_{NS} = 2.0M_{\odot}$ (right panel) with varying M_{χ} and fixed $k_F^{DM} = 0.01$ GeV in each panel. The theoretical calculations are com-

pared with the observational data of pulsars namely Cas A, RX J0822-43, 1E 1207-52, RX J0002+62, XMMU J17328, PSR B1706-44, Vela, PSR B2334+61, PSR B0656+14, Geminga, PSR B1055-52 and RX J0720.4-3125 shown by dots with error bars from left to right

admixed DD2. We considered different neutron star masses namely $1.0 M_{\odot}$, $1.4 M_{\odot}$ and $2.0 M_{\odot}$ for the calculations. In case of DM admixed DD2, we explored the effect of variation of DM mass (50 GeV, 200 GeV and 500 GeV) and DM Fermi momentum k_F^{DM} (0 GeV, 0.01 GeV, 0.02 GeV, 0.03 GeV and 0.06 GeV) on the cooling of NSs. It is important to mention here that $k_F^{DM} = 0$ GeV means dark matter density is zero but effective mass of nucleons will be effected due to non-zero Higgs-nucleon Yukawa coupling (Eq. 4). For

demonstrating DM-effect on neutron star cooling we plot the variations of luminosity with time (Figs. 4, 5, 6) and effective temperature with time (Figs. 7, 8, 9). As seen in all the plots (Figs. 4, 5, 6, 7, 8, 9, 10, 11, 12, 13, 14), shortly after birth, NS cooling becomes dominated by neutrino emitting processes as mentioned earlier. When the internal temperature has sufficiently dropped in nearly about 10^4 – 10^5 year then the cooling is dominated by photon emission from the NSs surface. In Figs. 4, 5, 6, luminosity vs time are plotted for dif-

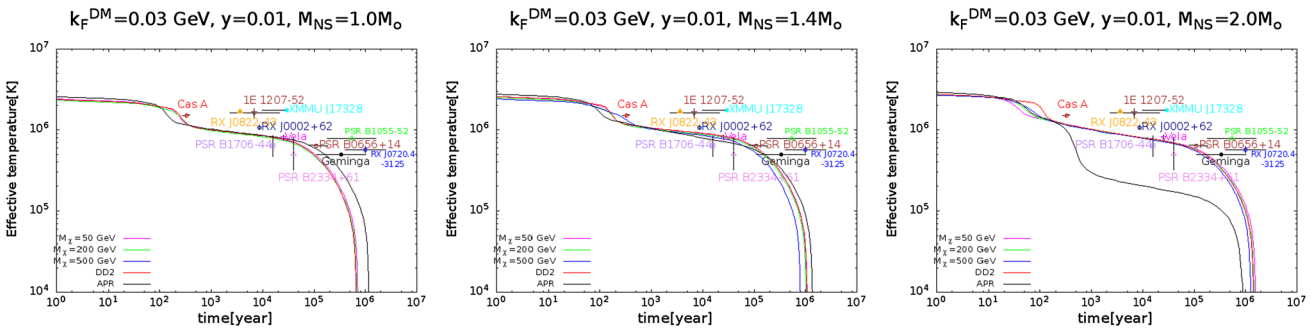


Fig. 13 Same as in Fig. 12 but for $k_F^{DM} = 0.03$ GeV

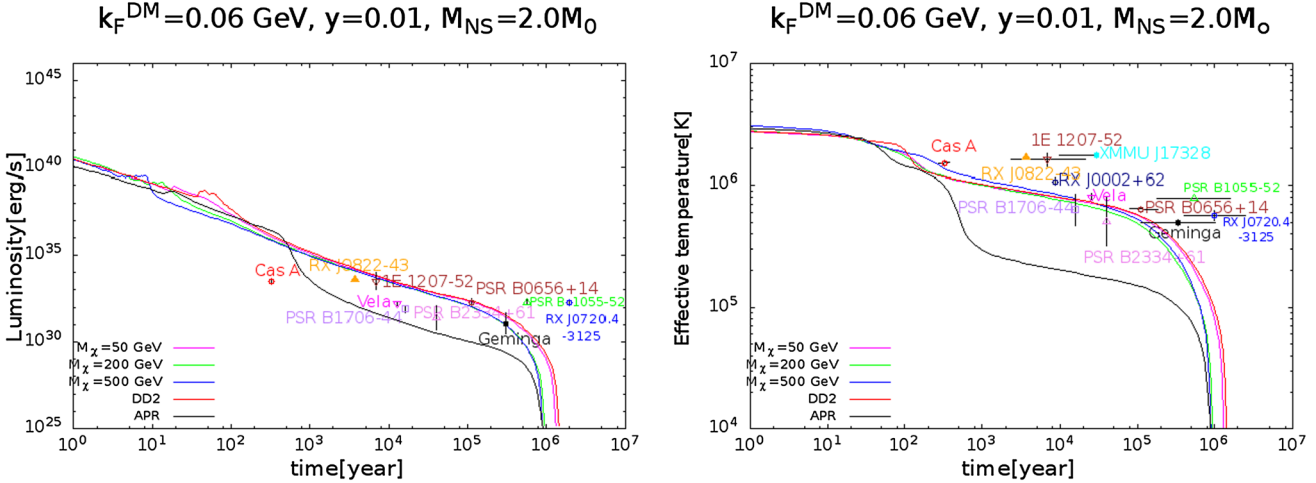


Fig. 14 Left panel is for luminosity vs time and right panel is for effective temperature vs time with varying M_χ and fixed $k_F^{DM} = 0.06$ GeV in both panels. The theoretical calculations are also compared with the observational data of all chosen pulsars

ferent NS masses and for every NS mass different EOSs are considered. For lower NS masses, cooling with DD2 is fastest and with APR it is slowest. Moreover, for fixed DM mass, cooling is faster for higher values of DM Fermi momentum. But in heavier NSs, cooling with APR becomes fastest which might be due to appearance of direct Urca neutrino emitting channels and variation due to k_F^{DM} is the same as previously. The effect of k_F^{DM} on cooling of heavier NSs becomes more and more prominent at higher values of DM mass as is evident from the right most panels of Figs. 5 and 6. Figs. 7, 8, 9 are effective temperature vs time profiles and these can be explained the same way as Figs. 4, 5, 6. In Figs. 10, 11 and 14 (left panel) for luminosity vs time, DM Fermi momentum is fixed and DM mass is varied for both heavier and lighter NSs. These figures clearly show that the cooling is faster for higher values of DM mass and in this case also cooling for heavier NSs is fastest with APR EOS. Figures 12, 13 and 14 (right panel) are effective temperature vs time plots for lighter and heavier NSs where k_F^{DM} is fixed and DM mass is varied. These Figures can be explained the same way as Figs. 10, 11 and 14 (left panel). In this case (Figs. 10, 11, 12, 13), effect on cooling due to varying DM masses becomes more evident

for lower mass NSs except for the case of $k_F^{DM} = 0.06$ GeV where variation due to DM mass is prominent even for heavier mass NS (Fig. 14) which is due to very high DM Fermi momentum. For all masses of DM admixed NSs, all chosen DM Fermi momenta are considerably consistent with cooling data of pulsars namely PSR B0656+14, Geminga, Vela, PSR B1706-44 and PSR B2334+61 as evident from the Figs. 4, 5, 6, 7, 8, 9, 10, 11, 12, 13, 14. It is noted that Cas A barely agrees with the cooling curves corresponding to higher values of dark matter Fermi momenta and DM mass. These observed pulsars might contain dark matter (WIMP) with lower to moderate mass. Furthermore, as seen from left most panels of Figs. 10, 11, 12, 13, it is evident that if small mass and super cold NSs are found in future astronomical cooling observations, we can say that heavier WIMPS may actually exist inside NSs.

For demonstrating the effect of superfluidity on cooling, we plotted luminosity vs time and temperature vs time profiles in Fig. 15 considering different pairing gap models inside the NSCool code because the actual value of neutron 3P_2 gap is unknown [74]. In Fig. 15, ‘pairing 0’ means no pairing is considered and ‘pairing a, b, c’ correspond to

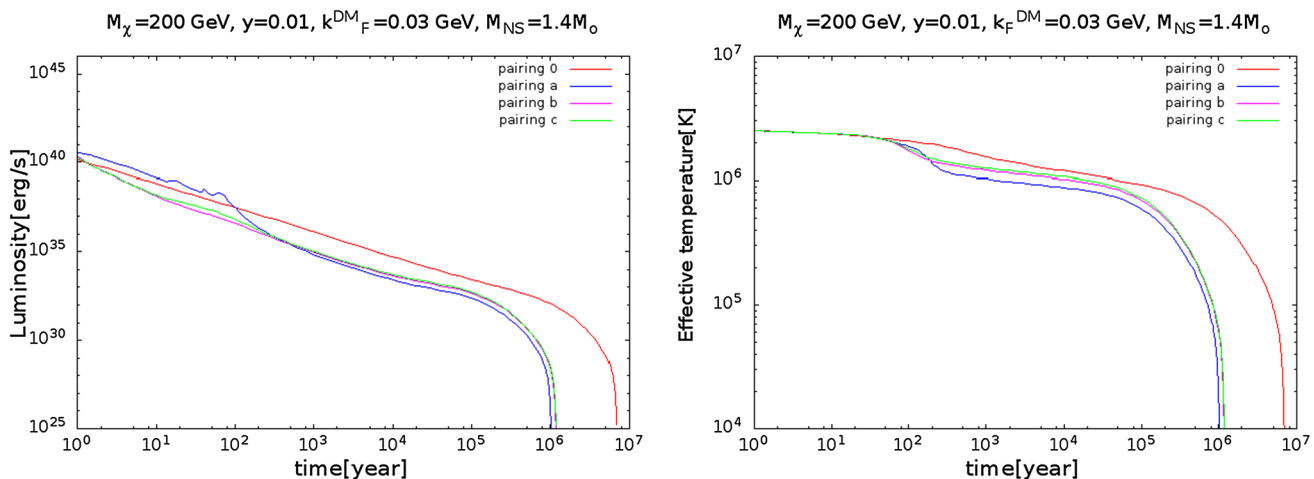


Fig. 15 Left panel is for luminosity vs time and right panel is for effective temperature vs time with different pairing gap models keeping M_χ and k_F^{DM} fixed in both the panels

three different 3P_2 pairing gap models. The details of these models are given in Ref. [74] and the references therein. It is evident that cooling is faster when pairing is considered and among the three pairing models, cooling with ‘pairing a’ is slightly faster. Hence, we have considered ‘pairing a’ model throughout the work.

6 Summary and conclusions

In this work, we first prepared dark-matter admixed DD2 equation of state and explored the effect of dark matter mass and Fermi momentum on the neutron star equation of state. Dark matter-Higgs coupling is constrained using dark matter direct detection experiments namely XENON-1T, PandaX-II, LUX and DarkSide-50. Then, we studied cooling of normal NSs using APR and DD2 equation of states and DM admixed neutron stars using dark-matter modified DD2 with varying dark matter mass and Fermi momentum for fixed DM-Higgs coupling. We have done our analysis by considering three neutron star masses one each from the lighter ($1.0 M_\odot$), medium ($1.4 M_\odot$) and heavier ($2.0 M_\odot$) NSs. We demonstrate our results by choosing three different DM masses namely 50 GeV, 200 GeV and 500 GeV and different Fermi momenta k_F^{DM} namely 0.01 GeV, 0.02 GeV, 0.03 GeV and 0.06 GeV. We calculated the variations of luminosity and temperature of the above mentioned neutron star masses with time and compared our calculations with the observed astronomical cooling data of pulsars namely Cas A, RX J0822-43, 1E 1207-52, RX J0002+62, XMMU J17328, PSR B1706-44, Vela, PSR B2334+61, PSR B0656+14, Geminga, PSR B1055-52 and RX J0720.4-3125. We found that APR EOS agrees well with the pulsar data for lighter and medium mass NSs whereas for DM admixed DD2 EOS, it is found for all

considered NS masses, all chosen DM Fermi momenta are consistent with the observational data of PSR B0656+14, Geminga, Vela, PSR B1706-44 and PSR B2334+61. Cooling becomes faster as compared to normal NSs in case of increasing DM masses and Fermi momenta. It is observed from the calculations that if low mass super cold NSs are observed in future that may support the fact that heavier WIMP can be present inside neutron stars.

Data Availability Statement This manuscript has no associated data or the data will not be deposited. [Authors’ comment: Data sharing not applicable to this article as no datasets were generated or analysed during the current study.]

Open Access This article is licensed under a Creative Commons Attribution 4.0 International License, which permits use, sharing, adaptation, distribution and reproduction in any medium or format, as long as you give appropriate credit to the original author(s) and the source, provide a link to the Creative Commons licence, and indicate if changes were made. The images or other third party material in this article are included in the article’s Creative Commons licence, unless indicated otherwise in a credit line to the material. If material is not included in the article’s Creative Commons licence and your intended use is not permitted by statutory regulation or exceeds the permitted use, you will need to obtain permission directly from the copyright holder. To view a copy of this licence, visit <http://creativecommons.org/licenses/by/4.0/>.

Funded by SCOAP³.

References

1. N.K. Glendenning, *Astrophys. J.* **293**, 470 (1985)
2. N.K. Glendenning, *Compact Stars, Nuclear Physics, Particle Physics and General Relativity* (Springer, New York, 1997)
3. M. Rho, D. Wilkinson (eds.), *See Mesons in Nuclei* (North-Holland, Amsterdam, 1979)
4. D.B. Kaplan, A.E. Nelson, *Phys. Lett. B* **175**, 57 (1986)
5. J.C. Collins, M.J. Perry, *Phys. Rev. Lett.* **34**, 1353 (1975)
6. G. Panotopoulos, I. Lopes, *Phys. Rev. D* **96**, 083004 (2017)

7. A. Das, T. Malik, A.C. Nayak, Phys. Rev. D **99**, 043016 (2019)
8. A. Quddus, G. Panotopoulos, B. Kumar, S. Ahmad, S.K. Patra, [arXiv:1902.00929 \[nucl-th\]](https://arxiv.org/abs/1902.00929) (2019)
9. D. Bandyopadhyay, S.A. Bhat, P. Char, D. Chatterjee, Eur. Phys. J. A **54**, 26 (2018). [arXiv:1712.01715 \[astro-ph.HE\]](https://arxiv.org/abs/1712.01715)
10. J.D. Walecka, Ann. Phys. **83**, 491 (1974)
11. B.D. Serot, J.D. Walecka, Int. J. Mod. Phys. E **6**, 515 (1997)
12. B.P. Abbott et al., Phys. Rev. Lett. **119**, 161101 (2017)
13. B.P. Abbott et al., Astrophys. J. Lett. **848**, L13 (2017)
14. H.T. Cromartie et al, [arXiv:1904.06759 \[astro-ph.HE\]](https://arxiv.org/abs/1904.06759) (2019)
15. C. Weniger, JCAP **1208**, 007 (2012)
16. T. Bringmann, X. Huang, A. Ibarra, S. Vogl, C. Weniger, JCAP **1207**, 054 (2012)
17. O. Adriani et al. [PAMELA Collaboration], Nature **458**, 607 (2009)
18. M. Aguilar et al., AMS collaboration, Phys. Rev. Lett. **113**, 121102 (2014)
19. G. Ambrosi et al., DAMPE Collaboration, Nature **552**, 63 (2017)
20. G. Jungman, M. Kamionkowski, K. Griest, Phys. Rept. **267**, 195 (1996). [arXiv:hep-ph/9506380](https://arxiv.org/abs/hep-ph/9506380)
21. A. Paul, D. Majumdar, A.D. Banik, JCAP **05**, 029 (2019). [arXiv:1812.10791 \[hep-ph\]](https://arxiv.org/abs/1812.10791)
22. A.D. Banik, D. Majumdar, A. Biswas, Eur. Phys. J. C **76**, 346 (2016)
23. A. Biswas, D. Majumdar, P. Roy, JHEP **1504**, 065 (2015)
24. A. Biswas, D. Majumdar, A. Sil, P. Bhattacharjee, JCAP **1312**, 049 (2013)
25. R.D. Peccei, Lect. Notes Phys. **741**, 3 (2008)
26. S. Weinberg, Phys. Rev. Lett. **40**, 223 (1978)
27. C.E. Yaguna, JHEP **1108**, 060 (2011)
28. E. Molinaro, C.E. Yaguna, O. Zapata, JCAP **1407**, 015 (2014)
29. A. Lidz, L. Hui, Phys. Rev. D **98**, 023011 (2018)
30. N.C. Amorisco, A. Loeb, [arXiv:1808.00464 \[astro-ph.GA\]](https://arxiv.org/abs/1808.00464) (2019)
31. L. Bergstrom, M. Fairbairn, L. Pieri, Phys. Rev. D **74**, 123515 (2006)
32. J. Fuller, C. Ott, Mon. Not. R. Astron. Soc. **450**, L71 (2015)
33. L. Braye, P. Tinyakov, Phys. Rev. Lett. **109**, 061301 (2012)
34. F. Sandin, P. Ciarcelluti, Astropart. Phys. **32**, 278 (2009)
35. D. Page, J.M. Lattimer, M. Prakash, A.W. Steiner, Astrophys. J. **707**, 1131 (2009)
36. D. Page, J.M. Lattimer, M. Prakash, A.W. Steiner, Astrophys. J. Suppl. **155**, 623 (2004)
37. D.G. Yakovlev, C.J. Pethick, Ann. Rev. Astron. Astrophys. **42**, 169 (2004)
38. A.Y. Potekhin, J.A. Pons, D. Page, Space Sci. Rev. **191**(1–4), 239 (2015)
39. A.Y. Potekhin, G. Chabrier, Astron. Astrophys. **609**, A74 (2018)
40. W.-B. Ding et al., Chin. Phys. Lett. **36**, 049701 (2019)
41. C. Kouvaris, Phys. Rev. D **77**, 023006 (2008)
42. K. Hamaguchi, N. Nagata, K. Yanagi, Phys. Lett. B **795**, 484 (2019)
43. S. Banik, M. Hempel, D. Bandyopadhyay, Astrophys. J. Suppl. **214**, 22 (2014)
44. S. Typel et al., Phys. Rev. C **81**, 015803 (2010)
45. H. Grigorian, D.N. Voskresensky, K.A. Maslov, Nucl. Phys. A **980**, 105 (2018)
46. H. Grigorian, D.N. Voskresensky, D. Blaschke, Eur. Phys. J. A **52**, 67 (2016)
47. D.N. Voskresensky, Lect. Notes Phys. **578**, 467 (2001)
48. K. Yanagi, N. Nagata, K. Hamaguchi, Mon. Not. R. Astron. Soc. **492**, 5508 (2020)
49. D. Viganò, N. Rea, J.A. Pons, R. Perna, D.N. Aguilera, J.A. Miralles, Mon. Not. R. Astron. Soc. **434**, 123 (2013)
50. A. De Luca, P.A. Caraveo, S. Mereghetti, M. Negroni, G.F. Bigianni, Astrophys. J. **623**, 1051 (2005)
51. A. Sedrakian, Phys. Rev. D **93**(6), 065044 (2016)
52. H. Umeda, N. Iwamoto, S. Tsuruta, L. Qin, K. Nomoto, [arXiv:astro-ph/9806337](https://arxiv.org/abs/astro-ph/9806337) (2019)
53. A. Paul, D. Majumdar, K.P. Modak, Pramana **92**, 44 (2019). [arXiv:1801.07928 \[hep-ph\]](https://arxiv.org/abs/1801.07928)
54. A. Akmal, V.R. Pandharipande, D.G. Ravenhall, Phys. Rev. C **58**, 1804 (1998)
55. S.A. Bhat, D. Bandyopadhyay, J. Phys. G **46**, 014003 (2019). [arXiv:1807.06437 \[astro-ph.HE\]](https://arxiv.org/abs/1807.06437)
56. S. Banik, D. Bandyopadhyay, Phys. Rev. C **66**, 065801 (2002)
57. S. Typel, Phys. Rev. C **71**, 064301 (2005)
58. S. Typel, H.H. Wolter, Nucl. Phys. A **656**, 331 (1999)
59. J.M. Cline, K. Kainulainen, P. Scott, C. Weniger, Phys. Rev. D **88**, 055025 (2013). (Erratum: Phys. Rev. D **92**, 039906 (2015))
60. X. Li, F. Wang, K.S. Cheng, JCAP **10**, 031 (2012)
61. J.R. Oppenheimer, G.M. Volkoff, Phys. Rev. **55**, 374 (1939)
62. E. Aprile et al., XENON Collaboration, JCAP **1604**, 027 (2016)
63. A. Tan et al., PandaX-II Collaboration, Phys. Rev. Lett. **117**, 121303 (2016)
64. D.S. Akerib et al., LUX Collaboration, Phys. Rev. Lett. **118**, 021303 (2017)
65. L. Marini et al., DarkSide Collaboration, Nuovo Cim. C **39**, 247 (2016)
66. D. Page, U. Geppert, F. Weber, Nucl. Phys. A **777**, 497 (2006). Kindly provide necessary details details for the Refs. [67, 68, 71], if possible.
67. <http://www.astroscu.unam.mx/neutrones/NSCool/>. Dany Page, Cooling of Neutron Stars, Lecture 2
68. <http://www.astroscu.unam.mx/neutrones/NSCool/>. We use the file Crust-EOS-Cat-HZD-NV.dat for the equation of state input
69. D.G. Yakovlev, A.D. Kaminker, O.Y. Gnedin, P. Haensel, Phys. Rept. **354**, 1 (2001)
70. C.O. Heinke, W.C.G. Ho, Astrophys. J. **719**, L167 (2010)
71. D. Page, M. Prakash, J.M. Lattimer, A.W. Steiner, Phys. Rev. Lett. **106**, 081101 (2011)
72. W.C.G. Ho, M.J.P. Wijngaarden, P. Chang, C.O. Heinke, D. Page, M. Beznogov, D.J. Patnaude, A.I.P. Conf. Proc. **2127**, 020007 (2019)
73. K. Yanagi, [arXiv:2003.08199 \[hep-ph\]](https://arxiv.org/abs/2003.08199) (2018)
74. [http://www.astroscu.unam.mx/neutrones/NSCool\(NSCool_Guide_0.0_Control.pdf\)](http://www.astroscu.unam.mx/neutrones/NSCool(NSCool_Guide_0.0_Control.pdf))

Dark matter admixed neutron star properties in the light of gravitational wave observations: a two fluid approach

Arpan Das^{1,*}, Tuhin Malik^{2,†}, and Alekha C. Nayak^{3,‡}

¹*Institute of Nuclear Physics Polish Academy of Sciences, PL-31-342 Kraków, Poland*

²*BITS-Pilani, Department of Physics, Hyderabad Campus, Hyderabad - 500078, India. and*

³*Department of Physics, NIT Meghalaya, Bijni Complex, Laitumkhrah Shillong-793003, Meghalaya, India.*

(Dated: November 4, 2020)

We consider the effect of density dependent dark matter on the neutron star mass, radius, and tidal deformability. Nuclear matter (normal matter) as well as the fermionic dark matter sector is considered in a mean field model. We adopt the two fluid formalism to investigate the effect of dark matter on the neutron star properties. In the two fluid picture, there is no direct interaction between the dark matter and the nuclear matter. Rather these two sectors interact only through gravitational interaction. The nuclear matter sector is described by the $\sigma - \omega - \rho$ meson interaction in the “FSU2R” parameterization. In the dark matter sector, we use the Bayesian parameter optimization technique to fix the unknown parameters in the dark matter equation of state. In the two fluid picture, we solve the coupled Tolman-Oppenheimer-Volkoff (TOV) equations to obtain the mass and radius of dark matter admixed neutron stars (DANSs). We also estimate the effect of the density dependent dark matter sector on the tidal deformability of dark matter admixed neutron stars (DANSs).

PACS numbers:

I. INTRODUCTION

The Universe has only $\sim 6\%$ visible matter and the remaining $\sim 94\%$ is composed of dark matter (26%) and dark energy (68%). A strong hint for the existence of dark matter (DM) came from the observations of the kinematics of self-gravitating objects such as galaxies and clusters of galaxies. Further cosmological observations indicate that DM may be baryon free and it must be a new form of matter which can interact with the rest of the standard model particles but only very weakly (for a recent review on dark matter physics see [1]). An exciting possibility of baryonic dark matter, where the dark matter is composed of quark matter nugget can be found in Ref.[2] and the references therein. Although the exact properties of the dark matter particles are not known, extensive studies on dark matter models from a particle physics point of view have put strong constraints on the mass and the coupling of the dark matter particles [1]. Among various dark matter models weakly interacting massive particle (WIMP) scenario has gained favor because in this model one can get the measured relic abundance of the dark matter very naturally using only the weak interaction scale physics. Since WIMP is associated with the weak interaction scale, this allows us to study these weak scale particles in the terrestrial laboratories [3].

In recent years one of the indirect methods that have gained attention is the study of the DM effects on compact stars properties. Compact stars like neutron stars (NS) provide us ample opportunities to study multidisciplinary physics such as the general theory of relativity, low energy nuclear physics, QCD under extreme conditions, etc. A neutron star is one the possible outcome of the gravitational collapse that a dying star undergoes, with a mass range between $1.4\text{--}3.0 M_{\odot}$ (M_{\odot} denotes the solar mass). In hydrostatically stable neutron stars gravitational collapse is balanced by the degeneracy pressure of neutrons which originates due to the quantum nature of neutrons. However, this neutron degeneracy pressure cannot make the star stable against the gravitational collapse if the mass of a dying star is very large. When the gravitational collapse becomes dominant as compared to the neutron degeneracy pressure, then the star cannot achieve hydrostatic equilibrium and the stellar remnant produces a black hole. Inside the neutron star, the matter density can be very large and it is generally considered to be as high as a few times nuclear saturation density ($n_0 = 0.16 \text{ fm}^{-3}$) [4]. Neutron stars are the only laboratories provided by Nature where such high-density matter can exist. Naturally interior of neutron stars gives us a unique opportunity to study the behavior of matter under extreme conditions. An important piece of information about the neutron star is its mass-radius

* arpan.das@ifj.edu.pl

† tuhin.malik@gmail.com

‡ alekhacu@gmail.com

relationship, which can be obtained by solving Tolman-Oppenheimer-Volkoff (TOV) equation, provided we know the nuclear equation of state (EoS) [5]. Tolman-Oppenheimer-Volkoff (TOV) equation has been studied extensively to put constraints on the nuclear EoS [4]. Independent measurements of the NS mass and radius can also be used to constrain the nuclear EoS [6-8]. Observations of quiescent low-mass X-ray binaries as well as X-ray bursters can place some constraints on the EoS [9-15]. NICER [16], LOFT [17, 18] which deals with X-ray pulse profile observations from a hot spot on the NS surface can also put strong constraints on the neutron star mass-radius. An alternative way has opened up to understand the neutron star structure and the underlying EoS of dense matter, due to the observation of gravitational waves (GW) from a merging binary NS [19]. In the neutron star binary merger, the tidal gravitational field of one neutron star induces a quadrupole deformation to its companion star. During the early inspiral stage, the orbital separation between the neutron stars is large therefore, the NSs do not feel the gravitational field of their companion strongly. As the inspiral proceeds, due to the energy loss by gravitational wave radiation, the orbital separation decreases. Now the gravitational tidal field of one of the neutron stars increases in magnitude at the position of its companion and thus creating a quadrupole deformation on the companion (and vice versa). In the binary mergers when the orbital separation between the neutron stars becomes comparable with the size of neutron stars, the details of the internal structure of the binary neutron stars become important. The induced quadrupole moment is related to the external tidal field through the tidal deformability. The tidal deformability is the response of the tidally induced quadrupole moment of an object subjected under an external tidal field. Tidal deformability is sensitive to the physical properties of a neutron star e.g., mass, radius, and tidal love number, which depend on the nuclear EoS. Hence using the observed tidal deformability of a neutron star merger, strong constraints can be put on the neutron star EoS [20].

It has been argued that dark matter (DM) can be captured in stars by losing their kinetic energy when the ambient dark matter particles scatter with ordinary matter in stars. Over a significant time scale, this capture of dark matter can lead to an accumulation of dark matter inside stars [21-26]. Hence it is natural that in the absence of any segregation mechanism between normal matter and dark matter, one expects the presence of dark matter in astrophysical objects. Further dark matter can be present during the formation processes of astrophysical objects. Depending upon the nature of the dark matter particles, the type of the accreting objects and their evolution history determines the total amount of dark matter that can be trapped inside an astrophysical object. Weakly interacting massive particles (WIMP) can accumulate inside neutron stars due to elastic scattering with nucleons. Due to a large density of normal matter inside neutron stars, the collisional energy loss of the dark matter particles can be quite significant. This makes the capture of dark matter inside these dense compact objects efficient. An interesting situation appears with the accumulation of dark matter inside the compact objects, if the mass fraction of the dark matter reaches a critical value, then the dark matter can form a self-gravitating dense core supported by degeneracy pressure (Fermi degeneracy pressure). Considering the collapses of the dark core into a black hole, if it reaches the Chandrasekhar mass, a possible bound on the density, cross-section, and mass of WIMPs can be put forward [27]. Further, the self-annihilating dark matter can heat old neutron stars in the galactic halo to a temperature detectable by infrared telescopes [21]. Self-annihilating dark matter can also affect the linear and angular momentum of compact objects [28]. This apart from the accumulation of non-self annihilating dark matter, such as asymmetric DM and mirror DM, inside the compact objects can also affect the structure of these compact objects. In this context, the dark-matter admixed neutron stars (DANSs) have been investigated extensively by many authors. In Refs. [29-31] authors considered the mirror dark matter in DANSs where both the normal matter (NM) and dark matter (DM) are present, but only interacting through gravity. It is important to note that due to the kinetic mixing of gauge bosons or due to unknown fields that can carry both ordinary and mirror charges, dark matter could also interact with ordinary matter through nongravitational interaction. The effect of dark matter on the neutron star properties due to nongravitational interaction also has been explored in literature. In Ref. [32], the authors considered nongravitational interaction between normal matter and dark matter by considering the Higgs portal mechanism. In Ref. [32] Walecka type relativistic mean field model including $\sigma - \omega$ interaction for the nucleonic sector [33-37] along with fermionic dark matter inside the neutron star has been considered. Using the mean field approximation effect of dark matter on the EoS and the corresponding mass-radius relation has been studied in Ref. [32]. Further in Ref. [38] considering an improved Walecka type relativistic mean field model including $\sigma - \omega - \rho$ meson interaction with NL3 parameterization [39, 40] effect of fermionic dark matter has been investigated on the neutron star EoS. It has been argued in Ref. [38] that the presence of a high mass (as compared to the nucleon mass) dark particles inside the neutron stars soften the equation state and lower the value of tidal deformability. This implies that stiff equations of states such as the Walecka model with NL3 parameterization which are disfavor by the GW170817 observation can satisfy the tidal deformability bound, in the presence of a dark matter component (with a uniform density) which is interacting with the normal matter through a nongravitational interaction.

It is important to mention that when one considers a nongravitational interaction between normal matter and the

dark matter, it is effectively a single fluid system. However one can also take an alternative and interesting approach by ignoring the nongravitational interaction between normal matter and the dark matter. This approach is also justified because the interaction between the normal matter and the dark matter can be very small, moreover, the in-medium properties of dark matter e.g. mass, self-interaction, etc., are still not known precisely. So if we ignore the nongravitational interaction between normal matter and dark matter then it is inherently a two-fluid system where normal matter and dark matter interact through gravitational interaction only. Alternative approaches have been discussed in the literature to study the two-fluid systems in the context of neutron star structure. Leung et al. in Ref [41], used the general relativistic two-fluid formalism based on the master function formalism, originally developed to study the effect of nuclear superfluid on the neutron star structure [42], to study DANSs. An alternative two fluid approach has been used by Sandin et.al. to study the effect of dark matter core on the structure of neutron star [29, 30]. The same approach as discussed in Refs. [29, 30], has been used for a broad variety of dark matter particles with various masses and interactions in neutron stars to examine the effects of dark matter on mass-radius relation of neutron stars [43]. Two-fluid formalism has been also used to study possible effects of a dark matter core on the mass-radius relation and the neutron star tidal deformability parameter for a self-interacting bosonic dark matter [44].

In the present investigation, we have considered the two-fluid formalism as developed in Refs. [29, 30, 43, 44] to study the effect of fermionic dark matter on the neutron star properties including tidal deformability, in a relativistic mean field approach. Here we consider the density dependent dark matter sector in a mean field description, i.e. relativistic mean field model (RMF) description analogous to the nuclear matter sector. So effectively here the dark matter sector is like a “mirror” to the normal matter sector, as has been considered in Ref. [43], but with a different equation of state as compared to the normal matter. It is important to note that in the relativistic mean field description of the normal matter all the coupling/parameters of the theory are fixed by the experimental observations. However, no such constraints are available for the density dependent dark matter sector. Therefore the parameters in the dark matter sector can be chosen in a wide range for an acceptable mass-radius relationship of neutron stars, as has been demonstrated in Ref. [43]. Naturally, with unknown parameters, we will get a large number of neutron star configurations some of which may or may not satisfy the known experimental observations. In the present investigation instead of choosing the unknown parameters in the dark matter sector arbitrarily, we use the Bayesian parameter optimization techniques to fix these unknown parameters using the knowledge of experimental and empirical information. Note that Bayesian parameter optimization techniques have been used extensively in the context of compact stars, e.g. Refs. [45–49]. Due to the Bayesian parameter optimization method, we get a distribution of the parameters in the dark matter sector and we also present the results for this range of optimized parameters. The rest of the paper is organized in the following manner.

In Sec. (I) we discuss the theoretical framework including discussions on the relativistic mean field approach to the normal matter as well as to the dark matter sector. We also include a brief discussion on Bayesian parameter optimization techniques required to fix the parameters in the dark matter sector. After the formalism part, in Sec. (III) we present the results and demonstrate the effects of fermionic dark matter in a two fluid approach. Finally in Sec. (IV) we conclude our results with an outlook to it.

II. THEORETICAL FRAMEWORK

In this section, we discuss the theoretical framework. In subsection (II A) we start with a brief discussion on the nuclear EoS in the Relativistic mean field (RMF) approach. Discussion of nuclear EoS will be followed up by a discussion on the dark matter EoS within the framework of RMF approach in subsection (II B). Further in subsection (II C) we discuss the theoretical framework of two fluid TOV equations along with the tidal deformability in the two fluid picture. Note that in the framework of RMF approach there are unknown parameters/couplings in the dark matter sector. We use Bayesian techniques to optimize these parameters. For completeness, we give a brief discussion on the Bayesian parameter optimization in subsection (II D).

A. Nuclear matter EOS

As stated earlier in this investigation we have considered the normal nuclear matter as well as the dark matter sector within the framework of relativistic mean field theory (RMF) [33, 34, 36, 37]. In the RMF approach nucleons behave like quasiparticles with an effective medium dependent mass. In this model nucleon-nucleon interaction is

mediated by meson exchange e.g. the exchange of σ and ω mesons. In general, σ mesons exchange gives rise to an attractive central force and a spin-orbit nuclear force. Further, the repulsive part of the nuclear potential can be incorporated if one also takes into account the ω -meson exchange interaction among the nucleons. However to explain nuclear saturation properties e.g. compressibility [50] we also have to include ρ meson exchange interaction between nucleons [40] along with σ and ω meson exchange. Since protons and neutrons only differ in terms of their isospin projections, the inclusion of ρ meson gives rise to a better understanding of the symmetry energy [51]. Further, for a charged neutral nuclear matter one can safely ignore the photon field.

The Lagrangian density of the nuclear matter sector including nucleon field, σ , ω , and ρ mesons and their interactions can be expressed as [52],

$$\begin{aligned} \mathcal{L}_{\text{NM}} = & \bar{\Psi}(i\gamma_\mu\partial^\mu - M_n + g_{\sigma N}\sigma - g_{\omega N}\gamma_\mu\omega^\mu - g_{\rho N}\gamma_\mu\vec{I}_N \cdot \vec{\rho}^\mu)\Psi \\ & + \frac{1}{2}\partial_\mu\sigma\partial^\mu\sigma - \frac{1}{2}m_\sigma^2\sigma^2 - \frac{\kappa}{3!}(g_{\sigma N}\sigma)^3 - \frac{\lambda}{4!}(g_{\sigma N}\sigma)^4 \\ & - \frac{1}{4}\Omega^{\mu\nu}\Omega_{\mu\nu} + \frac{1}{2}m_\omega^2\omega_\mu\omega^\mu + \frac{\zeta}{4!}(g_{\omega N}^2\omega_\mu\omega^\mu)^2 \\ & - \frac{1}{4}\vec{R}^{\mu\nu}\vec{R}_{\mu\nu} + \frac{1}{2}m_\rho^2\vec{\rho}_\mu\vec{\rho}^\mu + \Lambda_\omega g_{\rho N}^2\vec{\rho}_\mu\vec{\rho}^\mu g_{\omega N}^2\omega_\mu\omega^\mu \end{aligned} \quad (1)$$

In the above equation Ψ represents nucleon field, σ , ω_μ and $\vec{\rho}_\mu$ denotes σ , ω , ρ meson field respectively. \vec{I}_N denotes the isospin generators for the nucleons. m_σ , m_ω and m_ρ are the corresponding masses of the mesons and M_n denotes the bare nucleon mass which is different from the medium dependent nucleon mass $M_n^* = M_n - g_{\sigma N}\sigma$. The mesonic field strength tensors are $\Omega_{\mu\nu} = \partial_\mu\omega_\nu - \partial_\nu\omega_\mu$, $\vec{R}_{\mu\nu} = \partial_\mu\vec{\rho}_\nu - \partial_\nu\vec{\rho}_\mu$ for ω and ρ mesons respectively. Nuclear manybody dynamics is encoded in the coupling constants of the above Lagrangian. The couplings of the σ and ω mesons to the nucleons i.e. $g_{\sigma N}$ and $g_{\omega N}$ determine the energy per particle and density of the nuclear matter saturation point [53]. The $g_{\rho N}$ is the coupling of the isovector meson ρ to the nucleon, determines the nuclear symmetry energy. Couplings in the σ meson self-interaction terms i.e. κ and λ are important for successful descriptions of nuclear matter and finite nuclei within the framework of a relativistic theory [54, 55]. These couplings give rise to a softer EoS at moderate densities and allow realistic compressibility of nuclear matter. The non negative quartic self-coupling ζ gives rise to an attractive interaction that softens the nuclear EoS at high density. Therefore this term affects the structure and maximum mass of neutron stars [56, 57]. Further, the interaction between the ω meson and ρ meson denoted by the coupling Λ_ω affects the density dependence of the nuclear symmetry energy which also affects the pressure of neutron matter and the radii of neutron stars [58].

The covariant equation of motion or the Euler-Lagrange equation of the fundamental fields Ψ , σ , ω^μ and $\vec{\rho}_\mu$ can be obtained using the Lagrangian densities \mathcal{L}_{NM} . The Euler-Lagrange equation for any field φ having the Lagrangian density (\mathcal{L}_φ) is given by,

$$\partial_\mu \left(\frac{\partial \mathcal{L}_\varphi}{\partial(\partial_\mu\varphi)} \right) = \frac{\partial \mathcal{L}_\varphi}{\partial\varphi}. \quad (2)$$

The associated stress-energy tensor $T^{\mu\nu}$ is,

$$T_\varphi^{\mu\nu} = \frac{\partial \mathcal{L}_\varphi}{\partial(\partial_\mu\varphi)}\partial^\nu\varphi - g^{\mu\nu}\mathcal{L}_\varphi \quad (3)$$

where $g_{\mu\nu}$ denotes the metric tensor and is given by $g_{\mu\nu} = \text{diag}[1 - 1 - 1 - 1]$. The energy density ε_φ and pressure P_φ of the system in static case is then,

$$\begin{aligned} \varepsilon_\varphi &= \langle T_\varphi^{00} \rangle, \\ P_\varphi &= \frac{1}{3}\langle T_\varphi^{ii} \rangle. \end{aligned} \quad (4)$$

Using the Euler-Lagrange equation of the fundamental fields Ψ , σ , ω^μ and $\vec{\rho}_\mu$ and the definition of the energy density and pressure as given in Eq.(4) one can obtain the energy density (ε_{NM}) and pressure (P_{NM}) of the nuclear matter as (for a detailed discussion see Ref.[38, 59]):

M_n (MeV)	m_σ (MeV)	m_ω (MeV)	m_ρ (MeV)	$g_{\sigma N}^2$	$g_{\omega N}^2$	$g_{\rho N}^2$	κ (MeV)	λ	ζ	Λ_ω
939	497.479	782.500	763.000	107.5751	182.3949	206.4260	3.0911	-0.001680	0.024	0.045

TABLE I: Parameters of the FSU2R model considered in this investigation [52].

$$\varepsilon_{NM} = \frac{1}{\pi^2} \int_0^{k_p} dk k^2 \sqrt{k^2 + (M_n^*)^2} + \frac{1}{\pi^2} \int_0^{k_n} dk k^2 \sqrt{k^2 + (M_n^*)^2} \\ + \frac{1}{2} m_\sigma^2 \bar{\sigma}^2 + \frac{1}{2} m_\omega^2 \bar{\omega}^2 + \frac{1}{2} m_\rho^2 \bar{\rho}^2 + \frac{\kappa}{3!} (g_{\sigma N} \bar{\sigma})^3 + \frac{\lambda}{4!} (g_{\sigma N} \bar{\sigma})^4 + \frac{\zeta}{8} (g_{\omega N} \bar{\omega})^4 + 3\Lambda_\omega (g_{\rho N} g_{\omega N} \bar{\rho} \bar{\omega})^2, \quad (5)$$

$$P_{NM} = \frac{1}{3\pi^2} \int_0^{k_p} dk \frac{k^4}{\sqrt{k^2 + (M_n^*)^2}} + \frac{1}{3\pi^2} \int_0^{k_n} dk \frac{k^4}{\sqrt{k^2 + (M_n^*)^2}} \\ - \frac{1}{2} m_\sigma^2 \bar{\sigma}^2 - \frac{\kappa}{3!} (g_{\sigma N} \bar{\sigma})^3 - \frac{\lambda}{4!} (g_{\sigma N} \bar{\sigma})^4 + \frac{1}{2} m_\omega^2 \bar{\omega}^2 + \frac{\zeta}{4!} (g_{\omega N} \bar{\omega})^4 + \frac{1}{2} m_\rho^2 \bar{\rho}^2 + \Lambda_\omega (g_{\omega N} \bar{\omega})^2 (g_{\rho N} \bar{\rho})^2 \quad (6)$$

respectively. ρ_n and ρ_p are the neutron and proton number density with k_n and k_p are the corresponding Fermi momentum of neutron and proton, respectively. In a static and isotropic medium $\bar{\sigma}$, $\bar{\omega}$ and $\bar{\rho}$ represents the mean field values of the corresponding mesons. For a complete description of the EoS, the couplings have to be specified. In this investigation, we are considering the ‘FSU2R’ parametrization on the Lagrangian as given in Eq.(1). The numerical values of all these couplings/parameters are given in the Table (I) [52].

B. Dark matter EOS

Inspired by the success of the nuclear mean field approach to describe the nuclear matter, in this investigation we have modeled the dark matter sector using the mean field approach following Ref.[43]. It is important to mention that using our knowledge of mean field approach in the nuclear matter sector one can write advanced Lagrangian including various “dark hadrons” [43]. But this comes at a price with a large number of unknown parameters. Therefore to reduce the effect of the unknown parameters in the theory we consider the dark matter Lagrangian with a single fermionic component and the self interaction of the fermionic dark matter is mediated by ‘dark scalar’ and ‘dark vector’ boson particles. This choice is motivated by the fact that in this minimal model attractive as well as repulsive self interaction between the fermionic dark matter particles can be obtained due to the ‘dark scalar’ and ‘dark vector’ mediators respectively. Therefore the dark matter Lagrangian incorporating attractive and repulsive interaction can be expressed as,

$$\mathcal{L}_{DM} = \bar{\psi}_D [\gamma_\mu (i\partial^\mu - g_{vd} V^\mu) - (M_D - g_{sd} \phi_D)] \psi_D + \frac{1}{2} (\partial_\mu \phi_D \partial^\mu \phi_D - m_{sd}^2 \phi_D^2) \\ - \frac{1}{4} V_{\mu\nu,D} V_D^{\mu\nu} + \frac{1}{2} m_{vd}^2 V_{\mu,D} V_D^\mu. \quad (7)$$

Here ψ_D , ϕ_D , and V_D^μ represent fermionic dark matter, ‘dark scalar meson’, and ‘dark vector meson’ respectively. M_D is the ‘bare’ mass of the fermionic dark matter. m_{sd} and m_{vd} are the corresponding masses of the scalar and vector ‘dark mesons’ respectively. Similar to the nuclear matter equation of state one can also obtain the dark matter equation of state in the mean field approximation and is expressed as,

$$\varepsilon_{DM} = \frac{1}{\pi^2} \int_0^{k_D} dk k^2 \sqrt{k^2 + (M_D^*)^2} + \frac{g_{vd}^2}{2m_{vd}^2} \rho_D^2 + \frac{m_{sd}^2}{2g_{sd}^2} (M_D - M_D^*)^2, \quad (8)$$

$$P_{DM} = \frac{1}{3} \frac{1}{\pi^2} \int_0^{k_D} dk \frac{k^2}{\sqrt{k^2 + (M_D^*)^2}} + \frac{g_{vd}^2}{2m_{vd}^2} \rho_D^2 - \frac{m_{sd}^2}{2g_{sd}^2} (M_D - M_D^*)^2. \quad (9)$$

Here M_D^* is the medium dependent fermionic dark matter mass which can be given as $M_D^* = M_D - g_{sd}\phi_{D_0}$, ϕ_{D_0} being the mean field value of the ‘dark scalar meson’. ϕ_{D_0} can be expressed as, $\phi_{D_0} \equiv \frac{g_{sd}}{m_{sd}^2} \langle \bar{\psi}_D \psi_D \rangle$. ρ_D represents the density of the fermionic dark matter, which is associated with the mean field value of the ‘dark vector’ meson. It is important to note that although in the dark matter Lagrangian as given in Eq.(7) there are four parameters, i.e. m_{sd}, m_{vd}, g_{sd} and g_{vd} , but the dark matter energy density and pressure in the mean field approximation depends only on the ratios g_{sd}/m_{sd} and g_{vd}/m_{vd} . Note that this reduction of effective parameters is possible for this simple Lagrangian density in the dark matter sector. For a more completed Lagrangian density one has to deal with a large numbers of parameters in the relativistic mean field approach. For a complete description of the dark matter equation of state we need to specify the parameters g_{sd}/m_{sd} and g_{vd}/m_{vd} . As mentioned earlier, determination of unknown parameters in the dark matter sector using the Bayesian parameter optimization technique has been discussed in the subsequent sections.

C. The tidal deformability of neutron star : two fluid formalism

Once we have a complete description of the nuclear as well as dark matter EoS we can study the properties of the dark matter admixed neutron stars (DANSs). To study the properties of the dark matter admixed neutron stars, we adopt a two-fluid formalism where the nuclear matter and the dark matter sectors do not interact directly, rather the interaction between these two sectors is through the gravitational interaction. The DANSs structure can be obtained by solving the hydrostatic balance equation between inward gravitational pressure and outward fermion degeneracy pressure also known as TOV equations. The TOV equations for a two fluid system with energy density and pressure ε_1, P_1 and ε_2, P_2 , where it has been assumed that the energy momentum tensors of the two fluids are separately conserved, can be expressed as (see appendix (A) for details)[43],

$$\frac{dP_1}{dr} = -(P_1 + \varepsilon_1) \frac{4\pi r^3(P_1 + P_2) + m(r)}{r(r - 2m(r))}, \quad (10)$$

$$\frac{dP_2}{dr} = -(P_2 + \varepsilon_2) \frac{4\pi r^3(P_1 + P_2) + m(r)}{r(r - 2m(r))}, \quad (11)$$

where,

$$\frac{dm(r)}{dr} = 4\pi(\varepsilon_1(r) + \varepsilon_2(r))r^2. \quad (12)$$

Here ε_1, P_1 and ε_2, P_2 are the energy density and pressure of the two different fluids. For this investigation one can consider ε_1, P_1 are associated with NM and ε_2, P_2 are associated with DM or vice versa.

Apart from the mass and radius of NS, tidal deformability is also an important measurable structural property. In a coalescing binary neutron star system, during the final stages of inspiral, each NS develops a quadrupole deformation due to the tidal gravitational field induced by the companion neutron star. The tidal deformability is the measure of the degree of deformation of a neutron star due to the tidal field of the companion star. Tidal deformability depends on the structural properties of neutron star and is sensitive to the nature of the EoS. The tidal deformability is defined as,

$$\lambda = \frac{2}{3}k_2R^5, \quad (13)$$

where R is the radius of the NS. The value of k_2 is typically in the range $\simeq 0.05 - 0.15$ [60-62] for NSs and depends on the stellar structure. This quantity can be calculated using the following expression [60]

$$\begin{aligned} k_2 &= \frac{8C^5}{5} (1 - 2C)^2 [2 + 2C(y_R - 1) - y_R] \\ &\times \left\{ 2C(6 - 3y_R + 3C(5y_R - 8)) \right. \\ &+ 4C^3 [13 - 11y_R + C(3y_R - 2) + 2C^2(1 + y_R)] \\ &\left. + 3(1 - 2C)^2 [2 - y_R + 2C(y_R - 1)] \log(1 - 2C) \right\}^{-1}, \end{aligned} \quad (14)$$

where C ($\equiv M/R$) is the compactness parameter of the star of mass M with radius R . The quantity y_R ($\equiv y(R)$) for a two fluid system can be obtained by solving the following differential equation

$$r \frac{dy(r)}{dr} + y(r)^2 + y(r)F(r) + r^2Q(r) = 0, \quad (15)$$

with,

$$\begin{aligned} F(r) &= \frac{r - 4\pi r^3 ((\varepsilon_1(r) + \varepsilon_2(r)) - (P_1(r) + P_2(r)))}{r - 2m(r)}, \\ Q(r) &= \frac{4\pi r \left(5(\varepsilon_1(r) + \varepsilon_2(r)) + 9(P_1(r) + P_2(r)) + \frac{\varepsilon_1(r) + P_1(r)}{\partial P_1(r)/\partial \varepsilon_1(r)} + \frac{\varepsilon_2(r) + P_2(r)}{\partial P_2(r)/\partial \varepsilon_2(r)} - \frac{6}{4\pi r^2} \right)}{r - 2m(r)} \\ &\quad - 4 \left[\frac{m(r) + 4\pi r^3 (P_1(r) + P_2(r))}{r^2 (1 - 2m(r)/r)} \right]^2, \end{aligned}$$

along with TOV equation with proper boundary conditions [63, 64] (details can be found in appendix B). One can then define the dimensionless tidal deformability as $\Lambda = \frac{2}{3}k_2C^{-5}$. We should emphasize that for a two fluid system the evolution equation for the $y(r)$ gets modified due to presence of multiple fluid inside the neutron star. However the evolution equation of $y(r)$ outside the star remains unaltered.

D. Bayesian parameter optimization

Here we discuss a framework to estimates the unknown coupling/parameters in the dark matter sector while incorporating all the necessary information at our disposal. In this context, we use the Bayesian formulation of the parameter estimation. For the parameter estimation, the use of priors is well motivated, however, we should keep in mind that priors can bias the parameter extraction as has been discussed in Ref. [65, 66]. Here we are not going into a deep discussion of the use of prior because it is not our goal here. For a detailed discussion on the choice of prior and its use see Ref. [65]. In the Bayesian techniques, the central quantity is $p(A | B)$, which denotes the posterior probability distributions (PDF) of A given that B is true. The parameter estimation determines the posterior $p(A | B, I)$. $p(A | B, I)$ is the joint probability distribution for the full set of parameters/coefficients (in the present case couplings, etc.) denoted as “ A ”, given the data “ B ” (including their errors). I represents any other information. Using the basic rules of probabilistic inference, the sum and product rules along with Bayes’ theorem we can express $p(A | B, I)$ in terms of other probability distributions which we can calculate [67–69], e.g.,

$$p(A | B, I) = \frac{p(B | A, I)p(A | I)}{p(B | I)}. \quad (16)$$

Here $p(B | I)$ does not depend upon “ A ”, therefore can be determined by normalization. $p(B | A, I)$ and $p(A | I)$ represents *likelihood* and *prior* respectively. In the Bayesian procedure one can identify a *likelihood* function based on the available experimental data and assigning an appropriate prior, “ A ” can be estimated by analyzing the properties of the posterior for “ A ”. Note that in the estimation of “ A ” using Bayesian techniques the choice of the prior is important. One could choose it to be uniform prior, which has been used as a baseline for many analyses. Note that in the present investigation we are estimating the parameters or couplings in the density dependent dark matter sector and we have a little prior knowledge about these parameters. Therefore we consider a uniform prior for the Bayesian analysis. Note that an important feature of Bayesian analysis is the dependence of the results on the choice of prior. However only if the data used in the analysis is not constraining then the results can depend on the choice of the prior.

For the prior PDFs, we choose the dark matter model parameters, i.e. the ratio of scalar coupling to the scalar meson mass (g_{sd}/m_{sd}), the ratio of vector coupling to the vector meson mass (g_{vd}/m_{vd}), dark matter bare mass (M_D) and the ratio of the dark matter central energy density to the normal matter central energy density ($f_D \equiv \varepsilon_{DM}^c/\varepsilon_{NM}^c$) with a uniform prior. Note that in the dark matter sector the parameters are not experimentally restricted. Therefore the choice of the dark matter parameters is guided by valuable previous investigation as has been done in Ref. [43].

Likelihood of the model parameters $\mathbf{a}(a_1, a_2 \dots a_j)$ with respect to the corresponding experimental data $(b_1^{\text{exp}}, b_2^{\text{exp}} \dots b_i^{\text{exp}})$ has been considered in the following form,

$$p(B(b_1^{\text{exp}}, b_2^{\text{exp}} \dots b_i^{\text{exp}}) | A(\mathbf{a}), I) = \prod_i \frac{1}{\sqrt{2\pi}\sigma_i} \exp\left(-\frac{(b_i^{\text{th}} - b_i^{\text{exp}})^2}{2\sigma_i^2}\right), \quad (17)$$

σ_i denotes the width of the likelihood function. The b_i^{th} is the theoretically calculated observable with parameters “ \mathbf{a} ”. The index i runs from 1 to number of data. Note that sometimes models can be overfitted due to the order of the number of model parameters quite larger than the order of the number of fit data. To overcome this overfitting problem one can design a *likelihood function* with explicit dependence on parameter space. However, in the present analysis, the number model parameter and fit data are in the same order. Therefore, our choice of the *likelihood function* is not an explicit function of parameter space.

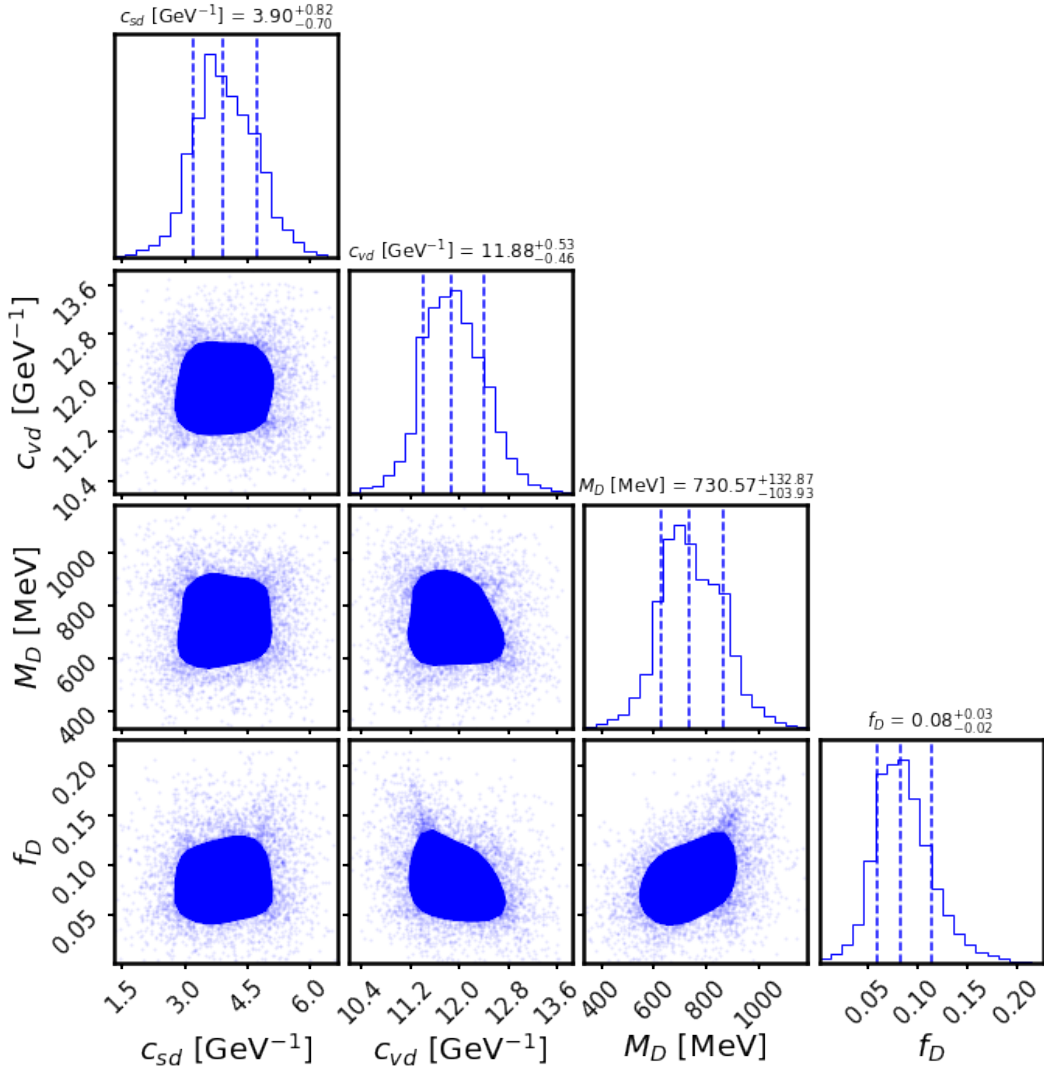


FIG. 1: Distribution of the dark matter sector parameters c_{sd} , c_{vd} , M_D and f_D as obtained by the Bayesian parameter optimization. For the Bayesian parameter optimization we have considered neutron star maximum mass, neutron star radius at $1.4 M_\odot$, and tidal deformability at $1.4 M_\odot$ as input data. Further for the parameters c_{sd} , c_{vd} , M_D and f_D we considered a uniform prior. The posterior distribution for these parameters is given in the plot as well mentioned in the table [\(II\)](#).

III. RESULTS

To see the effects of the dark matter component on the structure of neutron stars we have to solve the TOV equations for the two fluid system as given in Eqs. (10), (11) and (12) once we have the full information about the equation of states (EoS) of the normal matter as well as of the dark matter. In the nuclear matter sector, various EoS has been studied extensively. As mentioned earlier in this investigation we are considering the “FSU2R” model in the nuclear matter sector [52]. However in the dark matter sector we need to fix the following parameters, $c_{sd} \equiv g_{sd}/m_{sd}$, $c_{vd} \equiv g_{vd}/m_{vd}$, M_D . Note that these parameters are not fixed by any laboratory experiments. Therefore one can take some suitable choice of these parameters to fix the dark matter EoS as has been done in Ref. [43]. Apart from the dark matter EoS we also need information about the dark matter central density to solve the coupled TOV equations. We parameterize the dark matter central density as a fraction of the nuclear matter central density, ($f_D \equiv \frac{\varepsilon_{DM}^c}{\varepsilon_{NM}^c}$). Although f_D does not enter into the dark matter EoS, neutron star properties will be dependent upon the fraction of the dark matter component. The fraction of the dark matter inside neutron stars depends upon the process of the dark matter capture in compact objects. Here we also consider f_D as a free parameter. We further emphasize that in the dark matter EOS, $m_{sd}, g_{sd}, m_{vd}, g_{vd}$ are all not independent. Interestingly the dark matter EOS, as obtained in the mean field approximation only depend upon the ratios $c_{sd} \equiv g_{sd}/m_{sd}$ and $c_{vd} \equiv g_{vd}/m_{vd}$. Therefore to solve the couple TOV equation we need to fix the following parameters: c_{sd} , c_{vd} , M_D and f_D . One is free to choose these parameters appropriately to see their effects on the neutron star structure. It is expected that with these four unknown parameters one can come up with very exotic mass-radius plots [43].

In the present investigation we take an alternative approach to fix c_{sd} , c_{vd} , M_D and f_D . Our choice of these parameters is guided by experimental and empirical information available on the properties of neutron stars. Here we use the Bayesian parameter optimization as discussed earlier to give the posterior of these four unknown parameters using the known result of the neutron star mass, neutron star radius at $1.4 M_\odot$ and the tidal deformability Λ at $1.4 M_\odot$ [70–75]. It is important to know that due to the absence of any prior knowledge of c_{sd} , c_{vd} , M_D , and f_D in the dark matter sector we take a uniform prior for the analysis. After the Bayesian parameter optimization the obtained posterior for these parameters are given in Table (II) and the distributions of these parameters are given in Fig. (I). For various parameters, we mention the central value of the posterior distribution along with the one sigma deviation from the central value. From Fig. (I) it is clear that the parameters c_{sd} , c_{vd} , M_D and f_D are generally not correlated.

Note that with central values of these parameters, i.e. c_{sd} , c_{vd} , M_D , and f_D , along with the deviation from the central values there will be a large number of dark matter EoS which also corresponds to a distribution of the neutron star properties, i.e its mass, radius and the tidal deformability for a given nuclear matter EoS. Using the values of the parameters c_{sd} , c_{vd} , M_D and f_D as obtained from the Bayesian parameter optimization we show the distributions for the neutron star maximum mass, neutron star radius at $1.4 M_\odot$, tidal deformability at $1.4 M_\odot$ along with other physical properties, e.g. neutron star radius corresponding to maximum mass R_{tot} , tidal deformability at $1.0 M_\odot$ and tidal deformability at $1.8 M_\odot$ in Fig.(2). Further to demonstrate the effect of dark matter on the neutron star mass, radius, and tidal deformability we also provide the mass-radius and tidal deformability plots in the presence, as well as in the absence of dark matter component in Fig.(3). In Fig.(3) for the dark matter sector we have only considered the central values of the parameters c_{sd} , c_{vd} , M_D and f_D for convenience. For such configuration, from Fig.(3) it can be observed that with dark matter the maximum mass of the neutron star decreases, and the corresponding radius increases. Note that tidal deformability and love number scales with radius. Therefore with an increasing radius, the tidal love number and the tidal deformability also increases. This is a very distinct result as compared to our previous investigation in Ref. [38], where we had considered the effect of the heavy fermionic dark matter on the neutron star mass, radius, and tidal deformability. However in Ref. [38] we considered the normal matter and the dark matter in a single fluid picture, where the dark matter interacts with the normal matter through a Higgs portal interaction. In such a single fluid picture the maximum mass as well the corresponding radius decreases in the presence of a dark matter component. This may be an important difference between the single fluid picture and the two fluid picture as investigated here.

IV. CONCLUSIONS

In the present investigation, we consider the effect of density dependent dark matter on the neutron star properties in a two fluid framework. We modeled the density dependent dark matter within the framework of mean field theory keeping in mind the success of the nuclear mean field theory for the compact objects. In the two fluid approach neutron star properties depend on the nuclear matter equation of state as well as the dark matter equation of state. Contrary

Data		Parameters		
	value	Flat Prior	Posterior	
NS maximum mass (M_{\odot})	2.01 ± 0.04 [70]	c_{sd} (Gev $^{-1}$)	1 – 7	$3.90^{+0.82}_{-0.70}$
$R_{1.4}$ (Km.)	11.3 ± 1.0 [71–74]	c_{vd} (Gev $^{-1}$)	10 – 14	$11.88^{+0.53}_{-0.46}$
$\Lambda_{1.4}$	70-580 [75]	M_D (MeV)	200 – 1200	$730.57^{+132.87}_{-103.93}$
		f_D	0.0 – 0.25	$0.08^{+0.03}_{-0.02}$

TABLE II: Table of information considered for the estimation of the unknown parameters in the dark matter sector along with the optimized parameters using the Bayesian parameter optimization. Here \pm indicates the error in the values of various quantities.

to the nuclear matter, parameters in the density dependent dark matter sector are not fixed. Using the Bayesian parameter optimization technique we fix the parameters in the dark matter sector. For a fixed nuclear equation of state, we obtain a distribution of parameters in the dark matter sector. The parameters in the dark matter sector also give rise to a distribution of various configurations of the dark matter admixed neutron stars (DANSs). Interestingly there are some configurations of DANSs where the maximum mass of the neutron star decrease in the presence of dark matter but the corresponding radius increases. For such configurations tidal deformability and the love number increase in the presence of dark matter components. In Ref.[38] earlier we obtained that in a single fluid picture where the dark matter interacts with the normal matter through the Higgs portal mechanism neutron star maximum mass and the tidal deformability decreases in the presence of dark matter. Therefore the effect of the density dependent dark matter on the neutron star properties in a two fluid approach can be significantly different as compared to the results obtained in a single fluid picture in Ref.[38]. Note that in the present investigation we modeled the dark matter sector using a specific mean field model incorporating attractive and repulsive interactions. Therefore naturally the results presented here are not model independent. A model independent analysis of density dependent dark matter on the neutron star properties will be discussed in future investigations.

Acknowledgements

T.M. would like to thank Prof. Hiranmaya Mishra for his support and acknowledges the hospitality provided by Physical Research Laboratory (PRL), Ahmedabad, India, during his visit, where the work was initiated. T.M would like to acknowledge the DAE-BRNS grant No.37(3)/14/12/2018-BRNS for support. The work of A.D. is supported by the Polish National Science Center Grants No. 2018/30/E/ ST2/00432. A.D. would also like to thank Wei-Zhou Jiang for very useful clarification about the parameter fixing in the dark matter sector in their work.

Appendix A: Two fluid TOV

We start with the background Einstein equation in the presence of two distinct fluids with conserved energy momentum tensors $\bar{T}_{\mu\nu}^{(1)}$ and $\bar{T}_{\mu\nu}^{(2)}$ respectively,

$$\begin{aligned}\bar{G}_{\mu\nu} &= 8\pi\bar{T}_{\mu\nu} = 8\pi(\bar{T}_{\mu\nu}^{(1)} + \bar{T}_{\mu\nu}^{(2)}), \\ &= \text{diag}(e^\alpha\varepsilon, e^\beta P, r^2 P, r^2 \sin^2 \theta P),\end{aligned}\tag{A1}$$

where we have identified the total energy density (ε) and the total pressure (P) of the two fluid system as,

$$\varepsilon(r) = \varepsilon_1(r) + \varepsilon_2(r),\tag{A2}$$

$$P(r) = P_1(r) + P_2(r),\tag{A3}$$

respectively. The background spherically symmetric static metric and its inverse in the spherical polar coordinate system $x^\mu \equiv (t, r, \theta, \phi)$, can be given as,

$$g_{\mu\nu}^{(0)} = \text{diag}\left(-e^{\alpha(r)}, e^{\beta(r)}, r^2, r^2 \sin^2 \theta\right),\tag{A4}$$

$$g^{(0)\mu\nu} = \text{diag}\left(-e^{-\alpha(r)}, e^{-\beta(r)}, 1/r^2, 1/r^2 \sin^2 \theta\right).\tag{A5}$$

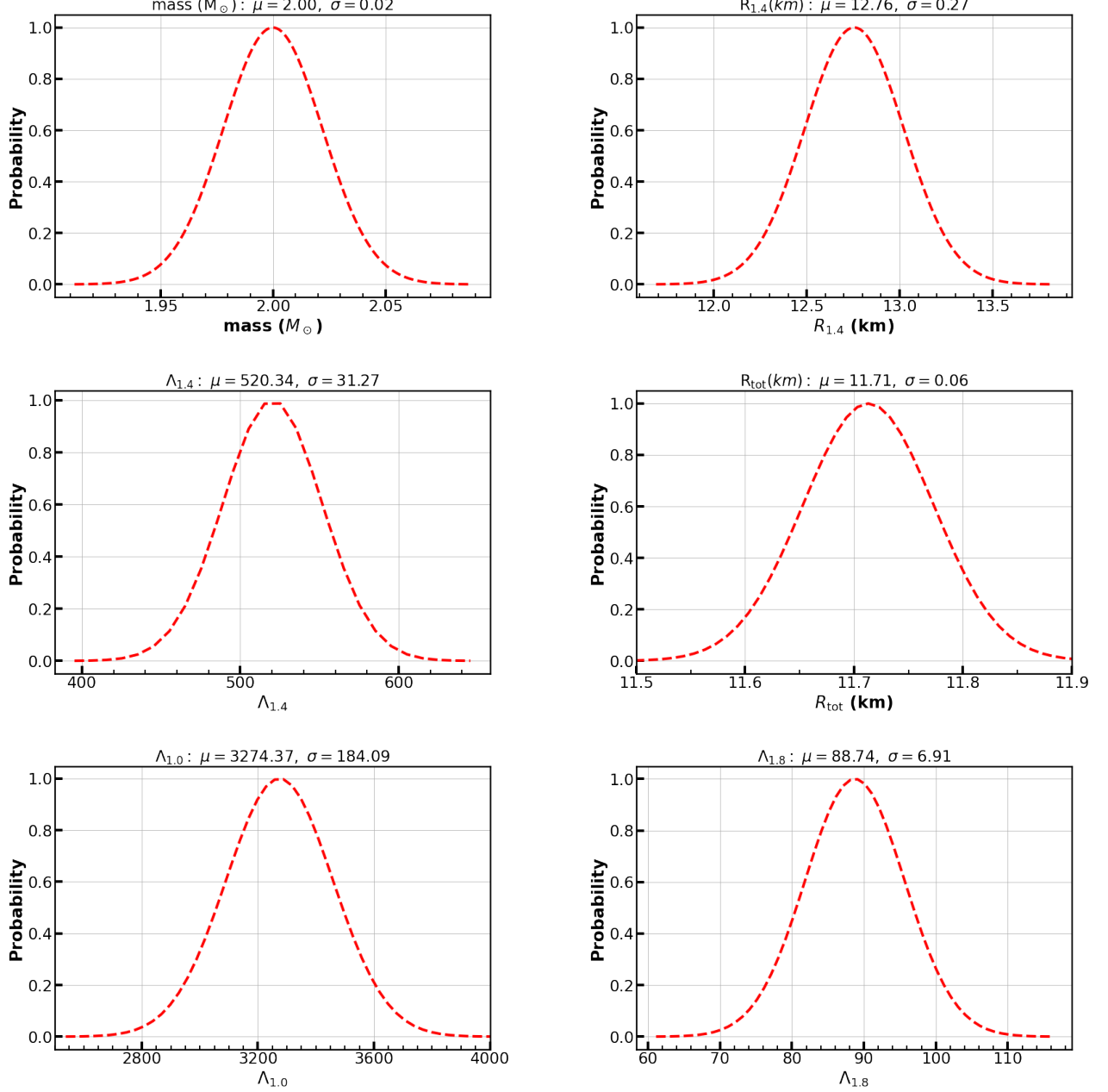


FIG. 2: In this figure we show the distribution of various physical properties of neutron star, i.e. neutron star mass, neutron star radius at 1.4 M_{\odot} , tidal deformability at 1.4 M_{\odot} , total radius of the neutron star, tidal deformability at 1.0 M_{\odot} and tidal deformability at 1.8 M_{\odot} , for the distribution of the parameters c_{sd} , c_{vd} , M_D and f_D as obtained by the Bayesian parameter optimization. In these plots μ denotes the central value of the distribution and σ denotes the standard deviation.

The “ tt ” component of the background Einstein equation gives us,

$$\begin{aligned} \bar{G}_{tt} &= 8\pi\bar{T}_{tt} \\ \implies r\beta' &= 1 - e^{\beta} + 8\pi r^2(\varepsilon_1 + \varepsilon_2)e^{\beta}. \end{aligned} \quad (\text{A6})$$

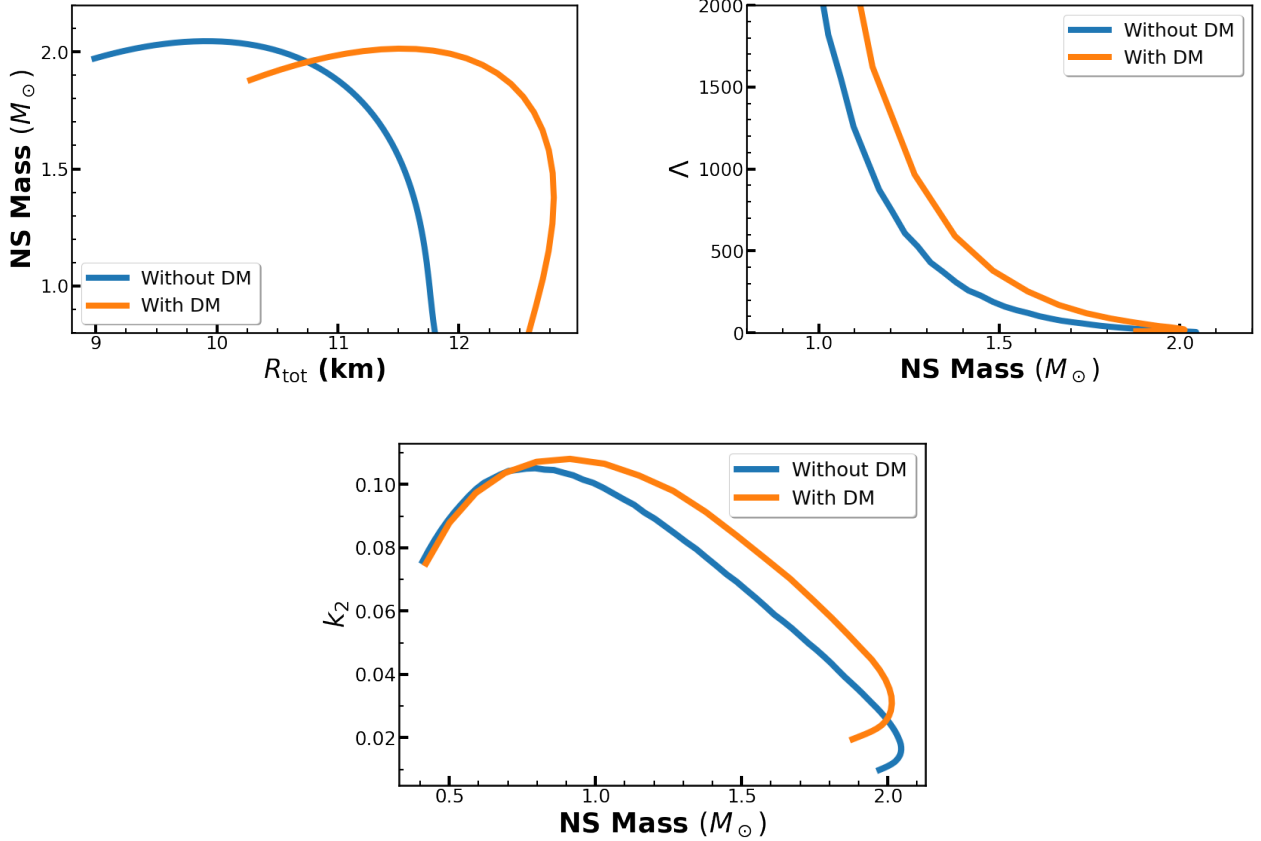


FIG. 3: Mass-radius plot, tidal deformability (Λ), and k_2 plot with and without the dark matter component. In this plots we have considered only the central values of the parameters c_{sd} , c_{vd} , M_D and f_D . For this configuration, we observe that the maximum mass of the neutron star decreases in the presence of the dark matter component. But the total radius corresponding to the maximum mass increases in the presence of a dark matter component. Also the tidal deformability (Λ) and k_2 increases in the presence of a dark matter component.

Similarly the “ rr ” component of the background Einstein equation gives us,

$$\begin{aligned} \bar{G}_{rr} &= 8\pi\bar{T}_{rr} \\ \implies r\alpha' &= 8\pi r^2(P_1 + P_2)e^\beta + e^\beta - 1. \end{aligned} \quad (\text{A7})$$

Eq. (A6) can be recasted as,

$$\begin{aligned} r\beta' &= 1 - e^\beta + 8\pi r^2(\varepsilon_1 + \varepsilon_2)e^\beta \\ \implies -\frac{d}{dr}(r(e^{-\beta} - 1)) &= 8\pi(\varepsilon_1 + \varepsilon_2)r^2 \\ \implies e^{-\beta} &= 1 - \frac{2m(r)}{r}, \end{aligned} \quad (\text{A8})$$

where the mass function $m(r)$ for the two fluid system is defined as,

$$m(r) \equiv 4\pi \int_0^r (\varepsilon_1(r') + \varepsilon_2(r'))r'^{-2}dr'. \quad (\text{A9})$$

In a similar way using Eq.(A8), Eq.(A7) can be written as,

$$\begin{aligned} r\alpha' &= 8\pi r^2(P_1 + P_2)e^\beta + e^\beta - 1 \\ \implies \frac{d\alpha}{dr} &= \frac{8\pi r^3(P_1 + P_2) + 2m(r)}{r(r - 2m(r))}. \end{aligned} \quad (\text{A10})$$

Further, the conservation of the energy momentum tensors of these two fluids imply,

$$\nabla_\mu T_{(1)}^{\mu\nu} = 0, \quad (\text{A11})$$

$$\nabla_\mu T_{(2)}^{\mu\nu} = 0. \quad (\text{A12})$$

Similar to the single fluid case, in a two fluid scenario conservation of energy-momentum tensor as given by Eqs.(A11) and (A12) boil down to,

$$\frac{dP_1}{dr} = -\frac{1}{2}(P_1 + \varepsilon_1)\frac{d\alpha}{dr}, \quad (\text{A13})$$

$$\frac{dP_2}{dr} = -\frac{1}{2}(P_2 + \varepsilon_2)\frac{d\alpha}{dr}. \quad (\text{A14})$$

Using Eq.(A10) back into Eqs.(A13) and Eq.(A14) we obtain,

$$\frac{dP_1}{dr} = -(P_1 + \varepsilon_1)\frac{4\pi r^3(P_1 + P_2) + m(r)}{r(r - 2m(r))}, \quad (\text{A15})$$

$$\frac{dP_2}{dr} = -(P_2 + \varepsilon_2)\frac{4\pi r^3(P_1 + P_2) + m(r)}{r(r - 2m(r))}, \quad (\text{A16})$$

with,

$$\frac{dm(r)}{dr} = 4\pi(\varepsilon_1(r) + \varepsilon_2(r))r^2. \quad (\text{A17})$$

Eq.(A15), Eq.(A16) along with Eq.(A17) constitutes the TOV equations for a two fluid system. One also gets the standard TOV equation for single fluid case by taking correct limit of the two fluid TOV equations. For an alternative approach to derive the two fluid TOV equations using the techniques of Lagrange multipliers, see Ref.[43].

Appendix B: Tidal deformability in a two fluid scenario

Keeping only terms up to first order in metric perturbation, the perturbed metric and the inverse metric can be expressed as [60],

$$\begin{aligned} g_{\mu\nu} &= g_{\mu\nu}^{(0)} + h_{\mu\nu}, \\ g^{\mu\nu} &= g^{(0)\mu\nu} - h^{\mu\nu}, \end{aligned} \quad (\text{B1})$$

respectively. Here $g_{\mu\nu}^{(0)}$ is the background spherically static metric and $h_{\mu\nu}$ is the associated metric perturbation. Note that $h_{\mu\nu}$ has correct tensorial properties in the background metric. Otherway stated space-time indices of $h_{\mu\nu}$ can be raised by $g^{(0)\mu\nu}$. Hence,

$$h^{\mu\nu} = g^{(0)\mu\lambda}g^{(0)\nu\sigma}h_{\lambda\sigma}. \quad (\text{B2})$$

The spherically symmetric static background metric and it's inverse can be expressed as,

$$g_{\mu\nu}^{(0)} = \text{diag}\left(-e^{\alpha(r)}, e^{\beta(r)}, r^2, r^2 \sin^2 \theta\right), \quad (\text{B3})$$

$$g^{(0)\mu\nu} = \text{diag}\left(-e^{-\alpha(r)}, e^{-\beta(r)}, 1/r^2, 1/r^2 \sin^2 \theta\right), \quad (\text{B4})$$

respectively. For $l = 2, m = 0$, static, even-parity metric perturbations ($h_{\mu\nu}$ and $h^{\mu\nu}$) in the Regge-Wheeler gauge can be expressed as (for a detailed discussion see [60]) ,

$$h_{\mu\nu} = \text{diag} \left(-e^{\alpha(r)} H(r) Y_{20}(\theta, \phi), -e^{\beta(r)} H(r) Y_{20}(\theta, \phi), r^2 K(r) Y_{20}(\theta, \phi), r^2 \sin^2 \theta K(r) Y_{20}(\theta, \phi) \right), \quad (\text{B5})$$

$$h^{\mu\nu} = \text{diag} \left(-e^{-\alpha(r)} H(r) Y_{20}(\theta, \phi), -e^{-\beta(r)} H(r) Y_{20}(\theta, \phi), \frac{1}{r^2} K(r) Y_{20}(\theta, \phi), \frac{1}{r^2 \sin^2 \theta} K(r) Y_{20}(\theta, \phi) \right). \quad (\text{B6})$$

Using the perturbed metric and energy-momentum tensor, the first order Einstein equations can be written as,

$$\delta G^t_t = 8\pi \delta T^t_t = -8\pi \delta \varepsilon, \quad (\text{B7})$$

$$\delta G^r_r = 8\pi \delta T^r_r = 8\pi \delta P, \quad (\text{B8})$$

$$\delta G^\theta_\theta = 8\pi \delta T^\theta_\theta = 8\pi \delta P, \quad (\text{B9})$$

$$\delta G^\phi_\phi = 8\pi \delta T^\phi_\phi = 8\pi \delta P, \quad (\text{B10})$$

$$\delta G^r_\theta = 0. \quad (\text{B11})$$

Here the components of the perturbed Einstein tensor are,

$$\delta G^t_t = \frac{e^{-\beta}}{2r^2} Y_{20}(\theta, \phi) \left[r \left\{ 2H' + K'(6 - r\beta') + 2rK'' \right\} + H(2 + 6e^\beta - 2r\beta') - 4Ke^\beta \right], \quad (\text{B12})$$

$$\delta G^r_r = \frac{Y_{20}(\theta, \phi)}{2r^2} e^{-\beta} \left[-4Ke^\beta + H(2 + 2r\alpha' - 6e^\beta) + r \left\{ 2H' + K'(2 + r\alpha') \right\} \right], \quad (\text{B13})$$

$$\begin{aligned} \delta G^\theta_\theta = & \frac{Y_{20}(\theta, \phi)}{4r} e^{-\beta} \left[2H(\alpha' - \beta') + Hr\alpha'(\alpha' - \beta') + H'(4 + 3r\alpha' - r\beta') \right. \\ & \left. + K'(4 + r\alpha' - r\beta') + 2rH'' + 2rK'' + 2rH\alpha'' \right], \end{aligned} \quad (\text{B14})$$

$$\delta G^r_\theta = -\frac{1}{2} e^{-\beta} \frac{\partial Y_{20}(\theta, \phi)}{\partial \theta} \left[\alpha' H(r) + H' + K' \right]. \quad (\text{B15})$$

Using Eq.(B9), Eq.(B10) and Eq.(B14) perturbation in total pressure of the two fluid system can be expressed as,

$$\begin{aligned} \delta P = & \frac{\delta G^\theta_\theta + \delta G^\phi_\phi}{16\pi} = \frac{\delta G^\theta_\theta}{8\pi} \\ = & \frac{Y_{20}(\theta, \phi)}{32\pi r} e^{-\beta} \left[2H(\alpha' - \beta') + Hr\alpha'(\alpha' - \beta') + H'(4 + 3r\alpha' - r\beta') \right. \\ & \left. + K'(4 + r\alpha' - r\beta') + 2rH'' + 2rK'' + 2rH\alpha'' \right]. \end{aligned} \quad (\text{B16})$$

The (r, θ) component of the perturbed Einstein equation allows us to write,

$$K'' = -H'' - \alpha' H' - \alpha'' H. \quad (\text{B17})$$

Using the “ tt ” and “ rr ” component of the perturbed Einstein tensor as given in Eq.(B7) and Eq.(B8) we obtain,

$$\begin{aligned} \delta G^t_t - \delta G^r_r &= 8\pi(\delta T^0_0 - \delta T^r_r), \\ \implies \delta G^t_t - \delta G^r_r + 8\pi \left(1 + \frac{d\varepsilon}{dP} \right) \delta P &= 0. \end{aligned} \quad (\text{B18})$$

Here we have expressed $\delta\varepsilon = (d\varepsilon/dP)\delta P$. Further using Eq.(B12), Eq.(B13), Eq.(B16) and Eq.(B17) allows us to recast Eq.(B18) as,

$$H'' + C_1 H' + C_0 H = 0, \quad (\text{B19})$$

where the coefficients of H' and H are,

$$C_1 = \frac{2}{r} + \frac{\alpha' - \beta'}{2}, \quad (\text{B20})$$

and,

$$C_0 = \left[-\frac{6}{r^2} e^\beta + \left(\alpha'' - \frac{\alpha' \beta'}{2} \right) - \frac{1}{2} \alpha'^2 + \frac{7}{2} \frac{\alpha'}{r} + \frac{1}{2r} \frac{d\varepsilon}{dP} \alpha' + \frac{3}{2} \frac{\beta'}{r} + \frac{1}{2r} \frac{d\varepsilon}{dP} \beta' \right], \quad (\text{B21})$$

respectively. Till this point the derivation of the evolution equation of $H(r)$ is general and does not assume any specific form of matter energy momentum tensor. Recall for a two fluid system,

$$r\alpha' = 8\pi(P_1 + P_2)r^2e^\beta + e^\beta - 1, \quad (\text{B22})$$

$$r\beta' = 1 - e^\beta + 8\pi(\varepsilon_1 + \varepsilon_2)r^2e^\beta. \quad (\text{B23})$$

Therefore C_1 as given in Eq. (B20) can be expressed as,

$$\begin{aligned} C_1 &= \frac{2}{r} + 4\pi r e^\beta ((P_1 + P_2) - (\varepsilon_1 + \varepsilon_2)) + \frac{e^\beta - 1}{r} \\ &= \frac{2}{r} + e^\beta \left(\frac{2m}{r^2} + 4\pi r ((P_1 + P_2) - (\varepsilon_1 + \varepsilon_2)) \right). \end{aligned} \quad (\text{B24})$$

Recall,

$$C_0 = -\frac{6}{r^2} e^\beta + \left(\alpha'' - \frac{\alpha' \beta'}{2} \right) - \frac{\alpha'^2}{2} + \frac{7}{2} \left(\frac{\alpha'}{r} \right) + \frac{1}{2r} \frac{d\varepsilon}{dP} \alpha' + \frac{3}{2} \frac{\beta'}{r} + \frac{1}{2r} \frac{d\varepsilon}{dP} \beta'. \quad (\text{B25})$$

Further using the background Einstein equation for $(\theta\theta)$ component allows us to write,

$$\begin{aligned} \bar{G}_{\theta\theta} &= 8\pi(P_1 + P_2)r^2 \\ \implies \alpha'' - \frac{\alpha' \beta'}{2} &= 16\pi(P_1 + P_2)e^\beta - \frac{\alpha'^2}{2} + \frac{\beta'}{r} - \frac{\alpha'}{r}. \end{aligned} \quad (\text{B26})$$

Using Eq. (B26), C_0 as given in Eq. (B25) can be simplified to,

$$C_0 = -\frac{6}{r^2} e^\beta + 4\pi e^\beta \left((P_1 + P_2) + (\varepsilon_1 + \varepsilon_2) \right) \frac{d\varepsilon}{dP} + 4\pi e^\beta \left(5(\varepsilon_1 + \varepsilon_2) + 9(P_1 + P_2) \right) - \alpha'^2. \quad (\text{B27})$$

For two fluid system assuming both fluids have a barotropic equation of state we get,

$$\frac{d\varepsilon}{dP} = \left(\frac{d\varepsilon_1}{dP_1} \right) \frac{\delta P_1}{\delta P_1 + \delta P_2} + \left(\frac{d\varepsilon_2}{dP_2} \right) \frac{\delta P_2}{\delta P_1 + \delta P_2}. \quad (\text{B28})$$

Further using two fluid TOV equations (Eqs. (A15) and (A16)) we can write,

$$\frac{\delta P_1}{\delta P_1 + \delta P_2} = \frac{P_1 + \varepsilon_1}{(P_1 + P_2) + (\varepsilon_1 + \varepsilon_2)}, \quad (\text{B29})$$

and

$$\frac{\delta P_2}{\delta P_1 + \delta P_2} = \frac{P_2 + \varepsilon_2}{(P_1 + P_2) + (\varepsilon_1 + \varepsilon_2)}. \quad (\text{B30})$$

Therefore for two fluid case,

$$C_0 = -6 \frac{e^\beta}{r^2} + 4\pi e^\beta \left[5\varepsilon_1 + 9P_1 + (P_1 + \varepsilon_1) \left(\frac{d\varepsilon_1}{dP_1} \right) + 5\varepsilon_2 + 9P_2 + (P_2 + \varepsilon_2) \left(\frac{d\varepsilon_2}{dP_2} \right) \right] - \alpha'^2. \quad (\text{B31})$$

Now let us introduce the dimensionless variable $y \equiv \frac{rH'}{H}$. In terms of $y(r)$ the evolution equation of $H(r)$ as given in Eq. (B19) can be expressed as,

$$r \frac{dy(r)}{dr} + y(r)^2 + y(r)F(r) + r^2Q(r) = 0, \quad (\text{B32})$$

with,

$$F(r) = \frac{r - 4\pi r^3 ((\varepsilon_1(r) + \varepsilon_2(r)) - (P_1(r) + P_2(r)))}{r - 2m(r)},$$

and

$$\begin{aligned} Q(r) &= \frac{4\pi r \left(5(\varepsilon_1(r) + \varepsilon_2(r)) + 9(P_1(r) + P_2(r)) + \frac{\varepsilon_1(r) + P_1(r)}{\partial P_1(r)/\partial \varepsilon_1(r)} + \frac{\varepsilon_2(r) + P_2(r)}{\partial P_2(r)/\partial \varepsilon_2(r)} - \frac{6}{4\pi r^2} \right)}{r - 2m(r)} \\ &- 4 \left[\frac{m(r) + 4\pi r^3 (P_1(r) + P_2(r))}{r^2 (1 - 2m(r)/r)} \right]^2, \end{aligned}$$

For the two fluid system only the Einstein equation inside the matter changes but the evolution equation of y outside matter remains unaltered (see Ref. [60] for details). The boundary conditions for $y(r)$ can be obtained by requiring regularity of $y(r)$ at $r = 0$. By considering only the leading order contribution to $y(r)$ at $r = 0$ one can easily obtain the boundary condition which is also same for a single fluid system (see Ref. [60]). This is because at $r = 0$ in the leading order, matter part does not contribute to $y(r)$. Therefore even for multiple fluids $y(r = 0) = 2$.

- [1] T. Plehn, [arXiv:1705.01987](#)
- [2] K. Lawson, A. R. Zhitnitsky, [arXiv:1305.6318](#)
- [3] F. Kahlhoefer, Int.J.Mod.Phys.A 32 (2017) 13, 1730006.
- [4] J. M. Lattimer, Ann.Rev.Nucl.Part.Sci. **62**, 485-515 (2012).
- [5] R. C. Tolman, Phys. Rev. 55, 364 (1939); J. R. Oppenheimer and G. M. Volkov, Phys. Rev. 55, 374 (1939).
- [6] J. M. Lattimer and M. Prakash 2001 ApJ 550 426.
- [7] Lattimer J M and Prakash M 2007 Phys. Rep. 442, 109–65
- [8] Ozel F 2013 Rep. Prog. Phys. 76016901
- [9] Steiner A W, Lattimer J M and Brown E F 2010 Astrophys. J. 722, 33–54
- [10] Ozel F, Baym G and Guver T 2010 Phys. Rev. D 82, 101301
- [11] Steiner A W, Lattimer J M and Brown E F 2013 Astrophys. J. 765 L5
- [12] Guver T and Ozel F 2013 Astrophys. J. 765 L1
- [13] Lattimer J M and Steiner A W 2014 Astrophys. J. 784, 123
- [14] Lattimer J M and Steiner A W 2014 Eur. Phys. J. A 50, 40
- [15] Ozel F, Psaltis D, Guver T, Baym G, Heinke C and Guillot S 2016 Astrophys. J. 82028.
- [16] T. E. Riley et.al., ApJL 887 L21 (2019).
- [17] Ray P S, Feroci M, den Herder J, Bozzo E, Stella L and LOFT Collaboration 2012 The large observatory for x-ray timing (LOFT): an ESA M-class mission concept American Astronomical Society Meeting Abstracts 219 vol 219 p 249.06
- [18] Feroci M et al 2012 LOFT: the large observatory for x-ray timing Soc. Photo-Opt. Instrum. Eng. 8443 84432D
- [19] B.P. Abbott et al., Phys. Rev. Lett. **119**, 161101 (2017).
- [20] B.P. Abbott et al., Phys. Rev. Lett. **121**, 161101 (2018).
- [21] N. Raj, P. Tanedo, H.B. Yu, Phys. Rev. **D97**, 043006 (2018).
- [22] I. Goldman, S. Nussinov, Phys.Rev. **D40**, 3221-3230 (1989).
- [23] A. Gould, B.T.Draine, R. W.Romani, and S. Nussinov, Phys. Lett. **B.238**, 337 (1990).
- [24] C. Kouvaris, Phys.Rev. **D77**, 023006 (2008).
- [25] C. Kouvaris, P. Tinyakov, Phys.Rev. **D82**, 063531 (2010).
- [26] A. de Lavallaz and M. Fairbairn, Phys.Rev. **D81** 123521 (2010).
- [27] T. Guver, A. E. Erkoca, M.H.Reno, and I. Sarcevic, JCAP **05**, 013 (2014).
- [28] M. Angeles, P. Garcia. J. Silk, Phys. Lett. B 711 6(2012).
- [29] F. Sandin, P. Ciarcellut, Astroparticle Phys. 32, 278 (2009).
- [30] P. Ciarcellut, F. Sandin, Phys. Lett. B 695, 19 (2011).

- [31] R. Ciancarella, F. Pannarale, A. Addazi, A. Marciano, arxiv: 2010.12904.
- [32] G. Panotopoulos, I. Lopes, Phys.Rev. **D96**, 083004 (2017).
- [33] J. D. Walecka, Ann. Phys.**83**, 491 (1974).
- [34] B. D. Serot and J. D. Walecka, Int. J. Mod. Phys. **E6**, 515 (1997).
- [35] J.Boguta and A.R.Bodmer, Nucl. Phys. **A292**, 413-428 (1977); J.Boguta and H.Stoecker, Phys.Lett. **B120** , 289-293 (1983); J.Boguta, Phys.Lett. **B106** 255-258 (1981) .
- [36] Y.K.Gambhir, P. Ring, and A. Thimet, Ann. Phys. (N.Y.) **198**, 132 (1990).
- [37] P. Ring, Prog. Part. Nucl. Phys. **37**,193 (1996).
- [38] A. Das, T. Malik, A. C. Nayak, Phys.Rev. **D 99** (2019) no.4, 043016.
- [39] J. Boguta, Phys.Lett. **B106** 245-249 (1981)
- [40] G. A. Lalazissis, J. Konig and P. Ring, Phys. Rev. **C55**, 540 (1997)
- [41] S.-C. Leung, M.-C. Chu, L.-M. Lin, Physical Review D 84, 107301 (2011).
- [42] G. L. Comer, D. Langlois and L. M. Lin, Phys. Rev. D60, 104025 (1999).
- [43] Qian-Fei Xiang, Wei-Zhou Jiang,Dong-Rui Zhang, and Rong-Yao Yang, Phys.Rev. **C89**, 025803 (2014).
- [44] J. Ellis, G. Hutsi,K. Kannike,L. Marzola,M. Raidal, V. Vaskonen, Phys.Rev. **D97**, 123007 (2018).
- [45] B. Biswas, R. Nandi, P. Char, S. Bose, N. Stergioulas, arXiv: 2010.02090
- [46] A. W. Steiner, J. M. Lattimer, E. F. Brown, Astrophys.J. 722 (2010) 33-54.
- [47] B.P. Abbott et. al., Phys.Rev.X 9 (2019) 1, 011001.
- [48] Soumi De, Daniel Finstad, James M. Lattimer, Duncan A. Brown, Edo Berger, et. al. Phys.Rev.Lett. 121 (2018) 9, 091102, Phys.Rev.Lett. 121 (2018) 25, 259902 (erratum).
- [49] T. E. Riley, A. L. Watts, S. Bogdanov, Paul S. Ray, Renee M. Ludlam et. al., Astrophys.J.Lett. 887 (2019) 1, L21.
- [50] K. C. Chung, C.S. Wang, A.J.Santiago, and J. W. Zhang, Eur.Phys.J.A11137-141 (2001).
- [51] N. K. Glendenning, Compact stars, 2nd edition, Springer, (2000).
- [52] Laura Tolos, Mario Centelles, Angels Ramos, Astronomical Society of Australia (PASA), Vol. 34, e065 (2017); arXiv: [arXiv:1708.08681](https://arxiv.org/abs/1708.08681)
- [53] Li, B.-A., Ramos, A., Verde, G., Vidana, I., EPJ, A50, 9 (2014).
- [54] Boguta, J., Bodmer, A. R., NucPh, A292, 413 (1977).
- [55] Boguta, J., Stoecker, H., PhL, B120, 289 (1983).
- [56] Bodmer, A. R. 1991, NucPh, A526, 703.
- [57] Mueller, H., Serot, B. D. 1996, NucPh, A606, 508.
- [58] Horowitz, C. J., Piekarewicz, J. 2001a, PhRvL, 86, 5647; Horowitz, C. J., Piekarewicz, J. 2001b, PhRv, C64, 062802.
- [59] J. P. W. Diener, [arXiv:0806.0747\[nucl-th\]](https://arxiv.org/abs/0806.0747)
- [60] T. Hinderer, Astrophys. **J.677**, 1216 (2008).
- [61] T. Hinderer, B. D. Lackey, R. N. Lang, and J. S. Read, Phys. Rev. **D81**, 123016 (2010).
- [62] S. Postnikov, M. Prakash, J. M. Lattimer, Phys.Rev. **D82** 024016, 2010.
- [63] T. Malik, N. Alam,M. Fortin, C. Providencia, B. K. Agrawal, T. K. Jha, B. Kumar and S. K. Patra, [arXiv:1805.11963](https://arxiv.org/abs/1805.11963)
- [64] K. Zhang, G. Z. Huang, F. L. Lin, arXiv: 2002.10961.
- [65] Wesolowski, S., Klco, N., Furnstahl, R.J., Phillips, D.R., Thapaliya, A., J. Phys. G, 43, 074001 (2016).
- [66] R.J. Furnstahl, N. Klco, D.R. Phillips, S. Wesolowski,Phys.Rev.C 92 (2015) 2, 024005.
- [67] R. T. Cox, American Journal of Physics 14, 1 (1946);
- [68] R. T. Cox, “Algebra of Probable Inference”, 2001.
- [69] E.T.Jaynes, Probability Theory The Logic of Science, edited by G. Larry Bretthorst, Cambridge University Press, 2003.
- [70] J. Antoniadis et al., Science 340, 6131 (2013).
- [71] Malik et al Phys.Rev.C 99 (2019) 5, 052801.
- [72] L. Baiotti Prog.Part.Nucl.Phys. 109 (2019) 103714.
- [73] Tews, I., Margueron, J., & Reddy, S. 2018, Phys. Rev. C, 98, 045804, doi: 10.1103/PhysRevC.98.045804
- [74] Annala, E., Gorda, T., Kurkela, A., & Vuorinen, A. 2018, Phys. Rev. Lett., 120, 172703, doi: 10.1103/PhysRevLett.120.172703
- [75] B. P. Abbott et al. (Virgo, LIGO Scientific), Phys. Rev. Lett. 121, 161101 (2018), [arXiv:1805.11581](https://arxiv.org/abs/1805.11581) [gr-qc]

Dark matter admixed neutron stars with a realistic nuclear equation of state from chiral nuclear interactions

Domenico Scordino^a, Ignazio Bombaci^{a,b},

^a*Dipartimento di Fisica “E. Fermi”, Università di Pisa, Largo B. Pontecorvo 3, I-56127 Pisa, Italy*

^b*INFN, Sezione di Pisa, Largo B. Pontecorvo 3, I-56127 Pisa, Italy*

(Dated: May 30, 2024)

We study the effects of dark matter on the structural properties of neutron stars. In particular we investigate how the presence of a dark matter component influences the mass-radius relation, the value of the maximum mass of a neutron star and others stellar properties. To model ordinary matter we use a state-of-the-art equation of state of β -stable nuclear matter obtained using the Brueckner-Hartree-Fock quantum many-body approach starting from two-body and three-body nuclear interactions derived from chiral effective field theory. The dark matter component of the star is modeled as a non-self-annihilating system of spin 1/2 fermions and its equation of state as an ideal relativistic Fermi gas. The equilibrium configurations of these dark matter admixed neutron stars (DANS) are calculated by solving a generalization of the Tolman-Oppenheimer-Volkoff equations to the case where the system consists of two perfect fluids interacting solely through gravity. We find that, depending on the dark matter particle mass m_χ , one can have somehow opposite effects on the stellar properties. In the case $m_\chi = 1 \text{ GeV}$, the stellar gravitational maximum mass M_{max} decreases, whereas in the case $m_\chi = 0.1 \text{ GeV}$, M_{max} increases with respect to the maximum mass of ordinary neutron stars. We also show that the presence of dark matter has indirect sizeable effect on the proton fraction in the ordinary matter fluid and, in the case $m_\chi = 1 \text{ GeV}$, results in a decrease of the threshold gravitational mass M_{tot}^{durca} for having direct URCA processes and fast stellar cooling. Finally we study the stability of dark matter admixed neutron stars with respect to radial perturbations.

I. INTRODUCTION

In spite of its many successes, Einstein’s theory of general relativity provides predictions that are at variance with astrophysical observational data on the kinematics of self-gravitating systems as galaxies and clusters of galaxies [1, 2]. In order to reproduce these data using general relativity requires the introduction of a new type of matter, known as dark matter (DM), that is not directly observable except through its gravitational effects on ordinary matter. Cosmological data, currently explained by the Λ -cold dark matter (Λ CDM) model [3], indicate that DM should be responsible for about 23% percent of the total energy density of the Universe while ordinary matter (OM) contributes only 4%. The remaining portion is due to dark energy responsible for the accelerated expansion of the Universe [4, 5].

The main feature of DM is that its cross section for electromagnetic processes must be extremely small or zero. As a result, DM cannot lose energy by emitting electromagnetic radiation, as in the case of ordinary matter, and thus DM does not collapse at the center of galaxies. In fact, the rotation curve profiles of disc galaxies (i.e. the plot of the orbital speeds of visible stars or gas in the galaxy versus their radial distance from the galaxy’s centre) are in agreement with the presence of an extended and diffuse halo of DM (see [6–8]).

None of the particles of the standard model meet the requirements for explaining the numerous astrophysical observations and cosmological data that require the existence of dark matter. Thus candidate particles to consti-

tute dark matter most often emerge from extensions of the standard model. A much-studied class of such particles are WIMPs (weakly interacting massive particles), and many active experiments are attempting to reveal their existence. No such experiments, however, have so far obtained convincing results on the existence of DM particles even though very stringent constraints on the interaction cross section of dark matter with ordinary matter have been produced (see e.g. [9]). If such a cross section is nonzero (although very small), it is conceivable that DM could be captured by stars or compact stellar objects, especially in environments such as the Galactic center, in a sufficient amount to produce observable effects.

Due to the very high densities ($10^{14} - 10^{15} \text{ g/cm}^3$) in their cores, the extreme surface gravity ($g \sim 10^{12} \text{ m/s}^2$) and their ages (up to 10^{10} yr), neutron stars are very good candidates where dark matter can be captured and can accumulate in sufficient amounts to influence their structural and evolutionary properties. Neutron stars can thus be used as natural detectors to identify DM and possibly unveil its nature [10–23].

In this paper we study the effects of the presence of DM on the structure and stability of neutron stars. In particular, we investigate, in a very detailed and systematic way, how the properties of these Dark matter Admixed Neutron Stars (DANS) are modified with respect to those of ordinary neutron stars in terms of the peculiarities and the fraction of DM present in the star.

The comparison of the results for the properties of DANS obtained in this work with some observational

properties of neutron stars, such as the values of their gravitational mass (especially those of "massive" stars with $M \sim 2 M_\odot$ that place stringent constraints on the value of the Oppenheimer-Volkoff mass limit) or the combined mass and radius measurements (obtained from NASA's NICER X-ray observatory) allowed us to derive constraints on the mass of the dark matter particles and the fraction of dark matter present in the star.

This work is organized as follows. In Section II, we introduce the two-fluids Tolman-Oppenheimer-Volkoff (TOV) stellar structure equations. In Section III, we discuss the equation of state for OM and for DM used in the present work. In Section IV we present results obtained by solving the two-fluids TOV equation and discuss the properties of DANS. In Section V we use observational data for properties of neutron stars to determine an upper limit to the dark matter particle mass. In Section VI, we study the stability of DANS equilibrium configurations with respect to small radial perturbations. Finally, in Section VII we give a brief summary of our work.

II. STRUCTURE EQUATIONS FOR DANS

Since the non-gravitational interaction between dark matter and ordinary matter is extremely small (e.g. [9, 24]), it is possible to split the total energy-momentum tensor as the sum of the energy-momentum tensor of each of the two fluids (OM and DM) and to have covariant conservation for both of them. Accordingly, the equation of state of OM is independent on the state variables of DM and vice versa. In addition, it is assumed that each of the two fluids be a perfect fluid. Based on these assumptions, and further assuming a spherically symmetric and stationary distribution of OM and DM, the stellar structure equations in general relativity for DANS take the following form (see e.g. [21]), which generalizes the TOV equations to the case of two fluids interacting exclusively through gravity:

$$\begin{aligned} \frac{dP_j}{dr} = & -G \frac{m_{tot}(r) \varepsilon_j(r)}{c^2 r^2} \left(1 + \frac{P_j(r)}{\varepsilon_j(r)} \right) \\ & \times \left(1 + \frac{4\pi r^3 P_{tot}^3(r)}{c^2 m_{tot}(r)} \right) \left(1 - \frac{2G m_{tot}(r)}{c^2 r} \right)^{-1} \end{aligned} \quad (1)$$

and

$$\frac{dm_j(r)}{dr} = \frac{4\pi}{c^2} r^2 \varepsilon_j(r), \quad (2)$$

where G is the gravitational constant, P_j and ε_j (with $j = \text{OM}, \text{DM}$) are the pressure and energy density for the OM and DM fluid, $m_j(r)$ is the gravitational mass enclosed within a sphere of radial coordinate r (surface area $4\pi r^2$) for each of the two fluids, $m_{tot}(r) = m_{\text{OM}}(r) + m_{\text{DM}}(r)$ is the total gravitational mass enclosed within a sphere of radial coordinate r and $P_{tot}(r) = P_{\text{OM}}(r) + P_{\text{DM}}(r)$ the total pressure.

A. Numerical integration

To solve the stellar structure equations (1) and (2) we need to specify the equation of state for the two fluids (see next section) and the appropriate boundary conditions at the center ($r = 0$) and at the surface ($r = R_j$, $j = \text{OM}, \text{DM}$) of the matter distribution for each fluid [21]:

$$m_j(0) = 0 \quad \varepsilon_j(0) = \varepsilon_{c,j}$$

We define the radius R_j of the distribution of fluid j by the following condition

$$P_j(R_j) = P_j^{surf}$$

where P_j^{surf} is a fixed value for the surface pressure of fluid j . For dark matter we use $P_{\text{DM}}^{surf} = 0$ while for ordinary matter we chose $P_{\text{OM}}^{surf} = P_{\text{OM}}(\rho^*)$, where $\rho^* = 7.86 \text{ g/cm}^3$ is the mass density of solid ^{56}Fe . For $r > R_j$ we define $P_j(r) = 0$. The total radius of the star is

$$R = \max\{R_{\text{OM}}, R_{\text{DM}}\} \quad (3)$$

Integrating Eq.(2) we get the total gravitational mass M_j for each of the two fluids ($j = \text{OM}, \text{DM}$)

$$M_j \equiv m_j(R_j) = \frac{4\pi}{c^2} \int_0^{R_j} r^2 \varepsilon_j(r) dr \quad (4)$$

and the total gravitational mass of the DANS is

$$M_{\text{tot}} = M_{\text{OM}} + M_{\text{DM}}. \quad (5)$$

III. EQUATION OF STATE

A. The equation of state of ordinary matter

In this work we model the OM fluid of a DANS as a uniform electric-charge-neutral fluid of neutrons, protons, electrons, and muons. Recently a new microscopic EOS for this system has been obtained in Ref. [25] (hereafter the BL EOS) for the zero temperature case, using the Brueckner-Hartree-Fock (BHF) quantum many-body approach (see [25] and references therein) starting from modern two-body and three-body nuclear interactions derived within chiral effective field theory (ChEFT) (e.g. [26, 27]). These chiral nuclear interactions reproduce with high accuracy the nucleon-nucleon (NN) scattering data and the experimental binding energies of light ($A = 3, 4$) atomic nuclei [28].

The BL EOS reproduces the empirical saturation point (i.e. saturation density $n_0 = 0.16 \pm 0.01 \text{ fm}^{-3}$, and energy per nucleon $E/A|_{n_0} = -16.0 \pm 1.0 \text{ MeV}$) of symmetric nuclear matter, and other empirical properties (symmetry energy E_{sym} and its slope parameter L , incompressibility) of nuclear matter at the saturation density n_0 (see

Tab. 2 in [25]). In particular the calculated $E_{sym}(n_0)$ and L for this EOS fulfill the bounds imposed by the unitary Fermi gas limit [29, 30]. As has been shown in ref. [29] several EOS models currently used in neutron star structure calculations, in supernova explosions and binary neutron star mergers simulations violate the unitary Fermi gas bounds.

Further the BL EOS is consistent (see figure 2 in [25]) with the measured elliptic flow of matter in heavy-ion collisions experiments [31].

At supranuclear densities ($n > n_0$) the BL EOS model predicts a symmetry energy $E_{sym}(n)$ which is in very good agreement with the empirical constraints derived in [32] using the excitation energies of isobaric analog states in nuclei and with additional constraints from neutron skin thickness of heavy nuclei [33]. As is well known, the symmetry energy $E_{sym}(n)$, and particularly its density dependence is a crucial ingredient to determine the proton fraction in β -stable nuclear matter [34–37] and ultimately it has an impact on the value of stellar radius and on the thickness of the crust [38, 39] and on the possibility of having direct URCA processes [40] (see Section IVB) and thus rapid cooling of neutron stars [41].

When computing static ordinary neutron star configurations the BL EOS (for the β -stable case) gives [25] a maximum mass $M_{max} = 2.08 M_\odot$, with a corresponding central density $\rho_c = 2.74 \times 10^{15} \text{ g/cm}^3$ and radius $R(M_{max}) = 10.26 \text{ km}$ and a quadrupolar tidal polarizability coefficient $\Lambda_{1.4} = 385$ (for the $1.4 M_\odot$ neutron star [42]) compatible with the constraints derived from GW170817 [43].

Recently, the BL EOS has been extended [44] to finite temperature and to arbitrary proton fractions. This finite-temperature EOS model has been applied to numerical simulations of binary neutron star mergers [45–47].

Finally, to model the (ordinary) neutron star crust (i.e. for nucleonic density $\leq 0.08 \text{ fm}^{-3}$) we have used the Baym–Pethick–Sutherland [48] and the Negele–Vautherin [49] EOS.

B. The equation of state of dark matter

In the present work we consider non-self-annihilating fermionic DM. This so called fermionic asymmetric dark matter (ADM) [50, 51] carry a conserved charge which is analogous to the baryon number in the case of ordinary matter. We describe the ADM fluid as a non-interacting (ideal) gas of fermions with mass m_χ and spin 1/2. The corresponding EOS is well known (see e.g. [52]) and is given by the following expressions

$$\begin{aligned}\varepsilon(x) &= \alpha(m_\chi, \nu)\chi(x) \\ p(x) &= \alpha(m_\chi, \nu)\phi(x) \\ n(x) &= n_0(m_\chi, \nu)x^3\end{aligned}$$

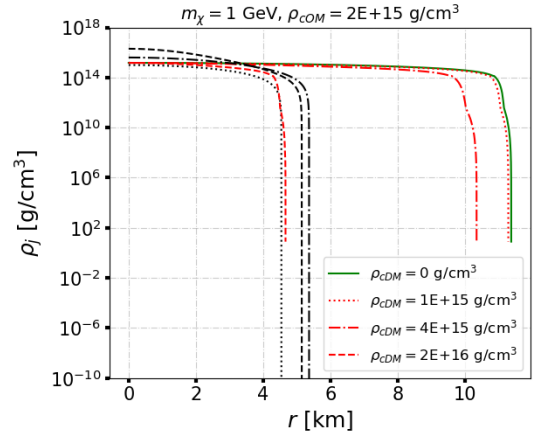


FIG. 1. Mass-density profiles of ordinary matter (red) and dark matter (black) to the two-fluids TOV equation for $m_\chi = 1 \text{ GeV}$, $\rho_{cOM} = 2 \times 10^{15} \text{ g/cm}^3$ and different values of the dark matter central densities ρ_{cDM} . Each line-style correspond to a different choice of ρ_{cDM} : $(\rho_{cOM}, 0)$ (green continuous line), $(\rho_{cOM}, 10^{15} \text{ g/cm}^3)$ (dotted lines), $(\rho_{cOM}, 4 \times 10^{15} \text{ g/cm}^3)$ (dash-dot lines), $(\rho_{cOM}, 2 \times 10^{16} \text{ g/cm}^3)$ (dashed lines).

ρ_{cDM} [g/cm³]	M_{OM} [M_\odot]	M_{DM} [M_\odot]	f_χ [%]	R_{OM} [km]	R_{DM} [km]
0	1.895	0	0	11.375	0
10^{15}	1.740	0.050	2.78	11.287	5.542
4×10^{15}	1.059	0.240	18.44	10.345	5.365
2×10^{16}	0.095	0.453	82.62	4.664	5.148

TABLE I. Values for the gravitational mass of ordinary matter and dark matter and total fraction of dark matter obtained for $m_\chi = 1 \text{ GeV}$, $\rho_{cOM} = 2 \times 10^{15} \text{ g/cm}^3$ and different values of the dark matter central mass-density.

where $x \equiv \hbar k_F / (m_\chi c)$ is the adimensional Fermi momentum, the degeneracy factor $\nu = 2$ for spin 1/2 particles and

$$\begin{aligned}\alpha(m_\chi, \nu) &= \nu \frac{\hbar c}{16\pi^2} \left(\frac{m_\chi c^2}{\hbar c} \right)^4 \\ n_0(m_\chi, \nu) &= \nu \frac{(m_\chi c^2)^3}{6\pi^2 (\hbar c)^3} \\ \chi(x) &= x(1+x^2)^{1/2}(1+2x^2) - \ln[x + (1+x^2)^{1/2}] \\ \phi(x) &= x(1+x^2)^{1/2} \left(\frac{2}{3}x^2 - 1 \right) + \ln[x + (1+x^2)^{1/2}]\end{aligned}$$

IV. DANS PROPERTIES

For a fixed values of the dark matter particle mass m_χ , a solution to the two-fluid TOV equations (1) and (2) is uniquely identified once we fix the central mass densities (central energy densities) ρ_{cOM} and ρ_{cDM} for the two fluids.

As an illustrative example, we display in Figure 1 the radial mass density profiles $\rho_{OM}(r)$ for OM (red curves)

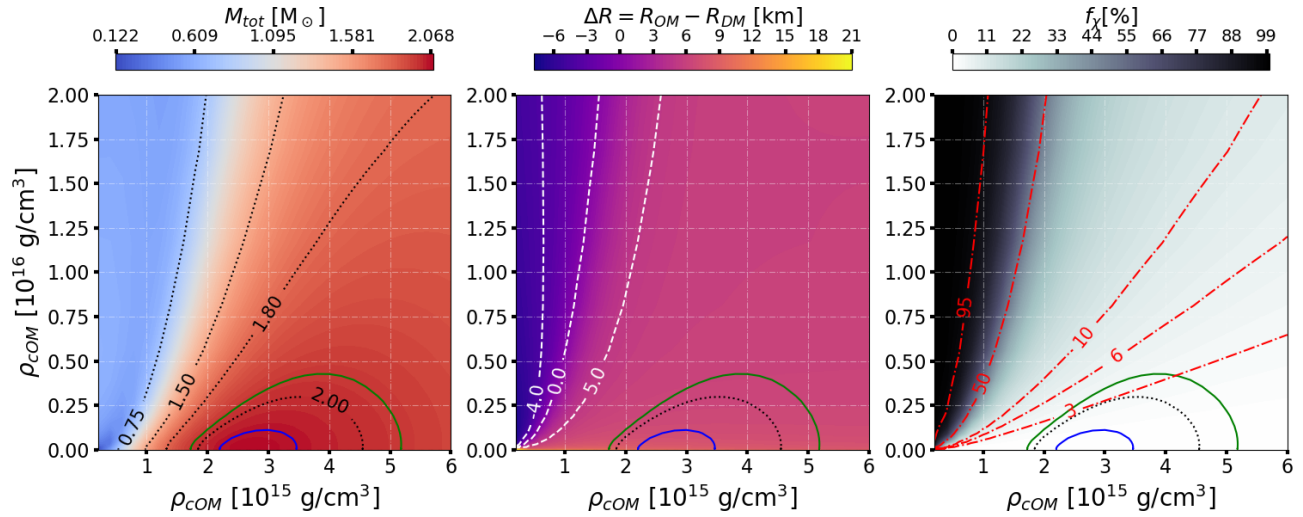


FIG. 2. Results for equilibrium configurations of DANS in the (ρ_{cOM}, ρ_{cDM}) plane for the case $m_\chi = 1$ GeV. The left panel shows the total gravitational mass of the star $M_{tot} = M_{tot}(\rho_{cOM}, \rho_{cDM})$ for different choices of the central mass densities. The central and right panel show the quantity $\Delta R = R_{OM} - R_{DM}$ and the stellar DM fraction in percent f_χ [%] respectively as function of the central mass densities. On each of the three panels we report the contour lines for M_{tot} (left), ΔR (central) and f_χ [%] (right). The green and blue lines in each panel delimit the region in the central mass density plane where the total gravitational mass M_{tot} is compatible with the measurement of the mass of the neutron star associated with the pulsar PSR J0348+0432 ($2.01 \pm 0.04 M_\odot$) [53].

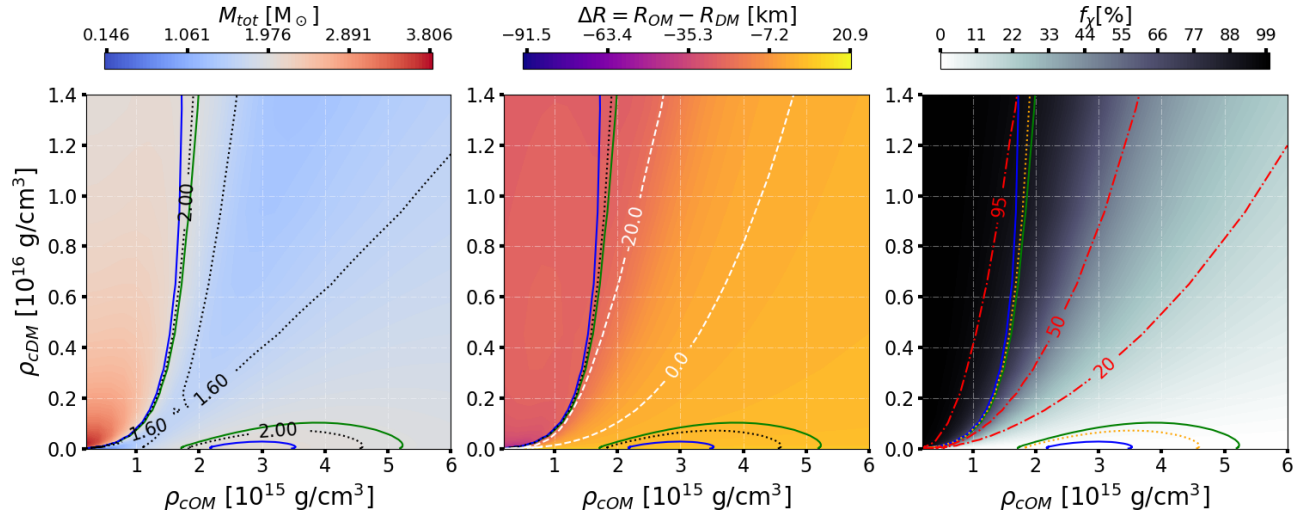


FIG. 3. Same as in Fig. 2 but now for the the case $m_\chi = 0.4$ GeV.

and $\rho_{DM}(r)$ for DM (black curves) obtained for a fixed value $\rho_{cOM} = 2 \times 10^{15}$ g/cm³ of the OM fluid central density and using different values ρ_{cDM} of the DM fluid central density. Each line-style in Figure 1 corresponds to the profiles obtained for a different value of ρ_{cDM} (see the figure caption for more details). As a baseline, we also plot in the same figure the mass density profile of an ordinary neutron star (green line). Taking the same stellar configurations considered in Figure 1, we report in Table I the total gravitational masses (eq.(4)) of the OM and DM stellar components, the corresponding radii R_{OM} and R_{DM} and the stellar DM fraction f_χ defined

as

$$f_\chi = \frac{M_{DM}}{M_{tot}}. \quad (6)$$

All the results reported in Figure 1 and in Table I are relative to the case $m_\chi = 1$ GeV. Coming back to Figure 1 we see that in the first two cases (dotted line and dash-dot lines), the radius of the dark matter distribution is smaller than the radius of the ordinary matter distribution ($R_{OM} \geq R_{DM}$) and thus we have a DANS with a dark matter core. In the third case reported in figure 1 (dashed lines) we have $R_{OM} < R_{DM}$ and thus

we have a DANS with a dark matter halo.

The results of our systematic calculations for hydrostatic equilibrium configurations of DANS in the (ρ_{cOM}, ρ_{cDM}) plane are reported in Fig (2) for the case $m_\chi = 1$ GeV. In particular, in the left panel we report, using a color scale, the total gravitational mass M_{tot} of the star. The black dotted lines represent the contour lines ($M_{tot} = \text{const}$), whereas the green and blue lines (reported in each of the three panels) are the contour lines which mark the region in the central mass densities plane where the calculated M_{tot} is compatible with the measured mass (2.01 ± 0.04) M_⊕ [53] of the neutron star associated to the pulsar PSR J0348+0432. In the central panel of Fig (2), we report, using a color scale, the difference $\Delta R = R_{OM} - R_{DM}$ between the radii of the OM and DM fluid distributions. The white dashed line labeled by "0.0" represents the contour line $\Delta R = 0$ and thus marks the boundary between DANS with a DM core (on the right of the $\Delta R = 0$ line) and those with a DM halo (on the left of the $\Delta R = 0$ line). Finally, in the right panel of Fig (2) we plot the DM fraction (in percent) $f_\chi [\%]$ and the contour lines for this quantity (red dash-dotted lines). The results in the right panel of Fig (2) ($m_\chi = 1$ GeV) clearly show that only DANS with a low DM fraction ($f_\chi < 4\%$) are compatible with the measured mass of the neutron star associated with PSR J0348+0432 and that these configurations are all characterized by the presence of a DM core (see middle panel). In Fig. (3) we show our results for DANS properties in the case $m_\chi = 0.4$ GeV. Now, in addition to the region of the (ρ_{cOM}, ρ_{cDM}) plane populated by DANS with a DM core and $f_\chi \lesssim 4.6\%$ and having $M_{tot} \sim 2$ M_⊕, there is a second region of the (ρ_{cOM}, ρ_{cDM}) plane populated by DANS with $M_{tot} \gtrsim 2$ M_⊕. All members of this second group of DANS have an extended DM halo and are almost completely formed by DM. In the $m_\chi = 0.4$ GeV case a large region of the (ρ_{cOM}, ρ_{cDM}) plane is populated by DANS with an extended DM halo and having a high DM fraction.

As a general trend, we have that for fixed values of the central mass densities of the two fluids, higher values of m_χ tend to favor the formation of a dark matter core, whereas lower values of m_χ tend to favor the formation of a dark matter halo.

A. Mass-radius relation for fixed f_χ

To investigate the effects of DM on observable properties of DANS, we consider stellar sequences with a fixed DM fraction f_χ . In other words, we solve the two-fluid structure equations by taking the central mass density of the OM fluid ρ_{cOM} and the DM fraction f_χ as independent variables.

In figure (4), for the case $m_\chi = 1$ GeV, we show the total gravitational mass of the star M_{tot} as a function of ρ_{cOM} (left panel) and M_{tot} as a function of the radius R_{OM}

of the OM fluid distribution (right panel). The surface of the OM fluid distribution is in fact the place where the electromagnetic radiation, that allows to determine R_{OM} , is generated. The light blue dash-dotted curve in both panels represents the ordinary neutron star sequence ($f_\chi = 0$). The other two curves represent DANS sequences with $f_\chi = 3\%$ (orange dash-dotted lines) and $f_\chi = 6\%$ (green dash-dotted lines). These two stellar sequences represent DANS having a DM core (see central and right panels in Fig (2)). The light green horizontal band represents the measured mass (2.08 ± 0.07) M_⊕ [54] of the neutron star associated to the pulsar PSR J0740+6620, whereas the pink horizontal band represents the measured mass (2.01 ± 0.04) M_⊕ [53] of the neutron star associated to the pulsar PSR J0348+0432. As we can see from the results reported in figure (4), the presence of DM with $m_\chi = 1$ GeV reduces the value of the maximum gravitational mass $M_{max} \equiv M_{tot,max}$ of the star with respect to the one for ordinary ($f_\chi = 0$) neutron stars. Considering DANS sequences with $f_\chi \gtrsim 3\%$ the calculated maximum mass is no longer compatible with the present measured masses of "heavy" neutron stars with $M \sim 2$ M_⊕ [53, 54]. We also note that the $M_{tot}(\rho_{cOM})$ curve is shifted towards higher value of the ordinary matter central density ρ_{cOM} compared to the ordinary neutron stars case ($f_\chi = 0\%$) as f_χ increases. The presence of DM also affects the value of the OM radius R_{OM} (right panel) making the OM distribution more compact [18, 19]. For example, considering an ordinary neutron star with a gravitational mass $M = 1.4$ M_⊕, a DM fraction $f_\chi = 6\%$ reduces the stellar observable radius R_{OM} by ~ 0.6 km i.e by $\sim 5\%$. These changes in the stellar radius are within the bounds of uncertainty of present instruments, as NICER, for measuring neutron star radii. The orange region, in the right panel of Fig. (4), marks the NICER measurement for the mass and radius of the neutron star in PSR J0030+0451 [55] while the gray and blue regions represent the portion of the mass-radius plane compatible with the data obtained from the GW170817 event (at 90% CL) [56].

In Fig. (5) we report DANS sequences for DM particles having a mass $m_\chi = 0.1$ GeV and for fixed DM fraction. In this case we get stars with a DM halo. This leads to a growth of the total gravitational maximum mass M_{max} of the star as f_χ increases. Since the ordinary neutron star sequence, calculated with the BL EOS, is compatible with the present measured masses of "heavy" neutron stars, the agreement with the same observational data will clearly hold for DANS sequences in the $m_\chi = 0.1$ GeV case.

To investigate in details how the maximum mass M_{max} of DANS depends on the DM fraction f_χ and on the DM particle mass m_χ , we show in Fig. (6) our results for the function $M_{max}(m_\chi, f_\chi)$ calculated for a few constant values of m_χ (curves in different colors). The black heavy dot on top of each curve denotes the minimum of the function $M_{max}(f_\chi)$. We see that for $m_\chi \approx 0.188$ GeV the minimum of the orange curve is equal to 2 M_⊕ (a

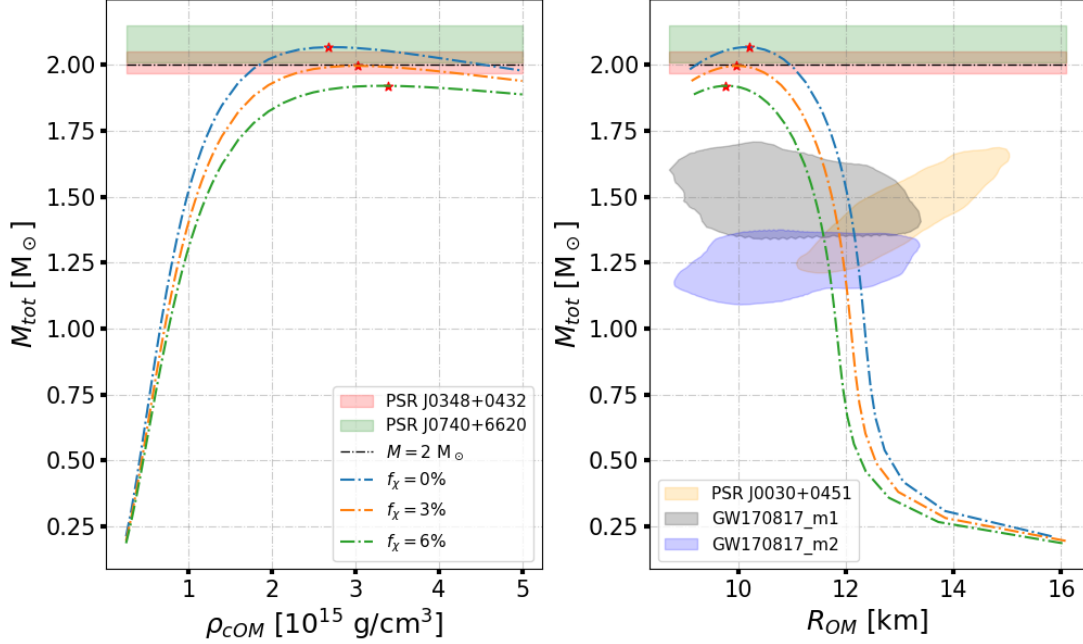


FIG. 4. Total gravitational mass of the star M_{tot} as a function of ρ_{cOM} (left panel) and M_{tot} as a function of the radius R_{OM} of the OM fluid distribution (right panel) for different values of the DM fraction ($f_\chi = 0\%, 3\%, 6\%$) and in the case $m_\chi = 1 \text{ GeV}$. The red star symbol on the top of each curve marks the maximum mass configuration. The light green and the pink horizontal bands represent respectively the measured mass of the neutron star associated to the pulsar PSR J0740+6620 [54] and to PSR J0348+0432 [53]. In the right panel, the orange region marks the NICER measurement for the mass and radius of the neutron star in PSR J0030+0451 [55] while the gray and blue regions represent the portion of the mass-radius plane compatible with the data obtained from the GW170817 event (at 90% CL) [56].

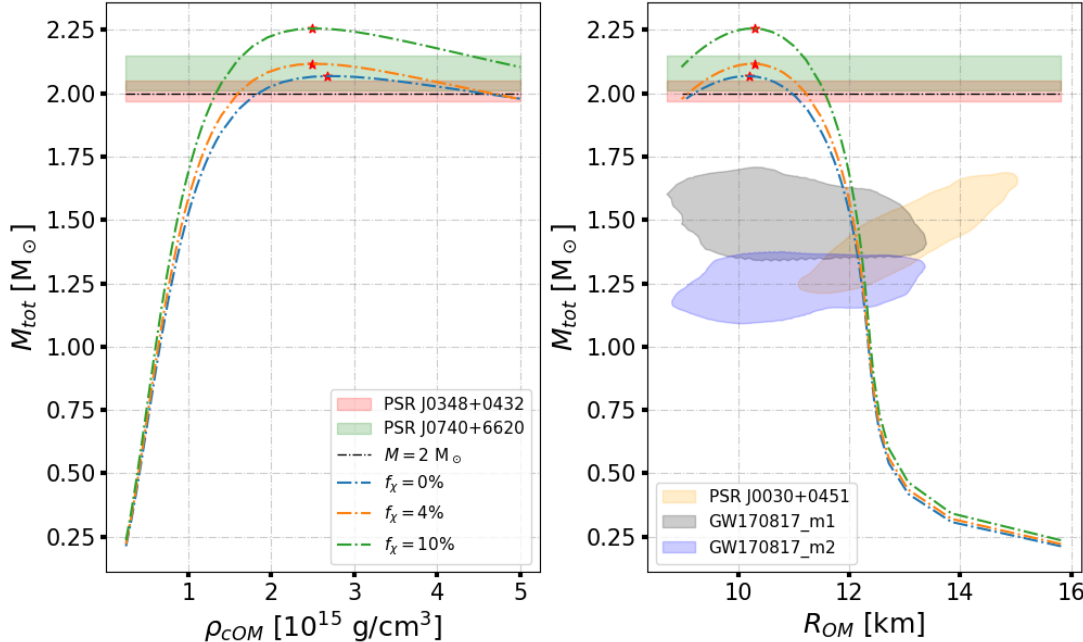


FIG. 5. Same as in Fig 4 but now for the the case $m_\chi = 0.1 \text{ GeV}$ and DM fraction $f_\chi = 0\%, 4\%, 10\%$.

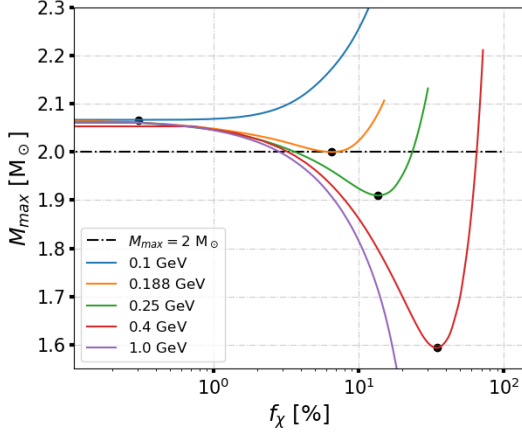


FIG. 6. Maximum mass for dark matter admixed neutron stars as a function of the dark matter fraction f_χ for fixed values of the dark matter particle mass m_χ . The black heavy dot on top of each curve denotes the minimum of each curve.

value we take as a reference for the measured masses of “heavy” neutron stars): this result means that for $m_\chi \leq 0.188$ GeV we obtain a value for M_{max} that is always compatible with measured neutron star masses for any value of f_χ .

Following [19, 57], for any fixed value of $m_\chi \geq 0.188$ GeV, we define a critical value of the DM fraction, and denote it with $f_\chi^{crit} = f_\chi^{crit}(m_\chi)$, as the solution of the equation $M_{max}(f_\chi, m_\chi) = 2 \text{ M}_\odot$.

From figure (6) we see that for $0.188 \text{ GeV} \leq m_\chi \leq 0.4 \text{ GeV}$ we get two critical values for f_χ and we observe that the largest of the two roots tends to $f_\chi = 100\%$ as m_χ increases. For the considered values $m_\chi \geq 0.4$ GeV we get one critical value for f_χ .

The exact value of $m_\chi > 0.188$ GeV that marks the transition from two critical values to one critical value for f_χ must lie in the range $0.4 < m_\chi/\text{GeV} < 0.56$. For this particular value of m_χ , the largest root of the equation $M_{lim}(f_\chi, m_\chi) = 2 \text{ M}_\odot$ is $f_\chi \approx 100\%$.

The critical DM fraction is shown in Fig. (7) by the heavy black curve labeled $f_\chi^{crit}(m_\chi)$. The green region in the same figure thus represents the portion of the (m_χ, f_χ) plane where the calculated maximum mass for DANS is compatible with the present measured masses of “heavy” neutron stars with $M_{tot} \sim 2 \text{ M}_\odot$ [53, 54]. It is useful to observe that, in the range $10 \leq m_\chi/\text{GeV} \leq 100$ the critical DM curve $f_\chi^{crit}(m_\chi)$ is well described by the following equation

$$f_\chi^{crit}(m_\chi) = 31.15 \left(\frac{1 \text{ GeV}}{m_\chi} \right)^2 + 6.62 \times 10^{-6} \quad (7)$$

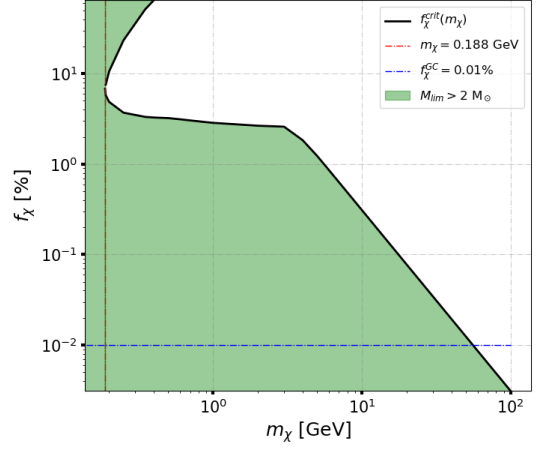


FIG. 7. Critical value of f_χ as a function of m_χ . In the green region and along the black line the maximum mass for DANS is compatible with observation.

B. Proton fraction and direct URCA processes in DANS

As we show in this subsection, the presence of DM influences not only the bulk properties (mass, radius, maximum mass) of a neutron star, but in addition has indirect sizeable effect (through gravitational interaction) on the particle fractions of the OM fluid constituents when considering DANS with a fixed total gravitational mass. In particular the value of f_χ influences the proton fraction $x_p = n_p/n$ (with $n = n_n + n_p$ being the baryon number density) in β -stable nuclear matter. As has been shown in Ref. [40], when the proton fraction x_p is larger than a threshold value, denoted as x_p^{durca} , the so-called direct URCA processes $n \rightarrow p + e^- + \bar{\nu}_e$, $p + e^- \rightarrow n + \nu_e$, can occur in neutron star matter. The direct URCA processes enhances neutrino emission and neutron star cooling rates by a very large factor compared to the so-called modified URCA processes $(n, p) + n \rightarrow p + e^- + \bar{\nu}_e$, $(n, p) + p + e^- \rightarrow n + \nu_e$, causing a fast cooling of the star [40, 41].

In β -stable nuclear matter the threshold proton fraction for direct URCA processes can be written [25]

$$x_p^{durca} = \frac{1}{1 + (1 + Y_e^{1/3})^3}, \quad (8)$$

where $Y_e = n_e/(n_e + n_\mu)$ is the leptonic electron fraction. Notice that below the muon threshold density $x_p^{durca} = 1/9$ while for asymptotically large baryon densities $x_p^{durca} \sim 14.77\%$.

In Fig. 8, we plot the proton fraction x_p in β -stable nuclear matter as a function of the radial coordinate r_{OM} in a DANS having a total gravitational mass $M_{tot} = 1.4 \text{ M}_\odot$ and considering three different values, $f_\chi = 0\%, 3.1\%, 5.41\%$, for the DM fraction (continuous lines) and taking $m_\chi = 1 \text{ GeV}$. Each of the three dash-dotted lines represents the threshold proton fraction x_p^{durca} for

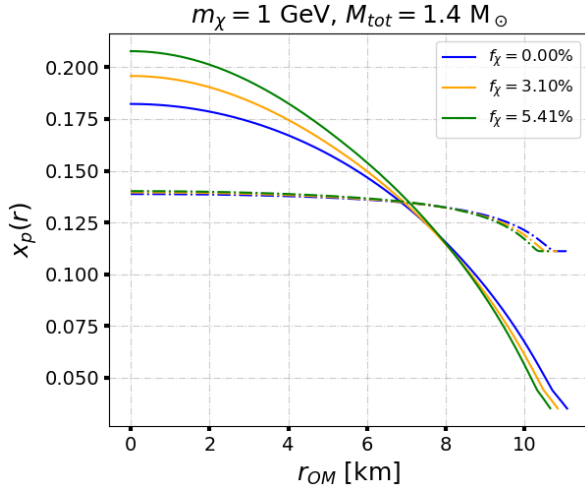


FIG. 8. Proton fraction $x_p(r)$ (continuous lines) and direct URCA processes threshold (x_p^{durca}) as functions of the radial coordinate in the ordinary matter fluid for a DANS having a gravitational mass $M_{tot} = 1.4 M_\odot$ in the case $m_\chi = 1$ GeV and different values of f_χ .

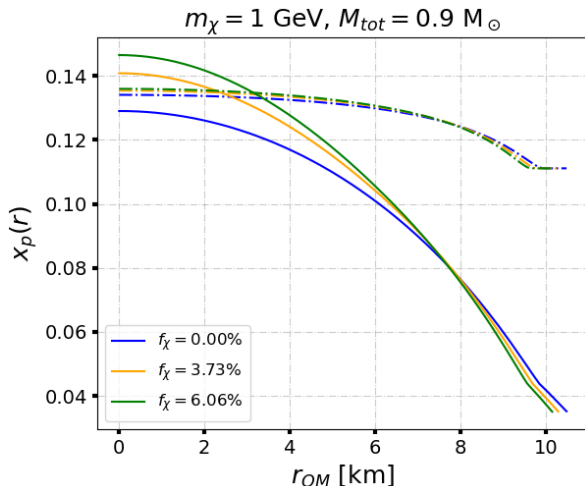


FIG. 9. Same as in Fig. 8 but now for $M_{tot} = 0.9 M_\odot$.

the direct URCA processes associated to the x_p curve with the same f_χ (curves with the same color). The intersection point between each couple of curves with the same color gives the value of the radial coordinate r_{OM}^{durca} below which direct URCA processes are possible. As is clearly seen in Fig. 8, the presence a DM core produces a significant increase in the proton fraction (particularly in the central region of the star) and small increase in the value of r_{OM}^{durca} . Notice that in the case of an ordinary neutron star ($f_\chi = 0$) with mass $M = 1.4 M_\odot$ described by the BL EOS, direct URCA processes are already possible [25]. Complementary to Fig. 8, we report in Tab. II some of the properties of a DANS with $M_{tot} = 1.4 M_\odot$ in the case $m_\chi = 1$ GeV.

Fig. 9 displays the same physical quantities as in the

$f_\chi [\%]$	$n(r=0) [\text{fm}^{-3}]$	$x_p(r=0)$	$r_{OM}^{durca} [\text{km}]$
0	0.497	0.182	6.84
3.10	0.539	0.196	6.94
5.41	0.578	0.208	7.08

TABLE II. Central baryon number density (second column), central proton fraction (third column) and the radial coordinate r_{OM}^{durca} below which direct URCA processes are possible in a $1.4 M_\odot$ DANS for different value of the dark matter fraction f_χ (first column). All the results are relative to the case $m_\chi = 1$ GeV.

$f_\chi [\%]$	$n(r=0) [\text{fm}^{-3}]$	$x_p(r=0)$	$r_{OM}^{durca} [\text{km}]$
0	0.345	0.129	/
3.73	0.377	0.141	2.40
6.06	0.393	0.147	3.13

TABLE III. Same as Tab. II but for $M_{tot} = 0.9 M_\odot$.

previous figure, but this time for DANS with a total gravitational mass $M_{tot} = 0.9 M_\odot$. Now in the case of ordinary neutron stars direct URCA processes are not possible ($x_P < x_p^{durca}$), but they can be switched on if a sufficient amount of DM is present in the star. Complementary to Fig. 9, we report in Tab. III some of the properties of a DANS with $M_{tot} = 0.9 M_\odot$ in the case $m_\chi = 1$ GeV.

The calculated values for the threshold baryon number density n^{durca} for having direct URCA processes and the corresponding threshold proton fraction $x_p(n^{durca})$ do not depend on the DM fraction, since these two quantities are exclusively determined by the nuclear interactions and particularly are strongly affected by the density dependence of the nuclear symmetry energy [27]. In the case of the BL EOS one has $n^{durca} = 0.361 \text{ fm}^{-3}$ and $x_p(n^{durca}) = 0.1347$ [25]. The stellar total gravitational mass $M_{tot}^{durca} \equiv M_{tot}(n_c = n^{durca})$ beyond which direct URCA processes are possible depends instead on the DM fraction. Its value together with the value of the gravitational maximum mass M_{tot}^{max} is reported in Tab. IV for some values of the DM fraction. As we see the presence of a DM core reduces the value of M_{tot}^{durca} and thus makes possible fast cooling of "light" neutron stars.

$f_\chi [\%]$	$M_{tot}^{durca} [M_\odot]$	$M_{max} [M_\odot]$
0	0.96	2.07
3.10	0.87	1.99
5.41	0.82	1.94

TABLE IV. Values for $M_{tot}^{durca} = M_{tot}(n^{durca})$ (second column) and for the maximum gravitational mass M_{max} for DANS sequences for different values of dark matter fraction (first column). The third column reports values of obtained for the corresponding f_χ value. All the results are relative to the case $m_\chi = 1$ GeV.

V. CONSTRAINTS FROM ASTROPHYSICAL OBSERVATIONS ON DM PROPERTIES

As discussed in [19], it is possible to give an upper limit to the dark matter particles mass by using the results obtained in figure (7) and comparing them with an estimation of the amount of dark matter that can be accumulated onto a neutron star. Such an estimation requires to evaluate the dark matter accretion rate at every evolutionary stage of the star, from the formation of the progenitor star to the stable neutron star stage.

Dark matter accretion rate onto neutron stars as been discussed in [58] and the total amount of dark matter accumulated in a given time t can be written as (see [19])

$$M_{DM}^{acc} \approx 10^{-14} \left(\frac{\rho_\chi}{0.3 \text{ GeV/cm}^3} \right) \left(\frac{\sigma_{\chi n}}{10^{-45} \text{ cm}^2} \right) \left(\frac{t}{1 \text{ Gyr}} \right) M_\odot \quad (9)$$

where ρ_χ is the local dark matter density and $\sigma_{\chi n}$ is the dark matter-nucleon interaction cross section.

Following [19], by using the Einasto profile for ρ_χ [59–62], assuming $\sigma_{\chi n} \sim 10^{-45} \text{ cm}^2$ and $t \sim 10 \text{ Gyr}$, we can estimate $M_{DM}^{acc} \sim (10^{-14} - 10^{-13}) M_\odot$ for a $2 M_\odot$ mass neutron stard in the disk of our galaxy. This values are to low to put a stringent upper limit on m_χ . As discussed in [19], using equation (9), for a $2 M_\odot$ mass neutron stars in the central region of our galaxy, we find that $f_\chi \leq 0.01\%$. Using this estimation, equation (7) give us an upper limit for the dark matter particles:

$$m_\chi \leq 56 \text{ GeV} \quad (10)$$

which is close to the result obtained in [19] ($m_\chi \leq 60 \text{ GeV}$) in spite the fact that we are using a different EOS for ordinary matter.

We observe that in the dark matter accretion rate estimation made in [58], only the dark matter-nucleon interaction cross-section is taken into account. If we assume a non zero self interaction between dark matter particles, the accretion rate and the result in equation (10) may change drastically.

VI. STABILITY OF DANS

A solution the two-fluid TOV equations (1) and (2) represents an equilibrium configuration. In this section we present results regarding the stability with respect to small radial perturbation of DANS. We assume that these perturbations don't modify the β -equilibrium condition of ordinary matter.

In the one-fluid limit (stars made only of ordinary matter or only of dark matter) it is well known that the critical point is the maximum of the $M(\rho_{c,j})$ curve [52]. Using the EOSs considered in this work we get the following value for the central mass densities of the critical config-

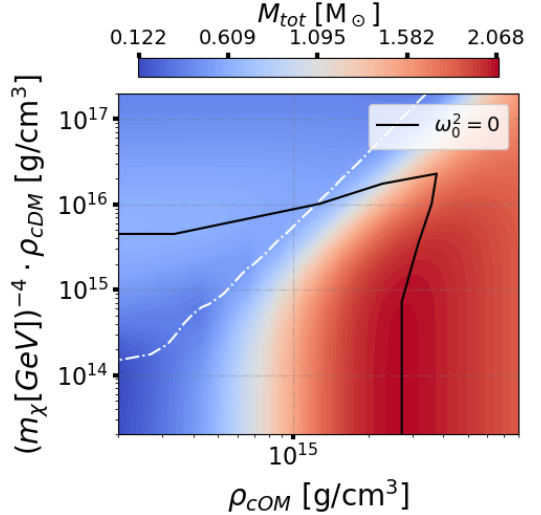


FIG. 10. Critical stability curve for $m_\chi = 1 \text{ GeV}$. The white dashed line is the $\Delta R = R_{OM} - R_{DM} = 0$ contour line.

uration

$$\text{OM stars: } \rho_{cOM} = 2.727 \times 10^{15} \text{ g/cm}^3$$

$$\text{DM stars: } \rho_{cDM} = 5.362 \times 10^{15} \left(\frac{m_\chi}{1 \text{ GeV}} \right)^4 \text{ g/cm}^3$$

In the two-fluids system case we get a critical stability curve in the (ρ_{cOM}, ρ_{cDM}) plane.

The stability analysis can be done in two different ways. The first method, discussed by Kain in [21], requires to solve a set of pulsation equations whose solution give the squared radial oscillation frequency ω^2 . If the squared radial oscillation frequency for the fundamental mode ω_0^2 is positive, than the corresponding solution is stable while, if $\omega_0^2 < 0$, the solution is unstable. This method requires to take the derivative of the EOSs of the fluids which is a problem if the EOSs aren't smooth enough.

The second method, developed by Henriques, Liddle and Moorhouse in [63], allow us to determine the critical stability curve without solving the pulsation equations. Their analysis give the following equation for the critical stability curve

$$\frac{dM_{tot}}{d\vec{\sigma}} = \frac{dN_{OM}}{d\vec{\sigma}} = \frac{dN_{DM}}{d\vec{\sigma}} = 0 \quad (11)$$

where M_{tot} , N_i ($i = OM, DM$) are the total gravitational mass and total fluid number of a static solution and $\vec{\sigma}$ is a vector in the parameter space that is simultaneously tangent to the level curves of M_{tot} and N_i . It can be shown [63] that if two of the quantities in (11) are zero, then the third is also zero so, to determine the critical stability curve, we can study the stationary point of M_{tot} along level curve of N_{DM} . As observed in [63], the stability region in the (ρ_{cOM}, ρ_{cDM}) plane must contain the stable structure in the one-fluid limit.

Figure (10) shows results obtained for $m_\chi = 1 \text{ GeV}$. This results are similar to those obtained by Kain in [22] and

show us that we can have stable DANS with both a core and a dark matter halo. We also note that there is a region inside the stability curve where DANS have an ordinary matter central density and/or a dark matter central density that exceed the critical value in the one-fluid limit.

VII. SUMMARY

In this paper we have studied the consequences of the presence of DM on the structural properties and the stability of neutron stars. Specifically, we explored how the properties of these DANS are modified with respect to those of ordinary neutron stars in terms of the DM particle mass m_χ and the fraction of DM present in the star. To model ordinary matter we used a state-of-the-art equation of state of β -stable nuclear matter obtained using the Brueckner-Hartree-Fock quantum many-body approach starting from two-body and three-body nuclear interactions derived from chiral effective field theory. This EOS, as discussed in Sect. III A, reproduces various empirical nuclear matter properties at the satu-

ration density n_0 and at supranuclear densities ($n > n_0$). Additionally, the calculated $E_{sym}(n_0)$ and L fulfill the bounds imposed by the unitary Fermi gas limit [29]. The dark matter component of the star has been modeled as a non-self-annihilating system of spin 1/2 fermions and its EOS as an ideal relativistic Fermi gas. We found that, depending on the dark matter particle mass m_χ , one can have somehow opposite effects on the stellar properties. In fact, in the case $m_\chi = 1 \text{ GeV}$, the stellar gravitational maximum mass M_{max} decreases, whereas in the case $m_\chi = 0.1 \text{ GeV}$ M_{max} increases with respect to the maximum mass of ordinary neutron stars. We studied M_{max} as a function of f_χ for some values of m_χ . Following [19], we defined the critical values $f_\chi^{crit}(m_\chi)$ as the roots of the equation $M(f_\chi, m_\chi) = 2 M_\odot$ for a given value of m_χ . Comparing an upper limit for the total dark matter fraction accumulated by a $2 M_\odot$ neutron star in the galactic center with the function $f_\chi^{crit}(m_\chi)$, we found an upper limit for the dark matter particles: $m_\chi \leq 56 \text{ GeV}$. We also shown that the presence of dark matter has indirect sizeable effect on the proton fraction in the ordinary matter fluid and, in the case $m_\chi = 1 \text{ GeV}$, results in a decrease of the threshold gravitational mass M_{tot}^{durca} for having direct URCA processes and fast stellar cooling.

-
- [1] E. Corbelli and P. Salucci, Monthly Notices of the Royal Astronomical Society **311**, 441 (2000).
 - [2] F. Nesti, P. Salucci, and N. Turini, Astronomy **2**, 90 (2023).
 - [3] P. J. E. Peebles, The Astrophysical Journal Letters **263**, L1 (1982).
 - [4] G. Goldhaber and S. Perlmutter, Physics Reports **307**, 325 (1998).
 - [5] P. M. Garnavich, R. P. Kirshner, P. Challis, J. Tonry, R. L. Gilliland, R. C. Smith, A. Clocchiatti, A. Diercks, A. V. Filippenko, M. Hamuy, C. J. Hogan, B. Leibundgut, M. M. Phillips, D. Reiss, A. G. Riess, B. P. Schmidt, R. A. Schommer, J. Spyromilio, C. Stubbs, N. B. Suntzeff, and L. Wells, Astrophysical Journal **493**, L53 (1998).
 - [6] Y. Sofue, Publications of the Astronomical Society of Japan **65**, 118 (2013).
 - [7] M. Pato, F. Iocco, and G. Bertone, Journal of Cosmology and Astroparticle Physics **2015**, 001 (2015).
 - [8] H.-N. Lin and X. Li, Monthly Notices of the Royal Astronomical Society **487**, 5679 (2019).
 - [9] E. Aprile, J. Aalbers, F. Agostini, M. Alfonsi, F. Amaro, M. Anthony, F. Arneodo, P. Barrow, L. Baudis, B. Bauermeister, et al., Physical Review Letters **119**, 181301 (2017).
 - [10] G. Bertone and M. Fairbairn, Physical Review D **77**, 043515 (2008).
 - [11] A. de Lavallaz and M. Fairbairn, Physical Review D **81**, 123521 (2010).
 - [12] C. Kouvaris and P. Tinyakov, Physical Review D **82**, 063531 (2010).
 - [13] C. Kouvaris and P. Tinyakov, Physical Review D **83**, 083512 (2011).
 - [14] S.-C. Leung, M.-C. Chu, and L.-M. Lin, Physical Review D **84**, 107301 (2011).
 - [15] P. Ciarcelluti and F. Sandin, Physics Letters B **695**, 19 (2011), arXiv:1005.0857 [astro-ph.HE].
 - [16] C. Kouvaris et al., Advances in High Energy Physics **2013** (2013).
 - [17] C. Kouvaris and N. G. Nielsen, Physical Review D **92**, 063526 (2015).
 - [18] J. Ellis, G. Hüttsi, K. Kannike, L. Marzola, M. Raidal, and V. Vaskonen, Physical Review D **97**, 123007 (2018).
 - [19] O. Ivanytskyi, V. Sagun, and I. Lopes, Physical Review D **102**, 063028 (2020).
 - [20] A. Del Popolo, M. Deliyergiyev, M. Le Delliou, L. Tolos, and F. Burgio, Physics of the Dark Universe **28**, 100484 (2020).
 - [21] B. Kain, Physical Review D **102**, 023001 (2020).
 - [22] B. Kain, Physical Review D **103**, 043009 (2021).
 - [23] S. Shakeri and D. R. Karkevandi, Phys. Rev. D **109**, 043029 (2024), arXiv:2210.17308 [astro-ph.HE].
 - [24] G. Bertone, D. Hooper, and J. Silk, Physics Reports **405**, 279 (2005).
 - [25] I. Bombaci and D. Logoteta, Astron. Astrophys. **609**, A128 (2018), arXiv:1805.11846 [astro-ph.HE].
 - [26] R. Machleidt and D. R. Entem, Phys. Rept. **503**, 1 (2011), arXiv:1105.2919 [nucl-th].
 - [27] H. W. Hammer, S. König, and U. van Kolck, Reviews of Modern Physics **92**, 025004 (2020).
 - [28] D. Logoteta, I. Bombaci, and A. Kievsky, Phys. Rev. C **94**, 064001 (2016), arXiv:1609.00649 [nucl-th].
 - [29] I. Tews, J. M. Lattimer, A. Ohnishi, and E. E. Kolomeitsev, Astrophysical Journal **848**, 105 (2017), arXiv:1611.07133 [nucl-th].

- [30] A. Kievsky, M. Viviani, D. Logoteta, I. Bombaci, and L. Girlanda, *Physical Review Letters* **121**, 072701 (2018), arXiv:1806.02636 [nucl-th].
- [31] P. Danielewicz, R. Lacey, and W. G. Lynch, *Science* **298**, 1592 (2002), arXiv:nucl-th/0208016.
- [32] P. Danielewicz and J. Lee, *Nuclear Physics A* **922**, 1 (2014).
- [33] X. Roca-Maza, M. Brenna, B. K. Agrawal, P. F. Bortignon, G. Colò, L.-G. Cao, N. Paar, and D. Vretenar, *Phys. Rev. C* **87**, 034301 (2013), arXiv:1212.4377 [nucl-th].
- [34] I. Bombaci and U. Lombardo, *Phys. Rev. C* **44**, 1892 (1991).
- [35] B.-A. Li, B.-J. Cai, W.-J. Xie, and N.-B. Zhang, *Universe* **7** (2021), 10.3390/universe7060182.
- [36] N.-B. Zhang and B.-A. Li, *The Astrophysical Journal* **921**, 111 (2021).
- [37] I. Bombaci, in *Astrophysics and Space Science Library*, Astrophysics and Space Science Library, Vol. 465, edited by S. Bhattacharyya, A. Papitto, and D. Bhattacharya (2022) pp. 281–317.
- [38] J. M. Lattimer and M. Prakash, *Astrophys. J.* **550**, 426 (2001), arXiv:astro-ph/0002232 [astro-ph].
- [39] A. W. Steiner, *Phys. Rev. C* **74**, 045808 (2006), arXiv:nucl-th/0607040 [nucl-th].
- [40] J. M. Lattimer, C. J. Pethick, M. Prakash, and P. Haensel, *Phys. Rev. Lett.* **66**, 2701 (1991).
- [41] D. Page, J. M. Lattimer, M. Prakash, and A. W. Steiner, *The Astrophysical Journal Supplement Series* **155**, 623 (2004), arXiv:astro-ph/0403657 [astro-ph].
- [42] D. Logoteta and I. Bombaci, *Universe* **5**, 204 (2019).
- [43] B. P. Abbott et al. (LIGO Scientific, Virgo), *Phys. Rev. Lett.* **119**, 161101 (2017), arXiv:1710.05832 [gr-qc].
- [44] D. Logoteta, A. Perego, and I. Bombaci, *Astron. Astrophys.* **646**, A55 (2021), arXiv:2012.03599 [nucl-th].
- [45] S. Bernuzzi et al., *Mon. Not. Roy. Astron. Soc.* **497**, 1488 (2020), arXiv:2003.06015 [astro-ph.HE].
- [46] A. Endrizzi, D. Logoteta, B. Giacomazzo, I. Bombaci, W. Kastaun, and R. Ciolfi, *Phys. Rev. D* **98**, 043015 (2018), arXiv:1806.09832 [astro-ph.HE].
- [47] A. Prakash, D. Radice, D. Logoteta, A. Perego, V. Nedora, I. Bombaci, R. Kashyap, S. Bernuzzi, and A. Endrizzi, *PHYSICAL REVIEW D* **104** (2021), 10.1103/PhysRevD.104.083029.
- [48] G. Baym, C. Pethick, and P. Sutherland, *Astrophys. J.* **170**, 299 (1971).
- [49] J. W. Negele and D. Vautherin, *Nucl. Phys. A* **207**, 298 (1973).
- [50] D. E. Kaplan, M. A. Luty, and K. M. Zurek, *Phys. Rev. D* **79**, 115016 (2009), arXiv:0901.4117 [hep-ph].
- [51] K. M. Zurek, *Phys. Rep.* **537**, 91 (2014), arXiv:1308.0338 [hep-ph].
- [52] S. L. Shapiro and S. A. Teukolsky, *Black holes, white dwarfs and neutron stars. The physics of compact objects* (1983).
- [53] J. Antoniadis, P. C. C. Freire, N. Wex, T. M. Tauris, R. S. Lynch, M. H. van Kerkwijk, M. Kramer, C. Bassa, V. S. Dhillon, T. Driebe, J. W. T. Hessels, V. M. Kaspi, V. I. Kondratiev, N. Langer, T. R. Marsh, M. A. McLaughlin, T. T. Pennucci, S. M. Ransom, I. H. Stairs, J. van Leeuwen, J. P. W. Verbiest, and D. G. Whelan, *Science* **340**, 448 (2013), arXiv:1304.6875 [astro-ph.HE].
- [54] E. Fonseca et al., *Astrophys. J. Lett.* **915**, L12 (2021), arXiv:2104.00880 [astro-ph.HE].
- [55] M. Miller, F. K. Lamb, A. Dittmann, S. Bogdanov, Z. Arzoumanian, K. C. Gendreau, S. Guillot, A. Harding, W. Ho, J. Lattimer, et al., *The Astrophysical Journal Letters* **887**, L24 (2019).
- [56] B. P. Abbott et al. (The LIGO Scientific Collaboration and the Virgo Collaboration), *Phys. Rev. Lett.* **121**, 161101 (2018).
- [57] V. Sagun, V. Sagun”, E. Giangrandi”, O. Ivanytskyi”, I. Lopes”, and K. Bugaev, in *Proceedings of Particles and Nuclei International Conference 2021* (Sissa Medialab) p. 313.
- [58] C. Kouvaris, *Physical Review D* **77**, 023006 (2008).
- [59] J. Einasto, *Trudy Astrofizicheskogo Instituta Alma-Ata* **5**, 87 (1965).
- [60] J. Einasto, *Astrofizika* **5**, 137 (1969).
- [61] D. Merritt, A. W. Graham, B. Moore, J. Diemand, and B. Terzić, *Astronomical Journal* **132**, 2685 (2006), arXiv:astro-ph/0509417 [astro-ph].
- [62] M. Baes, *Astronomy & Astrophysics* **667**, A47 (2022), arXiv:2209.03639 [astro-ph.GA].
- [63] A. Henriques, A. R. Liddle, and R. Moorhouse, *Physics Letters B* **251**, 511 (1990).

Effects of asymmetric dark matter on a magnetized neutron star: A two-fluid approach

Pinku Routaray¹, Vishal Parmar², H. C. Das³, Bharat Kumar¹, G. F. Burgio³, and H.-J. Schulze³

¹*Department of Physics and Astronomy, NIT Rourkela, 769008, India*

²*INFN Sezione di Pisa, Largo B. Pontecorvo 3, 56127 Pisa, Italy and*

³*INFN Sezione di Catania, Dipartimento di Fisica, Università di Catania, Via Santa Sofia 64, 95123 Catania, Italy*

(Dated: December 31, 2024)

We study the interaction between dark matter (DM) and highly magnetized neutron stars (NSs), focusing on how DM particle mass, mass fraction, and magnetic field (MF) strength affect NS structure and stability. We consider self-interacting, non-annihilating, asymmetric fermionic DM that couples to NSs only through gravitational interaction. Using the QMC-RMF4 relativistic mean-field model with density-dependent magnetic fields, we investigate the magnetized equation of state and examine the accumulation of DM under various conditions. Our results show that as the DM fraction increases, the maximum gravitational mass of the NS decreases, especially for heavier DM particles, while lighter DM particles can induce a transition from a dark core to a halo structure, increasing the maximum mass. Strong MFs soften the equation of state and reduce the dark mass a NS core can retain before transitioning to a halo. These findings provide key insights into how DM and MF jointly shape the mass-radius relation and the stability of DM-admixed magnetized NSs.

I. INTRODUCTION

The majority of matter within the Universe remains obscured in the form of dark matter (DM) [1]. Although numerous discoveries provide compelling evidence for the existence of DM [2–5], none elucidate the particle identity of DM, which remains an enigma. Comprehending the characteristics of DM will facilitate observational astrophysics to identify its nature. Methods such as direct detection, indirect detection, particle colliders, and astrophysical probes constitute the means for such observations. Neutron stars (NSs) stand out as invaluable probes for deciphering the elusive nature of DM and its scattering cross sections [6, 7]. Given their compact and dense composition, they have become indispensable tools for examining the particle characteristics of DM. The incorporation of DM into the constitution of NSs results in significant modifications of their observables, including changes in mass-radius profiles, tidal deformability, and luminosity [8, 9]. This phenomenon provides a distinctive indirect avenue for scrutinizing the properties of DM.

Given the substantial mass of these compact objects, their presence is predominantly observed in proximity to the Galactic center rather than its periphery. Moreover, the density distribution of DM is higher in these regions. Consequently, there is a non-negligible probability that DM may be captured within a NS due to its significant gravitational potential. The associated accretion rate is contingent upon various factors including (i) the nature of the DM particle, (ii) prevailing environmental conditions, and (iii) the star’s internal structure.

Numerous theories have been proposed over many years on the nature of DM and its impact on the properties of NSs, considering both gravitational and non-gravitational interactions [10–39]. Among these, asymmetric DM (ADM) interacting gravitationally with NSs has received significant attention recently, resulting in several theories on the nature of DM, both fermionic and bosonic. In [21], the authors considered a trace amount of ADM captured inside a NS, which self-interacts without annihilation. They also investigated how DM affects gravitational-wave (GW) emission and leads to the formation of a DM halo during inspiral, comparing results

for both fermionic and bosonic natures of DM. Subsequently, in [24], a permissible range for the mass of fermionic ADM and the mass fraction inside the two massive pulsars PSR J0348+0432 [40] and PSR J0740+6620 [41] was obtained. In [29] a Bayesian analysis was performed to determine the formation criterion for dark cores/halos and also investigate the impact of dark halos on the pulsar pulse profile. Similarly, presuming self-interacting fermionic DM with dark scalar and vector mediators, [25] investigated the impact of DM on NS properties and carried out a Bayesian analysis to constrain the DM parameters for a single NS model. Likewise, other studies assuming self-interacting bosonic ADM have been conducted to investigate their effects on NS properties [26, 27, 31, 35–37].

Nevertheless, the particular effect of DM on highly magnetized NSs remains a largely unexplored domain. NSs originate as dense remnants resulting from the explosive collapse of massive stars during core-collapse supernova events. Throughout this violent genesis, the magnetic fields are significantly amplified, reaching magnitudes ranging from 10^{11} to 10^{13} G [42, 43]. On rare occasions, magnetars exhibit even more intense fields, escalating to $10^{14–16}$ G, approximately 1000 times stronger than typical pulsars [44]. These extreme magnetic fields significantly affect the structure and evolution of NSs, influencing their deformations and, consequently, leading to substantial GW emissions.

Anomalous X-ray Pulsars [45] and Soft Gamma Repeaters [46], subsets of NSs characterized by high magnetic fields, provide valuable insights. These pulsars, distinguished by their intermittent emissions of X-rays and gamma rays, contribute to the understanding of the complex interplay between extreme magnetic fields (MFs) and the observable behavior of NSs [47]. As NSs experience dissipative processes over time, younger magnetars may exhibit even stronger MFs. This phenomenon warrants further exploration into the dynamic relationship between intense MFs and the intrinsic properties of NSs [48].

In this study, we explore ADM realized through self-interacting fermions, which interact with highly-magnetized NSs solely via gravitation. The mass of the DM particle, rang-

TABLE I. Saturation properties and NS observables predicted by the QMC-RMF4 EOS model: density ρ_0 , binding energy per nucleon E_0 , compressibility K_0 , symmetry energy S_0 , its derivative L_0 , maximum NS mass M_{\max} , radii of $1.4M_{\odot}$ and $2.08M_{\odot}$ NSs, and tidal polarizability $\Lambda_{1.4}$. Observational ranges are listed for comparison.

	ρ_0 [fm $^{-3}$]	$-E_0$ [MeV]	K_0 [MeV]	S_0 [MeV]	L_0 [MeV]	M_{\max} [M_{\odot}]	$R_{2.08}$ [km]	$R_{1.4}$ [km]	$\Lambda_{1.4}$
Exp.	0.162 $\sim 0.14\text{--}0.17$	16.1 $\sim 15\text{--}17$	279 220–260	30.4 28.5–34.9	31.3 30–87	2.20 $> 2.35 \pm 0.17$	11.81 12.35 ± 0.75	12.24 12.45 ± 0.65	454 70–580
Ref.	[49]	[49]	[50, 51]	[50, 51]	[52, 53]	[54]	[55]	[55]	[56]

ing from MeV to GeV scales, is treated as a free parameter, while the repulsive interaction strength is constrained by observational data on the DM particle cross section.

For the hadronic equation of state (EOS), we employ the QMC-RMF4 parameter set, developed within the relativistic mean field (RMF) formalism [57], and extend it to include density-dependent meson fields using the methodology described in [58–60]. This EOS is capable of producing a NS with a maximum mass of about $2.2M_{\odot}$. Considering the gravitational interaction between DM and magnetized NSs, we examine the impact of DM on macroscopic properties such as mass, radius, and tidal deformability of magnetized NSs. A crucial parameter for evaluating these effects is the DM mass fraction, defined as the ratio of the included DM mass to the total mass of the NS. We investigate the existence of dark cores and dark halos, accounting for all the free parameters of the DM-admixed magnetized NSs.

This paper is organized as follows. In Sec. II we illustrate the properties of the hadronic EOS and its extension to the magnetized case; we also discuss the DM EOS. In Sec. III we discuss the results, and finally in Sec. IV we draw our conclusions.

II. FORMALISM

A. Magnetized hadronic EOS

In this work, we employ a RMF model called “QMC-RMF4” that is derived by fitting parameters to the uniform pure-neutron-matter EOS obtained from chiral effective field theory [57]. The unified treatment of the crustal EOS is described in [61]. This EOS exhibits stiff behavior, with a maximum mass of $2.20M_{\odot}$, and a canonical radius which lies within the limits given by the NICER+XMM data [55]. Also the tidal deformability $\Lambda_{1.4}$ meets the GW170817 constraint [56]. In Table I we summarize the main properties of the EOS at saturation density, along with some NS observables.

In the presence of a uniform external MF aligned along the z direction ($\mathbf{B} = B\hat{\mathbf{z}}$), such that $\nabla \cdot \mathbf{B} = 0$ [62], the transverse momenta of charged particles with an electric charge q are quantized into discrete Landau levels [59]. The thermodynamic potential Ω [63], which is a function of the chemical potential μ , temperature T , and MF B , conforms to canonical relations $\Omega = -p_{\parallel} = \varepsilon - \sum_i \rho_i \mu_i$ and $p_{\perp} = p_{\parallel} - MB$. Here, ε represents the energy density, ρ_i denotes the density of the i th particle, μ_i the corresponding chemical potential, $M = -\partial \Omega / \partial B$ repre-

sents the system’s magnetization, and p_{\parallel} and p_{\perp} indicate the pressure in the directions parallel and transverse to the MF, respectively [58, 59, 63, 64].

In the present paper, following the seminal work of [58], we compute the magnetized EOS starting from the RMF effective Lagrangian given in [65–69]. A detailed description and derivation of the various quantities required to define the magnetized nuclear matter can be found in [58, 59, 63]. Here, we present the necessary formalism required in the zero-temperature limit.

The energy spectra of neutrons, protons, and charged leptons (electron and muon) are

$$E_n = \sqrt{k^2 + m_n^{*2}} + W + R/2, \quad (1)$$

$$E_p = \sqrt{k_z^2 + (\bar{m}_{v,\sigma_z}^{(p)})^2} + W - R/2, \quad (2)$$

$$E_l = \sqrt{k_z^2 + (\bar{m}_{v,\sigma_z}^{(l)})^2}, \quad (3)$$

where W and R are the omega and rho meson mean field, respectively [70, 71], k_z and $\sigma_z = \pm 1$ are the momentum and spin along the direction of the MF, and v is the principal quantum number. The masses of the charged particles get modified due to the Landau levels [58, 59],

$$(\bar{m}_{v,\sigma_z}^{(p)})^2 = m_p^{*2} + 2qB\left(v + \frac{1}{2} - \frac{1}{2}\sigma_z\right), \quad (4)$$

$$(\bar{m}_{v,\sigma_z}^{(l)})^2 = m_l^2 - 2qB\left(v + \frac{1}{2} + \frac{1}{2}\sigma_z\right), \quad (5)$$

where m_p^* is the effective mass of the proton.

The partial number and energy densities of the species $i = p, e, \mu$ in presence of the MF are then given by [58]

$$\rho_i = \frac{|q|B}{2\pi^2} \sum_{\sigma_z=\pm 1} \sum_{v=0}^{v_{\max}} k_{F,v,\sigma_z}^{(i)}, \quad (6)$$

$$\varepsilon_i = \frac{|q|B}{4\pi^2} \sum_{\sigma_z=\pm 1} \sum_{v=0}^{v_{\max}} \left[E_F^{(i)} k_{F,v,\sigma_z}^{(i)} + (\bar{m}_{v,\sigma_z}^{(i)})^2 \operatorname{arsinh} \left| \frac{k_{F,v,\sigma_z}^{(i)}}{\bar{m}_{v,\sigma_z}^{(i)}} \right| \right]. \quad (7)$$

In these equations, the Fermi momentum is defined by

$$k_{F,v,\sigma_z}^{(i)} = \sqrt{E_F^{(i)2} - (\bar{m}_{v,\sigma_z}^{(i)})^2}, \quad (8)$$

where the Fermi energies $E_F^{(i)}$ are fixed by the respective

chemical potentials,

$$E_F^{(l)} = \mu_l, \quad (9)$$

$$E_F^{(b=p,n)} = \mu_b - W \pm R/2. \quad (10)$$

The largest possible energy label v_{\max} for protons or leptons is the integer for which the Fermi momentum remains positive, i.e.,

$$v_{\max} \leq \frac{E_F^2 - m^*{}^2}{2|q|B}. \quad (11)$$

While the contribution of the neutrons to the pressure is straightforward [64, 70], that of the protons can be written in terms of parallel and perpendicular components along the local direction of the magnetic field [59, 72],

$$p_{\parallel} = \frac{|q|B}{4\pi^2} \sum_{\sigma_z=\pm 1} \sum_{v=0}^{v_{\max}} \left[E_F^{(i)} k_{F,v,\sigma_z}^{(i)} - (\bar{m}_{v,\sigma_z}^{(i)})^2 \operatorname{arsinh} \left| \frac{k_{F,v,\sigma_z}^{(i)}}{\bar{m}_{v,\sigma_z}^{(i)}} \right| \right], \quad (12)$$

$$p_{\perp} = \frac{|q|^2 B^2}{2\pi^2} \sum_{\sigma_z=\pm 1} \sum_{v=0}^{v_{\max}} v \operatorname{arsinh} \left| \frac{k_{F,v,\sigma_z}^{(i)}}{\bar{m}_{v,\sigma_z}^{(i)}} \right|. \quad (13)$$

Consequently, the energy-momentum tensor in the presence of a magnetic field can be expressed as [73, 74]

$$T_{\mu\nu} = T_{\mu\nu}^{\text{matter}} + T_{\mu\nu}^{\text{MF}}, \quad (14)$$

$$= \text{diag} \left(\varepsilon + \frac{B^2}{2}, p_{\perp} + \frac{B^2}{2}, p_{\perp} + \frac{B^2}{2}, p_{\parallel} - \frac{B^2}{2} \right). \quad (15)$$

In order to be able to employ the standard Tolman-Oppenheimer-Volkoff (TOV) equations that require an isotropic pressure (see the extended discussion in [75]), we average the spatial components of $T_{\mu\nu}$ to obtain an effective local isotropic pressure. Adhering to the “chaotic-magnetic-field” framework outlined in [73, 76–78], we express the total average pressure as

$$p = \frac{T_{11} + T_{22} + T_{33}}{3} = \frac{2p_{\perp} + p_{\parallel}}{3} + \frac{B^2}{6}. \quad (16)$$

Finally, the total energy density ε and pressure p of the EOS $p(\varepsilon)$ needed in the TOV equations are obtained by summing the nucleon and lepton contributions as detailed above, of asymmetric, beta-stable, and charge-neutral matter. The anomalous magnetic moment is excluded from our calculations as it does not significantly affect the EOS [74].

Regarding the MF strength profile inside the NS, we assume the standard parametrization [79–82] (but see [75] for a critical discussion)

$$B(\rho) = B_{\text{surf}} + B_c \left(1 - e^{-\beta(\rho/\rho_0)^{\gamma}} \right). \quad (17)$$

Here, ρ_0 is the saturation density, B_{surf} represents the surface MF assumed to be 10^{15} G, consistent with the observed surface MF of various magnetars [83, 84]. B_c pertains to the MF at the core of the star. The parameters $\beta = 0.01$ and $\gamma = 3$ are selected to reproduce the decaying behaviors of the MF [79].

B. DM EOS

In this study, the ADM EOS is realized by self-interacting fermions that do not undergo annihilation. The fermion mass varies from the MeV to GeV scale, as discussed in [8, 21, 29, 38], and the Lagrangian reads

$$\mathcal{L}_{\text{DM}} = (D_{\mu}\chi)^*(D^{\mu}\chi) - m_{\chi}^2 \chi^* \chi + \frac{1}{2} m_{\phi}^2 \phi_{\mu} \phi^{\mu} - \frac{1}{4} \Omega_{\mu\nu} \Omega^{\mu\nu}, \quad (18)$$

where χ and ϕ_{μ} represent the fermionic ADM field and vector boson field with masses m_{χ} and m_{ϕ} , respectively. $D_{\mu} = \partial_{\mu} + ig_{\chi}\phi_{\mu}$ is the covariant derivative, where g_{χ} is the interaction strength of χ with the ϕ_{μ} field. The strength tensor is defined as $\Omega_{\mu\nu} = \partial_{\mu}\phi_{\nu} - \partial_{\nu}\phi_{\mu}$. The corresponding DM energy density and pressure are [11, 38, 85]

$$\varepsilon_{\chi} = \frac{m_{\chi}^4}{8\pi^2} \left[x \sqrt{1+x^2} (2x^2+1) - \operatorname{arsinh}(x) \right] + \delta, \quad (19)$$

$$p_{\chi} = \frac{\partial(\varepsilon_{\chi}/n_{\chi})}{\partial n_{\chi}} n_{\chi}^2 = \frac{\partial\varepsilon_{\chi}}{\partial n_{\chi}} n_{\chi} - \varepsilon_{\chi} \\ = \frac{m_{\chi}^4}{8\pi^2} \left[x \sqrt{1+x^2} (2x^2/3 - 1) + \operatorname{arsinh}(x) \right] + \delta, \quad (20)$$

where

$$x = \frac{k_{\chi}}{m_{\chi}} = \frac{(3\pi^2 n_{\chi})^{1/3}}{m_{\chi}} \quad (21)$$

is the dimensionless kinetic parameter with the DM Fermi momentum k_{χ} and number density n_{χ} . Introducing the dimensionless interaction parameter $y \equiv g_{\chi} m_{\chi} / (\sqrt{2} m_{\phi})$, the self-interaction term is written as

$$\delta = \left(\frac{y n_{\chi}}{m_{\chi}} \right)^2. \quad (22)$$

Ref. [11] contains interesting scaling relations regarding the EOS and mass-radius relations of pure fermionic DM stars.

Within this model, m_{χ} and y are not independent free parameters, but constrained by limits imposed on the DM self-interaction cross section σ_{χ} through observation of the interaction of galaxies in different colliding galaxy clusters [86–89],

$$\sigma_{\chi}/m_{\chi} \sim 0.1 - 10 \text{ cm}^2/\text{g}. \quad (23)$$

In [90–93] it has been shown that the Born approximation

$$\frac{\sigma_{\chi}}{m_{\chi}} = \frac{y^4}{\pi m_{\chi}^3} \quad (24)$$

is very accurate for $m_{\chi} \lesssim 1$ GeV and in any case remains valid in the limit $y \rightarrow 0$ for larger masses. We therefore employ here this approximation, choosing for simplicity the fixed constraint

$$\sigma_{\chi}/m_{\chi} = 1 \text{ cm}^2/\text{g} = 4560/\text{GeV}^3, \quad (25)$$

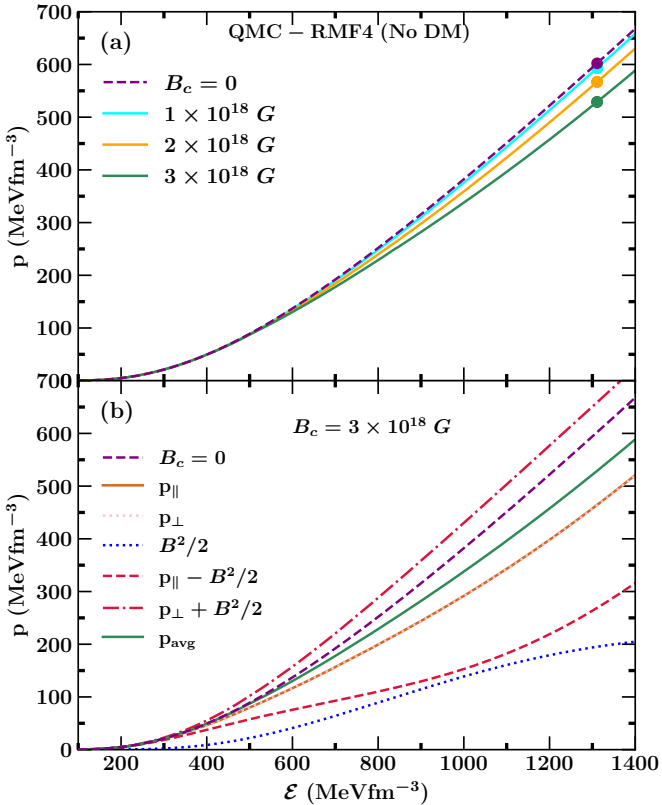


FIG. 1. Upper panel (a): QMC-RMF4 EOS for magnetized NS matter with different MF strengths B_c . The markers indicate the maximum-mass configurations. Lower panel (b): Different contributions to the pressure for $B_c = 3 \times 10^{18}$ G.

which appears compatible with all current observations. This implies

$$y^4 = \pi m_\chi^3 \sigma_\chi / m_\chi \approx \pi (16.58 m_1)^3, \quad (26)$$

$$y \approx 10.94 m_1^{3/4} \quad (27)$$

with $m_1 \equiv m_\chi / 1$ GeV. After this, the DM EOS depends only on the one parameter m_χ .

III. RESULTS AND DISCUSSION

In this section, we provide our numerical results for the DNS properties in presence of a MF. As mentioned earlier, the DM has only indirect effects on the properties of the magnetized NS; therefore, we mainly focus on explaining the results of the combined system with different scenarios in the following.

A. EOS of magnetized NSs

In Fig. 1(a) we present the EOS $p(\epsilon)$ for nucleonic NSs without DM, employing the QMC-RMF4 EOS under varying MF strengths $B_c = 1, 2, 3 \times 10^{18}$ G, comparing with the

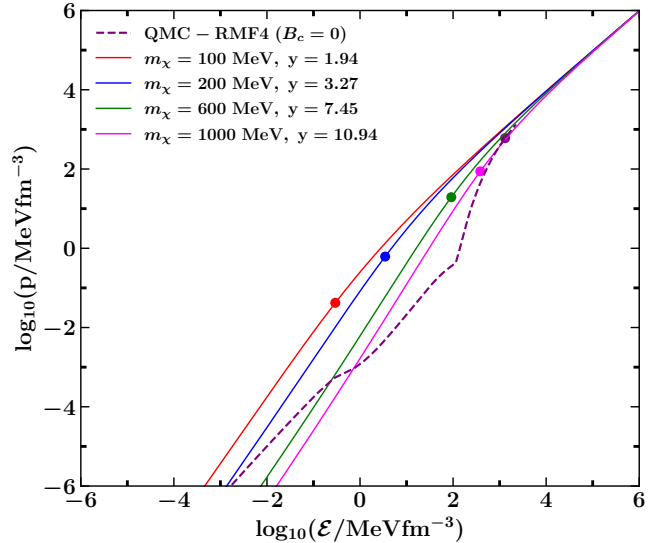


FIG. 2. Pure DM EOS with different masses m_χ in comparison with the nucleonic QMC-RMF4 EOS. The DM self-interaction parameter y , Eq. (27), is also listed. The markers indicate the maximum-mass configurations.

EOS without a MF ($B_c = 0$). Note that due to the assumption of a density-dependent magnetic field, Eq. (17), B increases with pressure or energy density along the curves, and this causes a progressive softening of the EOS [77], i.e., lower pressures for a given energy density, resulting in less massive and compact NSs [59, 77]. Thus, the MF's effect on the pressure profile of the NS is considerable, demonstrating that MFs can induce significant structural changes in NSs. The markers on the curves indicate the maximum-mass configurations for each EOS, anticipating that the maximum mass decreases with stronger MFs.

In the lower panel (b) we show individual contributions to the pressure at the highest field considered, $B_c = 3 \times 10^{18}$ G: The bare matter pressures p_\perp and p_\parallel , Eqs. (12,13), are practically identical and strongly reduced compared to the $B = 0$ pressure. The pure field contributions $\pm B^2/2$ to the components of $T_{\mu\nu}$, Eqs. (15), are of considerable size, such that also the contribution $B^2/6$ to the average pressure p , Eqs. (16), plotted in panel (a), is sizeable. However, the effect is not enough to compensate the reduction of p_\perp , p_\parallel relative to the $B = 0$ pressure. Note that the pressures shown in Fig. 1 always contain contributions of neutrons, protons, and leptons. These results corroborate earlier findings, which also showed that deviations from spherical symmetry, even in high-MF scenarios up to 10^{18} G, remain minimal (less than 1%) [64, 82, 94], thus, supporting the assumption that the structure of highly-magnetized NSs can still be effectively described assuming spherical symmetry.

B. EOS of ADM

The DM EOS is depicted in Fig. 2 for different DM candidate masses $m_\chi = 0.1 - 1$ GeV and the compatible DM self-

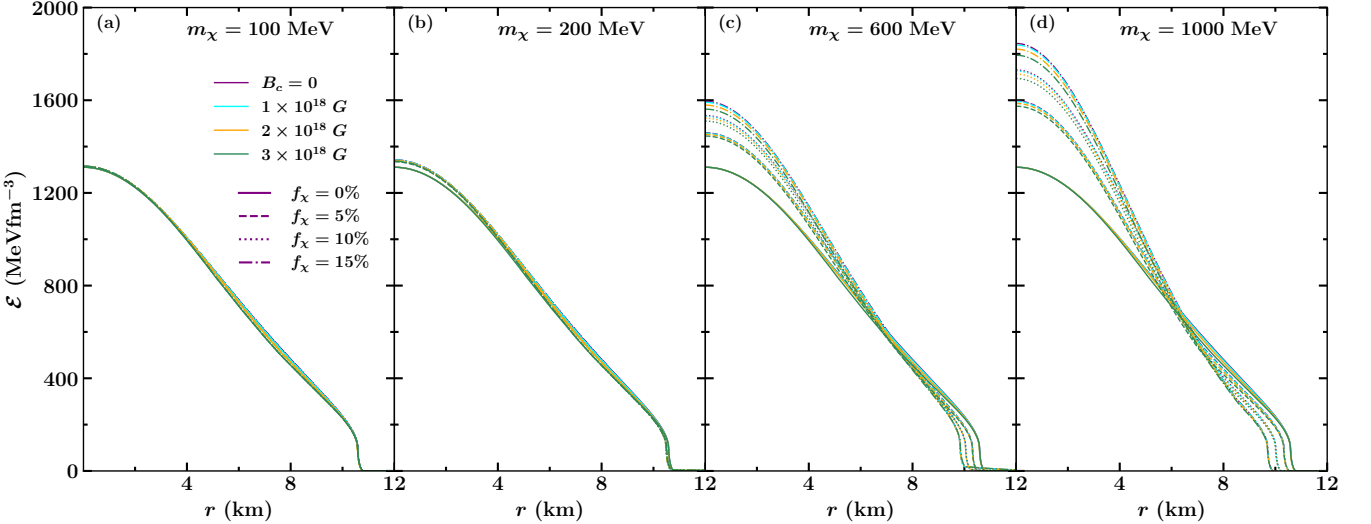


FIG. 3. The radial energy-density profiles of magnetized DNSs for the DM EOSs shown in Fig. 2. Several choices of DM fraction f_χ and magnetic field strength B_c are compared. The curves correspond to the respective maximum-mass configurations.

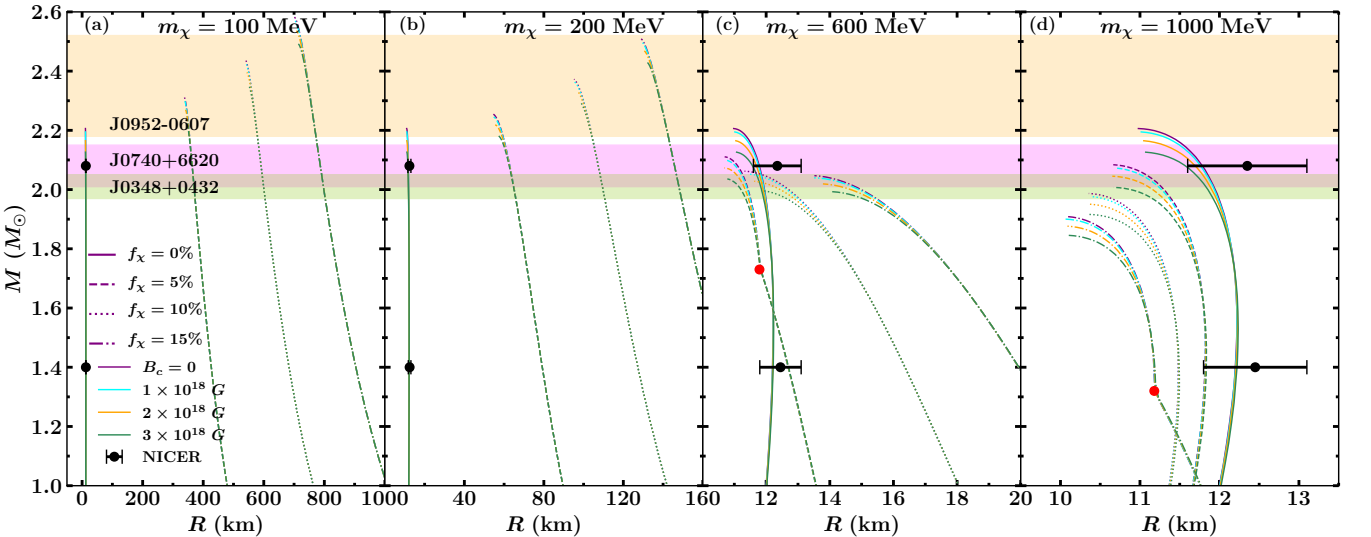


FIG. 4. The mass-radius profiles of magnetized DNS for the DM EOSs shown in Fig. 2, and several choices of DM fraction f_χ and magnetic field strength B_c . The radius is $R = \max(R_N, R_\chi)$, note the different scales. The mass constraints for PSR J0952-0607 [54], PSR J0740+6620 [41], and PSR J0348+0432 [40] are represented by shaded bars. The simultaneous $M - R$ constraints from NICER+XMM for PSR J0740+6620 [55] are also shown as horizontal error bars.

interaction parameter y , Eq. (27). The hadronic QMC-RMF4 EOS is shown for comparison, exhibiting different domains for core, inner crust, and outer crust. Markers indicate the maximum-mass configurations of pure dark stars or standard NSs. Within the range of interest, lighter DM masses result in a notably stiffer EOS, corresponding to larger DNS maximum masses, as is well known [8, 38].

C. Density profiles

The interaction between DM and a magnetized NS can result in either a DM-core or a DM-halo star, mainly determined by the DM particle mass m_χ (and the correlated interaction

strength), and the DM mass fraction $f_\chi = M_\chi/M$ [35, 38]. We are interested in the effect of a magnetic field on this feature.

In Fig. 3, the radial energy-density profiles of magnetized DNSs are shown for the maximum-mass configuration of each EOS, varying m_χ , f_χ , and B_c . The figure illustrates that as the DM particle mass or its fraction increase, the energy density rises, corresponding to a more compact star. As will be better seen in the next Fig. 4, for light DM masses, such as $m_\chi = 100, 200$ MeV, the DM extends beyond the normal matter radius R_N for all chosen values of f_χ , forming a DM-halo star, whereas for heavier DM masses like $m_\chi = 600, 1000$ MeV, the DM is entirely confined within the star regardless of the DM mass fraction f_χ . With increasing f_χ , also the dark radius R_χ increases, extending further the DM halo for ‘small’

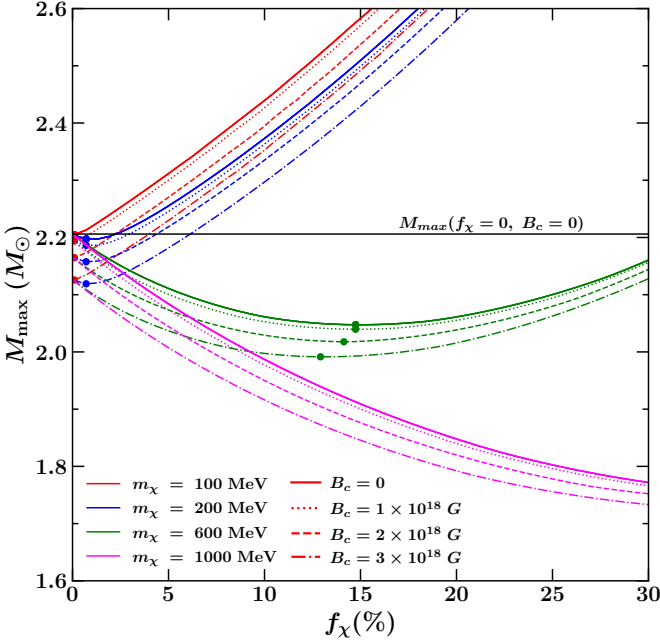


FIG. 5. The maximum gravitational mass as a function of DM fraction for different DM particle masses and magnetic fields. The markers indicate the transition from DM core to halo.

m_χ , whereas for ‘large’ m_χ the DM remains trapped within the DNS core, substantially increasing the star’s compactness.

An increasing MF also decreases the compactness by a few percent, but the effect is much weaker than varying the DM fraction in the figure.

D. Mass-radius relations

The density profiles of magnetized DNSs show clearly that the model parameters m_χ and f_χ determine the formation of either a DM-halo ($R = R_\chi$) or a DM-core ($R = R_N$) structure, and thus, impact significantly the radius and overall structure of the DNS, whereas the magnetic field appears of minor importance. This is also seen in the mass-radius profiles shown in Fig. 4, for the same conditions as in Fig. 3. As analyzed in more detail in [38], for ‘small (large)’ masses $m_\chi \lesssim (\gtrsim) 1 \text{ GeV}$ DM-halo (core) stars are formed, where both R and M_{\max} increase (decrease) with increasing (not too large) f_χ . Two typical contrasting cases are shown in the $m_\chi = 100 \text{ MeV}$ and $m_\chi = 1000 \text{ MeV}$ panels.

The $m_\chi = 600 \text{ MeV}$ panel illustrates the transition between both regimes: on the $f_\chi = 5\%$ curves one notes a $R_\chi = R_N$ configuration (red marker) with $M \approx 1.73M_\odot$ and $R \approx 11.79 \text{ km}$, where the R_N branch for larger masses deviates onto the R_χ branch for lower masses. The same occurs on the $f_\chi = 15\%$ curves for $m_\chi = 1000 \text{ MeV}$. Again we refer to [38] for a more extended discussion.

The figure also shows current maximum-mass constraints from PSR J0952-0607, PSR J0740+6620, and PSR J0348+0432, as well as NICER+XMM constraints of the radii $R_{1.4}$ and $R_{2.08}$. The nucleonic RMF EOS is compatible with

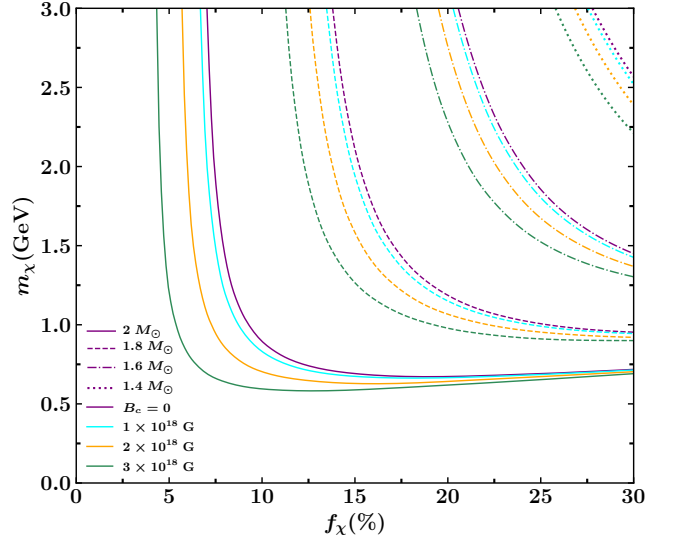


FIG. 6. M_{\max} contours in the (m_χ, f_χ) plane for different magnetic fields.

all of them, and some admixture of DM can currently not be excluded for the observed objects.

The effect of the magnetic field (reduction of M_{\max}) is not more than a few percent for all configurations and will be analyzed in more detail now.

E. Maximum mass

In Fig. 5 we show the maximum DNS gravitational mass as a function of DM fraction, for different m_χ and B_c values. For each EOS the transition from DM core to halo is indicated by a marker. In accordance with Fig. 4, for the ‘small’ masses $m_\chi = 100, 200 \text{ MeV}$ the DM-halo character sets in at low $f_\chi < 1\%$, increasing M_{\max} , while for ‘large’ $m_\chi = 600 \text{ MeV}$ the onset occurs at $f_\chi \approx 15\%$, and for $m_\chi = 1000 \text{ MeV}$, there are only DM-core configurations with lowered M_{\max} in the plot range. Again the effect of the magnetic field is very small, in particular there is a small reduction of the halo-core transition fraction.

Finally, Fig. 6 shows some contours of M_{\max} in the (m_χ, f_χ) plane for different magnetic fields. As the previous figure, it indicates that for greater m_χ , a smaller f_χ is sufficient to destabilize the DNS. Since a magnetic field decreases the maximum mass, it provides some degree of destabilization against DM-induced collapse, but the effect is again small compared to variation of f_χ .

F. Tidal deformability

In a binary system, the gravitational interaction with a companion object (either a NS or a BH) induces deformation in a NS. The dimensionless tidal deformability of the system, which quantifies this deformation, is represented by $\Lambda = (2/3)(R/M)^5 k_2$, where k_2 refers to its second Love number [96, 97]. Λ depends on the star’s mass and radius, and is

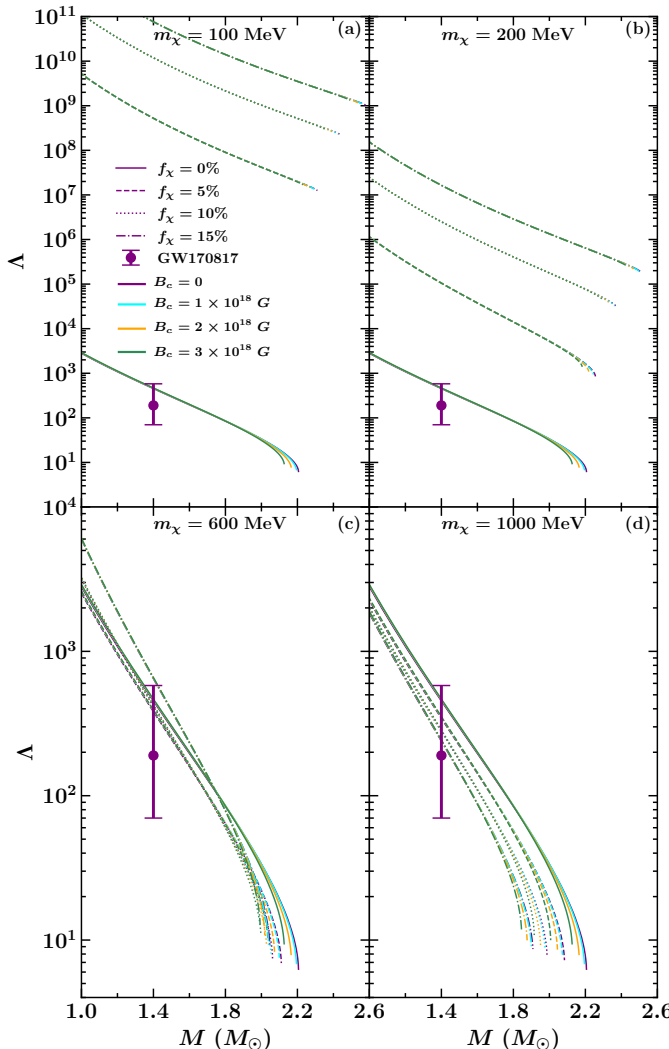


FIG. 7. The tidal deformability vs DNS mass for different values of m_χ , f_χ , and B_c . The GW170817 constraint [95] is also shown.

modulated by DM and magnetic fields. Within the two-fluid framework, it has been examined both with [64, 71, 98] and without [21, 25, 27, 28, 35, 38] the presence of a MF.

In Fig. 7, Λ is plotted vs the DNS mass for different values of m_χ , f_χ , and B_c . As $\Lambda \sim R^5$ is extremely sensitive to the gravitational radius, the DM-halo or -core character plays a decisive role: According to Fig. 4, the small- m_χ DM-halo stars feature very large radii and consequently enormous val-

ues of Λ , whereas the large- m_χ DM-core stars with their reduced radii exhibit also reduced Λ values.

Across all panels it is apparent that the effect of the MF is very small and only visible near the M_{\max} configurations. A stronger MF results in a more compact NS, thereby decreasing its deformability.

The pure NS EOS with $\Lambda = 454$ fulfills (by construction) the observational limits imposed by GW170817, but also here, the large error bar currently cannot exclude an admixture of DM.

IV. CONCLUSIONS

In this work, we examined the combined effects of DM and MF on DNS properties. We considered self-interacting, asymmetric, non-annihilating fermionic DM, obeying the self-interaction cross-section constraint imposed by the observed interaction of galaxies in various galaxy clusters. This left the DM particle mass as a free parameter. Combined with the nucleonic QMC-RMF4 EOS and density-dependent MFs of magnetar size, we investigated how DM particle mass, DM mass fraction, and MF strength influence key DNS properties such as maximum mass, mass-radius relations, tidal deformability, and the critical DM mass fraction needed for destabilization.

As is well known, the DM-halo or -core character of a DNS is mainly determined by a small (halo) or large (core) DM particle mass (compared to the nucleon mass), associated with possible increase or decrease of the DNS maximum gravitational mass, respectively.

We found that the influence of the MF on these features is generally very small, even for the strongest field values of magnetar size. The magnetized EOS is softer and consequently causes slightly smaller maximum masses and less stability against collapse, for example, for otherwise unchanged parameters. But as the same effects are caused by a small variation of the DM fraction, it will be real challenge to extract this information from observation, if such DNSs with large DM fraction exist.

ACKNOWLEDGMENTS

B. K. acknowledges partial support from the Department of Science and Technology, Government of India, with grant no. CRG/2021/000101. Part of this computation was performed using the CINECA cluster under the NEUMATT project.

-
- [1] G. Bertone, D. Hooper, and J. Silk, Phys. Rep. **405**, 279 (2005).
 - [2] V. C. Rubin and J. Ford, W. Kent, Astrophys. J. **159**, 379 (1970).
 - [3] V. C. Rubin, J. Ford, W. K., and N. Thonnard, Astrophys. J. **238**, 471 (1980).
 - [4] D. Clowe, M. Bradač, A. H. Gonzalez, M. Markevitch, S. W. Randall, C. Jones, and D. Zaritsky, Astrophys. J. **648**, L109 (2006).
 - [5] E. Komatsu *et al.*, Astrophys. J. Supplement Series **192**, 18 (2011).
 - [6] G. Bertone and M. Fairbairn, Phys. Rev. D **77**, 043515 (2008).
 - [7] N. F. Bell, G. Busoni, T. F. Motta, S. Robles, A. W. Thomas, and M. Virgato, Phys. Rev. Lett. **127**, 111803 (2021).
 - [8] B. Kain, Phys. Rev. D **103**, 043009 (2021).
 - [9] D. Rafiei Karkevandi, S. Shakeri, V. Sagun, and O. Ivanytskyi, Phys. Rev. D **105**, 023001 (2022).
 - [10] I. Goldman and S. Nussinov, Phys. Rev. D **40**, 3221 (1989).

- [11] G. Narain, J. Schaffner-Bielich, and I. N. Mishustin, Phys. Rev. D **74**, 063003 (2006).
- [12] C. Kouvaris, Phys. Rev. D **77**, 023006 (2008).
- [13] C. Kouvaris and P. Tinyakov, Phys. Rev. D **82**, 063531 (2010).
- [14] L. J. Hall, K. Jedamzik, J. March-Russell, *et al.*, JHEP **2010**, 80 (2010).
- [15] C. Kouvaris and P. Tinyakov, Phys. Rev. D **83**, 083512 (2011).
- [16] C. Kouvaris, Phys. Rev. Lett. **108**, 191301 (2012).
- [17] I. Goldman, R. Mohapatra, S. Nussinov, D. Rosenbaum, and V. Teplitz, Phys. Lett. B **725**, 200 (2013).
- [18] T. Han, Z. Liu, and S. Su, JHEP **2014**, 93 (2014).
- [19] G. Panotopoulos and I. Lopes, Phys. Rev. D **96**, 083004 (2017).
- [20] N. Bernal, M. Heikinheimo, T. Tenkanen, *et al.*, IJMP A **32**, 1730023 (2017).
- [21] A. E. Nelson, S. Reddy, and D. Zhou, JCAP **2019**, 012 (2019).
- [22] M. I. Gresham and K. M. Zurek, Phys. Rev. D **99**, 083008 (2019).
- [23] H. C. Das, A. Kumar, B. Kumar, S. K. Biswal, T. Nakatsukasa, A. Li, and S. K. Patra, Mon. Not. R. Astron. Soc. **495**, 4893 (2020).
- [24] O. Ivanytskyi, V. Sagun, and I. Lopes, Phys. Rev. D **102**, 063028 (2020).
- [25] A. Das, T. Malik, and A. C. Nayak, Phys. Rev. D **105**, 123034 (2022).
- [26] D. Rafiei Karkevandi, S. Shakeri, V. Sagun, and O. Ivanytskyi, Phys. Rev. D **105**, 023001 (2022).
- [27] K.-L. Leung, M.-C. Chu, and L.-M. Lin, Phys. Rev. D **105**, 123010 (2022).
- [28] M. Collier, D. Croon, and R. K. Leane, Phys. Rev. D **106**, 123027 (2022).
- [29] Z. Miao, Y. Zhu, A. Li, and F. Huang, Astrophys. J. **936**, 69 (2022).
- [30] P. Routaray, H. C. Das, S. Sen, B. Kumar, G. Panotopoulos, and T. Zhao, Phys. Rev. D **107**, 103039 (2023).
- [31] N. Rutherford, G. Raaijmakers, C. Prescod-Weinstein, and A. Watts, Phys. Rev. D **107**, 103051 (2023).
- [32] M. Mariani, C. Albertus, M. d. R. Alessandroni, M. G. Orsaria, M. A. Pérez-García, and I. F. Ranea-Sandoval, Mon. Not. R. Astron. Soc. **527**, 6795 (2023).
- [33] P. Routaray, A. Quddus, K. Chakravarti, and B. Kumar, Mon. Not. R. Astron. Soc. **525**, 5492 (2023).
- [34] P. Routaray, S. R. Mohanty, H. Das, S. Ghosh, P. Kalita, V. Parmar, and B. Kumar, JCAP **2023**, 073 (2023).
- [35] H.-M. Liu, J.-B. Wei, Z.-H. Li, G. F. Burgio, and H.-J. Schulze, Physics of the Dark Universe **42**, 101338 (2023).
- [36] D. Rafiei Karkevandi, M. Shahrbaf, S. Shakeri, and S. Typel, Particles **7**, 201 (2024).
- [37] S. Shakeri and D. R. Karkevandi, Phys. Rev. D **109**, 043029 (2024).
- [38] H.-M. Liu, J.-B. Wei, Z.-H. Li, G. F. Burgio, H. C. Das, and H.-J. Schulze, Phys. Rev. D **110**, 023024 (2024).
- [39] P. Routaray, H. Das, J. A. Pattnaik, and B. Kumar, International Journal of Modern Physics E **0**, 2450052 (0), <https://doi.org/10.1142/S0218301324500526>.
- [40] J. Antoniadis, P. C. C. Freire, N. Wex, *et al.*, Science **340**, 1233232 (2013).
- [41] E. Fonseca, H. T. Cromartie, T. T. Pennucci, *et al.*, Astrophys. J. Lett. **915**, L12 (2021).
- [42] V. M. Kaspi, Proceedings of the National Academy of Sciences **107**, 7147 (2010).
- [43] V. M. Kaspi and A. M. Beloborodov, Annu. Rev. Astron. Astrophys. **55**, 261 (2017).
- [44] K. Makishima, T. Enoto, J. S. Hiraga, T. Nakano, K. Nakazawa, S. Sakurai, M. Sasano, and H. Murakami, Phys. Rev. Lett. **112**, 171102 (2014).
- [45] B. Kern and C. Martin, Nature **417**, 527 (2002).
- [46] K. Hurley, Advances in Space Research **47**, 1326 (2011).
- [47] J. Lattimer, Ann. Rev. Nucl. Part. Sc. **71**, 433 (2021).
- [48] Y. Gao, L. Shao, G. Desvignes, D. I. Jones, M. Kramer, and G. Yim, Mon. Not. R. Astron. Soc. **519**, 1080 (2022).
- [49] J. Margueron, R. Hoffmann Casali, and F. Gulminelli, Phys. Rev. C **97**, 025805 (2018).
- [50] B.-A. Li and X. Han, Phys. Lett. B **727**, 276 (2013).
- [51] M. Oertel, M. Hempel, T. Klähn, and S. Typel, Rev. Mod. Phys. **89**, 015007 (2017).
- [52] S. Shlomo, V. M. Kolomietz, and G. Colò, Eur. Phys. J. A **30**, 23 (2006).
- [53] J. Piekarewicz, J. Phys. G **37**, 064038 (2010).
- [54] R. W. Romani, D. Kandel, A. V. Filippenko, T. G. Brink, and W. Zheng, Astrophys. J. Lett. **934**, L17 (2022).
- [55] M. C. Miller, F. K. Lamb, A. J. Dittmann, *et al.*, APJ **918**, L28 (2021).
- [56] B. P. Abbott *et al.*, Phys. Rev. Lett. **121**, 161101 (2018).
- [57] M. G. Alford, L. Brodie, A. Haber, and I. Tews, Phys. Rev. C **106**, 055804 (2022).
- [58] A. Broderick, M. Prakash, and J. M. Lattimer, Astrophys. J. **537**, 351 (2000).
- [59] M. Strickland, V. Dexheimer, and D. P. Menezes, Phys. Rev. D **86**, 125032 (2012).
- [60] V. Parmar, H. C. Das, M. K. Sharma, and S. K. Patra, Phys. Rev. D **107**, 043022 (2023).
- [61] V. Parmar, H. C. Das, A. Kumar, M. K. Sharma, and S. K. Patra, Phys. Rev. D **105**, 043017 (2022).
- [62] J. Fang, H. Pais, S. Pratapsi, *et al.*, Phys. Rev. C **95**, 062801 (2017).
- [63] A. Goyal, V. K. Gupta, K. Goswami, and V. Tuli, Int. J. Mod. Phys. A **16**, 347 (2001).
- [64] N. K. Patra, T. Malik, D. Sen, *et al.*, Astrophys. J. **900**, 49 (2020).
- [65] H. Müller and B. D. Serot, Nucl. Phys. A **606**, 508 (1996).
- [66] P. Wang, Phys. Rev. C **61**, 054904 (2000).
- [67] S. K. Patra, M. Centelles, X. Viñas, *et al.*, Phys. Rev. C **65**, 044304 (2002).
- [68] A. Kumar, H. C. Das, S. K. Biswal, *et al.*, Eur. Phys. J. C **80** (2020).
- [69] H. C. Das, A. Kumar, B. Kumar, *et al.*, JCAP **2021**, 007 (2021).
- [70] B. Kumar, S. K. Patra, and B. K. Agrawal, Phys. Rev. C **97**, 045806 (2018).
- [71] V. Parmar, H. C. Das, M. K. Sharma, *et al.*, Phys. Rev. D **107**, 043022 (2023).
- [72] S. Chakrabarty, Phys. Rev. D **54**, 1306 (1996).
- [73] M. Mariani, M. G. Orsaria, I. F. Ranea-Sandoval, *et al.*, Mon. Not. R. Astron. Soc. **489**, 4261 (2019).
- [74] M. Mariani, L. Tonetto, M. C. Rodríguez, M. O. Celi, I. F. Ranea-Sandoval, M. G. Orsaria, and A. Pérez Martínez, Mon. Not. R. Astron. Soc. **512**, 517 (2022).
- [75] D. Chatterjee, J. Novak, and M. Oertel, Eur. Phys. J. A **57**, 249 (2021).
- [76] I. Bednarek, A. Brzezina, R. Mańka, and M. Zastawny-Kubica, Nucl. Phys. A **716**, 245 (2003).
- [77] L. Lopes and D. Menezes, JCAP **2015**, 002 (2015), arXiv:1411.7209 [astro-ph.HE].
- [78] C. V. Flores, L. B. Castro, and G. Lugones, Phys. Rev. C **94**, 015807 (2016).
- [79] D. Bandyopadhyay, S. Chakrabarty, and S. Pal, Phys. Rev. Lett. **79**, 2176 (1997).
- [80] A. Rabhi, H. Pais, P. K. Panda, and C. Providência, J. Phys. G **36**, 115204 (2009).

- [81] R. Mallick and S. Schramm, Phys. Rev. C **89**, 045805 (2014).
- [82] G. H. Bordbar and M. Karami, Eur. Phys. J. C **82**, 74 (2022).
- [83] R. H. Casali, L. B. Castro, and D. P. Menezes, Phys. Rev. C **89**, 015805 (2014).
- [84] T. Güver, E. Göğüş, and F. Özel, Mon. Not. R. Astron. Soc. **418**, 2773 (2011).
- [85] M. F. Barbat, J. Schaffner-Bielich, and L. Tolos, Phys. Rev. D **110**, 023013 (2024).
- [86] M. Markevitch, A. H. Gonzalez, D. Clowe, A. Vikhlinin, W. Forman, C. Jones, S. Murray, and W. Tucker, Astrophys. J. **606**, 819 (2004).
- [87] M. Kaplinghat, S. Tulin, and H.-B. Yu, Phys. Rev. Lett. **116**, 041302 (2016).
- [88] L. Sagunski, S. Gad-Nasr, B. Colquhoun, A. Robertson, and S. Tulin, J. Cosmol. Astropart. Phys. **2021**, 024 (2021).
- [89] A. Loeb, Astrophys. J. Lett. **929**, L24 (2022).
- [90] S. Tulin, H.-B. Yu, and K. M. Zurek, Phys. Rev. D **87**, 115007 (2013).
- [91] C. Kouvaris and N. G. Nielsen, Phys. Rev. D **92**, 063526 (2015).
- [92] A. Maselli, P. Pnigouras, N. G. Nielsen, C. Kouvaris, and K. D. Kokkotas, Phys. Rev. D **96**, 023005 (2017).
- [93] K. M. Zurek, Phys. Rep. **537**, 91 (2014).
- [94] P.-C. Chu, X. Wang, L.-W. Chen, and M. Huang, Phys. Rev. D **91**, 023003 (2015).
- [95] B. P. Abbott *et al.* (The LIGO Scientific Collaboration and Virgo Collaboration), Phys. Rev. Lett. **119**, 161101 (2017).
- [96] T. Hinderer, Astrophys. J. **677**, 1216 (2008).
- [97] B. Kumar, S. K. Biswal, and S. K. Patra, Phys. Rev. C **95**, 015801 (2017).
- [98] I. A. Rather, U. Rahaman, V. Dexheimer, A. A. Usmani, and S. K. Patra, Astrophys. J. **917**, 46 (2021).

Exploring robust correlations between fermionic dark matter model parameters and neutron star properties: A two-fluid perspective

Prashant Thakur^{1,*}, Tuhin Malik^{2,†}, Arpan Das^{3,4,‡}, T. K. Jha^{1,§}, and Constança Providência^{2,||}

¹Department of Physics, BITS-Pilani, K. K. Birla Goa Campus, Goa 403726, India

²CFisUC, Department of Physics, University of Coimbra, P-3004-516 Coimbra, Portugal

³Institute of Nuclear Physics Polish Academy of Sciences, PL-31-342 Kraków, Poland

⁴Department of Physics, Birla Institute of Technology and Science, Pilani, Rajasthan-333031, India

(Received 9 August 2023; revised 10 December 2023; accepted 12 January 2024; published 15 February 2024)

We investigate the probable existence of dark matter in the interior of neutron stars. Despite the current state of knowledge, the observational properties of neutron stars have not definitively ruled out the possibility of dark matter. Our research endeavors to shed light on this intriguing mystery by examining how certain neutron star properties, including mass, radius, and tidal deformability, might serve as constraints for the dark matter model. In our investigation, we adopt a two-fluid approach to calculate the properties of neutron stars. For the nuclear matter equation-of-state (EOS), we employ several realistic EOS derived from the relativistic mean field model (RMF), each exhibiting varying stiffness and composition. In parallel, we look into the dark matter EOS, considering fermionic matter with repulsive interaction described by a relativistic mean field Lagrangian. A reasonable range of parameters is sampled meticulously. Our study primarily focuses on exploring correlations between the dark matter model parameters and different neutron star properties using a rich set of EOSs. Interestingly, our results reveal a promising correlation between the dark matter model parameters and stellar properties, particularly when we ignore the uncertainties in the nuclear matter EOS. However, when introducing uncertainties in the nuclear sector, the correlation weakens, suggesting that the task of conclusively constraining any particular dark matter model might be challenging using global properties alone, such as mass, radius, and tidal deformability. Notably, we find that dark-matter admixed stars tend to have higher central baryonic density, potentially allowing for non-nucleonic degrees of freedom or direct Urca processes in stars with lower masses. There is also a tantalizing hint regarding the detection of stars with the same mass but different surface temperatures, which may indicate the presence of dark matter. With our robust and extensive dataset, we delve deeper and demonstrate that even in the presence of dark matter, the semiuniversal C-Love relation remains intact. This captivating finding adds another layer of complexity to the interplay between dark matter and neutron star properties.

DOI: 10.1103/PhysRevD.109.043030

I. INTRODUCTION

Neutron stars (NSs), with their compact nature, hold great fascination in the vast expanse of the cosmos. Although they are of great significance in astrophysics, the interiors of neutron stars remain mysterious [1–3].

One of the most intriguing puzzles is the nature of the dense matter that forms their cores. It is believed that these cores can reach densities 5–10 times greater than normal nuclear saturation density. However, the exact composition and behavior of this extreme matter under such extreme conditions elude our understanding. To unravel the secrets concealed within these dense cores, scientists have devoted considerable effort to studying the equation-of-state (EOS), which characterizes the interplay among pressure, density, and temperature within a specific substance [4,5].

The issue of galaxy rotation curves stands out as a prominent indication that galaxies may not be only composed of ordinary nuclear matter [6]. These rotation curves, which depict the rotational velocities of stars and gas in galaxies, exhibit unexpected behavior that cannot be explained solely by the presence of visible matter. This suggests the existence of an additional component known

*p20190072@goa.bits-pilani.ac.in

†tuhin.malik@uc.pt

‡arpan.das@ifj.edu.pl, arpan.das@pilani.bits-pilani.ac.in

§tkjha@goa.bits-pilani.ac.in

||cp@uc.pt

Published by the American Physical Society under the terms of the [Creative Commons Attribution 4.0 International license](#). Further distribution of this work must maintain attribution to the author(s) and the published article's title, journal citation, and DOI. Funded by SCOAP³.

as dark matter [7,8]. Dark matter, as its name suggests, does not interact directly with electromagnetic radiation and remains invisible to traditional telescopes. Its existence can be inferred indirectly through its gravitational effects on visible matter. The dense cores within neutron stars can act as gravitational traps for dark matter particles, potentially influencing their behavior and properties. The highly dense matter inside neutron stars [9–11] can enhance the dark matter capture process inside these objects. Several theoretical models propose the presence of dark matter within neutron star cores, with one possibility being the accumulation of dark matter particles, such as weakly interacting massive particles (WIMPs), due to gravitational attraction [12]. Significant accumulation of nonself-annihilating dark matter inside the compact objects can affect the structure of these compact objects [10–22]. From a particle physics point of view so far there are many candidates for dark matter particles, such as bosonic dark matter, axions, sterile neutrinos, and different possible WIMPs have been proposed in literature [7,23,24]. Since the nature of particle dark matter is uncertain, both bosonic and fermionic dark matter particles have been considered to study its effect on the neutron star dynamics [17,18,25–27]. Naively for fermionic dark matter particles modeled by the ideal Fermi degenerate gas, it is the degeneracy pressure that allows for a stable neutron star configuration [26]. But for the bosonic dark matter particle one must include self-interaction to obtain stable neutron star configurations [17]. Practically neutron star EOS in the presence of dark matter can be much more complicated.

The advent of multi-messenger observations of compact astrophysical objects and the discovery of gravitational waves from neutron star-neutron star mergers by advanced LIGO and VIRGO collaborations [28,29] have not only opened new avenues for exploring the EOS of dense matter but also offer a fresh perspective on the study of dark matter in compact objects, whether fermionic or bosonic [30,31]. Recent advancements in this field of research have shed new light on the presence of dark matter inside neutron stars [19,22,32–37]. Progress in numerical simulations and theoretical models has provided insights into the behavior of dark matter within the cores of neutron stars. Recently, a number of studies have been conducted using statistical Bayesian methods to constrain the EOS of neutron stars using astrophysical observations [38–42]. In constraining the EOS, the correlation has proven useful, with nuclear matter parameters (NMPs) as its key components [43,44]. Modern studies have documented correlations between empirical nuclear parameters and neutron star observables [45–47]. Although some studies have suggested the existence of dark matter (DM) inside neutron stars [16,48–52], up to our knowledge most of these studies have not extensively examined correlations with measurable properties, including dark matter parameters and neutron star astrophysical observable.

The motivation behind this study is to explore potential correlations between the dark matter sector and the global properties of neutron stars while taking into account the inherent uncertainties in the EOS within the baryonic sector. It is crucial to consider the uncertainties associated with the EOS in the baryonic sector, as they can affect our understanding of the overall behavior of neutron stars.

Using the well-known Kendall rank correlation studies we look into the relationship between the dark matter sector and neutron star properties. We seek to uncover any connections or influences that may exist, providing valuable insights into both the properties of dark matter and the behavior of these enigmatic cosmic objects. Furthermore, we aim to explore new avenues to constrain the dark matter sector by investigating its effects on neutron star cooling, which is a key observable, or by examining the viability of direct Urca processes.

The paper has the following organization. In Sec. II, we introduce the basic formalism of the equation-of-state for nuclear matter and dark matter, as well as the two-fluid formalism of the Tolman-Oppenheimer-Volkoff equation and the Kendall rank correlation coefficient. In Sec. III, we present and discuss the results of the current study. Finally, in Sec. IV, we provide concluding remarks.

II. METHODOLOGY

A. Nuclear matter EOS

Our study considers the relativistic mean field (RMF) description [53] of the nuclear matter EOS: a mean-field theory approach that includes nonlinear meson terms, both self-interactions and mixed terms.

$$\mathcal{L} = \mathcal{L}_N + \mathcal{L}_M + \mathcal{L}_{NL} \quad (1)$$

with

$$\begin{aligned} \mathcal{L}_N &= \bar{\Psi} [\gamma^\mu (i\partial_\mu - g_\omega \omega_\mu - g_\varrho \mathbf{q} \cdot \mathbf{q}_\mu) - (m - g_\sigma \sigma)] \Psi \\ \mathcal{L}_M &= \frac{1}{2} [\partial_\mu \sigma \partial^\mu \sigma - m_\sigma^2 \sigma^2] - \frac{1}{4} F_{\mu\nu}^{(\omega)} F^{(\omega)\mu\nu} + \frac{1}{2} m_\omega^2 \omega_\mu \omega^\mu \\ &\quad - \frac{1}{4} \mathbf{F}_{\mu\nu}^{(\varrho)} \cdot \mathbf{F}^{(\varrho)\mu\nu} + \frac{1}{2} m_\varrho^2 \mathbf{q}_\mu \cdot \mathbf{q}^\mu. \\ \mathcal{L}_{NL} &= -\frac{1}{3} b m g_\sigma^3 \sigma^3 - \frac{1}{4} c g_\sigma^4 \sigma^4 + \frac{\xi}{4!} g_\sigma^4 (\omega_\mu \omega^\mu)^2 \\ &\quad + \Lambda_\omega g_\varrho^2 \mathbf{q}_\mu \cdot \mathbf{q}^\mu g_\omega^2 \omega_\mu \omega^\mu, \end{aligned}$$

In this context, the field Ψ represents a Dirac spinor that describes the nucleon doublet (consisting of neutron and proton) with a bare mass m . The couplings of the nucleons to the meson fields σ , ω , and ϱ are denoted by g_σ , g_ω , and g_ϱ respectively, with corresponding masses m_σ , m_ω , and m_ϱ . The parameters b , c , ξ , and Λ_ω , which determine the strength of the nonlinear terms, are determined alongside

TABLE I. Parameters of the employed nuclear matter EOS: EOS1, EOS2, EOS3, and EOS4. The B and C are $b \times 10^3$, and $c \times 10^3$ respectively [53].

EOS	g_σ	g_ω	g_ρ	B	C	ξ	Λ_ω
EOS1	10.411847	13.219028	11.180337	2.541001	-3.586261	0.000845	0.027999
EOS2	11.150279	14.420375	13.806001	2.036239	-1.635468	0.018019	0.037600
EOS3	8.695491	10.431351	9.821776	3.975509	-2.615425	0.006394	0.039323
EOS4	9.608190	11.957725	12.191950	3.117923	-4.098400	0.000255	0.058744

the couplings g_i (where $i = \sigma, \omega, \rho$) by imposing a set of constraints.

We chose four samples from the EOS generated in [53], which we designate as EOS1, EOS2, EOS3, and EOS4. They have been constrained to several nuclear matter properties, in particular, the saturation density, binding energy, incompressibility, symmetry energy at saturation, and the pure neutron matter pressure calculated with chiral effective field theory. It was also imposed that the pure neutron matter pressure must be an increasing function of the baryonic density and stars with at least $2.0M_\odot$ must be described. The parameters of all these four models are presented in Table I. Figure 1 displays these four EOS, along with their corresponding neutron stars (NS) properties. The graph depicts the pressure, denoted as P , as a function of baryon density ρ_B in the left plot. The middle plot showcases the NS mass, denoted as M , as a function of radius R . Additionally, the right plot illustrates the relation between the NS mass (M) and the square of the speed of sound (c_s^2) for the four nuclear matter EOSs. The EOS1 is the stiffest and EOS3 is the softest one. The nuclear saturation properties along with star properties can be accessed from Table II. It can be seen from the table that the NS maximum mass of these four EOSs ranges from 2.10 to $2.74M_\odot$. The radius and tidal deformability for a $1.4M_\odot$ NS are in the range of 12.55 – 13.78 km and 462 – 844 , respectively.

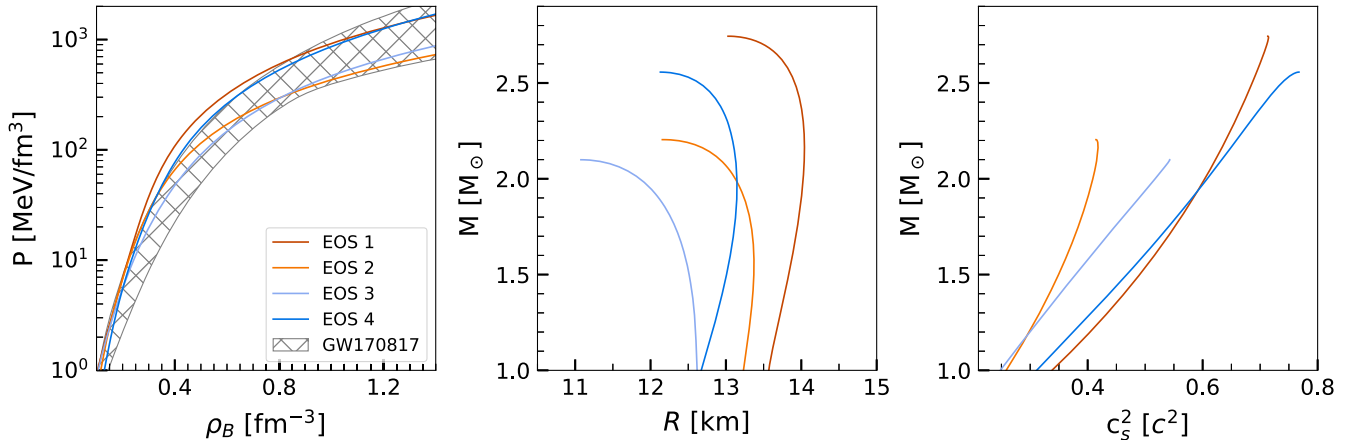


FIG. 1. (left plot) The pressure P as a function of baryon density ρ_B , (middle plot) the NS mass M as a function of radius R , and (right plot) NS mass M as a function of the square of the speed of sound c_s^2 for nuclear matter EOS: EOS1, EOS2, EOS3, and EOS4, respectively.

B. Dark matter EOS

Similar to the Lagrangian of the nuclear model, one can apply the knowledge from the nuclear mean field approach to describe the Lagrangian for the fermionic dark matter sector. We consider the simplest dark matter Lagrangian with a single fermionic component (χ_D) and we assume that a dark vector meson V_D^μ that couples to the conserved DM current through $g_{vd}\bar{\chi}_D\gamma_\mu\chi_D V_D^\mu$. The dark matter model Lagrangian and the corresponding EOS in the mean field approximation is expressed as [48,49]

$$\mathcal{L}_\chi = \bar{\chi}_D [i\partial^\mu - g_{vd}V_D^\mu] \chi_D - \frac{1}{4}V_{\mu\nu,D}V_D^{\mu\nu} + \frac{1}{2}m_{vd}^2V_{\mu,D}V_D^\mu \quad (2)$$

$$\epsilon_\chi = \frac{1}{\pi^2} \int_0^{k_D} dk k^2 \sqrt{k^2 + m_\chi^2} + \frac{1}{2}c_\omega^2\rho_D^2 \quad (3)$$

$$P_\chi = \frac{1}{3\pi^2} \int_0^{k_D} dk \frac{k^4}{\sqrt{k^2 + m_\chi^2}} + \frac{1}{2}c_\omega^2\rho_D^2 \quad (4)$$

Here $c_\omega \equiv \frac{g_{vd}}{m_{vd}}$ and m_χ is the bare mass of fermionic dark matter. These two parameters along with the dark matter Fermi momenta determine the dark matter EOS. The dark matter Fermi momenta determines the accumulated dark

TABLE II. Nuclear saturation properties—(i) For symmetric nuclear matter–energy per nucleon ε_0 , incompressibility coefficient K_0 , and skewness Q_0 ; and (ii) For symmetry energy–symmetry energy at saturation $J_{\text{sym},0}$, its slope $L_{\text{sym},0}$; and (iii) neutron star properties—maximum mass M_{max} , radius R_{max} , radius $R_{1.4}$ for $1.4M_\odot$ and $R_{2.08}$ for $2.08M_\odot$ neutron stars, tidal deformability $\Lambda_{1.4}$ for 1.4 solar mass neutron stars, the square of speed-of-sound c_s^2 at the center of maximum mass neutron stars, the neutron star mass at which the direct Urca process occurs M_{dUrca} , and the direct Urca density $\rho_{B,x}$ for $x \in [1.4, 1.6, 1.8]$ solar mass neutron stars.

EOS	NMP							NS									
	ρ_0 (fm $^{-3}$)	ε_0	K_0	Q_0	$J_{\text{sym},0}$	$L_{\text{sym},0}$	M_{max}	R_{max}	$R_{1.4}$	$R_{2.08}$	$\Lambda_{1.4}$	c_s^2	M_{dUrca}	ρ_{dUrca}	$\rho_{B,1.4}$	$\rho_{B,1.6}$	$\rho_{B,1.8}$
EOS1	0.155	-16.08	177	-74	33	64	2.74	13.03	13.78	14.04	844	0.713	2.06	0.366	0.298	0.316	0.336
EOS2	0.154	-15.72	190	614	32	60	2.20	12.16	13.36	13.00	709	0.414	1.83	0.443	0.344	0.382	0.432
EOS3	0.157	-16.24	260	-400	32	57	2.10	11.08	12.55	11.53	462	0.543	2.07	0.829	0.432	0.491	0.570
EOS4	0.156	-16.12	216	-339	29	42	2.56	12.13	12.95	13.14	638	0.767	2.55	0.747	0.345	0.370	0.399

matter density/mass fraction inside neutron stars. The properties of dark matter admixed neutron stars depend on the dark matter EOS along with dark matter mass fraction. Procedure to determine the dark matter EOS has been discussed in subsequent sections.

C. Two fluid formalism

We have employed a two-fluid Tolman-Oppenheimer-Volkoff (TOV) formalism to analyze the structure of neutron stars with a mixture of dark matter, referred to as dark matter admixed neutron stars (DANSs) [48]. Dark matter and baryonic matter are treated separately within this framework and interact solely through gravitational interaction. Consequently, each fluid follows its conservation of energy-momentum tensor.

To describe the combined effects of the two fluids, we introduce the total pressure $P(r)$ and total energy $\varepsilon(r)$, which can be expressed as the sum of the respective contributions from baryonic matter and dark matter:

$$P(r) = P_B(r) + P_\chi(r) \quad (5)$$

$$\varepsilon(r) = \varepsilon_B(r) + \varepsilon_\chi(r) \quad (6)$$

Here, the subscripts “ B ” and “ χ ” represent the baryonic and dark matter components, respectively. The TOV equations governing the behavior of this two-fluid system are given by [35,48]:

$$\frac{dP_B}{dr} = -(P_B + \varepsilon_B) \frac{4\pi r^3(P_B + P_\chi) + M(r)}{r(r - 2M(r))} \quad (7)$$

$$\frac{dP_\chi}{dr} = -(P_\chi + \varepsilon_\chi) \frac{4\pi r^3(P_B + P_\chi) + M(r)}{r(r - 2M(r))} \quad (8)$$

$$\frac{dM(r)}{dr} = 4\pi(\varepsilon_B + \varepsilon_\chi)r^2 \quad (9)$$

When investigating the influence of admixed dark matter, it proves useful to define a dark matter mass fraction F_χ [35]:

$$F_\chi = \frac{M_\chi(R_\chi)}{M(R)} \quad (10)$$

Here, $M_\chi(R_\chi) = 4\pi \int_0^{R_\chi} r^2 \varepsilon_\chi(r) dr$ represents the total accumulated dark matter gravitational mass within R_χ , where the dark matter pressure reaches zero. Based on this DM mass fraction, it is possible to determine how much gravitational mass the DANS contributes to the star’s total mass.

Besides mass and radius, neutron stars’ tidal deformability plays a crucial role in their structural characteristics. The tidal gravitational field generated by their companion causes the two neutron stars in a binary neutron star system to undergo quadrupole deformations during the final stages of inspiration. As a result of the tidal forces exerted by the partner star of a neutron star, the magnitude of the deformation that occurs is described as tidal deformability, which quantifies the extent to which it distorts under those forces.

The dimensionless tidal deformability is defined as

$$\Lambda = 2/3 k_2 C^{-5} \quad (11)$$

where C ($\equiv M/R$) and k_2 are known as the compactness and Love number of the deformed star. k_2 for the two-fluid system can be obtained by solving the differential equation for radial perturbation,

$$r \frac{dy(r)}{dr} + y(r)^2 + y(r)F(r) + r^2 Q(r) = 0, \quad (12)$$

$$\begin{aligned}
F(r) &= \frac{r - 4\pi r^3((\varepsilon_B(r) + \varepsilon_\chi(r)) - (P_B(r) + P_\chi(r)))}{r - 2M(r)} \\
Q(r) &= \frac{4\pi r(5(\varepsilon_B(r) + \varepsilon_\chi(r)) + 9(P_B(r) + P_\chi(r)) + \frac{\varepsilon_B(r) + P_B(r)}{\partial P_B(r)/\partial \varepsilon_B(r)} + \frac{\varepsilon_\chi(r) + P_\chi(r)}{\partial P_\chi(r)/\partial \varepsilon_\chi(r)} - \frac{6}{4\pi r^2})}{r - 2M(r)} \\
&\quad - 4 \left[\frac{M(r) + 4\pi r^3(P_B(r) + P_\chi(r))}{r^2(1 - 2M(r)/r)} \right]^2,
\end{aligned} \tag{13}$$

together with the two-fluid TOV equation with proper boundary conditions [48,54].

D. Sampling

To compute the structure of neutron stars (NS), we have utilized four distinct nucleonic equation-of-states (EOSs) and a diverse range of dark matter EOSs constructed through the relativistic mean field (RMF) formalism, as detailed in Secs. II A and II B respectively. We have sampled a total of 50,000 dark matter parameter combinations, namely c_ω , m_χ , and F_χ from uniform distributions within the ranges specified in Table III. In Fig. 2 we represent EOS for normal matter and dark matter components. There were 50K dark matter EOSs solved individually for each nucleonic EOS, resulting in a total of 200,000 mass-radius (M-R) calculations. To determine the dark matter EOS here we consider the dark matter with a mass range $0.5 \text{ GeV} \leq m_\chi \leq 4.5 \text{ GeV}$ [24], dark matter self-interaction measure in the range, $0.1 \text{ fm} \leq c_\omega \leq 5 \text{ fm}$ [49], and dark matter mass fraction in the range $0 \leq F_\chi \leq 25\%$ [55]. Note that the dark matter mass fraction crucially depends on the dark matter capture rate inside neutron stars. Depending upon the generic modeling of the nucleon-dark matter interaction inside the high-density region of neutron stars, the dark matter capture rate can be of the order of 10^{25} GeV/sec for dark matter mass near 1 GeV [56]. Such an estimate of the capture of dark matter particles in the interior of neutron stars over its lifetime ($\sim 10^{17}$ seconds) indicates that it may be difficult for a neutron star to accumulate a significant fraction of dark matter. Instead, some other mechanism, such as the production of dark matter in the star during supernovae (SN) [57], may be necessary for a neutron star to have a large dark matter fraction. Conversion of the neutrons into dark matter particles might also allow a significant fraction of the

nuclear matter to be converted into dark matter particles inside neutron stars. Non-standard conversion of neutrons into scalar dark matter particles has been explored in the context of dark matter admixed neutron stars in Ref. [17] and references therein. The dark matter capture rate can crucially depend on the Pauli blocking factor in the degenerate nuclear matter, multiple scattering among dark matter particles and nucleons, neutron star internal structure, momentum dependent form factors of hadrons, etc [58–60]. Note that apart from the degenerate neutrons, protons, electrons, and muons are also present in the beta-equilibrated nuclear matter. The interaction between the leptonic sector and the dark matter sector can also account for the dark matter capture within neutron stars [58]. Furthermore, the capture of dark matter particles by neutron stars can be enhanced in a close binary system. This amplification stems from the energy loss of dark matter particles resulting from their gravitational interaction with moving companions (gravitational slingshot) [61]. This effect is maximum when the velocities of the companions are comparable to the asymptotic velocity of dark matter particles [61].

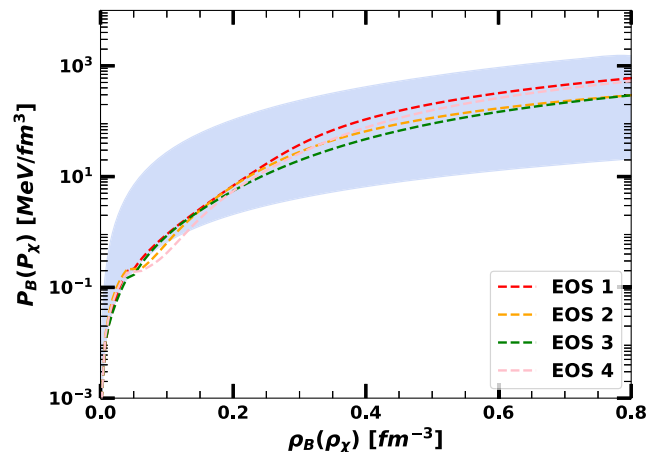


FIG. 2. The shaded blue domain represents the sampled dark matter EOS, i.e., the pressure (P_χ) as a function of density (ρ_χ). The colored dashed lines depict the nuclear matter EOS, i.e., the variation of baryonic matter pressure (P_B) with baryon number density (ρ_B).

TABLE III. The prior set for dark matter model parameters.

m_χ GeV		c_ω fm		F_χ %	
Min	Max	Min	Max	Min	Max
0.5	4.5	0.1	5	0	25

TABLE IV. Summary of neutron star properties and their corresponding values obtained from filtered two-fluid solutions with EOS1, EOS2, EOS3, and EOS4. The table presents the median values, along with the lower and upper bounds of the 90% confidence intervals (CI), for various neutron star properties. These properties include the maximum mass of neutron stars (M_{\max}), the total radius ($R_{t,x}$) for values of x in the range of [1.2, 1.4, 1.6, 1.8, 2.0], the dimensionless tidal deformability (Λ_x) for x in the range of [1.4, 1.6, 1.8], the fraction of dark matter energy density over nuclear matter ($f_{d,x}$), and the nuclear matter baryon density ($\rho_{B,x}$) for x in the range of [1.4, 1.6, 2.0]. The values are based on comprehensive analyses using EOS1, EOS2, EOS3, and EOS4 as the equation-of-state models for neutron stars.

NS	Units	EOS1			EOS 2			EOS 3			EOS 4				
		90% CI		Median	90% CI										
		Min	Max		Min	Max		Min	Max		Min	Max		Min	Max
M_{\max}	M_{\odot}	2.454	2.067	2.710	2.107	2.067	2.710	2.051	2.067	2.710	2.351	2.067	2.710	2.067	2.710
$R_{t,2.0}$		13.16	11.77	13.87	12.68	11.77	13.87	11.50	11.77	13.87	12.50	11.77	13.87		
$R_{t,1.8}$		13.16	12.00	13.81	13.00	12.00	13.81	12.04	12.00	13.81	12.56	12.00	13.81		
$R_{t,1.6}$	km	13.11	12.04	13.73	13.13	12.04	13.73	12.27	12.04	13.73	12.54	12.04	13.73		
$R_{t,1.4}$		13.02	12.01	13.63	13.17	12.01	13.63	12.40	12.01	13.63	12.48	12.01	13.63		
$R_{t,1.2}$		12.92	11.94	13.53	13.18	11.94	13.53	12.48	11.94	13.53	12.40	11.94	13.53		
$\Lambda_{1.8}$...	18	7	29	16	7	29	9	7	29	13	7	29		
$\Lambda_{1.6}$		36	17	57	36	17	57	23	17	57	28	17	57		
$\Lambda_{1.4}$		76	39	114	82	39	114	58	39	114	62	39	114		
$f_{d,2.0}$		0.47	0.14	0.68	0.27	0.14	0.68	0.20	0.14	0.68	0.40	0.14	0.68		
$f_{d,1.6}$		0.43	0.12	0.65	0.26	0.12	0.65	0.19	0.12	0.65	0.37	0.12	0.65		
$f_{d,1.4}$		0.41	0.11	0.63	0.24	0.11	0.63	0.18	0.11	0.63	0.34	0.11	0.63		
$\rho_{B,2.0}$	fm^{-3}	0.408	0.350	0.576	0.589	0.350	0.576	0.788	0.350	0.576	0.489	0.350	0.576		
$\rho_{B,1.6}$		0.339	0.303	0.394	0.399	0.303	0.394	0.500	0.303	0.394	0.395	0.303	0.394		
$\rho_{B,1.4}$		0.314	0.283	0.354	0.352	0.283	0.354	0.435	0.283	0.354	0.361	0.283	0.354		

III. RESULTS AND DISCUSSION

We aim to investigate whether NS observational properties such as mass, radius, and tidal deformability, can uniquely constrain the dark matter model parameters. To explore this, we have employed a two-fluid scenario to calculate neutron star properties Sec. II C. For the nuclear matter, we utilize four realistic EOS, namely EOS1, EOS2, EOS3, and EOS4 (see Sec. II A for details). In the dark matter sector, a total of 50K dark matter EOSs were sampled within the reasonable prior range (see Table III, Sec. II B and Sec. II D for details). These large combinations of nuclear matter and dark matter EOS give rise to 200K mass-radius curves by solving the two-fluid TOV equations. All of these mass-radius relations are not practically relevant as we use the filter that NS must have a mass greater than $1.9M_{\odot}$, set by the pulsars PSR J0348 + 0432 and PSR J0740 + 6620 within $\sim 3\sigma$. We also consider that the dark matter admixed neutron stars only produce non-halo configurations, which means the dark matter admixed radius is smaller than the luminous radius. Following the application of this filter, the remaining values of samples for EOS1, EOS2, EOS3, and EOS4 are 25K, 14K, 10K, and 20K, respectively. The median values, along with the lower and upper bounds of the 90% confidence intervals (CI), for various neutron star properties for these sets are listed in Table IV. These properties include the maximum mass of neutron stars (M_{\max}), the total radius ($R_{t,x}$) for values of x in

the range of [1.2, 1.4, 1.6, 1.8, 2.0], the dimensionless tidal deformability (Λ_x) for x in the range of [1.4, 1.6, 1.8], the fraction of dark matter energy density over nuclear matter ($f_{d,x}$), and the nuclear matter baryon density ($\rho_{B,x}$) for x in the range of [1.4, 1.6, 2.0].

To study the relation between dark matter parameters and various neutron star properties, we employ the Kendall rank correlation coefficient analysis. The Kendall rank correlation can be considered a nonparametric test that allows us to quantify the strength of dependence between two variables. Unlike Pearson correlation, it accounts for nonlinearity in the correlation, making it suitable for analyzing relationships that may not follow a linear pattern [62]. Our strategy involves first selecting a fixed nuclear EOS and then assessing the correlation coefficients using the chosen set of dark matter EOS. In this way, we can explore the uncertainty only in the dark matter sector. Lastly, we explore the combined effects of all four combinations of nuclear equations and the entire set of dark matter equation-of-states. This approach helps us to comprehend the impact of uncertainty in the nuclear EOS on these correlations. In Fig. 3 we plot the Kendall rank correlation coefficients, where we consider the nuclear EOS1 and the entire set of filtered dark matter equation-of-state sets, i.e., with NS having a maximum mass above $1.9M_{\odot}$ and NS having to be nonhalo (as mentioned earlier). As portrayed in Figs. 3, and 4 includes the complete dataset with all four nuclear EOSs employed. Please note that in this context, the

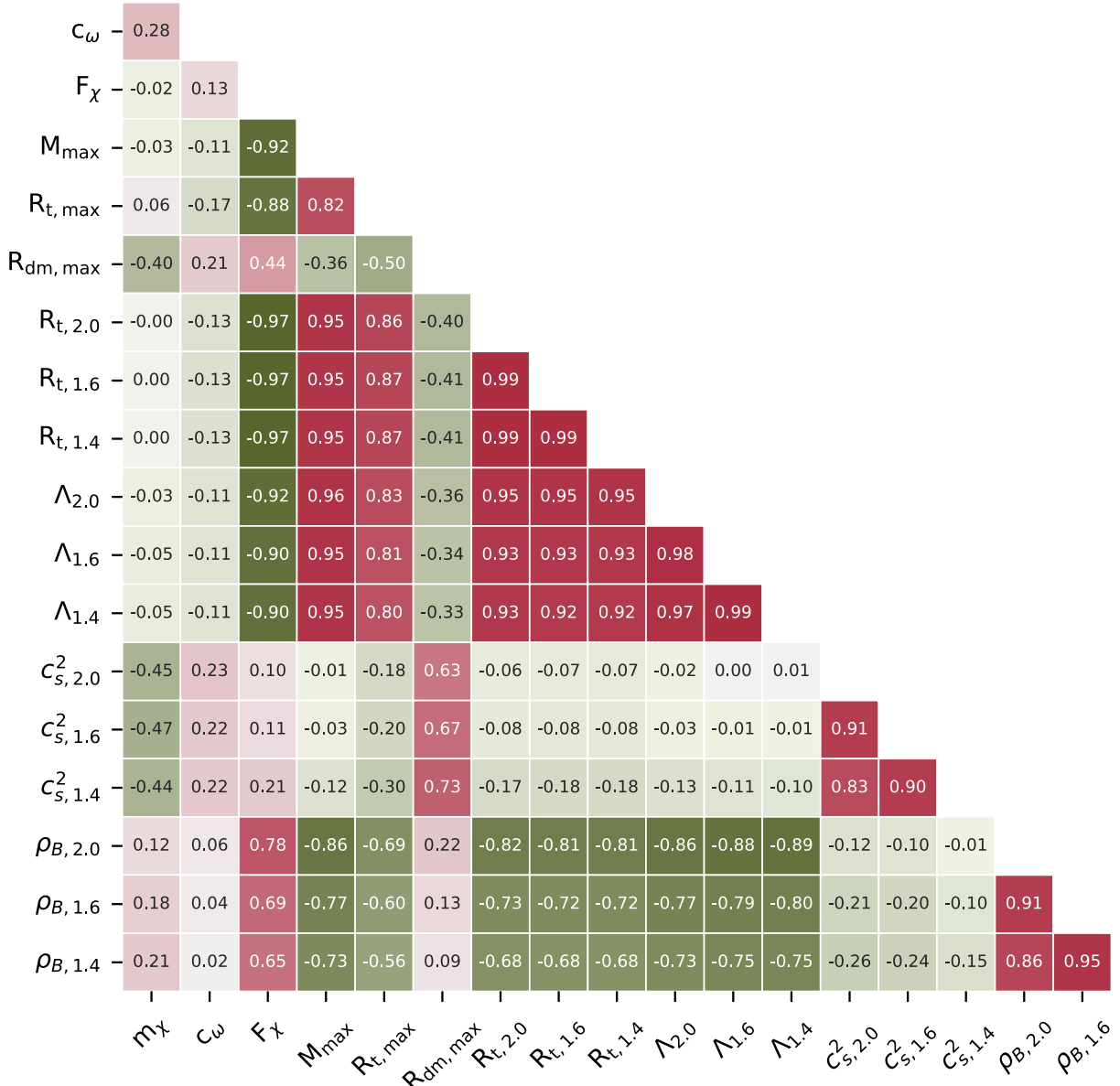


FIG. 3. With only one nuclear EOS, namely EOS1, we compute the Kendall rank correlation coefficients linking various dark matter parameters to neutron star properties, and with the entire set of dark matter EOS sets after applying the filter (see text).

subscript “ t ” denotes the total radius of the neutron star, while the subscript dm represents the radius specifically associated with the admixed dark matter.

The following comments are in order:

- (i) We have observed in Fig. 3 a strong negative correlation ~ 0.9 between the dark matter mass fraction, F_χ , and the maximum gravitational mass of a neutron star (NS). Additionally, there is a notable correlation ~ 0.9 between F_χ and the radius as well as the tidal deformability of NS at masses of 1.4, 1.6, and $2.0M_\odot$ respectively. However in Fig. 4, when incorporating uncertainty in the nuclear sector and considering all four nuclear matter equation-of-states (EOSs) alongside the sampled dark matter

EOSs, the previously mentioned correlation disappears.

- (ii) Furthermore, our findings have revealed a notable positive correlation between F_χ and the central baryonic density ρ_B (at different NS masses 1.4, 1.6, and $2.0M_\odot$) for EOS1. However, once again when we account for the uncertainties associated with nuclear matter, as can be seen in Fig. 4, those correlations disappear.
- (iii) Nonetheless, the correlations between radii, tidal deformability, mass, and central baryon density persist even when considering uncertainties in the nuclear sector, i.e., including the entire dark matter admixed set for all nuclear EOS. It is worth noting

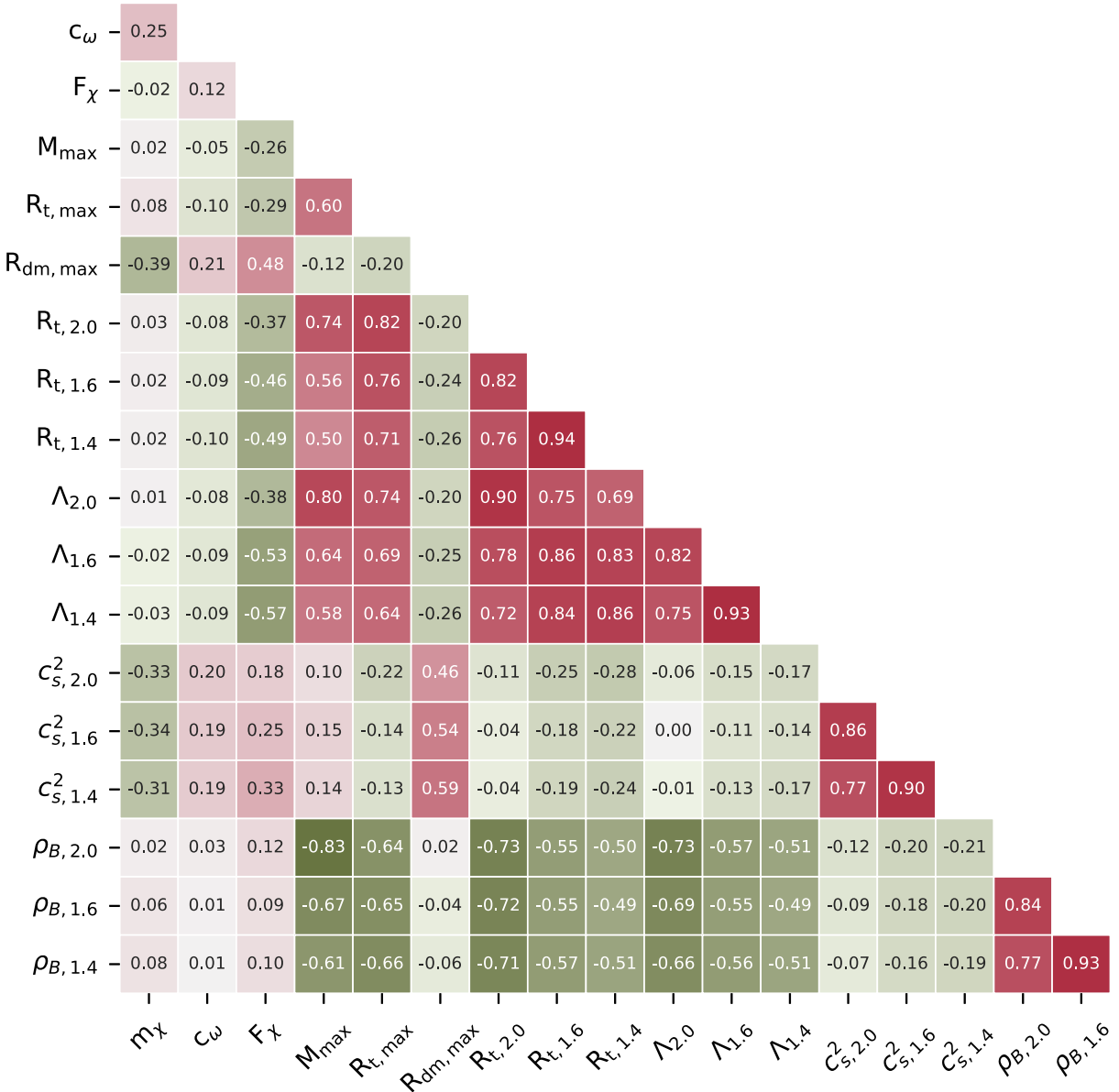


FIG. 4. Same as Fig. 3 but with the data where all four nuclear EOS are employed.

that there is a robust and strong correlation between the central baryon density and the star radius even when dark matter is not considered [53,63]. However, this correlation is found to break in the case of modified gravity [64]. This interestingly allows us to distinguish between the effects of modified gravity and dark matter in neutron stars (NS).

Figure 5 displays the corner plot featuring the dark matter parameters c_ω , m_χ , and F_χ corresponding to EOS1, EOS2, EOS3, and EOS4 after applying the filtration process. A corner plot is a visualization used to explore the multivariate distribution of parameters in a dataset. It allows us to observe the relationships and correlations between different variables simultaneously, providing valuable insights into the underlying data structure. When considering a fixed nuclear EOS

and only varying the dark matter EOS within the two-fluid formalism, there exists a direct correlation between the fraction of dark matter F_χ and M_{\max} , as depicted in Fig. 3. Consequently, the maximum mass constraints of $1.9M_\odot$ depend on the softness or stiffness of the EOS for each individual nuclear matter EOS. Each nuclear matter EOS is capable of sustaining a different percentage of dark matter F_χ . For example, the softest EOS3 can sustain only up to $\approx 10\%$ of dark matter, whereas EOS1, EOS2 and EOS4 can sustain $\approx 24\%$, 14% and 22% of dark matter respectively. Therefore, depending on the stiffness of the employed EOS, we can observe variations in the percentage of dark matter fraction F_χ ranging from 0% to 25%.

In Fig. 6, we demonstrate the outcomes of mass-radius calculations obtained through a collection of EOSs

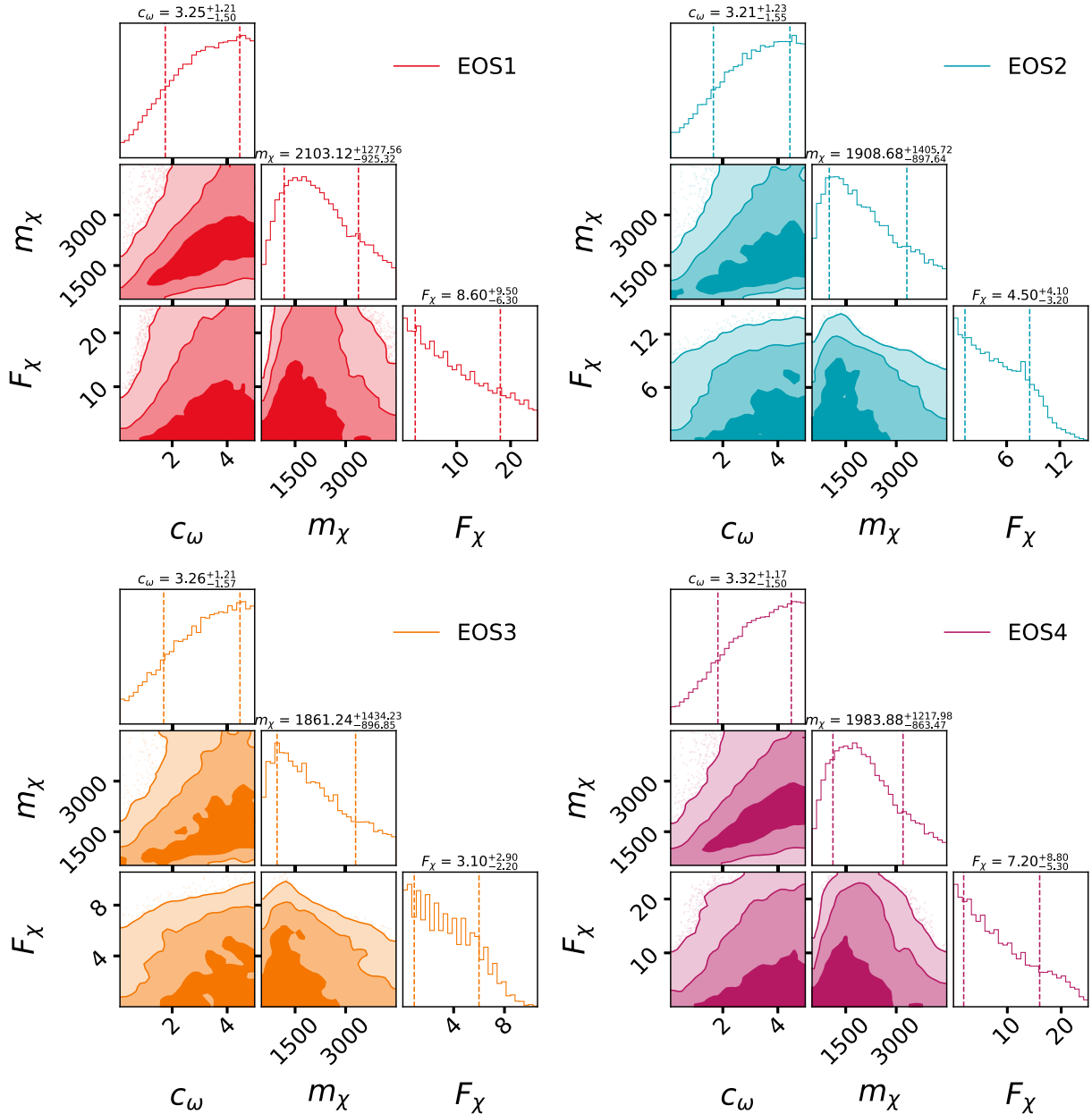


FIG. 5. The distribution of dark matter parameters, i.e., c_ω , m_χ (in MeV units), and F_χ for the prior set mentioned in Table III after applying the filter that NS must have a mass greater than $1.9M_\odot$.

ensemble. The upper panels illustrate the results for EOS1 and EOS2, whereas the lower panels correspond to EOS3 and EOS4, respectively. The vertical color bar, which ranges from 0% to 25%, visually illustrates the spread of dark matter mass fractions. It provides insight into the resulting variations in the mass-radius curve influenced by the parameter F_χ . Interestingly, when the percentage of F_χ increases, it noticeably leads to a decrease in the maximum mass of neutron stars. The dashed lines present in each plot correspond to the properties of neutron stars computed exclusively based on the nuclear EOS, without taking into account the influence of dark matter. To assess the validity

of our findings, we compare them with recent observational constraints, represented by skin lines. These constraints encompass the binary components of GW170817 [65], along with their corresponding 90% and 50% credible intervals (CI). Furthermore, we illustrate the 1σ (68%) CI for the two-dimensional posterior distribution in the mass radii domain obtained from NICER x-ray data for the millisecond pulsars PSRJ0030 + 0451 (cyan and yellow) and PSRJ0740 + 6620 (violet). The horizontal (radius) and vertical (mass) error bars reflect the 1σ credible interval derived from the 1-dimensional marginalized posterior distribution of the same NICER data. From this figure,

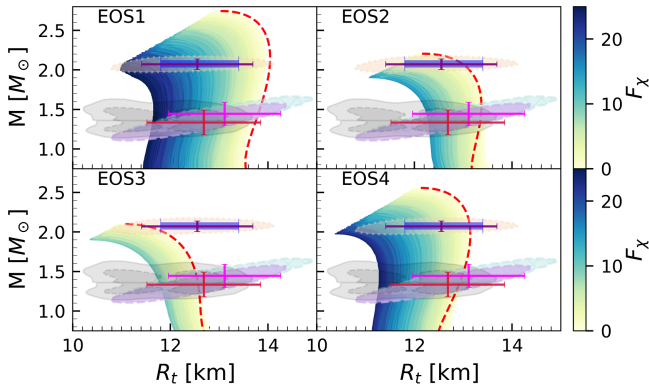


FIG. 6. The domain of neutron star (NS) mass-radius using a two-fluid scenario, considering our entire set of dark matter EOSs in conjunction with different nuclear EOSs. The vertical color bar with the panel depicts the dark matter mass fraction F_χ from 0 to 25%. The dashed lines on each plot correspond to NS properties computed using only nuclear EOS in single fluid TOV, without dark matter. We compare the M-R domains with current observational constraints. The gray region depicts the constraints from the binary components of GW170817 [65], along with their 90% and 50% credible intervals(CI). The $1\sigma(68\%)$ CI for the 2D posterior distribution in the mass-radii domain for millisecond pulsar PSRJ0030 + 0451 (cyan and yellow) [66,67] as well as PSRJ0740 + 6620 (violet) [68,69] from the NICER x-ray data are also shown.

one may observe that as the percentage of the dark matter component increases, both the mass and radius decrease for different neutron star mass sequences. It is worth noting that the current observational constraints on mass and radius, whether from NICER or GW observations, are not able to precisely determine the dark matter fraction F_χ . Therefore, using the robust investigation presented in this Fig. 6, we suggest that the dark matter fraction can be as high as 25% when $1.9M_\odot$ NS maximum mass constraint is imposed.

Figure 7 illustrates the relation between the dimensionless tidal deformability (Λ) and the mass of neutron stars (NS) for different nuclear equation-of-states (EOSs) in separate panels. The dashed lines represent the properties of NS computed solely using the nuclear EOS in a single fluid TOV calculation, excluding the presence of dark matter. The color bar on the side indicates the dark matter mass fraction (F_χ), with the color tone varying from yellow to blue, representing DM mass fractions ranging from 0% to 25%. From the figure, it is clear that the inclusion of dark matter leads to a decrease in tidal deformability for all masses, the same as obtained in the previous figure for the radius. As can be seen from the figure, dimensionless tidal deformability of different NS masses was negatively correlated with dark matter mass fraction F_χ . The inclusion of observational constraints from GW170817 is represented by the blue bars, depicting the tidal deformability at $1.36M_\odot$, $\Lambda_{1.36} < 720$, [65]. The inclusion of dark matter could potentially lead to a reduction in the higher tidal

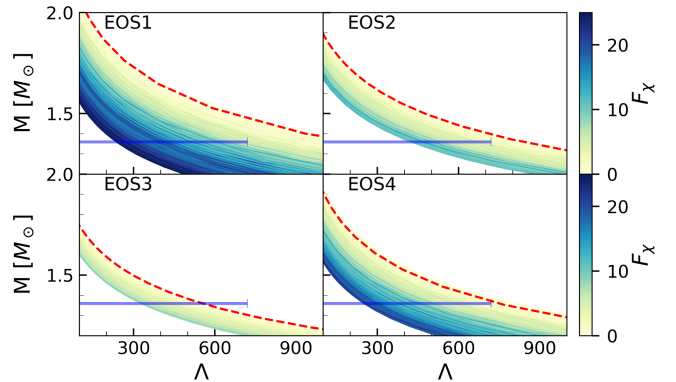


FIG. 7. The graphical representation illustrates the relationship between tidal deformability (Λ) and the mass (M_\odot) of neutron stars (NS). Meanwhile, the dashed lines depicted in each plot correspond to the computed properties of neutron stars solely based on the nuclear EOS in single fluid TOV, incorporating the observational constraint (blue bars) depict the tidal deformability at $1.36M_\odot$ [65]. Additionally, the color gradient on the side denotes the proportional dark matter mass fraction F_χ , encompassing values from 0% to 25%.

deformability attributed to the stiff nuclear EOS. This similarity holds even for bosonic dark matter when employing a two-fluid approach, as demonstrated in previous studies Refs. [17,35,54,70]. The same behavior was obtained with a fermionic dark matter model based on RMF description incorporating short-range correlations within a single fluid approach [71], and with the linear sigma-omega fermionic dark matter model together with a two-fluid approach [48].

Figure 8 illustrates the representation of Λ_1 and Λ_2 , the dimensionless tidal deformability parameters obtained with

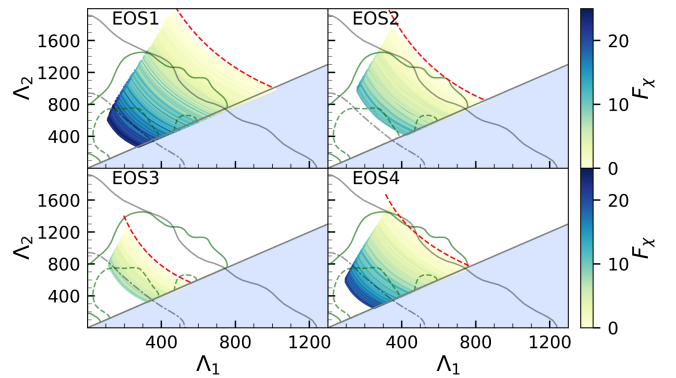


FIG. 8. The graphical representation of Λ_1 , and Λ_2 with a fraction of dark matter F_χ from 0 to 25%, where Λ_1 , and Λ_2 are the dimensionless tidal deformability parameters of the binary neutron star merger from the GW170817 event, using the observed chirp mass of $M_{\text{chirp}} = 1.186M_\odot$. The green and gray solid (dashed) lines represent the 90% (50%) CI from the marginalized posterior for the tidal deformabilities of the two binary components of GW170817 using a parametrized EOS, with (green) and without (gray) a maximum mass of $1.97M_\odot$ requirement.

nuclear matter EOS: EOS1, EOS2, EOS3, and EOS4 for the binary neutron star merger event GW170817. For this calculation, we have fixed the chirp mass (M_{chirp}) $1.186M_{\odot}$ which is observed in the GW170817 event. In the plot, for the comparison we have included the constraints in the gray solid (dashed) line corresponding to the 90% (50%) confidence interval (CI) obtained from the marginalized posterior, which represents the tidal deformability of the two binary components of neutron star merger event GW170817. Furthermore, the green solid (dashed) lines depict the 90% (50%) CI derived from the marginalized posterior, indicating the tidal deformability of the two binary components of GW170817 based on an equation-of-state which is parametrized with a requirement that the maximum mass of at least $1.97M_{\odot}$. Here it can be seen that, for EOS1 in the absence of any dark matter component lies outside the boundary of observational constraints, but in the presence of dark matter as F_{χ} increases this comes inside the boundaries which results that the stiff nuclear EOS with admixed dark matter, comes inside the boundaries defined by the constraints on tidal deformability. As it is discussed in Fig. 5 EOS2 and EOS3 can only sustain up to $\approx 14\%$ and 10% of dark matter respectively, if the $1.9M_{\odot}$ constraint is imposed. As a consequence, the acceptable $\Lambda_1 - \Lambda_2$ domain is quite small, whereas for EOS1 and EOS4 the domain is wider because these EOS can sustain, respectively, 24% and 22% of dark matter.

In Fig. 9, we investigate the effect of DM on the NS central density. The main effect is the compression of matter inside a star which results in a decrease of the NS radius as the fraction of DM increases and the

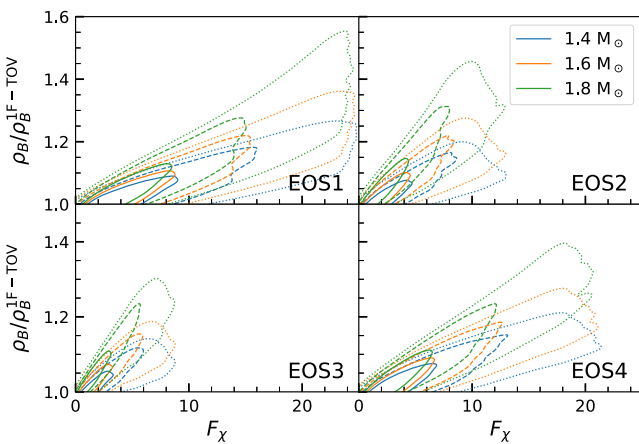


FIG. 9. The central baryonic density $\rho_B/\rho_B^{1F-\text{TOV}}$ where $\rho_B^{1F-\text{TOV}}$ represents the central baryon density in the absence of dark matter (single fluid TOV) as a function of dark matter mass fraction F_{χ} for NS masses equal to $1.4M_{\odot}$ (blue), $1.6M_{\odot}$ (orange), $1.8M_{\odot}$ (green). The top panels are for EOS1 and EOS2, whereas the bottom panels are for EOS3 and EOS4. The solid line in each panel represents 68% confidence interval whereas dashed and dotted lines represent 95% and 99%, respectively.

gravitational mass is kept constant. We consider all four equation-of-states (EOSs) to examine how dark matter affects this compression. The plot shows the scaled central density $\rho_B/\rho_B^{1F-\text{TOV}}$ of stars where $\rho_B^{1F-\text{TOV}}$ represents the central baryon density in the absence of dark matter (single fluid TOV) for masses 1.4 , 1.6 , and $1.8M_{\odot}$ as a function of the percentage of dark matter F_{χ} . The solid line in each panel represents 68% confidence interval whereas dashed and dotted lines represent 95% and 99% CI, respectively. From the figure, it is evident that, for each EOS, as the percentage of dark matter (F_{χ}) increases, the central density for masses ranging from 1.4 to $1.8M_{\odot}$ increases in all cases. In Fig. 10, we plot the density profile of $1.4M_{\odot}$ NS with different fractions of DM. The presence of DM increases the gravitational interaction at the star center. As a consequence, mass is pushed to the center, the central baryonic density increases, and the radius of the star decreases. This is an interesting result because it indicates that due to the presence of DM, processes that are otherwise not favorable are now allowed, e.g., the onset of hyperons or of the nucleonic direct Urca, etc. may open in smaller mass stars with the DM presence. The increase in central baryon density due to the compression of matter may also give rise to quark hadron phase transition inside the core of dark matter admixed neutron stars. Model calculations indicate that onset densities for hadron-quark pasta phases and pure quark matter phase can be of the order of 0.4 – 0.7 fm $^{-3}$ [72]. These results also imply that the accumulation of dark matter inside neutron stars can trigger the QCD phase transition. This is a novel but model-dependent result and it needs further detailed studies.

In the following, we discuss how the presence of dark matter leads to a decrease in the mass of the star where nucleonic direct Urca processes start to occur, which we designate as M_{dUrca} . In Fig. 11, the scaled Urca mass $M_{\text{dUrca}}/M_{\text{dUrca}}^{1F-\text{TOV}}$ is plotted as a function of the fraction of

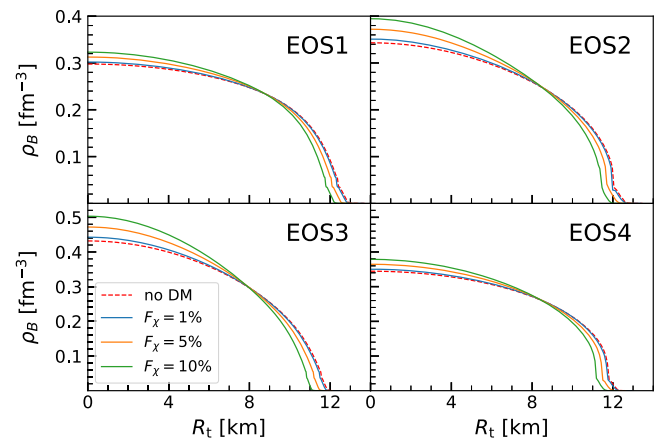


FIG. 10. The baryon density ρ_B plotted against the NS radius R_t for a $1.4M_{\odot}$ NS. The plot includes four panels, each representing a different nuclear EOS, along with a generic dark matter EOS.

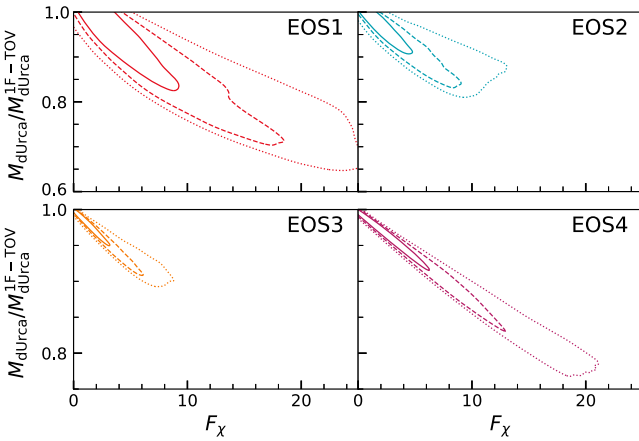


FIG. 11. The ratio $M_{d\text{Urca}}/M_{d\text{Urca}}^{1F-\text{TOV}}$ where where $M_{d\text{Urca}}^{1F-\text{TOV}}$ represents the Urca mass in the absence of dark matter (single fluid TOV) as a function of dark matter mass fraction F_χ . The top panels are for EOS1 and EOS2, whereas the bottom panel represents results for EOS3 and EOS4. The solid line in each panel represents 68% confidence interval whereas dashed and dotted lines represent 95% and 99% CI, respectively.

dark matter, where $M_{d\text{Urca}}^{1F-\text{TOV}}$ represents the Urca mass with single fluid TOV, obtained for the four nuclear matter EOSs. A strong correlation between the dark matter fraction and the Urca mass for each individual case is observed. Notice that the decrease in the $M_{d\text{Urca}}$ can be large for stiff EOSs. This is because stiff EOSs can allow a large dark matter fraction inside the neutron stars.

In a previous study conducted by Malik *et al.*, [73], it was argued that the Urca mass exhibits a robust correlation with nuclear symmetry energy. The presence of dark matter may, however, affect our perception of the central baryonic density, resulting in a wrong estimation of the proton density, in particular, a larger proton fraction, and, therefore larger nuclear symmetry energy. To gain a comprehensive understanding of these phenomena, further investigations are required in the future.

There has been a large interest in the finding of universal relations that involve several NS properties and are independent of the NS mass, see for instance [74–77]. Although universal relations for neutron stars are inherently insensitive to the EOS and, therefore, cannot be utilized to differentiate between different EOS models, they hold the potential to serve as powerful tools for inferring the properties of neutron stars in connection with other measurements. Besides, if a particular NS composition breaks the universal relation, this feature may be considered a smoking gun to identify that special composition. We may, therefore, question whether DM will break some of the known universal relations. In the following, we will analyze the universal relation $C - \Lambda$ proposed in [77], and discussed in [74]. The C-Love relationships are depicted in Fig. 12. We begin by fitting the data related to EOS to a simple curve represented by the equation:

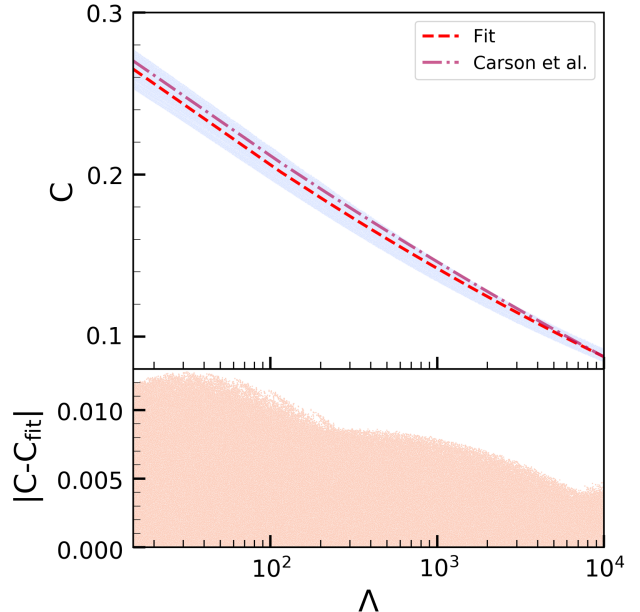


FIG. 12. C-Love universal relation for all EOS. The red line is fitted with Eq. (14) In the lower panel the residuals for the fitting are calculated. Furthermore, we conduct a comparison with the findings presented in Ref. [74] for the scenario of single fluid TOV without dark matter (highlighted in pink-red).

$$C = \sum_{k=0}^2 a_k (\ln \Lambda)^k. \quad (14)$$

By performing this fitting process, we obtain the following values for the coefficients: $a_0 = 0.36054566$, $a_1 = -0.0375908$, and $a_2 = 0.00086283$. In the lower panel of Fig. 12, the absolute difference from the fits is displayed. The absolute difference is approximately equal to 1%, and furthermore, it decreases to about 0.5% for higher values of Λ . We have also compared our results with Figure 4 in Ref. [74], where they used $a_0 = 0.3617$, $a_1 = -0.03548$, and $a_2 = 0.0006194$ for the constrained EOS. This constrained EOS shows an absolute difference of less than 1%, while the unconstrained EOS is around 1%. We conclude that DM does not break the universal relation $C - \Lambda$.

IV. CONCLUSIONS

In conclusion, this study has shed light on the connection between dark matter and neutron star properties, while considering the uncertainties in the equation-of-state within the baryonic sector. Dark matter was considered to be formed by fermionic particles with a mass of the order of a few GeVs that interact with a dark vector meson. By employing a two-fluid scenario and sampling 50,000 dark matter EOSs, we analyzed the structure of dark matter admixed neutron stars. It was considered that dark matter is confined within the visible radius of neutron stars, i.e., only no-halo configurations were studied. We have imposed the

dark-matter admixed star should have a maximum mass above $1.9M_{\odot}$, a value within 3σ the PSR J0348 + 0432 mass, $2.01 \pm 0.04M_{\odot}$. The results revealed interesting correlations between dark matter parameters and various neutron star properties, consistent with results discussed in the literature: the larger the fraction of dark matter the smaller the maximum mass and the smaller the NS radius and tidal deformability [17]. In fact, the dark matter mass fraction within a neutron star was found to have a strong negative correlation with its maximum gravitational mass if a single nuclear model was considered. However, it was shown that this correlation disappears when accounting for the uncertainties associated with nuclear matter EOS. The maximum mass constraints of dark-matter admixed neutron stars depend on the softness or stiffness of the nuclear matter EOS employed, with some equation-of-states being able to sustain a significant fraction of dark matter, and still describing approximately two solar mass stars.

The inclusion of dark matter led to a decrease in the radius and the tidal deformability for all masses, indicating the influence of dark matter on the structural characteristics of neutron stars. Through the analysis of various observational constraints and data, it was demonstrated the potential of dark matter to affect the compression and central energy density of baryonic matter inside neutron stars. The presence of dark matter originates a nuclear matter compression that translates itself into a larger central baryonic density, a smaller radius, and a smaller crust thickness. The increase of the central baryonic density has important consequences on the neutron star properties: it favors the onset of non-nucleonic degrees of freedom inside less massive stars and may affect the onset of direct Urca processes, affecting the neutron star cooling. In particular, our study has highlighted the impact of dark matter on the cooling process and nuclear symmetry energy of baryonic matter. The detection of stars with similar masses but different surface temperatures could indicate that the cooler ones can be dark-matter admixed stars. Additionally, the

study explored universal relations, known as the C-Love relationships [74,77], which provide insights into neutron star properties that are not easily measurable. We have verified that within 1% the C-Love universal relation was not broken by the presence of dark matter, confirming the results of [55].

Overall, this research contributes to our understanding of the complex interplay between dark matter and neutron star properties. By uncovering these connections, we are moving closer to unraveling the mysteries concealed within neutron stars.

ACKNOWLEDGMENTS

The author, P. T., would like to acknowledge CFisUC, University of Coimbra, for their hospitality and local support during his visit in May–June 2023 for the purpose of conducting part of this research. This work was partially supported by national funds from FCT (Fundação para a Ciência e a Tecnologia, I.P, Portugal) under projects UIDB/04564/2020 and UIDP/04564/2020, with DOI identifiers 10.54499/UIDB/04564/2020 and 10.54499/UIDP/04564/2020, respectively, and the project 2022.06460.PTDC with the associated DOI identifier 10.54499/2022.06460.PTDC. T. M. would like to acknowledge the support of FCT—Fundação para a Ciência e a Tecnologia, within Project No. EXPL/FIS-AST/0735/2021. The authors acknowledge the Laboratory for Advanced Computing at the University of Coimbra for providing HPC resources that have contributed to the research results reported within this paper, [78]. A. D. would like to acknowledge Polish National Science Centre Grant No. 2018/30/E/ST2/00432. A. D. also acknowledges the New Faculty Seed Grant (NFSG), NFSG/PIL/2024/P3825, provided by the Birla Institute of Technology and Science, Pilani, India. We thank the anonymous referee for pointing out the dark matter capture rate inside the neutron star available in the literature. The insightful constructive criticism has prompted us to seek a more cautious assessment of the dark matter fraction in neutron stars.

-
- [1] N. K. Glendenning, *Compact Stars* (Springer New York, New York, 1996).
 - [2] P. Haensel, A. Y. Potekhin, and D. G. Yakovlev, *Neutron Stars 1: Equation of State and Structure* (Springer, 2007), Vol. 326.
 - [3] *The Physics and Astrophysics of Neutron Stars*, edited by L. Rezzolla, P. Pizzochero, D. I. Jones, N. Rea, and I. Vidaña (Springer, New York, 2018), Vol. 457.
 - [4] J. M. Lattimer and M. Prakash, *Astrophys. J.* **550**, 426 (2001).
 - [5] S. Ghosh, D. Chatterjee, and J. Schaffner-Bielich, *Eur. Phys. J. A* **58**, 37 (2022).
 - [6] V. C. Rubin, W. K. Ford, Jr., and N. Thonnard, *Astrophys. J. Lett.* **225**, L107 (1978).
 - [7] M. Bauer and T. Plehn, *Yet Another Introduction to Dark Matter: The Particle Physics Approach*, Lecture Notes in Physics Vol. 959 (Springer, New York, 2019).
 - [8] P. Salucci, *Astron. Astrophys. Rev.* **27**, 2 (2019).
 - [9] G. Bertone and M. Fairbairn, *Phys. Rev. D* **77**, 043515 (2008).
 - [10] A. de Lavallaz and M. Fairbairn, *Phys. Rev. D* **81**, 123521 (2010).
 - [11] T. Güver, A. E. Erkoca, M. Hall Reno, and I. Sarcevic, *J. Cosmol. Astropart. Phys.* **05** (2014) 013.

- [12] I. Goldman and S. Nussinov, *Phys. Rev. D* **40**, 3221 (1989).
- [13] N. Raj, P. Tanedo, and H.-B. Yu, *Phys. Rev. D* **97**, 043006 (2018).
- [14] A. Gould, B. T. Draine, R. W. Romani, and S. Nussinov, *Phys. Lett. B* **238**, 337 (1990).
- [15] C. Kouvaris, *Phys. Rev. D* **77**, 023006 (2008).
- [16] C. Kouvaris and P. Tinyakov, *Phys. Rev. D* **82**, 063531 (2010).
- [17] J. Ellis, G. Hüttsi, K. Kannike, L. Marzola, M. Raidal, and V. Vaskonen, *Phys. Rev. D* **97**, 123007 (2018).
- [18] G. Panotopoulos and I. Lopes, *Phys. Rev. D* **96**, 083004 (2017).
- [19] A. Das, T. Malik, and A. C. Nayak, *Phys. Rev. D* **99**, 043016 (2019).
- [20] H. C. Das, A. Kumar, B. Kumar, S. Kumar Biswal, T. Nakatsukasa, A. Li, and S. K. Patra, *Mon. Not. R. Astron. Soc.* **495**, 4893 (2020).
- [21] L. Tolos, J. Schaffner-Bielich, and Y. Dengler, *Phys. Rev. D* **92**, 123002 (2015); **103**, 109901(E) (2021).
- [22] S. Shirke, S. Ghosh, D. Chatterjee, L. Sagunski, and J. Schaffner-Bielich, *J. Cosmol. Astropart. Phys.* **12** (2023) 008.
- [23] J. Silk *et al.*, *Particle Dark Matter: Observations, Models and Searches*, edited by G. Bertone (Cambridge University Press, Cambridge, England, 2010).
- [24] X. Calmet and F. Kuipers, *Phys. Lett. B* **814**, 136068 (2021).
- [25] R. F. Diedrichs, N. Becker, C. Jockel, J.-E. Christian, L. Sagunski, and J. Schaffner-Bielich, *Phys. Rev. D* **108**, 064009 (2023).
- [26] K.-L. Leung, M.-c. Chu, and L.-M. Lin, *Phys. Rev. D* **105**, 123010 (2022).
- [27] G. Narain, J. Schaffner-Bielich, and I. N. Mishustin, *Phys. Rev. D* **74**, 063003 (2006).
- [28] B. P. Abbott, R. Abbott, T. Abbott, M. Abernathy, F. Acernese, K. Ackley, C. Adams, T. Adams, P. Addesso, R. Adhikari *et al.*, *Phys. Rev. Lett.* **116**, 061102 (2016).
- [29] B. P. Abbott, R. Abbott, T. Abbott, F. Acernese, K. Ackley, C. Adams, T. Adams, P. Addesso, R. Adhikari, V. B. Adya *et al.*, *Phys. Rev. Lett.* **119**, 161101 (2017).
- [30] L. Baiotti and L. Rezzolla, *Rep. Prog. Phys.* **80**, 096901 (2017).
- [31] L. Baiotti, *Prog. Part. Nucl. Phys.* **109**, 103714 (2019).
- [32] H. C. Das, A. Kumar, and S. K. Patra, *Phys. Rev. D* **104**, 063028 (2021).
- [33] Z. Miao, Y. Zhu, A. Li, and F. Huang, *Astrophys. J.* **936**, 69 (2022).
- [34] M. Hippert, E. Dillingham, H. Tan, D. Curtin, J. Noronha-Hostler, and N. Yunes, *Phys. Rev. D* **107**, 115028 (2023).
- [35] N. Rutherford, G. Raaijmakers, C. Prescod-Weinstein, and A. Watts, *Phys. Rev. D* **107**, 103051 (2023).
- [36] Y. Dengler, J. Schaffner-Bielich, and L. Tolos, *Phys. Rev. D* **105**, 043013 (2022).
- [37] S. Shakeri and D. R. Karkevandi, [arXiv:2210.17308](https://arxiv.org/abs/2210.17308).
- [38] M. W. Coughlin, T. Dietrich, B. Margalit, and B. D. Metzger, *Mon. Not. R. Astron. Soc.* **489**, L91 (2019).
- [39] T. Dietrich, M. W. Coughlin, P. T. Pang, M. Bulla, J. Heinzel, L. Issa, I. Tews, and S. Antier, *Science* **370**, 1450 (2020).
- [40] M. F. O’Boyle, C. Markakis, N. Stergioulas, and J. S. Read, *Phys. Rev. D* **102**, 083027 (2020).
- [41] P. T. Pang, I. Tews, M. W. Coughlin, M. Bulla, C. Van Den Broeck, and T. Dietrich, *Astrophys. J.* **922**, 14 (2021).
- [42] B. K. Pradhan, D. Chatterjee, M. Lanoye, and P. Jaikumar, *Phys. Rev. C* **106**, 015805 (2022).
- [43] I. Vidana, C. Providência, A. Polls, and A. Rios, *Phys. Rev. C* **80**, 045806 (2009).
- [44] C. Ducoin, J. Margueron, and C. Providencia, *Europhys. Lett.* **91**, 32001 (2010).
- [45] Z. Carson, A. W. Steiner, and K. Yagi, *Phys. Rev. D* **99**, 043010 (2019).
- [46] W.-J. Xie and B.-A. Li, *Astrophys. J.* **883**, 174 (2019).
- [47] J. Zimmerman, Z. Carson, K. Schumacher, A. W. Steiner, and K. Yagi, [arXiv:2002.03210](https://arxiv.org/abs/2002.03210).
- [48] A. Das, T. Malik, and A. C. Nayak, *Phys. Rev. D* **105**, 123034 (2022).
- [49] Q.-F. Xiang, W.-Z. Jiang, D.-R. Zhang, and R.-Y. Yang, *Phys. Rev. C* **89**, 025803 (2014).
- [50] C. Kouvaris, *Phys. Rev. Lett.* **108**, 191301 (2012).
- [51] N. F. Bell, G. Busoni, and S. Robles, *J. Cosmol. Astropart. Phys.* **06** (2019) 054.
- [52] A. Hook and J. Huang, *J. High Energy Phys.* **06** (2018) 036.
- [53] T. Malik, M. Ferreira, M. B. Albino, and C. Providência, *Phys. Rev. D* **107**, 103018 (2023).
- [54] D. R. Karkevandi, S. Shakeri, V. Sagun, and O. Ivanytskyi, *Phys. Rev. D* **105**, 023001 (2022).
- [55] R. Ciancarella, F. Pannarale, A. Addazi, and A. Marciano, *Phys. Dark Universe* **32**, 100796 (2021).
- [56] N. F. Bell, G. Busoni, S. Robles, and M. Virgato, *J. Cosmol. Astropart. Phys.* **09** (2020) 028.
- [57] W. DeRocco, P. W. Graham, D. Kasen, G. Marques-Tavares, and S. Rajendran, *Phys. Rev. D* **100**, 075018 (2019).
- [58] F. Anzuini, N. F. Bell, G. Busoni, T. F. Motta, S. Robles, A. W. Thomas, and M. Virgato, *J. Cosmol. Astropart. Phys.* **11** (2021) 056.
- [59] N. F. Bell, G. Busoni, S. Robles, and M. Virgato, *J. Cosmol. Astropart. Phys.* **03** (2021) 086.
- [60] N. F. Bell, G. Busoni, T. F. Motta, S. Robles, A. W. Thomas, and M. Virgato, *Phys. Rev. Lett.* **127**, 111803 (2021).
- [61] L. Brayeur and P. Tinyakov, *Phys. Rev. Lett.* **109**, 061301 (2012).
- [62] S. Ghosh, B. K. Pradhan, D. Chatterjee, and J. Schaffner-Bielich, *Front. Astron. Space Sci.* **9**, 864294 (2022).
- [63] J.-L. Jiang, C. Ecker, and L. Rezzolla, *Astrophys. J.* **949**, 11 (2023).
- [64] K. Nobleson, S. Banik, and T. Malik, *Phys. Rev. D* **107**, 124045 (2023).
- [65] B. P. Abbott *et al.* (LIGO Scientific and Virgo Collaborations), *Phys. Rev. X* **9**, 011001 (2019).
- [66] T. E. Riley *et al.*, *Astrophys. J. Lett.* **887**, L21 (2019).
- [67] M. C. Miller *et al.*, *Astrophys. J. Lett.* **887**, L24 (2019).
- [68] T. E. Riley *et al.*, *Astrophys. J. Lett.* **918**, L27 (2021).
- [69] M. C. Miller *et al.*, *Astrophys. J. Lett.* **918**, L28 (2021).
- [70] O. Ivanytskyi, V. Sagun, and I. Lopes, *Phys. Rev. D* **102**, 063028 (2020).
- [71] O. Lourenço, C. H. Lenzi, T. Frederico, and M. Dutra, *Phys. Rev. D* **106**, 043010 (2022).

- [72] M. Ju, J. Hu, and H. Shen, *Astrophys. J.* **923**, 250 (2021).
- [73] T. Malik, B. K. Agrawal, and C. Providêncio, *Phys. Rev. C* **106**, L042801 (2022).
- [74] Z. Carson, K. Chatzioannou, C.-J. Haster, K. Yagi, and N. Yunes, *Phys. Rev. D* **99**, 083016 (2019).
- [75] K. Yagi and N. Yunes, *Science* **341**, 365 (2013).
- [76] K. Yagi and N. Yunes, *Phys. Rep.* **681**, 1 (2017).
- [77] A. Maselli, V. Cardoso, V. Ferrari, L. Gualtieri, and P. Pani, *Phys. Rev. D* **88**, 023007 (2013).
- [78] Laboratory for Advanced Computing, Laboratory for Advanced Computing–University of Coimbra, <https://www.uc.pt/lca>.